Process manufacturing of functional food particles from lignin-rich feed

James Christopher Huscroft, BSc (Hons) RSci MIFST MIFT

Thesis submitted to the University of Nottingham for the degree of Doctor of Philosophy in Food Science

Division of Food Sciences
School of Biosciences
University of Nottingham
Loughborough
LE12 5RD

October 2019

The research leading to these results has received funding from the University of Nottingham, the Engineering and Physical Sciences Research Council (EPSRC) and Campden BRI.

University of Nottingham
UK | CHINA | MALAYSIA

Campden BRI
food and drink innovation

Abstract

The aim of the work presented in this thesis was to investigate various manufacturing routes to create hydrophobic particulate emulsifiers from lignin-rich by-products. In turn creating a functional material from ordinary waste materials.

Lignin, the second most abundant natural polymer after cellulose, is found in many different feedstocks. These are generated at multiple stages of food and drink production. Lignin provides structural support to the plant cell wall. Brewers' Spent Grain (BSG) which, was milled and dried, was used as the chosen lignin-rich feedstock for conversion into particulate emulsifiers. Differential Scanning Calorimetry (DSC) was used to register the thermal transition of the lignin in the BSG prior to hydrothermal processing. Ordinarily, an Acetyl Bromide Soluble Lignin assay is used to quantify lignin content in a biomass, however here a newly devised solid state Nuclear Magnetic Resonance (NMR) method was used to calculate lignin content based on carbon resonance ratios in the produced spectrum. This is compared to the standard Acetyl Bromide Soluble Lignin assay as well as a known Thermogravimetric Analysis (TGA) method to allow for a three way comparison using different quantification techniques.

Hydrothermal processing was used as a route to relocate lignin to the surface of the particulate emulsifier in the form of droplets. This in turn changed the particle hydrophobicity. In order to achieve this relocation, the feedstock requires processing above the quantified lignin transition temperature whereby the lignin undergoes a physical phase transition and as a result of cell wall collapse migrates through the to the surface of the particles. Numerous temperatures either side of this point of reference were tested and the highest temperature and time condition was found to have the greatest effect on the production of droplets. Scanning Electron Microscopy

(SEM) was used to confirm the production of droplets and their composition was quantified with NMR. Particle size of particulate emulsifiers is crucial for production of emulsions and the size of the droplets produced. Methods of particle size reduction i.e. high pressure homogenisation did not generate particles which were in the order of magnitude desired (<10μm). Although particle size reduction did occur, this was as a result of removing primary cell wall constituents during the high pressure process. This removal proved critical in generating a greater number of droplets at the surface of a smaller particle once they were hydrothermally treated. Droplet coated particles have been shown to produce water-in-oil emulsions whereas the untreated feedstocks produced oil-in-water emulsions. As such, the newly created particles in this work will enable the formation of a range of emulsions with varying concentrations of oil and water in their composition.

Acknowledgements

It is with great pleasure that I am able to thank everyone who has made the completion of this PhD possible.

Firstly, I would like to thank my primary supervisors at the University of Nottingham for their continued support throughout my PhD. Professor Bettina Wolf and Dr Eleanor Binner, I could not have done this without you. Your assistance over the last 3 years, combined with writing support, has enabled me to submit this thesis. We have shared many exciting moments throughout my research, and you have both motivated me to strive for more.

Secondly, I am extremely grateful to the Engineering and Physical Sciences Research Council (EPSRC), the University of Nottingham School of Biosciences and Chemical Engineering as well as to Campden BRI for providing the financial support for my PhD research.

I would also like to thank my third UoN supervisor, Dr Bill MacNaughtan for his invaluable insight on NMR and the food science world in general. Without you, there would be many more unanswered questions in this thesis. Steven Johnson cannot go unmentioned because you have supported me technically in and out of the lab and enabled me to succeed whilst exploring new science throughout the PhD. My thanks to Val Street and Darrell Cobon for continual technical support, Professor Ed Lester for help on pressure calculations and to Christine Grainger-Boultby for acquisition of the SEM images.

Thirdly, I would like to thank certain staff members at Campden BRI for their support over the last 5 years continuing through this PhD.

The first of those has to be Dr Graham Bown. Together, we have shared many wonderful memories (both inside and outside long factory nights in Swansea…) but your constant mentorship, guidance in challenging assumptions and never settling has helped mould me into the scientist I am today and for that I am indebted.

Onto Graham's successor in this PhD – Andrew Bosman who has provided a totally new angle to my way of thinking and getting the crucial research data. Technical support was provided by Robert Davis, Dr Tom Wood, Dr Martin Whitworth and Dr Richard Akkermans. Professor Sam Millar must be mentioned for his continued mentorship over the last 5 years pushing me to succeed. Lastly, Professor Steven Walker must also be included since the input you have provided to me, both during and outside of the PhD has enabled me to build such strong foundations at the start of my food industry career.

Lastly, there are a few individuals who cannot go unmentioned, my family, past and present. Throughout my life, all of you have supported me and kept me focussed striving to follow my dreams and passions. Mum and Dad (Anne and Chris Huscroft) need an extra special mention because whatever life has thrown at us, we have come out stronger as a trio. As Winston Churchill would so elegantly orate "Difficulties mastered are opportunities won" and the three of us have most definitely flourished.

With that being said, this thesis is dedicated to you both.

List of abbreviations and symbols

α	Alpha
β	Beta
BSG	Brewers' Spent Grain
CSL	Calcium Stearoyl Lactylate
^{13}C	Carbon-13 Isotope
cm	Centimetres
CPVC	Cross Polarisation Variable Contact Time
CPMAS	Cross Polarised Magic Angle Spinning
°C	Degrees Celsius
DE	Degree of Esterification
Δ	Delta
δ	Delta (Small Letter)
DATEM	Diacetyl Tartaric Acid Esters of Monoglycerides
Dicots	Dicotyledon
DSC	Differential Scanning Calorimetry
E	Electric Field (V/cm)
EU	European Union
°F	Degrees Fahrenheit
F	Frequency (GHz)
FV	Fill Volume
GSlignin	G&S Lignin Region on the NMR Spectrum (120 - 165 ppm)
GHz	Gigahertz
Tg	Glass Transition Temperature
g	Grams
G	Guaiacyl
HPH	High Pressure Homogenisation
Hz	Hertz
^{1}H	Hydrogen-1 Isotope
H	Hydroxyphenol
kPa	Kilopascals
kg	Kilograms
kHz	Kilohertz
kJ	Kilojoules
LCM	Lignocellulosic Material
l	Litres
MPa	Megapascals
Methoxy	Methoxy Region on the NMR Spectrum (54.5 - 58.5 ppm)
m/s	Metres Per Second
µ	Micro Sign
µm	Micrometer(s) (1 X 10^{-6} meters)
mg	Milligram(s) (1 X 10^{-3} grams)
ml	Millilitres(s) (1 X 10^{-3} litres)
mmHg	Millimeter Of Mercury
mm	Millimeter(s) (1 X 10^{-3} meters)

ms	Milliseconds
min	Minutes
Mol	Mole
Monocots	Monocotyledon
nm	Nanometer(s) (1 X 10^{-9} meters)
NQS	Non-Quaternary Suppression
NMR	Nuclear Magnetic Resonance
I	Nuclear Spin
O/W	Oil-in-Water
ω	Omega (lower case) - Angular Velocity
ppm	Parts Per Million
Pa	Pascals
π	Pi
PGPR	Polyglycerol-Polyricinoleate
P_v	Power Absorbed per Unit Volume (W/cm^3)
r	Radius
ϵ''	Relative Dielectric Loss Factor
Psat	Saturation Vapour Pressure
SEM	Scanning Electron Microscopy
SS-NMR	Solid State NMR
N	Speed (Revolutions per Minute)
T_0	Start Temperature
S	Syringyl
V_t	Tangential Velocity
T	Temperature
TEM	Transmission Electron Microscopy
TGA	Thermogravimetric Analysis
3D	Three Dimensional
tpa	Tons Per Annum
Total	Total NMR Spectra Region (0 - 250 ppm)
2D	Two Dimensional
UV	Ultraviolet
V	Volt
Vf_{liq}	Liquid Volume Fraction
W/O	Water-in-Oil
W/O/W	Water-in-Oil-in-Water
w/w	Weight for weight
wt%	Weight Percentage
wwb	Wet Weight Basis

Contents

1 Thesis Outline 1

1.1 Motivation 1

1.2 Overall aim and research objectives 3

1.3 Thesis layout 4

2 Scientific literature review and fundamentals 7

2.1 Plant cell wall structure 7

2.1.1 Cellulose 9

2.1.2 Hemicelluloses 11

2.1.3 Pectin 13

2.1.4 Lignin 14

2.2 Sources of lignin and their monolignol composition 17

2.3 Biomass processing methods 23

2.3.1 Chemical methods 24

2.3.2 Non-chemical methods for lignin liquefaction 26

2.4 Emulsification - principles 34

2.4.1 Pickering stabilised emulsions 37

2.5 Principles of key measurement methods applied in this PhD research 39

2.5.1 Principles of Nuclear Magnetic Resonance 39

2.5.2 Thermal properties 48

3 Method development and validation 52

3.1 Particle functionality assay 52

3.1.1 Angular velocity and tangential velocity calculations for using different high shear mixer heads 54

3.2 Particle size analysis 56

3.3 Microstructure methods 57
3.3.1 Bright field illumination 57
3.3.2 Fluorescence illumination 58
3.3.3 Scanning electron microscopy 58
3.4 Acetyl Bromide soluble lignin assay 59
3.5 Hydrothermal processing 62
3.5.1 Thermal process validation of hydrothermal process 62
3.5.2 Heat rate calculations for use in Microwave Synthesis Reactor 65
3.5.3 Hydrothermal processing in microwave synthesis reactor 67
3.5.4 Pressure calculations during the hydrothermal process 67
3.6 Nuclear Magnetic Resonance 75
3.6.1 Processing NMR spectra using MNOVA 75
3.6.2 Quantifying lignin from NMR spectra 76
3.7 Thermogravimetric analysis of lignin-rich feedstock 78
3.8 Method for Emulsion droplet analysis in W/O emulsions .. 80
3.9 Production of hydrophobic particles without the use of temperature 84
3.10 Production of lignin-emulsifier based cake 89
4 The Quantification of lignin content: a comparison of analytical methods. 92
4.1 Introduction 94
4.1.1 Lignin 94
4.1.2 Methods used for lignin quantification 94
4.2 Materials and methods 104

4.2.1 Materials 104
4.2.2 ^{13}C CPMAS solid state NMR 106
4.2.3 Acetyl Bromide Soluble Lignin (ABSL) Assay 108
4.2.4 Thermogravimetric analysis for lignin percentage quantification 109
4.3 Results and Discussion 109
4.3.1 Model lignin compounds characterised by two different analytical methods (Wet chemistry spectroscopy vs NMR spectroscopy) 110
4.3.2 Application of both methods for lignin quantification in three lignin-rich feedstocks 119
4.4 Conclusions 128
5 Hydrothermal processing as a route to yielding particulate emulsifiers from Brewers' Spent Grain as a lignin-rich by-product of the brewing industry 132
5.1 Introduction 134
5.2 Materials and methods 137
5.2.1 Materials 137
5.2.2 Hydrothermal process and extraction methods processes 138
5.2.3 Physicochemical Analysis Methods 140
5.2.4 Particle functionality assay 142
5.3 Results and Discussion 143
5.3.1 Thermal properties and composition 143
5.3.2 Surface morphology and emulsion functionality 154
5.4 Conclusions 167

6 Process design of an improved hydrophobic Pickering particle from Brewers' Spent Grain 170
6.1 Introduction 172
6.2 Materials and Methods 178
6.2.1 Materials 178
6.2.2 Processing 178
6.2.3 Physical material property analyses 183
6.2.4 Compositional analyses methods 184
6.2.5 Particle functionality assay 184
6.2.6 Lignin-based Pickering emulsifiers used to replace conventional emulsifiers during cake baking 186
6.3 Results and Discussion 187
6.3.1 Effects of the Microfluidizer step on the BSG particles 187
6.3.2 Hydrothermal processing 199
6.3.3 Particulate emulsifying capability 208
6.3.4 Additional particle functionality (cakes) 216
6.4 Conclusions 220
7 Final conclusions and proposed next steps 223
7.1 Final Conclusions 223
7.1.1 Feedstock selection 223
7.1.2 Time and Temperature hydrothermal processing parameters 224
7.1.3 High pressure processing technology applied for particle size reduction and emulsion droplet size reduction 225
7.1.4 Relevant droplet size for food industry applications 226

7.1.5 Lignin Percentage Quantification - Acetyl Bromide Soluble Lignin Assay, Thermogravimetric analysis and ^{13}C solid state NMR 226

7.2 Proposed next steps 229

References 232

Appendices 247

A1. Supplementary information for Paper 1 (Chapter 5) – All Scanning Electron Micrographs produced from different hydrothermal processing conditions 247

A2. Preliminary results for Lignin-based Pickering emulsifiers used to replace conventional emulsifiers during cake baking 253

A3. MATLAB code for calculating lignin percentage from NMR data 264

1 Thesis Outline

In this PhD research entitled "Process manufacturing of functional food particles from lignin-rich feed" the process technologies required to create hydrophobic particles from a selected lignin-rich by-product, for the stabilisation of Pickering emulsions were developed. The following outline gives the motivation and objectives behind this work as well as the layout of the thesis.

1.1 Motivation

Globally the food industry is facing a crisis of having to feed nearly 10 billion people by the year 2050 (United Nations, 2015), but also against a background of the area of arable land capable of growing foods remaining constant. Global food security is a key factor which has come to the forefront with the ever-growing global population. It is defined as the access to safe and nutritious food capable of meeting the requirements for a healthy life, whilst also having minimal environmental impact and ensuring that the planet can sustain these requirements in the future (FAO, 2002).

In the UK, it is estimated that post farm food waste is around 10 million tonnes per annum (WRAP, 2018). Despite the majority of this coming from households, there is still a large generation of food waste and by-products in the manufacturing sector and supply chain prior to the consumer that has been shown to amount to 1.85 million tonnes in 2015 (WRAP, 2018). These by-products could be an option capable of tackling the problem of global food security either by recycling or reuse and the generation of new products or ingredients. Globally, food businesses are tackling this problem with their own sustainability goals. Two examples scheduled for 2025 are PepsiCo, targeting a zero waste to landfill policy in line with their Performance with Purpose goal; and Mondelēz, who have set the objective of making its packaging fully recyclable (PepsiCo, 2006, Mondelēz International, 2018).

By-products are being used to formulate new products. Some recent developments in food innovation that follow the concept of recycling and reuse in the supply chain before reaching the consumer are innovative edible upcycled products, such as protein bars produced from brewers' grains (ReGrained, 2019) and the production of beer using out of specification Rice Krispies and Coco Pops, by Kelloggs (Hyslop, 2019). Upcycling is where a product of lower quality is reused for a different purpose/product of greater quality.

A vast proportion of by-products are of plant origin and currently used as animal feed if not going to landfill. From Brewers' Spent Grain to Apple Pomace, and bread to seed shells, businesses are sending greater proportions of materials to animal feed as a component of the circular economy of food production (Crawshaw, 2009). As lignin is the second most abundant plant cell wall material, it is present in a number of different materials. In 2007, it was estimated that around 200 billion metric tons of lignocellulosic materials (LCM) were produced globally (Zhang *et al.*, 2007, Ruiz *et al.*, 2013). The majority of sources, which are classed as LCM, are from agricultural residues and various types of wood, as well as co-products from a range of industries (Ruiz *et al.*, 2013). The variability of these materials at a molecular level is based on the maturity of the plant cell wall, and for lignin, this is characterised by the ratio of the monomeric components which bond to make the polymer. Plant cell wall material, specifically lignin has been shown to have many functional properties. One possibility is that lignin, which is intrinsically hydrophobic compared to other plant cell wall components, could potentially behave as an emulsifier (Gould *et al.*, 2016).

A number of lignin-rich feedstocks, when modified to change their functionality, could, potentially be converted to create sustainable,

clean label, environmentally and label friendly emulsifiers for use in a number of products.

1.2 Overall aim and research objectives

The overall aim of this PhD research was to develop a broad scientific understanding necessary for the generation of hydrophobic particulate emulsifiers from a lignin-rich by-product of the food and drink manufacturing supply chain. The interest in emulsifiers of this type lies in the current trend for fat reduction through the replacement of the entire or part of the fat by water-in-oil emulsions for fat-continuous products (e.g. chocolate) or water-in-oil-in-water emulsions for aqueous continuous products (e.g. salad dressings). There is also the possibility that these emulsifiers could be used as a clean-label emulsifier in foam-type products such as cakes and bread.

Specific objectives in this research were:

1. The selection of an appropriate lignin-rich feedstock for use in the experimental work
2. To explore processing parameters and routes for particle generation; specifically, the time and temperature of the hydrothermal process necessary to form a hydrophobic Pickering emulsifier
3. To explore whether an additional high pressure fluid process prior to hydrothermal processing generated particles of greater hydrophobicity than previously demonstrated and confirm whether this is linked to better emulsion stability with smaller particles and dispersed phase droplets
4. To confirm whether these emulsions are usable in current food industry applications

5. To quantify the lignin percentage in the particles using a newly developed method (Nuclear Magnetic Resonance) and compare this to the established wet chemical assay used widely in wood research and known as the Acetyl Bromide Soluble Lignin Assay

1.3 Thesis layout

The layout for the remainder of the thesis is as follows:

- **Chapter 2** provides a review of the literature relevant to the thesis. Some of this literature is again reviewed but in more detail in subsequent chapters (4–6), where relevant to the research results. These chapters (4–6) are written in the style of scientific paper manuscripts. The reviewed literature includes plant cell wall structure, biomass as sources of lignin, biomass processing methods, principles of emulsification, principles of key measurement methods and legislative considerations for particulate plant-based emulsifiers.

- **Chapter 3** introduces the method development section. In this section, newly devised techniques and their subsequent validation are explored.

- **Chapter 4** comprises the first results and discussion chapter. The intention is that this chapter will form the basis of a collaborative manuscript aiming for submission to the Royal Society of Chemistry Journal "Green Chemistry" from a number of researchers in both Food Science and Chemical Engineering. The Chapter title is "Comparison of different analytical methods for quantifying lignin in biomass". Lignin is notoriously difficult to quantify, and the benchmark technique is a wet chemical assay. This chapter explores the mechanism

of the Acetyl Bromide Soluble Lignin assay for lignin quantification and compares it to a newly devised NMR method, both for lignin precursor alcohols and also for known lignin-rich feedstocks. Two additional alternative methods for the quantification of lignin: Thermogravimetric analysis (TGA) and Pyrolysis Gas Chromatography Mass Spectrometry (Py-GCMS) are also considered. The TGA method was used in this study on the selected three feedstocks but Py-GCMS was not included with these results being collected by another researcher in Chemical Engineering and as such are not discussed in this thesis.

- **Chapter 5** is the second results and discussion chapter and forms the basis of a manuscript for publication in the Institution of Chemical Engineers journal "Food and Bioproducts Processing" entitled "Hydrothermal processing as a route to yielding particulate emulsifiers from Brewers' Spent Grain". The fundamental properties of Brewers' Spent Grain (BSG) are explored. Additionally, time and temperature conditions for hydrothermal processing were explored to understand the conditions under which a hydrophobic Pickering emulsifier from BSG is created.

- **Chapter 6** is the third results and discussion chapter forming the basis of a manuscript for publication in Elsevier's "Journal of Food Engineering". It is entitled "Process design of an improved hydrophobic Pickering particle from Brewers' Spent Grain". This research used the most severe time/temperature profile from the previous chapter and included a high pressure homogenisation (HPH) step prior to hydrothermal processing in order to decrease the size of the particles which were then

used to generate improved particulate emulsifiers from BSG. NMR was used as a tool to understand where lignin is distributed internally, whether it had become successfully relocated to the surface of the BSG particles, and to see if any fundamental changes in particle composition occurred. The effects of high pressure prior to hydrothermal processing on the thermal properties of BSG samples were tested. Additional work included in this chapter attempted to create hydrophobic particles using only HPH; image analysis of the W/O emulsions stabilised by 3PHT BSG and also the application of 3PHT BSG particles to replace a conventional emulsifier in cake baking.

- **Chapter 7** is the final conclusions and proposed future work section. Some of the hypotheses behind the suggested future work have already been tested in preliminary experiments, the results of which are shown and discussed in Appendices A2–A5.

- **References**

- **Appendices**

A1: Supplementary work and figures for Chapter 5.

A2: Preliminary results for Lignin-based Pickering emulsifiers used to replace conventional emulsifiers during cake baking.

A3: MATLAB code for calculating lignin percentage from NMR data.

2 Scientific literature review and fundamentals

In this chapter, the scientific background literature relevant to this PhD is covered, together with the scientific principles underlying the methods. Specific literature relevant to the results chapters is explored later in more detail in the introduction of the manuscript style results chapters.

2.1 Plant cell wall structure

Plant-based biomass is considered to be the most abundant form of renewable energy sources on the planet but only accounts for 4% contribution in the UK, whereas other renewable sources such as wind and solar power account for 12% and 11%, respectively (Hartley, 2019). In 2015, wood and waste biomass accounted for 26% of utilised renewable sources in the U.S. for energy (National Academies of Sciences, 2019). These biomasses are formed of a plant cell wall network which is made up of different polymers and polysaccharides, namely: cellulose, hemicellulose, pectin and lignin.

Figure 2.1 shows a simplified model of the plant cell wall matrix and where the different components are located (Rytioja *et al.*, 2014). The main components of the primary cell wall are cellulose, pectin and hemicellulose whereas in the secondary cell wall no pectin is found but instead lignin is present (Figure 2.1). The composition of a typical primary cell wall in a grass is 20–30% cellulose, 40–50% hemicellulose, 10–15% pectin, and 1–2% protein (Albersheim *et al.*, 2011). In the primary cell wall, an aqueous phase (water) is another constituent which can account for up to 70% of the total cell wall weight. Within this aqueous phase, soluble proteins, ions and newly manufactured cell wall components can be found. In the secondary plant cell wall, the amount of water present is greatly reduced and replaced by extra cellulose and, of most importance for this research, lignin (Albersheim *et al.*, 2011). Lignin is absent in the primary cell wall across most plant species and combined, cellulose and lignin

can account for up to 80% of the total secondary cell wall. Secondary cell walls mainly contain cellulose, hemicellulose (mainly xylan and glucomannan) and lignin (Zhong and Ye, 2015).

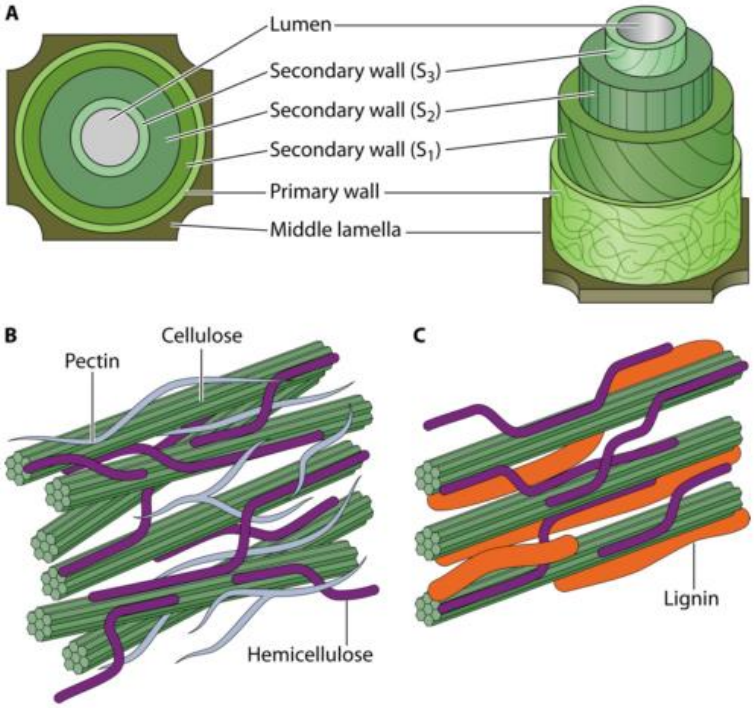


Figure 2.1: Simplified model of the plant cell wall structure, (A) Main structural layers, (B) Primary cell wall layer, (C) Secondary cell wall layer taken from (Rytioja et al., 2014)

Within the plant cell wall of most feedstocks, cellulose, hemicellulose and lignin are present but for some, BSG for example (reasons for selection shown in Section 2.2), also contains ferulic acid. This component is the most abundant hydrocinnamic acid in the plant world acting as a structural component within the cell wall itself and adding to strength whilst helping to keep it rigid (Mathew and Abraham, 2004). In barley and barley products, the levels of ferulic acid have been reported to vary depending on the constituent of the barley and whether or not it had been processed or merely harvested (Felizardo and Freire, 2018). Ferulic groups are also linked to arabinose sidechains in BSG (Bartolomé *et al.*, 2002). As shown by Hernanz *et al*. (2011), a mechanical shearing fractionation process produced barley fractions which had a large variation in the amount

of ferulic acid and ρ-coumaric acid present. Of the different barley fractions, husk and outer layers (F1), intermediate fractions (F2) and the endosperm fraction (F3), the F1 fraction had the greatest proportion of ferulic acid and ρ-coumaric acid at levels between 77.7–82.3% (w/w) and 78.0–86.3% (w/w), respectively. It should also be mentioned that BSG was around 5 times richer in both of these fractions compared with barley (Hernanz *et al.*, 2001). The ferulic acid present in plant cell walls binds to structural proteins, polysaccharides and lignin in the grass cell wall and forms cross-links between these components (de Oliveira *et al.*, 2015). Another impact of ferulic acid in beer is that when it is thermally or enzymatically degraded, a compound termed 4-ethyl-2-methoxyphenol is produced which creates a characteristic flavour in white beer. As such this could be transferred into the final product for the emulsifiers in this work (Olszewski *et al.*, 2019).

2.1.1 Cellulose

Cellulose is the most abundant material in the plant-based world. It provides structural support to the plant cell wall. Cellulose is a high molecular weight polysaccharide made up of glucose units (specifically anhydro-D-glucose units) linked with β–1,4 linkages (Figure 2.2). Cellulose is found in both the primary and the secondary cell walls with the primary cell wall being 20–30% cellulose whereas the secondary cell wall can contain up to around 50% cellulose (w/w) (Albersheim *et al.*, 2011).

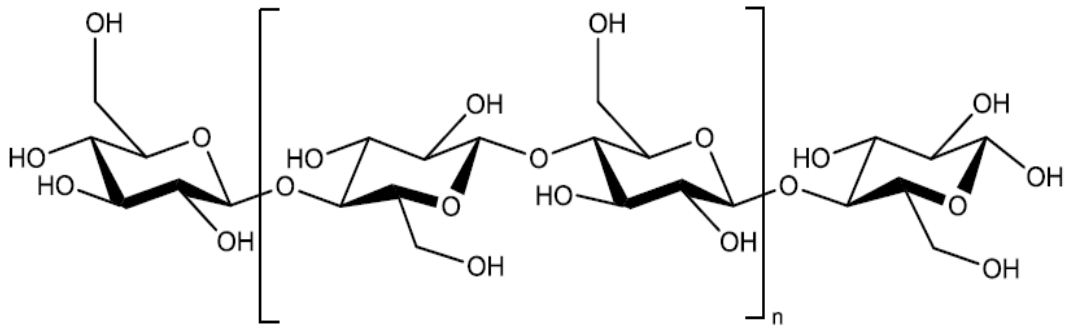


Figure 2.2: Chemical structure of cellulose (Chawla et al., 2015)

Cellulose has four different allomorphs (I to IV) and Cellulose allomorph I is considered "native" cellulose. Upon the use of an alkaline treatment, Cellulose I is converted into type II fibres and the difference being the hydrogen bonding patterns in the cellulose structure. Cellulose I and II can be converted into Cellulose III with the use of liquid ammonia which causes either parallel or antiparallel chains (I and II respectively) but this can be reversible. Cellulose III fibres can be converted into Cellulose IV fibres only with heat treatment in Glycerol at 260°C. The hierarchical structure of cellulose is as follows: Cellulose fibres (~10μm); cellulose bundle network (~1μm); microfibril bundle (~10nm); individual microfibril (~3nm); cellulose chain (~1nm) (Paajanen *et al.*, 2019). Due to the ordered formation of the glucan chains in cellulose microfibrils, it is often considered to be a crystalline material. Despite this, the highly organised crystalline regions are separated by amorphous regions. The difference in crystallinity of the crystalline and amorphous regions can be characterised by such techniques as X-ray Diffraction as well as solid state ^{13}C Nuclear Magnetic Resonance (NMR). The arrangement of these microfibrils has been observed using different forms of electron microscopy (SEM & TEM) and consists of random mesh and loose parallel sheets.

2.1.2 Hemicelluloses

These are comprised of several different polysaccharides, for example, xylans, xyloglucans, arabinoxylans, glucomannans, galactomannans and galactoglucomannans. These different polysaccharides are made up of various amounts of the monomeric sugars shown in Figure 2.3. For different angiosperms and gymnosperms, the main component hemicellulosic polysaccharides are the xyloglucans and the arabinoxylans (Albersheim *et al.*, 2011). Depending on the species, the relative abundance of these two polysaccharides varies. For example in gymnosperms, the total cell wall can contain up to 35% xyloglucan with less than 5% being from arabinoxylan whereas in monocots, up to 40% of the cell wall can be arabinoxylans with minimal xyloglucan (Albersheim *et al.*, 2011). The secondary cell wall is where xylans, glucomannans, galactomannans and galactoglucomannans are likely to be found. The structures of the different hemicellulose polysaccharides are shown in Figure 2.4.

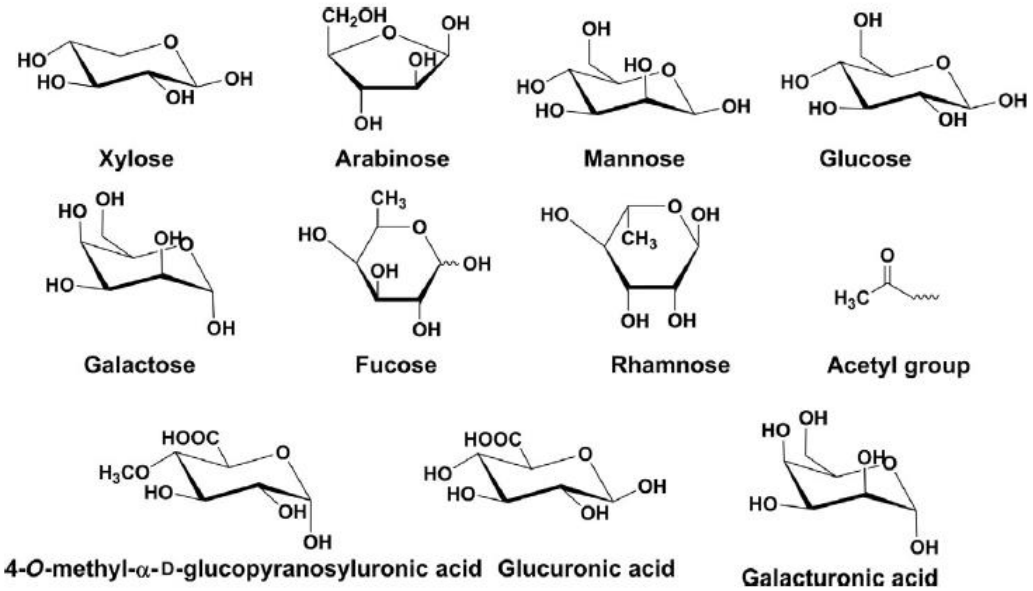


Figure 2.3: Building blocks of hemicellulose (Zhou et al., 2016)

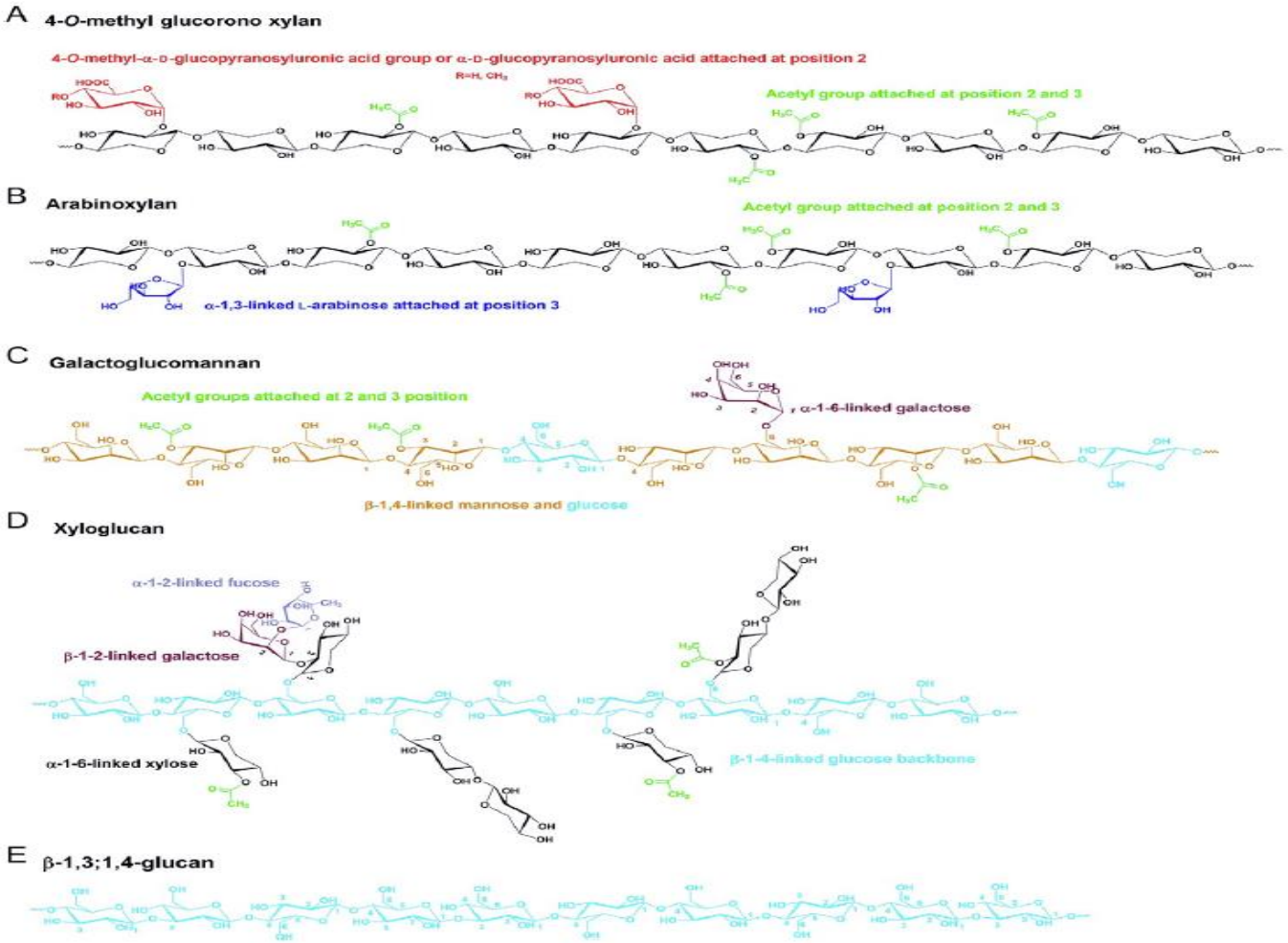


Figure 2.4: Structure of major hemicellulose polysaccharides: (A) 4-O-methyl-D-glucorono-D xylan (glucuronoxylan), (B) arabinoxylan, (C) galactoglucomannan, (D) xyloglucan, and (E) β-1,3;1,4-glucan (Zhou et al., 2016)

2.1.3 Pectin

The primary cell wall polysaccharide matrix as previously mentioned contains cellulose, hemicellulose and pectin. The pectic polysaccharides are classed as those which can usually be dissolved in hot water or by weak chemical (acid or alkali) treatment in complete contrast to the cellulose and hemicelluloses (Albersheim *et al.*, 2011). The pectic polysaccharides found in the primary plant cell wall are homogalacturonan, xylogalacturonan, rhamnogalacturonan I and rhamnogalacturonan II. Their structures are shown in Figure 2.5. Hemicellulose and pectin are the other main constituents in the primary cell wall matrix where the cellulose microfibrils are embedded (Harholt *et al.*, 2010). The ratio of the different pectic polysaccharides varies depending on source material. Characteristically, of these polysaccharides, homogalacturonan is found in the greatest quantity in the pectin structure accounting for around 65%; rhamnogalacturonan I is the second most abundant accounting for 20–35% and both rhamnogalacturonan II and xylogalacturonan accounting for less than 10% each (Zandleven *et al.*, 2007, Mohnen, 2008, Harholt *et al.*, 2010).

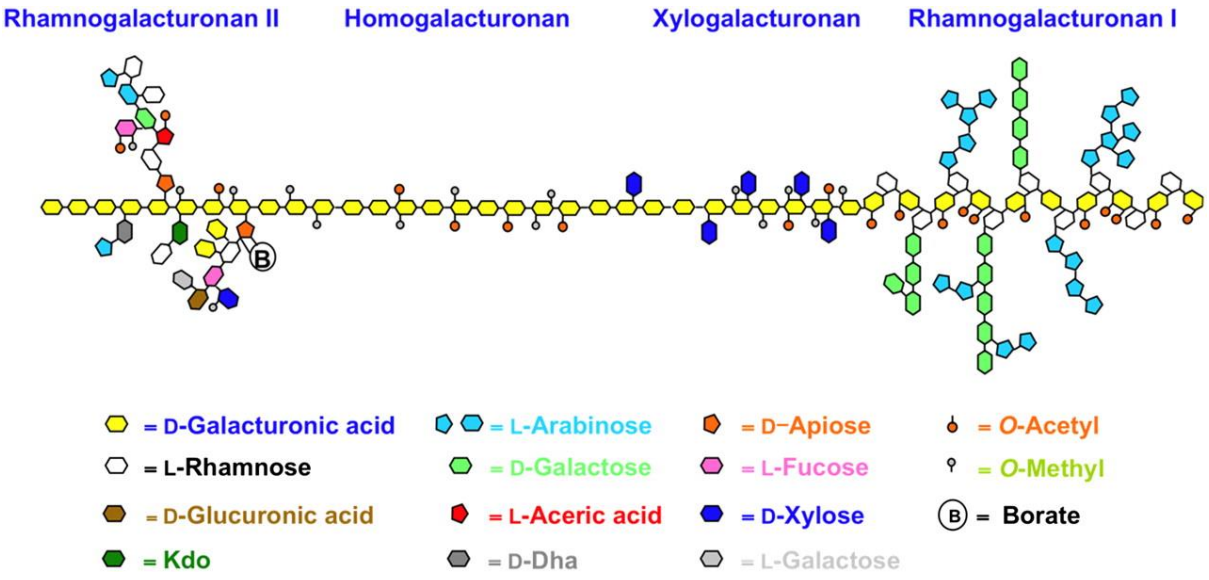


Figure 2.5: Schematic structure of pectin and the four different types of pectic polysaccharides (Harholt et al., 2010). Dha is 3deoxy-lyxo-2-heptulosaric acid, and Kdo is 3-deoxy-manno-2-octulosonic acid (Voragen et al., 2009).

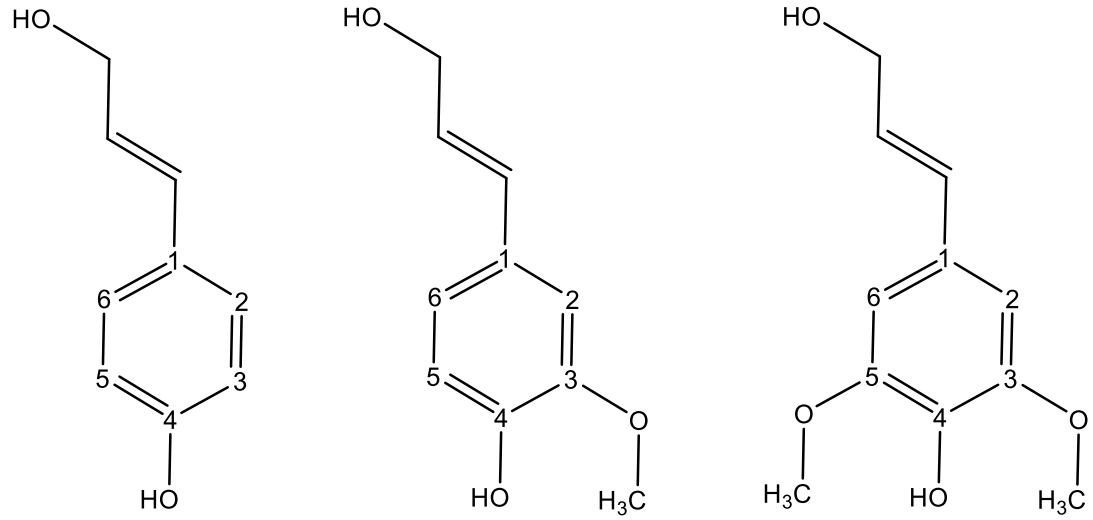
The pectin structure is a block-based polysaccharide where specific sections have specific structures. Unlike cellulose, pectin is a heavily branched polymer with homogalacturonan blocks which can be esterified by methyl groups (Jarvis, 1984, Ha *et al.*, 2005). In pectin structures, the degree of esterification (DE) refers to the amount of methyl groups present where a high methoxy pectin is a sample which has a DE of above 50% whereas a low methoxy level pectin is one which has a DE of less than 50% (Morris *et al.*, 2000).

2.1.4 Lignin

Lignin is made up of the three organic alcohols (ρ-coumaryl, coniferyl and sinapyl). In addition to what has been said before, another key role of lignin is that is provides a barrier to both pests and pathogens which may cause harm to the plant (Albersheim *et al.*, 2011). Lignin provides a physical barrier against initial pathogen colonisation and the lignin content of a feedstock being an important factor shown by a positive correlation in aiding resistance of the plant to vascular pathogens (Miedes *et al.*, 2014).

These alcohols form the basis of the primary monomers for the monolignols which are ρ-hydroxyphenol (H), guaiacyl (G) and syringyl (S) units shown in Figure 2.6. These monolignols are synthesised within the plant from the amino acid, phenylalanine. The type of lignin found in these plant materials are classified into three based on the monomers and enzyme-initiated dehydrogenative polymerisation (Santos *et al.*, 2012). These monomers are formed at different stages of the lignification process. Lignification is the process by which the three different monomers form together to create the macromolecule (Hatfield and Vermerris, 2001). During the early stages of plant growth, the primary wall contains precursor copolymers of G and H lignin in derived compounds from phenylalanine. For development of the secondary plant cell wall, a

greater proportion of sinapyl alcohol is copolymerised to form mixed G and S lignin (Grabber, 2005). Lignin is considered to have no known fixed structure due to the changing composition from species to species with regards to the G: H: S ratio. Lignin is also considered to be hydrophobic and provides structural support as well as fundamental strength to the plant cell wall. The crosslinking of lignin with other polysaccharides enables the plant cell wall to be a barrier to water.



coumaryl alcohol (H) coniferyl alcohol (G) sinapyl alcohol (S)

Figure 2.6: Allocation of carbon atoms in the benzene ring numbered on H-lignin but also the same for G and S lignin adapted from (Manders, 1986)

In the wheat grain for example, the amount of lignin present depends on the stage of maturity. However, the molar ratio (S/G) remains constant throughout various stages of maturity having a value of 0.8. Over the four stages (termed A, B, C, D) of maturation, as categorised by Beaugrand *et al.* (2004), the lignin remains undetectable in the first two stages. However, it was found to be a component of the peripheral tissues for the developing wheat grain in the last two stages. The molar ratio decreases in total lignin from 4.8μmol/g in stage C to 4.3μmol/g in stage D (Beaugrand *et al.*,

2004). Lignin monomers are formed from their precursors depending on the formation of the monolignols and their interactions with ferulic acid. The formation of the lignin monomers begins by the conversion of phenylalanine through a series of steps into the lignin precursors (de Oliveira *et al.*, 2015).

The linkages involved in the lignin molecule and the ratios of these linkages differ between different materials as shown in Table 2.1 and Figure 2.7. The coupling of the monomeric components whether major or minor (aldehydes, esters or diols) subunit monomers can be by either ether linkages, carbon-carbon bonds or sometimes bonds where they are bonded to more than one phenylpropane unit. Due to the stability of the free radicals which form the bonds at specific locations, there is a high probability as to which carbon atom will become the bonded host to a specific free radical. As a result of this, specific linkages are preferred between the lignin sub-units which form the large polymeric structure (Haghdan *et al.*, 2016). As lignin contains a variety of linkages (Table 2.1), it forms a highly heterogeneous polymer which has a complex branched three-dimensional structure (Haghdan *et al.*, 2016).

Table 2.1: Predominant Lignin Linkages (Patil, 2012, Santos et al., 2013)

Linkage Type	**Dimer Structure**	**Percentage Linkages in Softwood (%)**	**Percentage Linkages in Hardwood (%)**
β-O-4	Arylglycerol β–aryl ether	45–50	60
5-5	Biphenyl and Dibenzodioxocin	18–25	20–25
β-5	Phenylcoumaran	9–12	6
β-1	1,2–Diaryl propane	7–10	7
α-O-4	Phenylpropane α-aryl ether	6–8	7
4-O-5	Diaryl ether	4–8	7
β- β	β–β linked structures	3	3

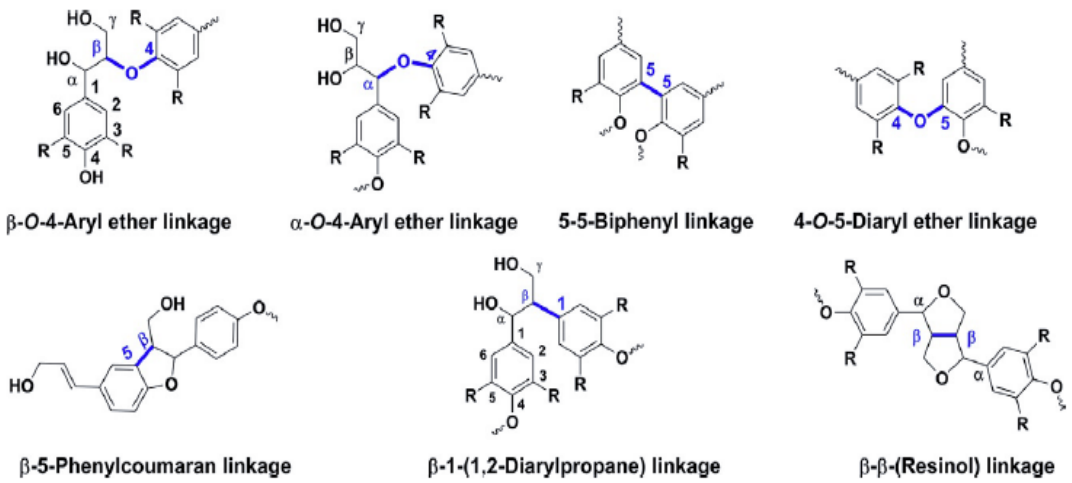


Figure 2.7: Seven major linkages (β-O-4, α-O-4, 5-5, 4-O-5, β-5, β-1, and β-β) in lignin (Zhou et al., 2016)

2.2 Sources of lignin and their monolignol composition

Lignin, which is the main plant polysaccharide of interest in this research, is found in numerous feedstocks. For example, grasses, often contain 5% to 10% lignin (Novaes *et al.*, 2010). The amount of lignin present in lignin-rich feedstocks varies from species to species and the monolignol composition is greatly affected by the maturity and absolute age of the plant/feedstock (Albersheim *et al.*, 2011). Examples of lignin-rich feedstocks in the food and drink industry are spent coffee grounds, composed of between 20–27 % lignin by weight (Pujol *et al.*, 2013, Ballesteros *et al.*, 2014), Brewers' Spent Grain (BSG), which is a by-product of wort production in the brewing industry, and oat husk, which is generated from the separation process when oats are rolled (Welch *et al.*, 1983). The main component of BSG is barley and BSG is often considered to be between 12 and 28% lignin depending on the origin of the ingredients and the inclusion of other malts (Mussatto *et al.*, 2006, Mussatto *et al.*, 2007, Lynch *et al.*, 2016). Other sources of lignin are shown in Table 2.2.

Table 2.2: Sources of lignin in food

Source	Percentage lignin (%)	Reference
Barley Straw	27.57	(Chen *et al.*, 2007)
Brewers' Spent Grain	12–28	(Lynch *et al.*, 2016)
Chestnut (Hull)	21.9 ± 1.3	(Saura-Calixto *et al.*, 1983)
Coir (coconut fibre) *	43–49	(Faruk, 2016)
Oat Husk (Finnish)	13.7	(Welch *et al.*, 1983)
Corn stalks	35	(Faruk, 2016)
Spent Coffee Grounds	23.9 ± 1.7	(Ballesteros *et al.*, 2014)
Sugarcane bagasse	20	(Faruk, 2016)
Wheat, by-products, bran	15.5	(Theander *et al.*, 1995)
White Asparagus	5	(Schafer *et al.*, 2016)
White Asparagus 7 days at 20°C	9.5	(Schafer *et al.*, 2016)
Spinach	4.1	(Anderson and Bridges, 1988)
Kiwi	8.9	(Bunzel *et al.*, 2005)
Carrot	3.2	(Bunzel *et al.*, 2005)
Rhubarb	9	(Bunzel *et al.*, 2005)
Softwood*	27–33	(Azadi *et al.*, 2013)
Hardwood*	18–25	(Azadi *et al.*, 2013)

*Non-food source comparison

Two feedstocks were selected as an example of lignin-rich feedstocks (spent ground coffee and BSG) and annual production was used as reference of scale. These two feedstocks were selected based on the amount of lignin present and also the abundance of production in the food industry. In London, there are a total of 1522 chain coffee shops (e.g. Starbucks/Costa), and account for almost one third of the national total for the UK (Prynn and Sinmaz, 2012). Annually these produce around 200,000 tonnes of spent coffee (Burrows, 2015). The brewing industry in Europe produced 52.1 billion litres of beer in 2016 (Kirin, 2017). With an approximate amount of 20kg of spent grain generated per 100L of beer (Reinold, 1997, Mussatto *et al.*, 2006), this equates to 10.42 million tpa of BSG (Kirin, 2017). BSG is predominantly malted barley however, other ingredients can be used depending on the type of beer produced (e.g. crystal malts or types of hops). Pre-production steps also generate lignin-rich by-

products. One example is the production of pearled barley. The pearling process for barley grains involves the removal of the fibrous hull and the outer bran layer of the endosperm through the use of a pearling machine (Felizardo and Freire, 2018). The end product of pearled barley (the endosperm and embryo of the grain) represents about 80% weight of the whole grain (Evers and Millar, 2002). The remaining 20% waste component contains the husk, the aleurone and the pericarp. The husk represents 13% of the whole grain and the husk itself contains 23% lignin (Olkku *et al.*, 2005). Barley production worldwide was approximately 140.6 million tonnes of grain in 2018/19 (Statista, 2019a, Statista, 2019b). Approximately 40% of global barley production is produced in the European Union (56.35 million metric tons) (Statista, 2019a, Statista, 2019b). For the total barley production in the EU in 2018/19, this equates to 7.33 million metric tons of barley husk per annum. As a percentage of this, annual lignin production equals 1.68 million metric tons in the European Union alone.

The composition of lignin in the agricultural supply chain differs depending on the feedstock origin. The proportions of the G, H and S monomers for specific lignins show how composition varies from source to source and how plant growth conditions impact on the cell wall (Table 2.3). The composition is based on the relative percentage of G, H and S in the overall feedstock. For example, lignin in softwood is rich in coniferyl alcohol. Hardwood consists of equal amounts of coniferyl and sinapyl alcohols and grasses consist of the same levels as hardwood with 10–20% amounts of ρ-coumaryl alcohol (Boerjan *et al.*, 2003). The relative proportions and the differences in composition are shown more clearly in Figure 2.8 using data taken from Table 2.3.

As can be seen on Figure 2.8, the proportions of the G, H and S lignin monomers for wheat straw and rhubarb are almost identical in terms

of monomeric compositions. Straw is the by-product of harvesting many cereal grain crops worldwide. In the example of wheat harvest, the straw remains as a by-product once the grains have been gathered. When the plant has gone to seed, nutrients are delivered to the wheat kernels to enable them to grow and upon harvest the lignin-rich straw remains.

From Table 2.3, the main noticeable difference between the two tree woods is the S/G ratio for the two materials. Softwoods have a much larger amount of coniferyl alcohol (guaiacyl lignin) with a relatively small proportion of sinapyl alcohol (syringyl lignin) whereas in hardwoods, the split between the S & G lignins is 50/50, implying that structurally hardwoods are more mature in growth terms than softwoods (Azadi *et al.*, 2013).

Compositionally, fresh white asparagus has a similar lignin monomer composition to that of a softwood (Table 2.3) whereas wheat and rhubarb have a similar composition to hardwood. The two food-based sources which display different compositional data to hard and softwoods are BSG and coir or coconut fibre.

Table 2.3: Lignin G, H, S proportions of food sources

Source	Proportion G (%)	Proportion H (%)	Proportion S (%)	Reference
Brewers' Spent Grain (MWL)	56	24	20	(Rencoret *et al.*, 2015)
Oat	38.5	n/a	61.5	(Lupoi *et al.*, 2015)
Coir	29	n/a	71	(Rencoret *et al.*, 2013)
Hemp (Industrial)	13	53	34	(Gutierrez *et al.*, 2006)
White Asparagus fresh	79.3	Trace	20.7	(Schafer *et al.*, 2016)
White Asparagus 7 days at 20°C	61.7	1	37.3	(Schafer *et al.*, 2016)
Wheat	49	5	56	(Tolbert *et al.*, 2014)
Wheat Straw	6	64	6	(del Rio *et al.*, 2012)
Sugarcane Bagasse (MWL)	38	2	60	(del Rio *et al.*, 2015)
Rhubarb	47	n/a	53	(Bunzel *et al.*, 2005)
Softwood*	90–95	-	5–10	(Azadi *et al.*, 2013)
Hardwood*	50	-	50	(Azadi *et al.*, 2013)
Grasses	5	75	25	(Azadi *et al.*, 2013)

n/a = not known, * Non-food source comparison, (MWL) = Milled Wood Lignin

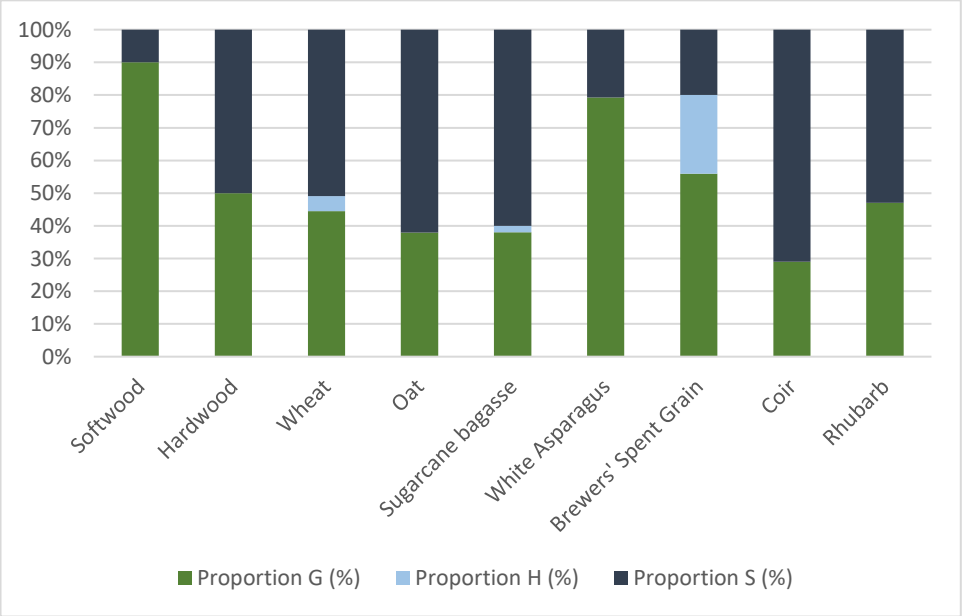


Figure 2.8: Differences in lignin composition for different lignin-rich sources from data presented in Table 2.3

The ratio of S/G depends on the maturity of the plant cell wall. The higher the proportion of syringyl lignin present and, therefore, the higher the S/G ratio, the older the plant tissue. The significance of this is that the lower the S/G ratio and, therefore, the greater proportion of G present, the greater is the cell wall degradability (He

et al., 2018). It was hypothesised by Jung and Deetz (1993) that the reason why the syringyl units were less accessible for cell wall degradability was because there were fewer sites capable of undergoing polymerisation reactions unlike the guaiacyl units (Jung and Deetz, 1993, He *et al.*, 2018). Counter to the hypothesis of Jung and Deetz (1993), Filley *et al*., (2002) emphasized that the G-lignin was in fact more chemically and biologically resistant than S-lignin (Filley *et al.*, 2002, He *et al.*, 2018). An example of the changing percentages of overall monomeric lignin content in a feedstock can be seen for white asparagus. Schafer *et al.* (2016) showed that the percentage of lignin appeared to alter depending upon storage conditions post-harvest. Taking the fresh asparagus as a reference, storing the asparagus at 20°C for a period of 3 days in the dark at a relative humidity (RH) of 60–80%, increased the molar percentage of H-lignin from trace amounts to 1%. S-lignin increased from just over 20% to 31% and caused a decrease in the G-lignin monomer from 79% to 68% as a molar percentage. After being held at 20°C for 7 days, the total molar percentage of G-lignin decreased to just under 62% with S-lignin being just over 37% (Schafer *et al.*, 2016). If however, the asparagus was held at 1°C, in the dark at an RH of 60–80%, the initial percentage of G-lignin increased to 81%. However, over 28 days, it decreased to 73.5% with this decrease mirrored by a corresponding increase in molar percentage of S-lignin (Schafer *et al.*, 2016).

The diversity of lignin compositions within food and plant materials have been shown in Table 2.2 and Table 2.3. There are a large number of possible feedstocks which could be used as a starting material in this research to generate functional particulate emulsifiers.

The current use for most of these by-products is animal feed, however some are also used in the production of biofuels. Table 2.4

shows the current alternative use for the by-products which can be classified as rich in lignin.

Table 2.4: Types of lignocellulosic material and their current uses (Howard et al., 2003)

Lignocellulosic material	Residues	Current use
Grain harvesting Wheat, rice, oats barley and corn	Straw, cobs, stalks, husks	Animal feed, burnt as fuel, compost, soil conditioner
Processed grains Corn, wheat, rice, soybean	Wastewater, bran	Animal feed
Fruit and vegetable harvesting	Seeds, peels, husks, stones, rejected whole fruit and juice	Animal and fish feed, some seeds for oil extraction
Fruit and vegetable processing	Seeds, peels, wastewater, husks, shells, stones, rejected whole fruit and juice	Animal and fish feed, some seeds for oil extraction
Sugar cane other sugar products	Bagasse	Burnt as fuel
Oils and oilseed plants Nuts, cotton seeds, olives, soybean etc.	Shells, husks, lint, fibre, sludge, press-cake, wastewater	Animal feed, fertiliser, burnt fuel

These by-products are currently surplus to requirements from a food industry perspective since they are not used to make products and therefore could potentially be used for something other than animal feed. Such by-products are a part of creating food products during the primary production stages. The process of adding value to these by-products is a way of minimising the overall amount of waste that is created through all stages of the food and beverage supply chain through using these current by-products to make new products or ingredients.

2.3 Biomass processing methods

Lignin as a constituent of wood poses a problem during the production of paper due to its role in the structuring of a plant cell well. The pulping industry is used here as an example because the lignin present in a plant cell wall must be removed in order to

produce paper. If lignin is not removed, then it causes problems in processing and production of the paper. The pulping industry in Europe uses two predominant processes to produce paper, chemical and non-chemical. The two methods produce differing amounts of paper of varied quality and have different production costs. Chemical methods, discussed in 2.3.1, account for two-thirds of the pulp produced in Europe every year and this pulp produces higher quality paper (CEPI, 2019). Non-chemical methods (mainly mechanical processes) account for the other third of the production and produces lower quality paper but is cheaper than the chemical counterpart (CEPI, 2019). The specific process of interest, hydrothermal processing, is discussed in its own section in 2.3.2.1.

2.3.1 Chemical methods

Prior to any of the pulping methods mentioned below, wood goes through a wood chipper to regulate the size of the chips and to ensure that there is uniform chemical penetration during the delignification process ensuring minimal batch to batch variation (Benjamin *et al.*, 1969).

2.3.1.1 Kraft Pulping Process

The primary method of lignin removal in the pulping process is known as Kraft Pulping. This occurs when wood chips are processed in a liquid known as "white liquor", an aqueous solution containing sodium sulphide and sodium hydroxide which in turn dissolves the lignin out of the wood chips into solution (US-EPA, 1990). The mechanism by which this occurs is the physical breakdown of the plant cell wall by the dissolution of hemicellulosic polysaccharides enabling lignin to be removed (Sun *et al.*, 1995). Sodium Hydroxide can also effectively transform cellulose I into cellulose II (Chen *et al.*, 2017). The process by which alkali has an impact on cellulose fibres in known as Mercerisation. Mercerisation is the process by

which irreversible swelling of cellulose fibres occurs (Mercer, 1850, Dinand *et al.*, 2002). Mercerisation is the physical change to the crystallinity structure and the morphology of the cellulose fibres (e.g. the change from Type I to Type II fibres).The swelling of cellulose fibres occurs during the first mercerisation step whereby the alkaline solvent penetrates the cellulose in the plant cell wall (specifically the amorphous regions) and in turn leads to fibre swelling (Budtova and Navard, 2015). Using NaOH as solvent, cellulose fibres can exhibit uniform swelling under specific conditions (-5 8°C, 7.6% of NaOH deemed optimal by Cuissinat and Navard, (2006)) whereby large swelling occurs in the form of ballooning as well as the partial dissolution of the fibre whilst still maintaining the shape (Cuissinat and Navard, 2006). Temperature has also been shown to have an impact on the use of NaOH for the swelling and dissolution of cellulose. Temperature was shown to reduce the quality of the solvent enable the swelling to occur of the cellulose but with no ballooning or dissolution of the fibres occurring (Cuissinat and Navard, 2006).

This process is usually conducted in a batch protocol. However, there are continuous flow systems. The temperatures used in the pulping process can be as high as 355°F (179°C), achieved through the use of steam inside of the digester vessel (Benjamin *et al.*, 1969). In the batch process, post-processing at temperature, the mixture is transferred to a tank where the liquid is separated from the wood chip pulp to remove the lignin. The wood pulp is then washed to remove any residual lignin liquor.

2.3.1.2 Acid Sulphite Pulping

This process is very similar in mechanism to the Kraft Pulping Process detailed in 2.3.1.1. However, the chemicals used in the pulping liquor differ and as such make the entire process acidic rather than alkaline. Sulphuric acid is used as the main chemical

component of the liquor along with a buffering solution containing a combination of different bisulphites (sodium, magnesium, ammonium, etc.). The processing is conducted at high temperature and pressure and can be in both batch and continuous procedures (US-EPA, 1990). Upon removal of the liquor, the pulp is washed again to remove any residual liquor and separate any fibre knots into strands before being dried.

2.3.1.3 Neutral Sulphite Semi-Chemical Pulping

In this process, wood chips are cooked in a liquor as in the above processes. However, this solution is neutral since it contains both sodium sulphite and sodium carbonate. This method removes lignin as in the Kraft and Acid Sulphite processes; the main difference being that only a portion of the lignin is removed from the wood chips. To increase lignin removal, the wood chips are further processed by mechanical disintegration.

The main non-chemical method of pulp production uses mechanical processes. This originally occurred by producing a pulp using a mechanical operation where wood was ground between rotating stones lubricated with water (CEPI, 2019). The generated heat from the grinding process aids the removal of lignin by softening and separating it from the wood fibres to produce a product known as "groundwood". Nowadays, the process occurs by using a high shear rotating disc and fixed plate (CEPI, 2019). There have been slight modifications made to the process, such as softening some of the woodchips are softened prior to processing with the use of heat to enable a greater degree of fibrillation.

2.3.2 Non-chemical methods for lignin liquefaction

Lignin liquefaction is the process by which a wet biomass is converted into another product; often crude oil or bio oil. Bio oil

ordinarily is a rich liquor fraction contain phenolic compounds as a result of the thermal conversion of biomass into hydrophobic compounds with a high solubility in polar solvents. Liquefaction often occurs at high pressure and moderate temperatures. The temperature range for lignin liquefaction is often in the sub-critical region of water, but not always. For best results, temperatures range from 150–400°C, with desired results occurring between 280°C and 380°C (Kozliak *et al.*, 2016, Schuler *et al.*, 2017, Belkheiri *et al.*, 2018).

The use of steam or microwave radiation (field coupling) are effective methods of heating a product and have been widely applied in the food industry. If alternative heating methods are used, the conductive, convective or radiative heat-transfer coefficients and field capacity must be considered and are required for process design. The main heating mechanisms occurring in the hydrothermal process in this work are conduction and convection, where conduction heating through a solid body (e.g. the walls of the processing vessel) and convection in the fluid (e.g. the water in the hydrothermal process). Heating by conduction occurs in solid bodies where the molecules in the food vibrate passing the heat energy through the material. The point-to-point transfer of heat occurs from areas of higher temperature to those of lower temperature (Singh and Heldman, 2014). The main principle of heat transfer by conduction is through this temperature gradient, can be described by Fourier's law. This states that the rate at which heat flows past any plane of the material is proportional to the negative temperature gradient across an area at right angles to the gradient through which the heat flows, the constant of proportionality being the thermal conductivity of the material (Hayhurst, 1997). Heating by convection is the mechanism by which heat is transferred through fluids (gas or liquid) which is what would occur during a hydrothermal process.

Following conduction of heat from a solid body (e.g. conduction through the walls of the processing vessel), heat is exchanged from the solid body to the fluid if there is a temperature gradient between the two media. Convection comes in two forms: forced convection or free convection. Forced convection is where an external mechanical source i.e. a pump, piston or fan physically induces movement within the fluid. Free convection is where density differences in the product cause a turbulent effect which is induced by temperature gradients (Singh and Heldman, 2014). For example, in the process of canning (which is relevant to hydrothermal processing due to the inclusion of headspace air in the vessel and the vessel being sealed), the air headspace volume is crucial in the convection within the product to allow it to heat. The air in the headspace is displaced due to heating of the fluid product. This in turn causes the product to heat more rapidly resulting from induced convection currents. The main difference between conduction and convection is that conduction heats point-to-point (vibrating atoms/molecules) whereas convection heats by induced motion, whether it is forced or naturally occurring as a result of density differences.

2.3.2.1 Hydrothermal processing

The use of a hydrothermal process in the treatment of lignocellulosic material (LCM) is a cost-effective way of processing biomass (Ruiz *et al.*, 2013). A hydrothermal process involves applying high temperature and pressures in order to either extract or modify the structure of materials within the LCM. The benefit of using a hydrothermal process to modify the material is that this does not require the addition, and therefore recovery, of chemicals to the system other than water. Therefore, a hydrothermal process is considered to be environmentally friendly (Garrote *et al.*, 2003).

Depending on the type of hydrothermal process applied to the LCM, the outcome and resultant products will differ. In 2012, Ye *et al.*, using cornstalk lignin showed that increasing the residence time, changing the temperature of the hydrothermal treatment and also some work by varying the ethanol content of the solvent increased the yields of solid and liquid products produced (Ye *et al.*, 2012). When LCM is processed hydrothermally, bonds between lignin and hemicellulose are broken (Ruiz *et al.*, 2013).

Kurian *et al.* (2015) showed the difference between using steam and microwave treatments to fractionate sorghum bagasse. The two treatments used were: 1) a steam-assisted process which took place at 121°C for 30–120 min; and 2) a microwave-assisted process under same temperature and time conditions. The aim of both of these processes was to hydrothermally treat the product, and resulted in the creation of a residue from which, after subsequent processing, lignin was extracted (Kurian *et al.*, 2015). The subsequent treatment involved the use of calcium hydroxide (lime) heated to 121°C to extract as much lignin as possible from the residue. The efficiency of the two processes and subsequent treatments is shown in Figure 2.9. It is hypothesised that the pH change associated with processing in lime will affect the amount of lignin removal in a similar way to if the biomass was processed in sodium hydroxide. These modifications to the plant cell wall suggest that increasing the pH will aid in improving the amount of lignin which is extracted during processing.

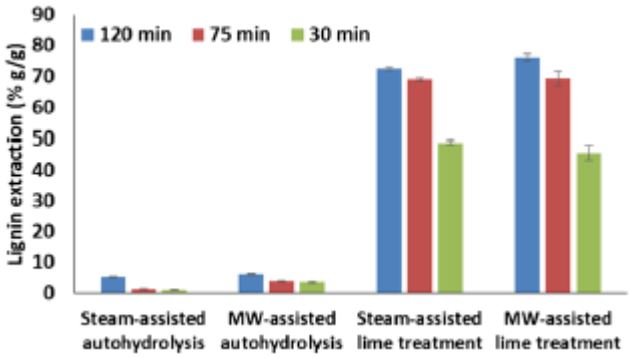


Figure 2.9: Comparison of lignin extraction during the steam-assisted and microwave-assisted treatments of Sweet Sorghum Bagasse (Kurian et al., 2015)

2.3.2.2 Microwave processing

The use of microwave heating in the production of bioenergy from biomass is an innovative pre-treatment option compared to conventional methods. Presently, and into the foreseeable future, there is an ever-increasing demand for energy. Biomass is proposed as an efficient alternative to regular hydrocarbons since solar energy post photosynthesis is stored within the feedstock itself. This stored energy is then released when it is burned or undergoes conventional pyrolysis (McKendry, 2002). The main reason for using microwave heating to process biomass is that it provides advantages compared to conventional heating processes. For example, rapid and efficient heating of a product can be induced in a controlled environment which sometimes leads to up to 80% shorter reaction times (Kostas *et al.*, 2017). Torrefaction is the process by which biomass is transformed into a coal-like material for the production of biofuels (Chen *et al.*, 2015). Microwave-induced wet-torrefaction of biomass is the conversion of biomass into char through heating the biomass as a suspension in water in the subcritical range (100–374°C). Usually the chosen temperature is between 180°C and 250°C. The relevance of torrefaction to this research is that the temperature ranges are equivalent to those of the hydrothermal processing temperatures used, as well as the biomass being suspended and processed in water. Since this occurs in a sealed vessel similar to

most hydrothermal processes, the pressure inside the vessel is self-generated through the thermal expansion of water (Kostas *et al.*, 2017). The benefit of wet torrefaction is that since the reaction occurs in the presence of water, the reaction pathway follows conventional hydrolysis instead of decarboxylation, de-carbonisation or de-methoxylation reactions. Since the hydrolysis occurs in an aqueous environment, the activation energy for biomass depolymerisation is reduced (Libra *et al.*, 2011).

The principle behind microwave technology involves the rapid movement of charged molecules following a cyclical electromagnetic field. The forces the molecules experience are frictional viscous forces which in turn generate heat. Everything possesses dielectric properties which makes food products and biomass also susceptible to microwave radiation. Dielectric materials absorb heat from oscillating electromagnetic fields which in turn polarize the charged molecules but because foods cannot follow this constant change, some of the energy absorbed is lost as heat (Metaxas and Meredith, 1988, Coronel *et al.*, 2009). Water and other ionic compounds present in foods are responsible for the loss of microwave energy in a food upon absorption of this energy which is then released in the form of heat (Coronel *et al.*, 2009). Dielectric molecules couple with the electromagnetic field in the microwave. When water couples with the magnetic field, the dipole attempts to reorient its position with regards to the oscillating field (in line with the field or against the field). Depending on the strength of the field, this reorientation can move in time with the field or cannot be affect or even lag behind the changing field oscillation. When the water dipole lags behind the oscillating field, energy loss from the field occurs as a result of heating.

Continuous flow microwave heating systems have emerged as an alternative to the currently well-established thermal processing

(Coronel *et al.*, 2009). The main difference between a thermal process and a microwave process is that a microwave process can selectively heat different materials within the food material. The properties of the food itself will impact on the heating rates of the product. Microwaves also heat volumetrically so therefore, they theoretically heat more uniformly than a conventional heating process (Coronel *et al.*, 2009).

The microwave power absorption into a food based on its dielectric properties is shown in Equation 2.1. For a food, the dielectric loss factor for the product varies. For a non-absorbing food, the loss factor is zero, however if the food is highly absorbent this dielectric loss factor will increase to 20 to 30 (Buffler, 1993). Some examples of highly absorbing foods are salted products and hams because they contain ions which are able to be selectively heated.

$$P_v = (5.56 \times 10^{-4}) \times f\epsilon'' E^2$$

Equation 2.1: Power absorbed by the material (Buffler, 1993)

Where:

- P_v = power absorbed per unit volume (W/cm^3)
- f = frequency (GHz)
- ϵ'' = relative dielectric loss factor
- E = electric field (V/cm)

Numerous factors can have an impact on the dielectric properties of a food such as temperature, moisture, fat and salt contents, as well as the frequency of the microwave used. These factors all impact directly on how the food behaves in the presence of the electromagnetic field (Tang, 2005). In foods with a high moisture content or those which are rehydrated, the dielectric properties are controlled by the water present. Water in the food however can be

divided into three categories: free water; water with mobility between free and bound water; and water bound to sites of solid food components. The differences between these water categories are that the free water will act similarly to bulk water, whereas the water which is bound to solid foods will behave similarly to ice when looking at its dielectric properties (Tang, 2005).

Temperature distribution in foods which are heated by microwaves is determined by the thermo-physical properties of the food product. In turn, this is affected by the composition of the food and therefore the distribution of the absorbed microwave energy within that food (Wäppling-Raaholt and Ohlsson, 2005).

2.3.2.3 Mechanical disruption in a high pressure homogenisation

High pressure homogenisation is a mechanical process where a fluid or liquid product is forced through a narrow gap or nozzle at high pressure (KU Leuven, 2012). This technology has primarily been used in the food industry to subject liquid products (e.g. dairy products, low fat mayonnaise or spreads) to high pressure and shear to create fine emulsion droplets.

Recently, the use of high pressure homogenisation (HPH) on plant cell wall material has become another utilised method for causing mechanical induced changes to the plant cell wall structure (e.g. fibrillation of cellulose). With regard to lignocellulosic material however, the primary application of HPH is to cause mechanical fibrillation i.e. to produce nano-fibrillated cellulose since the mechanical size reduction caused by HPH has been shown to enable complete cell wall breakdown into fibrils in woody materials (Hu *et al.*, 2015, Kucharska *et al.*, 2018). Fibrillation of cellulose into nanofibrils occurs by the application of compression forces to the plant cell wall which in turn causes partial delamination (Hubbe, n.d.). This partial delamination creates a hairy-like appearance

(formed of micro and nano-scale fibrillated fibres) on the surface of the wetted cellulose macrofibril fibre. Occasionally an enzymatic treatment (endoglucanase) is included prior to the use of HPH to promote cell wall delamination which in turn prevents blocking in the chamber of the machine (Missoum *et al.*, 2013). The primary use for cellulose nanofibrils has been to improve the overall strength of cellulose derived composite films (Lee *et al.*, 2009). However recently, nanofibrils containing lignin, have been formed from the pulp fractions in the Kraft process (see 2.3.1.1). Following procedures such as acid hydrolysis which breaks down the cellulose and hemicellulose in LCM biomass to form the individual sugar molecules prior to the usual fermentation into bioethanol (Lenihan *et al.*, 2010), the residual pulp has been processed using HPH to create a multitude of different lignin containing cellulose fibrillated samples (Wang *et al.*, 2012).

HPH has also been used to create nanolignin particles which have particle size of <100nm after 4 hours of mechanical induced homogenisation. These particles were used in nanolignin-polyvinyl alcohol (PVA) blends and had an increased thermal stability compared to the original lignin-PVA blends (Nair *et al.*, 2014). Depending on the processing parameters used in HPH, the increased shear rate can often deform the fluid through the rearrangement of microstructure (or in this case reduce particle size) resulting in an increase in the velocity of the fluid. This is most often seen in non-aggregating concentrated suspensions (Hayhurst, 1997).

2.4 Emulsification - principles

Innovation in emulsion technology has recently led to the creation of emulsion-based delivery systems through encapsulation of functional ingredients and improved stability and efficiency in drug delivery (Padalkar *et al.*, 2011, Berton-Carabin and Schroën, 2015,

Gutiérrez-Valenzuela *et al.*, 2018, Bhattacharjee *et al.*, 2018, Linke and Drusch, 2018). An emulsion is formed when two immiscible liquids form a stable dispersion with one acting as the continuous phase and the other acting as the dispersed phase. Emulsions themselves are not thermodynamically unstable since the two immiscible liquids are stabilised by some form of emulsifier or stabiliser to enable one to be dispersed in the other without phase separation.

Many different types of emulsion are present in products across the food sector specifically: oil-in-water (O/W); water-in-oil (W/O); water-in-oil-in-water (W/O/W). In the food industry, there are numerous products which are emulsions such as: mayonnaise; salad dressing; salad cream; fondants; butter; margarine; cake batters; ice cream, and even some soups (McClements, 2016b). Depending on the application, the type of emulsifier or stabiliser used will vary. For example, in mayonnaise, lecithin in egg yolks is used to stabilise the oil to form an oil-in-water emulsion (McGee, 2004, Magnusson and Nilsson, 2012). Commercially, lecithin is produced by extraction from soya bean oil or rapeseed oil. In baked goods, the use of crumb softeners and dough stabilisers help to strengthen the dough during gluten formation to aid with gas retention, improve the texture of the final product and help with increasing the volume within the structure. Such examples of these stabilisers are: sodium stearoyl lactylate (ssl); calcium stearoyl lactylate (csl) and diacetyl tartaric acid esters of monoglycerides (datem) (Brandt, 1996). The predominant emulsifier used for W/O emulsions in food applications are mono/diglycerides of fatty acids, or distilled monoglycerides of fatty acids. another emulsifier more often used in chocolate is polyglycerol-polyricinoleate (PGPR/E476) with legal limits of 5000 mg/kg in cocoa-based confectionary (EurLex, 2011). PGPR is an oil soluble surfactant and only requires a small amount (0.3% in a final

product) to stabilise water droplets below 1 μm in diameter for use in oral and dermal water-based products (Wolf *et al.*, 2013).

The thermodynamics of emulsion stabilisation can be characterised by how the dispersed droplets behave with respect to one another in such phenomena as Ostwald ripening, coalescence and flocculation (Kabalnov, 1998). Ostwald ripening is when smaller dispersed phase emulsion droplets are dissolved into the continuous phase before being redeposited onto the structure of the larger droplets increasing their size (McClements, 2016a). The smaller droplets keep dissolving and being redeposited onto the larger droplets until they either further coalesce or directly cream in phase separation (Kulkarni and Shaw, 2016, McClements and Jafari, 2018). The mechanism of transfer from the small droplet to the large droplet is a spontaneous process driven by thermodynamics where the larger droplets are favoured energetically due to increased order as a result of pressure differentials. This increased order is as a result of minimising the energy by decreasing the interfacial area in the system e.g. one large droplet has a lower interfacial area than multiple small droplets in the same space (Ratke and Voorhees, 2002). Coalescence is where two fluid droplets merge at their interface upon collision into one larger droplet as a result of film thinning and subsequent rupture (Eggers *et al.*, 1999). This normally occurs when the attractive forces between the droplets are greater than the repulsive forces (McClements and Jafari, 2018). Flocculation differs from coalescence since instead of combining to form one larger droplet, attractive forces (e.g. van der Waals interactions) between the dispersed phase droplets cause the droplets to stick together and flocculate to form clumps of small droplets. In flocculation, the attractive forces are stronger than the electrostatic forces of repulsion which causes the droplets to stick (Gupta *et al.*, 2016, McClements and Jafari, 2018). The stability of

emulsion or colloidal based systems could change and again become unstable by depletion flocculation (Jenkins and Snowden, 1996). This is when the surfactant or emulsifier is present in excess and is dissolved in the continuous phase solvent. Osmotic pressures are generated between the droplets and the surrounding aqueous phase since the concentration of surfactant is greater than that between the droplets. As a result, the aqueous phase migrates to where the concentration of solute is greater. As such the droplets, are attracted to one another when the solute has migrated towards the higher concentration leaving an increase in partial pressures between the droplets (Jenkins and Snowden, 1996).

2.4.1 Pickering stabilised emulsions

Particle stabilisation is a method of emulsion stabilisation which has been shown to have unrivalled stability against coalescence and is specifically relevant to this PhD. The reason for the unrivalled stability is because the amount of energy required to desorb particles from the interface between the two liquids is greater than that required to adsorb the same particles to the interface (Pickering, 1907, Dickinson, 2010, Binks *et al.*, 2010, Lam *et al.*, 2014, Xiao *et al.*, 2016, Dickinson, 2019). For example, the hydrophobicity of the particles can cause an initial O/W emulsion to phase invert to a W/O emulsion. Similarly, the concentration of particles and the ratios of oil and water in the system has been shown to cause phase inversion (Binks *et al.*, 2010). Duffus *et al.* (2016) conducted a study where different food grade particles are used to stabilise O/W and W/O particle stabilised (Pickering) emulsions (Duffus *et al.*, 2016). The study looked at the effects of particle size, pH and particle surface character (wettability and interfacial tension). It was found that the main prerequisites for producing emulsions with small internal phase droplets are the size of the particles which are adsorbed to the interface between the oil and the water and that the particle surface

activity, although this was a less significant factor (Duffus *et al.*, 2016). Additional work has used solid-lipid particles to stabilised the interface between water and the oil continuous phase through the formation of sintered fat shells around the water droplets (Pawlik *et al.*, 2016).

Recently, particles created from waste materials have been used to stabilise the interface of emulsions. One such material is lignin-droplet coated particles produced through hydrothermally treating spent coffee grounds (Gould *et al.*, 2016). Another innovative method of stabilisation is using cellulose nanocrystals to stabilise the interface between the oil and water (Kalashnikova *et al.*, 2011, Bai *et al.*, 2018). Cellulose nanofibers were used to induce a depletion effect to get different variants of creaming types in the nanocrystal stabilised emulsions (Bai *et al.*, 2018). Cellulose microfibers have also been used to stabilise oil-in-water Pickering emulsions by using mechanical treatments in the form of high pressure homogenisation to stabilise emulsions with a low concentration (1% microfibers) previously added to the continuous water phase ahead of processing (Sanchez-Salvador *et al.*, 2019). Other Pickering particles have been produced specifically nano-particles originating from a number of natural origins. As mentioned earlier, polysaccharides (in the form of cellulose nanocrystals and fibres, chitin or chitosan) can be used to stabilise emulsions and the method of production of these fibres often results from multi-step processes including the use of heat, strong bleaching chemicals and acid or enzymatic hydrolysis (Lam *et al.*, 2014, Calabrese *et al.*, 2018). The use of polymers, starch and proteins has also been reported for use as the stabiliser in Pickering emulsions (Murray *et al.*, 2011). Starches such as quinoa starch granules effectively showed that they can stabilise O/W Pickering emulsions with the droplet size being dependent on the concentration of starch granules added to the formulation (Rayner

et al., 2012). The use of quinoa starch granules was not only shown to produce smaller internal emulsion droplet sizes compared to egg yolk and egg yolk granules but also to have better frozen storage stability of particle stabilised mayonnaises over a 70 day period using the $D_{4,3}$ or the volume moment mean of the emulsion droplet size as the measurement parameter (Rayner *et al.*, 2014). Proteins isolated from peanuts in the form of microgel particles were found to be able to stabilise O/W emulsions with a high internal phase volume of 87% edible peanut oil which showed that these could be used as an edible replacement to partially hydrogenated oils (Jiao *et al.*, 2018). Lignin from the pulping industry in the presence of aqueous solution or alkaline lignin (extracted from furfural residues) has been found to produce particles which could reversibly stabilise Pickering emulsions from inducing a reduction in pH (Calabrese *et al.*, 2018). The selection of lignin-rich materials suitable for potentially stabilising a W/O emulsion involved selecting a material with a relatively high percentage lignin abundance in nature, to make it potentially commercially viable and also the milling capability of the feedstock.

2.5 Principles of key measurement methods applied in this PhD research

2.5.1 Principles of Nuclear Magnetic Resonance

Nuclear Magnetic Resonance (NMR) is a multi-faceted technique which has been adapted to make many different measurements from traditional spectroscopic identification through diffusion and kinetics to medical imaging. The particular technique used here to characterise the bulk composition of the material is solid state NMR.

Cross Polarisation Magic Angle Spinning solid state NMR (CPMAS NMR) involves spinning a sample "rapidly" at the "magic angle" of 54.74° with respect to the magnetic field. This minimises any interaction in the material involving chemical shift and dipolar shielding ($1–3\cos^2\theta$) which at the magic angle is zero. Interactions

involving these terms, which can lead to the production of broadened peaks are dipolar coupling and chemical shift anisotropy. In addition, high power decoupling powers involving the use of high-power amplifiers further reduces the effect of dipolar broadening by "stirring" or flipping the protons between states (α, in line with magnetic field and β, against the magnetic field by 180°). Protons are the principal nucleus present and studied in biological samples, however in the solid state NMR experiments reported here both protons (^{1}H) and carbons (^{13}C) are irradiated enabling carbon to also be observed. Essential elements of solid state NMR to consider are dipolar interactions, cross polarisation, magic angle spinning, spin coupling, nuclear spin and interactions with the magnetic field B_0.

Dipolar interactions are the interactions between two nuclei which are spinning in the magnetic field. Such interactions are between the magnetic fields of nuclei themselves e.g. ^{1}H-^{1}H, ^{1}H-^{13}C, ^{13}C-^{1}H. The cross-polarisation stage of the CPMAS experiment makes use of dipolar interactions in that it allows the lower abundance and lower γ ^{13}C nucleus to be excited by the high abundance and high γ ^{1}H. In solid state powder samples, the magnetic field of one proton nucleus is coupled to those of other nuclei and this broadens the NMR spectrum due to the random placements of the nuclei. Spin-spin coupling is an interaction between different nuclei and/or electrons which in turn gives the different patterns seen in spectra e.g. doublets, triplets etc. For chemists, J-coupling is linked with spin-spin coupling and is related to the distance between the nuclei and relative orientation which provides information on the shape and structure of molecules. Nuclear spin (I) of the specific elements determines whether or not they will be able to undergo NMR (Keeler, 2010b, Günther, 2013b, Günther, 2013d).

The three types of nuclear spin are:

1) Even/Even. Nuclei containing even numbers of both protons and neutrons have I=0 and therefore cannot undergo NMR. Examples include ^{4}He, ^{12}C, ^{16}O and ^{32}S.

2) Odd/Odd. Nuclei with odd numbers of both protons and neutrons have spin quantum numbers that are positive integers. Examples include ^{14}N (I=1), ^{2}H (deuterium, I=1), and ^{10}B (I=3).

3) All others. The remaining nuclei (odd/even and even/odd) all have spins that are half integral. Examples include ^{1}H (I=½), ^{17}O (I=3/2), ^{19}F (I=½), ^{23}Na (I=3/2), and ^{31}P (I=½).

These spins can be orientated in a positive or negative direction relative to the imposed magnetic field. A positive value indicates that the nuclei spins in a clockwise direction, whereas a negative value is a counter-clockwise spin. The NMR experiments conducted in this PhD are based on the ^{13}C CPMAS method and for an intense signal, the spins of the nuclei are aligned in the lowest energy state for both ^{1}H and ^{13}C which is equivalent to +½ (Al-Jalali and Mahzia, 2014). Quadrupolar nuclei, which have I values of over ½, are not considered for this work.

Interactions with the magnetic field define the magic angle and the spin state. Quadrupole interactions are associated with an uneven charge distribution inside a nucleus. Hydrogen (deuterium and tritium) and Nitrogen nuclei exhibit quadrupolar behaviour. Quadrupole coupling is an interaction between the nuclear quadrupole with the electric field gradient at the nucleus (Keeler, 2010b, Günther, 2013a, Günther, 2013b).

There are many different types of solid state NMR experiments. Three types of experimental techniques are considered in this report.

The differences between these methods are:

1) CPMAS → cross polarisation magic angle spinning:

The polarisation for abundant nuclei (e.g. ^{1}H, ^{19}F, ^{31}P) is transferred to rare nuclei (e.g. ^{13}C, ^{15}N, ^{29}Si), enhancing the signals of rarer nuclei which allows for a reduction in experimental time. The properties of the protons which are measured indirectly during ^{13}C CPMAS are those which can transfer polarisation to the ^{13}C nuclei. In any attempt to quantify a CPMAS measurement, several characteristics of the measurement must be taken into account. The first is the usual consideration, as in most NMR measurements, of the T_1 of the different components present. The T_1 relaxation time, sometimes known as the longitudinal relaxation time, is the time constant describing the return to the equilibrium value of magnetisation in the external magnetic field after some perturbation. Different time relevant relaxations are applicable to solid state NMR. Namely T_1, $T_{1\rho}$ and T_2. T_1 relaxation is the spontaneous relaxation from the gain or loss of magnetisation in the longitudinal (z) direction to an equilibrium value (Keeler, 2010a). T_2 follows similar principles to T_1 however this spontaneous relaxation occurs in the x,y-direction reducing the magnetisation to the equilibrium value of zero (Keeler, 2010a). $T_{1\rho}$ describes the return of the magnetisation to an equilibrium value corresponding to an imposed magnetic field such as is present in an imposed pulse.

Pulse sequences such as the inverse recovery sequence can be used to measure T_1 accurately. Clearly in order to truly quantify a measurement the system must be completely relaxed i.e. at equilibrium. Only then will the measurement of areas under peaks be quantitatively accurate. One quick, rough and ready method of assessing whether the system has returned to equilibrium involves making measurements with different recycle delay times. If the area calculations return the same values, then within the accuracy of the

experiment, equilibrium has been reached and this part of the method at least is quantitative.

The ^{13}C CPMAS experiment is a dynamic experiment. The intensity of the peaks in a CPMAS spectrum is determined by 2 principal time constants i.e. the T_{C_H}, the time constant for the transfer of polarisation between protons and carbons, and the ^{1}H $T_{1\rho}$. The complete expression for intensity also contains a ^{13}C $T_{1\rho}$ term. Consideration of these equations behind the ^{13}C CPMAS method lead naturally on to a description of the variable contact time experiments.

2) CPVC → cross polarisation variable contact time:

CPVC is the same as CPMAS however, the contact time between the irradiated protons and carbons in the sample changes. A crucial parameter in this method is the time that the two spin systems (proton and carbon) are kept in contact during the cross polarisation. This is known as the contact time. Signal transfer from proton to carbon increases with contact time up to a maximum. The time constant of this signal increase reflects the number of protons in the immediate neighbourhood of the carbon as well as the solidity of the sample and consequently the ease of transfer of polarisation. After this maximum the signal decays. The time constant for this decay reflects the proton $T_{1\rho}$ value. The proton decay is due to the signal being spin locked along an axis in the x-y plane and decreasing to an equilibrium value; effectively zero. The rate at which this occurs gives useful information on the mobility of the system as well as the degree of cross transfer between protons on various parts of the molecule. By using 10–15 values for the contact time, the envelope of the rise and fall of the carbon intensity can be measured and estimates of the decay constants obtained.

So, for example, if a carbon has a different number of attached protons or indeed no directly attached protons, the T_{C_H} value will be different. In particular, if a carbon has no directly attached protons but is rather immersed in a surrounding sea of protons, the T_{C_H} can be very long with the consequence that the peak intensity appears much later in the contact time experiment. In view of the aromatic nature of Lignin, and many of the carbons having no directly attached protons, there is a suspicion that this might be the case here. It is important to carry out either a full or abbreviated variable contact time experiment. If this type of issue is occurring, then the choice of one contact time will give different intensities for the carbons of different components not necessarily related to content and hence quantification will be inaccurate. Differences in the ^{1}H $T_{1\rho}$ are related to mobility of the protons in the components, however differences are often minimised due to spin diffusion which averages the values between all protons. However, if there is phase separation between components, this is not the case, and the decay times being different for the carbons of the components in the different phases result in similar problems to those described and inaccuracies in quantification.

Once again, a check at several contact time values rather than complete experiments (which can use upwards of 12–24 hours of NMR time) can give an indication whether this type of event is occurring.

Changing the contact time alters the signal strength of the different carbons in the sample. The intensity of the signal peaks increases to a maximum at certain variable contact time and decreases to a minimum at extended times. Quantification with this method is notoriously difficult due to changes in the signal strength across the sample measured. The optimal contact time for carbons in one polymer producing higher intensities may produce a lower signal

intensity for another polymer present in the bulk sample, e.g. increase in lignin signal strength or intensity corresponds to a decreased cellulose signal intensity. The changes in the signal strength may not be directly correlated to content and as such quantification can be almost impossible. Information generated from CPVC experiments can enable the identification of more information for a specific compound or polymer with regards to chemical composition but not for quantification on the whole sample. $T_{1\rho}$ must also be taken into consideration for variable contact experiments. It is the time constant for the decay of magnetisation specifically along the radio field frequency. In cross polarisation experiments, this directly affects the intensity of the NMR signal in the spectra collected through the duration of the spin locking pulse.

3) NQS → non-quaternary suppression:

NQS suppresses signals of carbons having attached protons e.g. methyl groups hence cellulose and quaternary aromatic lignin carbons can be distinguished.

The basic, simple and original NQS measurement involved a gap in the sequence. The attached protons then de-phase the attached carbons and these signals disappear. Therefore only non-proton containing carbons are left in signal. There is an optimum time for this and also an added echo step in the more advanced sequences to return intensity. This leads to longer experiments as the signal is less intense firstly because of the removal of signals and secondly due to the nature of the pulse sequence itself.

Bonding interactions and the spin coupling of the nuclei is heavily dependent on the electronegativity of the atoms present. This in turn alters the chemical shift of the atoms measured. Electronegativity is defined as the power of an atom to attract electrons and the Pauling scale is used to describe this (Pauling, 1932). The most

electronegative element is Fluorine which has a value of 3.98 on the Pauling Scale, with the least electronegative element being Francium which has a value of 0.7. Since this work is predominantly on Carbon and Hydrogen for quantification of the feedstocks, these have their own values of electronegativity which correspond to 2.55 and 2.20 respectively (Al-Jalali and Mahzia, 2014). Depending on what the carbon is attached to, changes in the shielding impact on the chemical shift signals recorded since the positioning of the electrons in the C-H bonds will change. For example, if the C-H is bonded to a benzene ring which is a naturally electron withdrawing compound then the electrons will be drawn towards the benzene ring. This makes the carbon partially negatively charged and the hydrogen partially positively charged. The reverse will happen if the carbon is attached to something which is less electronegative than hydrogen. For examples, in a salt, where the carbon could be bonded to a sodium or potassium which are less electronegative than hydrogen, with values of 0.93 and 0.82 respectively (Murphy *et al.*, 2000), the electron pair will be drawn towards the hydrogen rendering it partially negatively charged and the carbon partially positively charged. All these changes will result in shielding differences at the nucleus which will mean that the effective magnetic field is different and so the carbon will resonate (produce a peak) at a different frequency or ppm value.

Literature was consulted to assign the respective carbon atoms and different constituents that comprise the BSG. For the peaks relevant to G & S lignin, a publication by Manders (1986) was used showing the G & S peaks in both hard and soft woods (Manders, 1986). With reference to Figure 2.10, C4 in the lignin H monomer was assigned to 160–162ppm, 136ppm corresponds to the C1 in G and also the C1 and C4 in S. The main difference between S and G was the peak at 153.5ppm. This was assigned to C3 and C5 in S which are O-

alkylated at C4. O-alkylation is the presence of an O-R bond attached to the carbon where the R refers to an alkylated group. These usually have the formula CnH2n+1. The up-field wing (towards 0ppm on the right-hand side of the peak) is assigned to C3 and C4 in G, however if the C3 and C5 in S are not O-alkylated at C4, these will appear at 148ppm. G lignin monomer has peaks at 134ppm for C1. For the cellulose and lignin peaks, Bernardinelli *et al.* in 2015 showed an assignment broadly in agreement with these values for a solid state ^{13}C spectrum (Bernardinelli *et al.*, 2015). In 2011, Sanna *et al.* showed the carboxyl carbon of long chain carboxylic acids such as palmitic or oleic fatty acids as well as carboxyl groups in pectin and methoxy groups in lignin (R-O-CH3) were located at 175-180ppm and 56ppm respectively (Gidley and Bociek, 1985, Gidley, 1992, Sanna *et al.*, 2011).

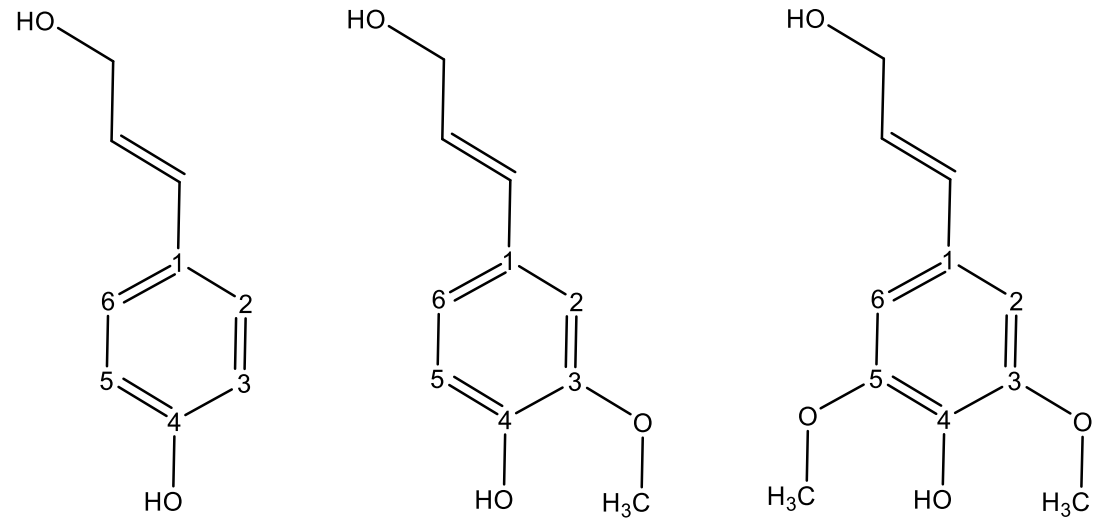


Figure 2.10: Numbering of carbon atoms in the benzene ring on H-lignin. The same nomenclature applies to G and S lignin (adapted from Manders, 1986)

High resolution solid-state NMR has also been used to characterise lipids in oil seed, measuring the relative mobility of crystalline polymorphs sites which were shown to be consistent with thermodynamic analysis, as well as trying to use NMR chemical shift

differences to characterise gluten to reflect baking quality (Gidley, 1992). Additionally, NMR has been used to characterise biopolymer conformation, e.g. the C1 carbon of α-1,4 linked glucans can be found at 100 ppm. Gidley's review article (1992) highlighted that for plant cell walls, due to their primary composition being from polysaccharides and structural proteins, that there is considerable scope for using such a technique for characterisation purposes (Gidley, 1992).

2.5.2 Thermal properties

There are three main thermal properties associated with food: the specific heat; thermal conductivity and thermal diffusivity. The specific heat capacity is defined as the amount of energy in the form of heat per unit mass of a body required to change the temperature of the body by 1°C without any change to its physical state.

The thermal conductivity of a material is crucial especially in thermal-related processing conditions since it impacts on the rate of heat transfer. It is defined as the amount of heat energy which will be transferred in a given unit of time through a specific thickness of material (perpendicular to the surface area) subject to a temperature gradient across the same thickness.

Thermal diffusivity differs to the thermal conductivity since it is a relationship between the thermal conductivity of said material, the density of the material and also the specific heat capacity of the material (Singh and Heldman, 2014).

Differential Scanning Calorimetry (DSC) is a technique that is used to directly assess the heat energy uptake into and release from a material. It measures heat capacity as well as molecular phase transitions in the material under a temperature profile in which the temperature is either increased or decreased at a known rate (Gill *et al.*, 2010).

Solid materials can have the properties of being amorphous, meaning that they have no clearly defined structure, or they can be crystalline, meaning that their atoms are arranged in a specific reproducible pattern. Depending on the structure, there could be regions of amorphous or crystalline solid (Lukas and LeMaire, 2009).

The principle of DSC is that during the heating of a product inside a sealed pan at a specific known rate of temperature change. Often this heating rate can be up to 10°C/minute ($\Delta T/\Delta t$). The properties of the material inside the pan will determine the amount and rate of thermal energy, which is delivered to the pan, which is known as the heat flow ($\Delta Q/\Delta t$). Using DSC, measurements of the heat flow into the material upon heating enables the calculation of the specific heat capacity of the material using $\Delta Q=mc_p\Delta T$. Changes in state are evidenced by an increase in the heat capacity which delivers more energy to the atoms within the material itself (Lukas and LeMaire, 2009). If melting were to occur in a material, this occurs with a change of state and increase in the amount of disorder of the molecules in the material increasing the entropy of the system. For materials consisting of multiple constituents, DSC can visualise the transitions of the various components. Upon melting, along with the change in entropy, a change in volume of the material may occur. Due to this phase transition the specific heat capacity of that component will also change (Lukas and LeMaire, 2009). For a material, the point at which the transition or melting temperature occurs is the position where the heat capacity reaches its maximum value (Raudino *et al.*, 2013).

The concept and theory of how a material melts were first introduced in 1910 by Lindemann. Lindemann showed that melting occurs when the fluctuation of atoms becomes so large that direct collisions between adjacent atoms occurs linking with the concept of entropy. The changing disorder within the system allows the material to

change state (Martin and O'Conner, 1977). The changes which occur to a typical material can be shown in Figure 2.11. A proposed mechanism by Donohoe *et al.*, (2008) of how lignin migrates through the structure of the cell wall is shown in Figure 2.12. The proposed mechanism shows that when lignin is heated above its melting temperature and breaking down the bonding structure causes lignin to coalesce and flow (Donohoe *et al.*, 2008). In this rubbery state, the lignin can migrate through the cell wall structure as a result of collapsing cellulose microfibrils and through thermal expansion, be redeposited onto the surface of the material where it once originated in the form of surface droplets (Donohoe *et al.*, 2008, Gould *et al.*, 2016).

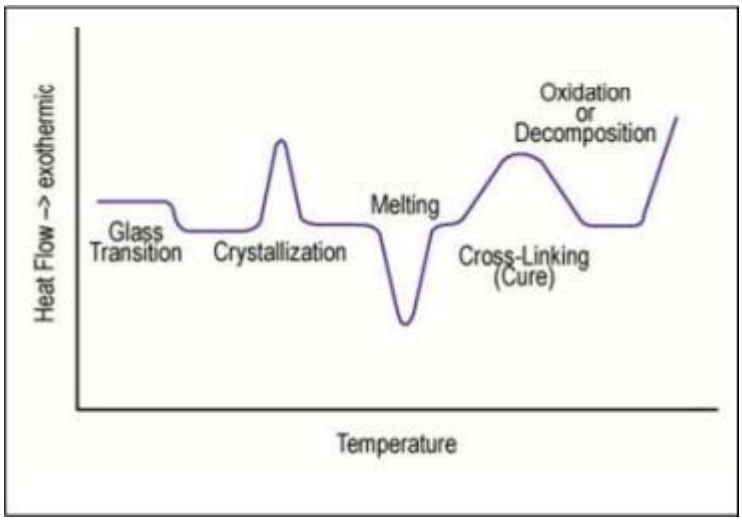


Figure 2.11: DSC profile and the associated transition with exothermic heat flow measured against temperature. (Courtesy: TA Instruments, Inc.) (Lukas and LeMaire, 2009)

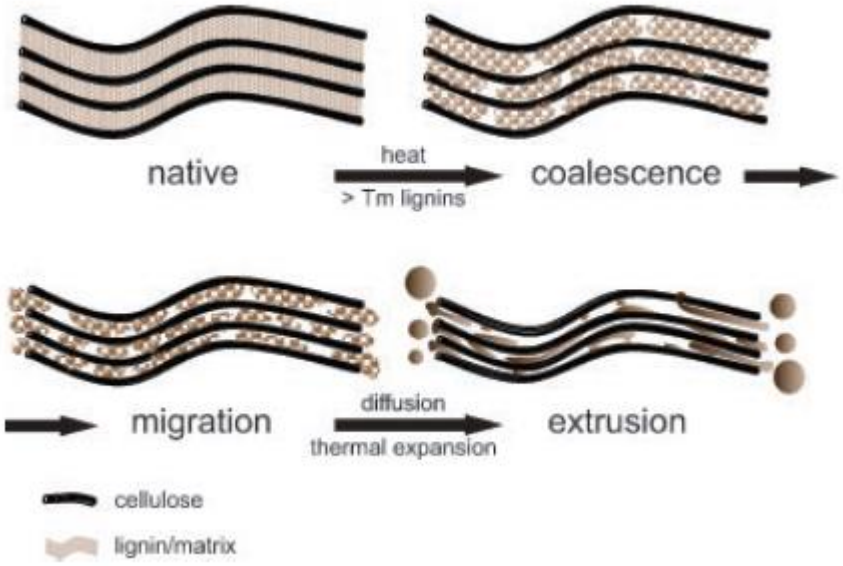


Figure 2.12: Model of a proposed mechanism for the driving force of lignin migration based on the melting of lignin, coalescence caused by the aqueous environment, and eventually the progressive collapse of microfibrils driving molten lignin to the surface of the biomass cell wall (Donohoe et al., 2008)

Lignin as a polymer from the range of sources mentioned earlier differs in composition but also have different melting properties. Lignin is also amorphous in nature (McCardy, 1991, Chen, 2014). The possible transitions which might occur for the polymer are shown in Figure 2.11, if lignin was to behave as a typical amorphous solid then a glass transition would be expected to be observed. As a result, the transition temperature of the lignin within a range of sources cover a wide possibility of temperatures. With regards to food sources, little research on characterising the lignin and its melting capabilities has been completed.

As such, if the lignin in the food sources used in this study were to behave as an amorphous polymer, it should undergo a glass transition changing state from a solid-like glass to a flowable rubber; this is discussed in more detail later.

3 Method development and validation

This chapter covers the fundamental methods which were developed during this PhD research. Any of these methods were subsequently validated to confirm any hypotheses which were considered during this research.

3.1 Particle functionality assay

This research involved making particulate emulsifiers from lignin-rich by-products. As such a particle functionality assay was developed to assess how the particles behaved as emulsifiers after processing. To begin with a published method was used with slight modifications (Gould *et al.*, 2016). This method follows advancement from the method that was used by Gould *et al.* (2016) with changes in scale and mixer-head speed. Different concentrations of particles (2% to 10%) were tested of untreated BSG to see how many particles were required to stabilise an emulsion which did not break down over time. A broken down emulsion was classified by visible phase separation. Emulsions were produced at either 50g or 100g scale containing the specific concentration of particles. The remaining percentage was split 50/50 between sunflower oil and reverse osmosis water. Similar emulsion processing parameters were taken from Gould *et al*. (2016) and was conducted using a high shear overhead mixer (L5M Series fitted with emulsor screen, Silverson, Chesham, UK) operating at 8000rpm for 2min.

The pre-weighed perceived dispersed phase was carefully added to the beaker and was placed into a plastic vessel for stability prior to processing before the addition of the particles and the perceived continuous phase.

The emulsions were then assessed by gravitational stability visually through the development of phase boundary layers in the storage vials (Figure 3.1). The emulsions were then stored at 6–8°C and

further assessed 1 day and 7 days after processing. A drop test was also used initially within the first hour of processing. The emulsions were assessed for phase continuity by observing whether a drop of the emulsion, pipetted with a wide tip plastic Pasteur pipette, would disperse in oil or water to indicate whether a W/O emulsion or an O/W emulsion had formed respectively with these results shown in Figure 3.1.

This was then used to find the minimum concentration capable of stabilising an emulsion as well as the optimal concentration to stabilise all of the dispersed phase. Figure 3.1 shows the 5 concentrations of particles tested and the results of the drop test. 4% particles was the minimum concentration able to stabilise all of the sunflower oil but the optimal concentration was found to be 8% with the produced oil-in-water emulsions. The minimal concentration was observed visually as the first concentration where no phase separation and free oil were visible whereas the optimal was where no free water was visible at the bottom of the vial. From Figure 3.1, when all of the emulsions from 4% onwards were pipetted into the sunflower oil, visible large droplets were formed compared (bonding of the emulsion phase) wheras the same emulsion was dispersed when pipetted into water (visible spreading of the emulsion) indicating that an O/W emulsion was produced.

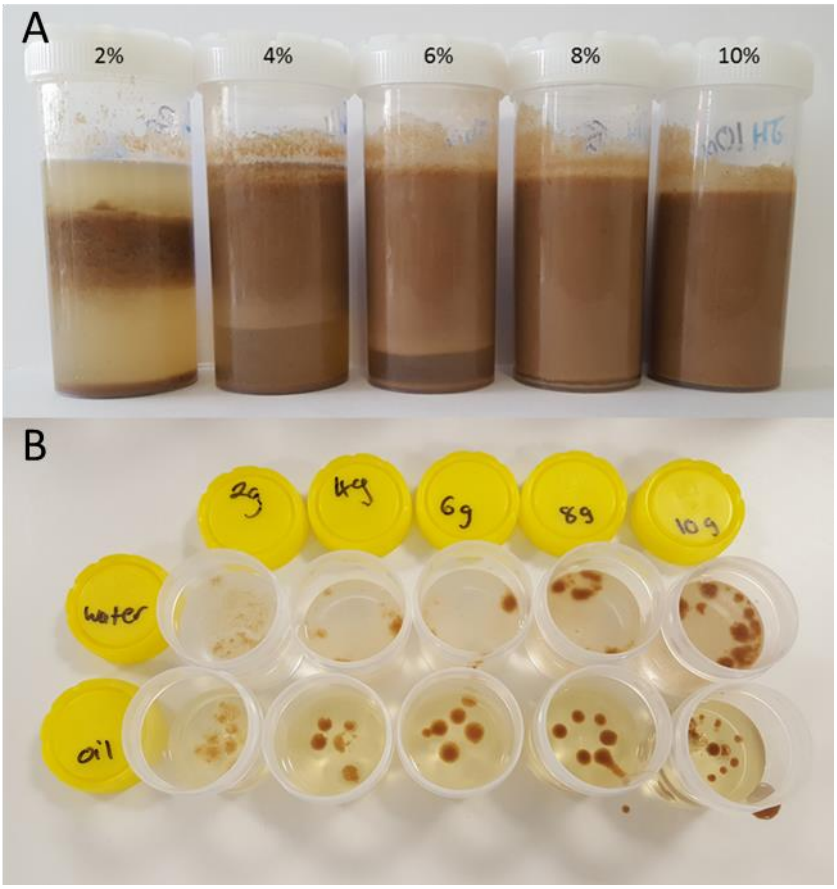


Figure 3.1: A) Different concentrations of Untreated BSG particles tested for optimal emulsification concentration and B) emulsion drop test results in both water and sunflower oil

3.1.1 Angular velocity and tangential velocity calculations for using different high shear mixer heads

The particle functionality assay outlined in 3.1, was used to produce the emulsions throughout this research. The final test of particle functionality in Chapter 6 using the different percentages of sunflower oil and water involved using smaller quantities of particles, oil and water and as such a different high shear overhead mixer had to be used. Consequently, a smaller processing head was used and thus calculations were made to create similar conditions which were previously used on larger quantities. Angular velocity and tangential velocity parameters were calculated to further calculate the change in rpm required since the gap between the head and the processing vessel were kept the same. The gap between the rotor and the stator in the mixer heads were also kept as close to parity as possible.

Angular velocity was calculated with ω denoting the angular velocity in rad/s and N is the speed in rpm (Equation 3.1) and the tangential velocity (V_t) in m/s was calculated by ω, the angular velocity in rad/s and r the radius of the mixer head in metres (Equation 3.2). If the tangential velocity was remaining constant throughout, this enabled to reverse calculate the speed required when using the T10 Basic Ultra-Turrax (IKA England Ltd, Oxford, UK) instead of the Silverson L5M. The parameters calculated for the Silverson L5M fitted with Emulsor screen (Silverson, Chesham, UK) are shown in Table 3.1. The parameters for the T10 Ultra-Turrax were reverse calculated from the Silverson data.

Equation 3.1: Angular velocity calculation using rpm

$$\omega = \frac{2\pi N}{60}$$

Equation 3.2: Tangential velocity calculation using angular velocity and radius of mixer head

$$V_t = \omega r$$

Table 3.1: Calculated parameters when changing overhead mixer head in the particle functionality assay

Parameter	**Symbol**	**Silverson L5M + Emulsor Screen Medium**	**T 10 basic ULTRA-TURRAX**
Mixer Head Diameter (m)	d	25×10^{-3}	10×10^{-3}
Mixer Head Radius (m)	r	12.5×10^{-3}	5.00×10^{-3}
Speed (rpm)	N	6000	15000
Processing Time (min)	t	2	0.5
Angular velocity (rad/s)	ω	628	1570
Tangential velocity (m/s)	V_t	7.85	7.85

3.2 Particle size analysis

Particle size analysis was used to measure the size of the particles at various stages of the processing. This was to assess the particle size distribution post milling and after hydrothermal processing and also to show whether there was additional particle size reduction with the inclusion of the high pressure process prior to the hydrothermal processing. The particle size distributions were measured using a laser diffraction particle size analyser (Beckman-Coulter LS 13320, Meritics, Dunstable, UK). The software setting of "Fraunhofer theory" was select for the automatic analysis of the diffraction patterns. This was justified as the particles of interest in this PhD research were at least several micrometres in diameter as revealed by microscopy and illustrated in Figure 3.2.

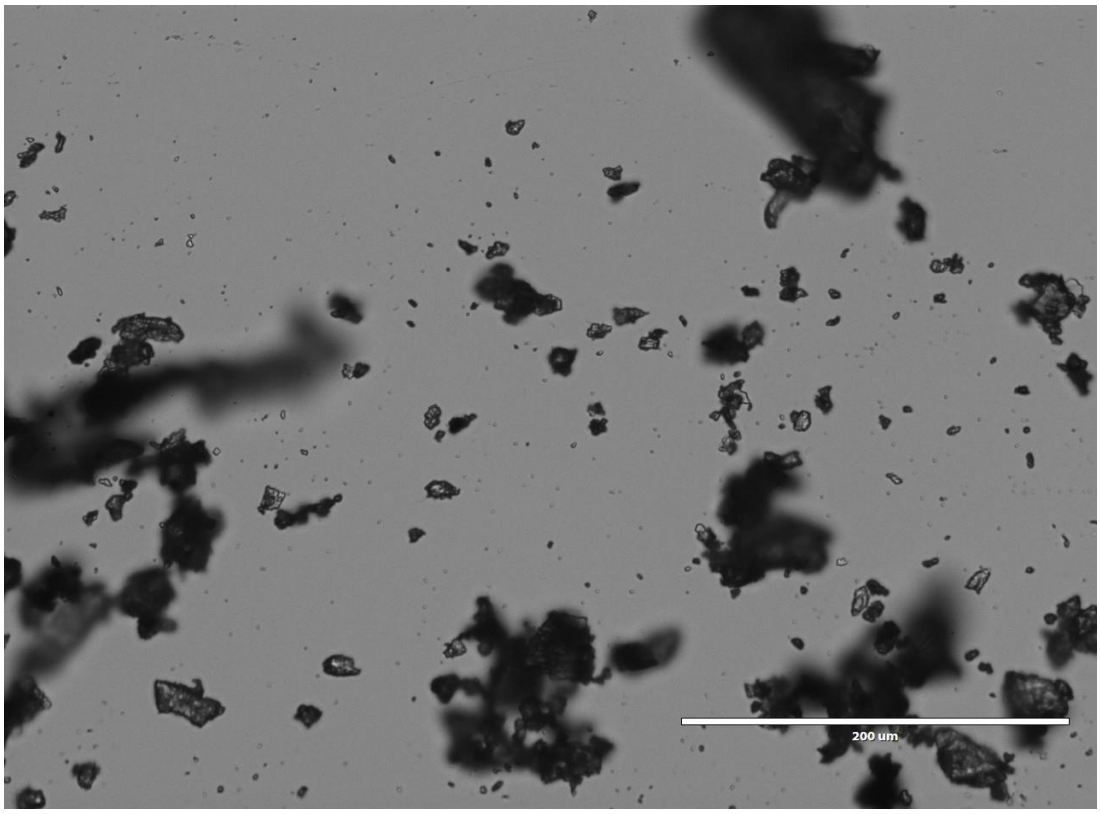


Figure 3.2: Milled Untreated BSG particles (200µm scale bar)

The principle of laser diffraction involves the particles passing through a laser beam and in doing so cause a change in the diffraction pattern of the light which is dependent on the size of the

particles. This laser beam was transmitted through a specific sample cell (liquid module) and was received by a Fourier lens. It should also be noted that the samples used were all diluted aqueous dispersions of selected particles. Particles were taken randomly across the batch. This lens is crucial because it ensures that the light diffraction from all particles is measured by the detectors giving a representative particle size distribution.

The attached dispersion cell filled with water was used to conduct the particle size analysis (Universal liquid module, LS13320, Beckman Coulter, High Wycombe, UK). Particles were pre-dispersed in water and then an aliquot was added to the water in the cell prior to commencing measurement, as indicated by the equipment software. The recirculation pump speed used was 85% to avoid sedimentation of the samples in the liquid module. Data is presented as volume based distributions.

For comparison, the $x_{90,3}$ was used to show the change in the particle size at various stages of the process. The $x_{90,3}$ refers to the diameter of the particles where 90 percent of the total particles falls below this diameter threshold for volume based distributions.

3.3 Microstructure methods

3.3.1 Bright field illumination

The size and shape of the BSG particles as well as the microstructure of the emulsions was visualised with a digital inverted microscope (EVOS FL Cell Imaging System, Fisher Scientific, Loughborough, UK) in bright field mode. Glass slides were utilised for the particles and oil-in-water (O/W) emulsions whereas the water-in-oil (W/O) emulsions were imaged on PTFE slides or petri-dishes to prevent coalescence of the hydrophilic droplet phase with the hydrophilic glass. Cover slips were not used because of the irregular shapes of the particles as the cover slips would not be level and in turn potentially diffracting the light and causing a distortion to the image.

Instead, the emulsions were spread in a thin layer across the respective slides using one droplet of around 1ml (the emulsion was highly viscous) and then using gravity to spread it into an even thin layer.

Emulsions were also observed immediately after homogenisation to gain an insight into droplet size of the dispersed phase using a Nikon Eclipse Ci-L Microscope with attachment DS-L3 image capture system (Nikon UK Ltd, Surrey, UK). Slides were prepared in the same way as for the EVOS above, but this was conducted in a food-grade environment immediately after production of the emulsions. No cover slip was used, and gravity was used to spread the emulsion thinly. The microscopy images produced here show full spectral illumination rather than greyscale which is produced by the EVOS FL mentioned previously.

3.3.2 Fluorescence illumination

One property of lignin which is useful for detection is that it is capable of auto-fluorescing. This can occur when excited at 357nm (Vavrčík *et al.*, 2008). The digital inverted microscope introduced in 3.3.1 can also be used in a multitude of fluorescent modes with the corresponding microscope specific light cubes (red, green and blue). The DAPI (blue) light cube (wavelength 340–380nm) in the digital inverted microscope (EVOS FL Cell Imaging System, Fisher Scientific, Loughborough, UK) allowed identification of lignin in the particles as well as to observe particles at the interface between the two emulsion phases due to lignin autofluorescence. As before, no cover slips were used.

3.3.3 Scanning Electron Microscopy

The surface structure of the particles was investigated using Scanning Electron Microscopy (SEM) (JSM 6060LV, JEOL, Tokyo, Japan). The particles were placed on SEM stubs with carbotape, dried under vacuum before being coated in gold using gold spluttering

(Leica SCD 0005, Leica Microsystems, UK). The samples were then transferred to the SEM stage for imaging.

3.4 Acetyl Bromide Soluble Lignin assay

This analysis was conducted by Robert Davis of the Food Composition Section of the Chemistry Department at Campden BRI (Chipping Campden, UK) using the following procedure. This procedure was adapted from literature reporting on the extraction and the isolation of lignin for the utilisation as a standard to determine lignin concentration using the Acetyl Bromide spectrophotometric method (Fukushima and Hatfield, 2001). The principle of the method involves using a dried and milled feedstock (capable of passing through 0.5mm sieve and ensure thorough mixing prior to use) which is then digested in Acetyl Bromide among other chemicals mentioned shortly. Acetyl Bromide is used for the formation of Acetyl derivatives in non-substituted OH groups and Bromide replacement of the α-carbon OH groups to allow the complete solubilisation of lignin under acidic conditions. This allows concentration measurement at 280nm by spectrophotometry in comparison to a calibration curve of a known lignin standard (namely, Sigma Aldrich low-sulphonate alkali lignin). The main reagents of the assay were: glacial acetic acid; 25% v/v Acetyl Bromide in glacial acetic acid, prepared by adding 25ml neat Acetyl Bromide to 75ml glacial acetic acid; lignin (Low sulphonated, pH 10.5, Sigma); 80% v/v dioxane, prepared by mixing 8ml of 1,4 dioxane with 2ml of water; 0.3M sodium hydroxide, prepared by dissolving 1.2g of sodium hydroxide in water and making up to 100ml in a volumetric flask; and 0.5M hydroxylamine hydrochloride solution, prepared by dissolving 3.475g solid in water and made to 100 ml in a volumetric flask. All of the reagents were purchased from Sigma Aldrich. All of the steps in this method were to be carried out in a fume cupboard using the method as follows.

This method is a laboratory procedure which was carried out at Campden BRI using test method "Campden BRI DC: TES-AC-908: 11/18 (01)":

1. Weight 100mg ± 10mg of sample into a 20ml Teflon capped boiling tube using an analytical balance capable of weighing to 0.001 mg.
2. **Ensure all operations are carried out in Fume cupboard**. Add 4ml of 25% Acetyl Bromide in glacial acetic acid into each tube (prepared by adding 25ml of Acetyl Bromide to 75ml glacial acetic acid).
3. Seal tubes and incubate at 50°C ± 2°C in a water bath for 2 hours.
4. Cool tubes in tap water.
5. Add 12ml glacial acetic acid to each tube.
6. Prepare lignin standards. Weight 10mg of Lignin and dissolve in 5ml 80% aqueous dioxane (prepared by mixing 8ml of 1,4 dioxane with 2ml of water) and then pipette 0.05, 0.1, 0.2, 0.3, 0.4 and 0.5ml into separate Teflon capped boiling tubes each containing 0.5ml 25% Acetyl Bromide.
7. Prepare a blank by adding 0.2ml 80% aqueous dioxane to a Teflon capped boiling tube containing 0.5ml 25% Acetyl Bromide.
8. Seal tubes and incubate at 50°C ± 2°C in a water bath for 30 min.
9. Cool tubes in tap water and then make up analysis samples as follows in Table 3.2.

Table 3.2: Calibration standard compositional make up for ABSL

Components (ml)	Samples	Calibration standards						
		Blank	**0.05**	**0.1**	**0.2**	**0.3**	**0.4**	**0.5**
Sample volume (ml)	0.5	0.7	0.55	0.6	0.7	0.8	0.9	1.0
Glacial acetic acid	2.5	2.5	2.5	2.5	2.5	2.5	2.5	2.5
0.3M NaOH	1.5	1.5	1.5	1.5	1.5	1.5	1.5	1.5
0.5M Hydroxylamine HCL	0.5	0.5	0.5	0.5	0.5	0.5	0.5	0.5
Glacial acetic acid	5	4.8	4.95	4.9	4.8	4.7	4.6	4.5

- 0.3M NaOH prepared by dissolving 1.2g of sodium hydroxide in water and making up to 100ml in a volumetric flask
- 0.5M Hydroxylamine HCl prepared by dissolving 3.475g solid Hydroxylamine HCl in water and made to 100ml in a volumetric flask

Note: sample volume is amount of sample taken from supernatant, whereas standards and blank can proceed by adding the components to their boiling tubes

10. Carefully shake tubes to ensure contents are homogenous.
11. Measure the absorbance at 280nm ± 2nm in a quartz cell against blank. The quartz cell must include a lid to avoid any spillage and the path length in the Spectrophotometer must be 1cm.
12. Lignin content is calculated based on the absorbance of the supernatant relative to the standard calibration curve with the Sigma Lignin being used as the calibration material.
13. Every 10^{th} sample must be analysed in duplicate, at least one per batch as quality control.

3.5 Hydrothermal processing

Existing tubular reactors were used for this section on process validation. They were modified by fitting a welded steel boss to the end of one end cap. The boss and cap were then drilled with a metal sheath capable of housing a thermocouple probe, was welded into the cap. This was to enable the measurement of temperature in real time during processing of the vessel.

This data was then used later to design heating experiments which used microwaves as heating source rather than a conventional method in an oven.

3.5.1 Thermal process validation of hydrothermal process

It is important to understand the specific heating rates within the product. This will enable alternative processes to be considered to achieve the same end product. A modified steel reactor was used. The modification to one of the end caps enabled a thermocouple to measure the internal temperature at the geometric centre of the vessel as shown in Figure 3.3, with an AutoCAD representative design of the idea in Figure 3.3A and the actual finished assembled reactor shown in Figure 3.3B. The same conditions were used following the optimisation of the hydrothermal process to understand the exact heating profile and rates which generate the particles in Chapter 5 and Chapter 6. The optimisation followed work in Chapter 5 where a number of different time and temperature processing conditions were used. For this thermal process validation the most extreme conditions were quantified as these were the conditions which were to be used for experiments in Chapter 6.

Loaded reactors (4g of BSG suspended in 40ml of water was sealed in stainless steel tubular reactors: 150mm tube length and two end caps and inner diameter of 22mm) were heated in a deck oven (Model CPMK4MDU438, Compacta deck oven, Tom Chandley, Manchester, UK) for 120min at processing temperature 220°C

following initial work on process optimisation (Chapter 5). Due to the modifications to the reactor to enable a thermocouple to be inserted into the vessel, an additional safety precaution was used and at the conclusion of the heating period, the reactors were left in the oven overnight to cool down. The heating profile is shown in Figure 3.4 where it was split into different segments to enable a stepped profile input for the transition into heating with a microwave.

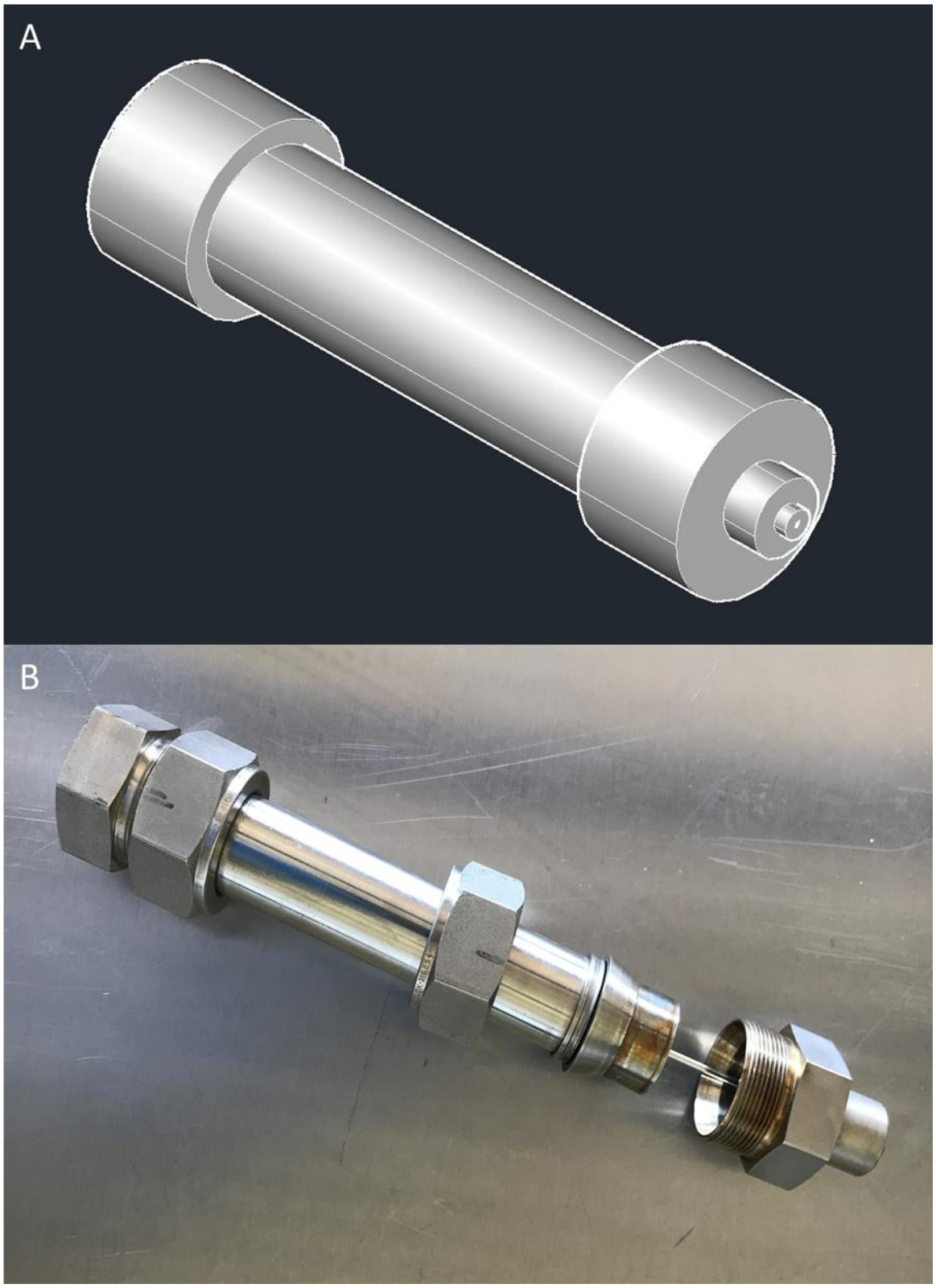


Figure 3.3: A: Modified steel reactor for use with thermocouple during thermal process validation experiments produced using AutoCAD, B: Actual Modified steel reactor including end caps with internal dimensions (L = 150mm or 180mm including two end caps, D = 22mm)

3.5.2 Heating rate calculations for use in Microwave Synthesis Reactor

The actual heating profile in the hydrothermal processing vessel is shown in Figure 3.4 and this was then used to transition into heating by microwaves at the end of Chapter 5 and 6 for the functionality test of the emulsifier. This new method was used as the previously used hydrothermal processing steel reactors were no longer in commission. The heating profile was broken down into segments to heat the product at the same rate despite the different heating mechanism. For the conventional hydrothermal process used in Chapters 5 and 6, the unmodified reactors were cooled at the conclusion of the 120min in the oven. As such, the profile in the microwave was adjusted slightly to be within the 2 hours scope of the oven time used throughout the course of the research. The specific details of the segmented heating rates and the breakdown of the calculations are shown in Table 3.3, using Equation 3.3, where T is the final step temperature (°C); T_0 is the start step temperature (°C) and t is the total time of the step (min). The measured average Hydrothermal T/t profile was carried out using a preheated oven operating at a set temperature of 220°C. The arrow in Figure 3.4 refers to the point at which the oven was manually turned off.

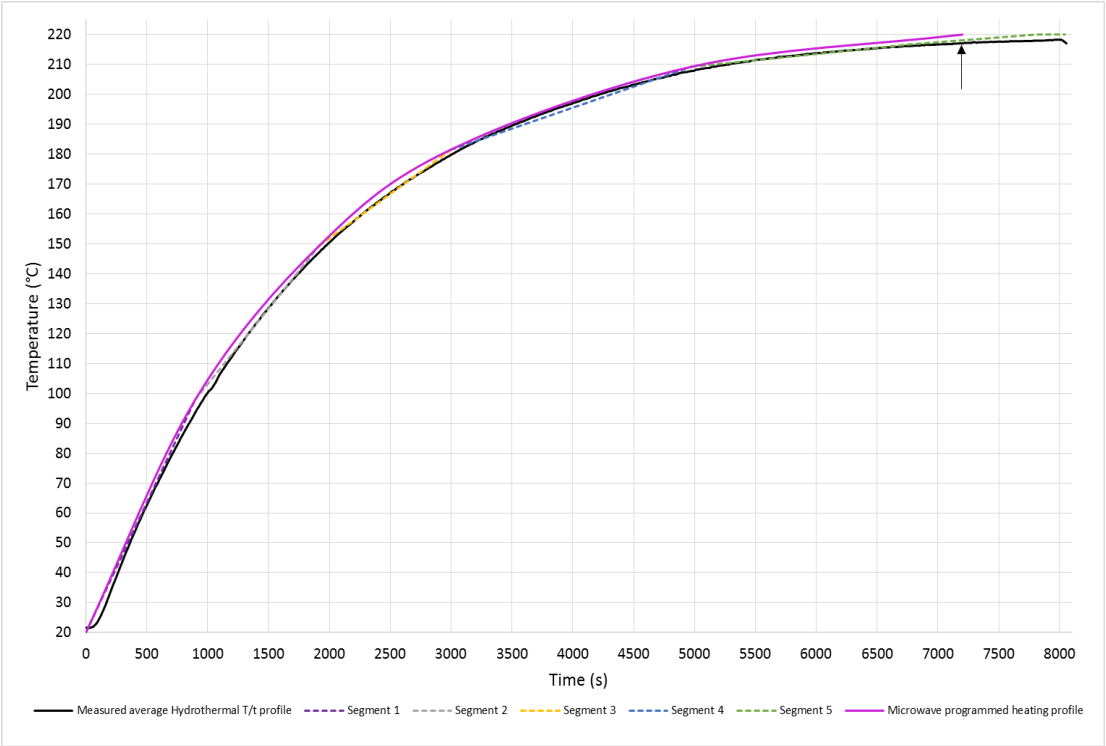


Figure 3.4: Segmented breakdown of hydrothermal process for transition from conventional heating to microwave heating (arrow signifying manual oven turn off)

Equation 3.3: Equation for calculating segmented heating rate

$$Heating\ rate = \frac{T - T_0}{t}$$

Table 3.3: Segment breakdown of hydrothermal process heating curve

Segment Number	Time t (min)	Start Temperature T_0 (°C)	End temperature T (°C)	Heating rate (°C/min)
1	15	20	98	5.20
2	17	98	149.51	3.03
3	18	149.51	181.55	1.78
4	33	181.55	209.27	0.84
5	37	209.27	220	0.29
*6	-	220	45	Compressed air controlled

*not on heating curve as controlled by the microwave synthesis reactor

3.5.3 Hydrothermal processing in microwave synthesis reactor

This profile outlined in Table 3.3 was translated for use in a microwave synthesis reactor. Particles which were produced using a Monowave 300 Microwave Synthesis Reactor (Anton Paar, Graz, Austria) were as a result of the smaller sample size required and after the rupture to the hydrothermal tubular reactors following pressure calculations to understand maximum fill level (3.5.4). The Monowave 300 was programmed to follow the same heating profile as in Table 3.3. The microwave heating profile as measured on the Monowave 300 is shown above in Figure 3.4. In the microwave synthesis reactor, a small magnetic mixing bar (5mm long x 2mm wide) was added to the 30ml vials. Along with the mixing bar, 2g of UT BSG and 16.5g of RO water was added. Throughout the process, a magnetic mixing bar was operated at 600rpm inside the synthesis reactor apart from during the cooling step. This was to ensure that the BSG dispersion did not sediment and stayed within the region where the microwaves penetrated the vial.

3.5.4 Pressure calculations during the hydrothermal process

Some background on the use of high pressure in the production of various food products will now be presented. In food production, processes involving high temperature and pressure are routinely used. In the production of canned food products, the use of over pressure in the processing vessel (e.g. retort) is used to enable the heating of the food to between 100°C and 130°C to deliver the required cook for *Clostridium botulinum* to render the shelf-stable food product safe. This is completed by adding compressed air to the retort environment and in turn increases the pressure inside the vessel to be the same or greater than the pressure internally in the product. For example, a routine retort sterilisation cook often occurs at 121°C and requires a minimum pressure of 1.03 barg (measured

pressure) to be achieved (based on steam saturation temperature). As such an over pressure normally equating to a minimum of 1.5 barg is often used in thermal processing of food products.

Pressure systems used in the bioenergy field differ slightly to those used in food production. For example, steam explosion is a process used in the pre-treatment of biomass to open up the fibres making the biomass more susceptible to subsequent processing for use in bioenergy and biofuel production. These processes are usually either fermentation or hydrolysis based. Steam explosion is often used due to the high mechanical strength of the biomass, especially if it is of woody origin and has a high lignin content (Stelte, 2013).

Often, the liquid phase of these processes is water. Processing at temperatures above 100°C require extra safety considerations, particularly if the vessel is a sealed container, due to the changes of state which water exhibits and the subsequent associated pressure changes. The phase state diagram of water is shown in Figure 3.5. For the purposes of this section, the region of interest is the one of sub-critical water. The temperature range of sub-critical water is between 100°C and 374°C. Sub-critical water is where water remains in a liquid state but at temperatures above its boiling point above atmospheric pressure. In order for water to remain in a liquid state above the ambient boiling point of 100°C, it must be subjected and compressed to increased pressure in a sealed vessel. Inside the sealed vessel, forces generated as a result of the water expansion increase the pressure in the vessel with the water remaining in a liquid state as the temperature is increased. If the pressure falls below the required pressure to keep water in its liquid state, then gaseous water vapour is produced. The water vapour pressure is the pressure at which water is in a thermodynamic equilibrium between a condensed state and a gaseous state (Engineering Toolbox, 2004). A fall in pressure can occur for example if the vessel which housed

the water failed and ruptured leading to a sudden pressure drop. The pressures associated with a temperature range of 100°C and 374°C are from 101kPa to 22089kPa. For the purposes of this work, the equivalent pressures in bar are 1bar and 220bar using a conversion factor of 1bar = $1x10^2$kPa (Perry, 1997).

Saturated vapour pressure occurs when water evaporates but in a sealed container there is no room for escape of the gaseous molecules. The greater the temperature, the greater the amount of kinetic energy in the system and therefore more water molecules can turn gaseous. There is a large difference in pressure between vapour pressure increases when compared with ideal gas pressure increases over the same range of temperatures. This is a result of the kinetic energy changes within the system as a whole (Joshua *et al.*, 2018).

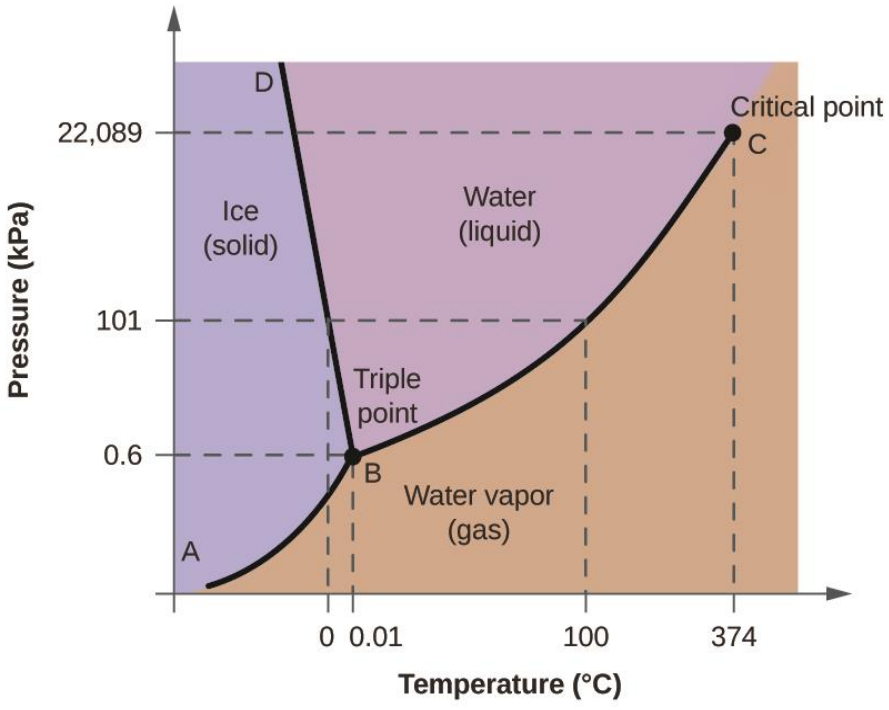


Figure 3.5: Phase diagram of water at different temperatures with associated pressure up to critical point (Flowers et al., 2018)

Pressure calculations are a necessary safety precaution for estimating the pressure inside of the system prior to use. The main reason for these calculations is to estimate the pressures likely to be

observed during a hydrothermal treatment in order to maintain the integrity of the system and to avoid vessel rupture, as shown in Figure 3.6. The hydrothermal processing vessel was scaled up from the 150mm (180mm including end caps as depicted in Figure 3.3) to 850mm using the same diameter of 22mm. This was necessary due to the requirement for additional material in the experimental stages of this research. Following the rupture of the new hydrothermal processing vessel when processing a different feedstock to the BSG normally used, pressure calculations were carried out retrospectively to understand what may have happened, leading to vessel rupture. The vessel rupture will depend on not only the pressure build up but also the vessel material properties. For example, the metal chosen as material for the vessel e.g. aluminium vs 316 stainless steel, will have very different pressure safety ratings.



Figure 3.6: Ruptured hydrothermal processing vessel due to over-pressurisation (22mm internal diameter tubing with 2mm wall thickness)

Calculations on filling ratios were conducted to generate optimal filling levels to avoid over-pressurisation of the vessel which could cause subsequent rupture of the wall (Lester, 2018). A pressure calculation using the Antoine Equation (Equation 3.4) was conducted to gain an insight into the pressure internally for the sealed vessel containing water and air. This equation (3.4) was also changed from pressure in mmHg to pressure in standard atmospheres (bar)

depending on whether the temperature was above or below 100°C (Equation 3.5 and Equation 3.6). It was also assumed that the volume of water (Equation 3.7) was incompressible meaning that the density of the liquid remains constant. The Henry's law constant is also calculated to determine how much gas is dissolved in the water based on fill volume (Equation 3.8 and Equation 3.9). The total number of moles of oxygen and nitrogen in the air were calculated (Equation 3.10 and Equation 3.11). The partial pressure of the oxygen and nitrogen in the system is also considered in order to give the total pressure (Equation 3.12, Equation 3.13 and Equation 3.14). This assumption is that if the volume fraction of the liquid is greater than 0.99˙ then the vessel will rupture (Tubing 316-T25M-S-2,0M-6ME and End Caps SS-1610-C, Swagelok, Warrington, UK).

Equation 3.4: Antoine Equation for vapour pressure calculation (mmHg) (Lester, 2018)

$$P = 10^{(A-\frac{B}{C+T})}$$

Equation 3.5: Antoine Equation for saturation vapour pressure calculation under 100°C (Psat) (Lester, 2018)

$$P = \frac{10^{(A1-\frac{B1}{C1+T})}}{750.06}$$

Equation 3.6: Antoine Equation for saturation vapour pressure calculation over 100°C (Psat) (Lester, 2018)

$$P = \frac{10^{(A2-\frac{B2}{C2+T})}}{750.06}$$

Table 3.4: Constants used in Antoine Equation (T in °C, P in mmHg) (DDBST GmBH, n.d., Lester, 2018)

Regression constants	For temperatures under 100°C
A1	8.07
B1	1730.63
C1	233.43
	For temperature over 100°C
A2	8.14
B2	1810.94
C2	244.49

Equation 3.7: Calculating volume fraction of the water in the system(Lester, 2018)

$$Vf_{liq} = \left((W \times T^3) + (X \times T^2) + (Y \times T) + Z\right) \times FV$$

Where W, X and Y are constants (see Table 3.5) and T is temperature in °C.

Table 3.5: Constants used for calculating the volume fraction of water at specific temperature which assumes that water is incompressible (Lester, 2018)

Constant	Value
W	-0.00000001
X	0.000006
Y	-0.00002
Z	0.99695
FV (Fill Volume)	0 to 1 (decimal)

Equation 3.8: Henry's law constant for oxygen as a function of temperature, in Kelvin (Lester, 2018)

$$H_{oxygen} = (4.342 \times 10^{-6}) \times e^{(\frac{1700}{T_{kelvin}})}$$

Equation 3.9: Henry's law constant for nitrogen as a function of temperature, in Kelvin (Lester, 2018)

$$H_{nitrogen} = (7.863 \times 10^{-6}) \times e^{(\frac{1300}{T_{kelvin}})}$$

Equation 3.10: Total moles of oxygen in the system (Lester, 2018)

$$Total\ moles_{oxygen} = \frac{0.21 \times (1 - Psat) \times (1 - FV)}{0.08314 \times T_{kelvin}} + (H_{oxygen} \times 0.21 \times (1 - Psat) \times FV)$$

Equation 3.11: Total moles of nitrogen in the system (Lester, 2018)

$$Total\ moles_{nitrogen} = \frac{0.79 \times (1 - Psat) \times (1 - FV)}{0.08314 \times T_{kelvin}} + (H_{nitrogen} \times 0.79 \times (1 - Psat) \times FV)$$

Equation 3.12: Partial pressure of oxygen in the system (Lester, 2018)

$$P_{oxygen} = \frac{Total\ moles_{oxygen}}{\left(\frac{1 - Vf_{liq}}{0.08314 \times T_{kelvin}}\right)} + (H_{oxygen} \times Vf_{liq})$$

Equation 3.13: Partial pressure of nitrogen in the system (Lester, 2018)

$$P_{nitrogen} = \frac{Total\ moles_{nitrogen}}{\left(\frac{1 - Vf_{liq}}{0.08314 \times T_{kelvin}}\right)} + (H_{nitrogen} \times Vf_{liq})$$

Equation 3.14: Total pressure in the system (Lester, 2018)

$$Total\ pressure = Psat + P_{oxygen} + P_{nitrogen}$$

The calculation of pressure was determined using the above equations (Lester, 2018). The main variable in these calculations was the fill volume of water in the main reactor chamber which determined whether or not the hydrothermal processing rig remained intact during heating. If the overall volume change for the water fill volume was too large (e.g. the space occupied became larger than the internal volume of the vessel) and the total air headspace was greatly reduced, then this could cause vessel rupture. Pressure changes at specific temperatures show whether the reactor will maintain integrity during the hydrothermal processing of lignin-rich feedstocks. In Table 3.6 the total space the water takes up inside of the vessel is shown as a decimal. During the calculation, the determination of the internal fill volume level aids in the understanding of whether the vessel would rupture or not. The maximum internal volume of the vessel is referred to as 100% in the calculation (or 1.00 as a decimal since this is how the result of the calculation are shown). In this instance, when the internal fill volume occupies a greater or equivalent space to 0.999 this was determined

to enable vessel rupture to occur even at low temperatures. Table 3.7 shows the associated pressure relating to the fill volume at a specific temperature. This shows that changes in the fill volume under heating generate different pressures internally at the same chosen temperature. For the relevance of this work, the maximum temperature used in these calculations was 240°C. This was to ensure that the fill volumes had a 20°C safety margin in case subsequent heat was generated exothermically by the feedstock during processing.

The results in Table 3.6 and Table 3.7 show that the greater proportion of the volume fraction taken up by the water fill volume, the greater the pressure generated. If the fill volume is too great e.g. at 0.95, then the vessel would rupture at a temperature as low as 120°C in contrast to a lower fill volume of 0.75 where the reactor would stay structurally sound when processing at 240°C.

Table 3.6: Table showing the space the liquid volume fraction takes up in the reactor at specific fill volume and temperature

	Vf(liq) at specific temperature					
Water Fill Volume in reactor	**40°C**	**80°C**	**120°C**	**160°C**	**200°C**	**240°C**
0.5	0.50	0.51	0.53	0.55	0.57	0.60
0.6	0.60	0.62	0.64	0.66	0.69	0.72
0.7	0.70	0.72	0.74	0.77	0.81	0.84
0.75	0.75	0.77	0.80	0.83	0.86	0.90
0.8	0.80	0.82	0.85	0.89	0.92	0.96
0.9	0.90	0.93	0.96	0.99	1.04	1.08
0.95	0.95	0.95	1.01	1.05	1.10	1.14

*Table 3.7: Table showing the associated pressure (bar) inside the reactor at specific fill volume and temperature (*N/A refers to no calculated pressure as vessel rupture)*

	Pressure at specific temperature (bar)					
Water Fill Volume in reactor	**40°C**	**80°C**	**120°C**	**160°C**	**200°C**	**240°C**
0.5	1.10	1.66	3.36	7.73	17.35	35.78
0.6	1.10	1.68	3.41	7.84	17.55	36.09
0.7	1.11	1.72	3.51	8.05	17.96	36.85
0.75	1.11	1.75	3.60	8.26	18.42	37.89
0.8	1.12	1.80	3.74	8.65	19.53	41.70
0.9	1.16	2.07	4.96	22.02	N/A	N/A
0.95	1.22	2.82	N/A	N/A	N/A	N/A

3.6 Nuclear Magnetic Resonance

3.6.1 Processing NMR spectra using MNOVA

The original FID (free induction decay) was generated by spinning a sample at the magic angle by non-equilibrium nuclear spin magnetisation in the magnetic field. The FID contains all the information collected during the experiment.

Using appropriate software (MNOVA, Mestrelab Research S.L., Santiago de Compostela, Spain) generates the spectra after the 1st Fourier Transform of the original FID. A Fourier Transform, when applied to NMR, takes the FID signal which was generated as a function of time (number of pulses) and generates a frequency amplitude which in turn creates a visible NMR spectrum based on signal intensity for a given chemical shift.

Due to the noise produced in lignocellulosic samples, an Apodization exponential function of 40–50 Hz must be applied to reduce the level of noise present in the spectrum. As the spectrum generated is already zero-filled to 16K, no further zero filling is applied in MNOVA (Mestrelab Research S.L., Santiago de Compostela, Spain). Automatic phase correction is applied initially to rephase the spectrum and subsequent manual phasing in both the zero and first

order are applied using the largest amplitude peak as reference. An automatic baseline correction is applied, and then further baseline correction can be manually applied using the Ablative method if the baseline still isn't accurate. After this point no further processing is applied to the spectrum and the file is extracted as an NMR CSV file in order to be processed for lignin quantification following the procedure in 3.6.2.

3.6.2 Quantifying lignin from NMR spectra

Lignin content and lignin distribution within particles calculated through carbon ratios. Carbon ratios are in this sense defined as the differences between the intensities of chemical shift carbon signals from the NMR spectrum. Table 3.8 shows the ppm ranges used to calculate the lignin percentage in the different samples. The intensity of the spectrum is the measured value which was generated during the NMR experiments.

The spectrum produced using ^{13}C solid –state NMR once processed in MNOVA (Mestrelab Research S.L., Santiago de Compostela, Spain) were then exported to Microsoft Excel (Microsoft Corporation, Washington, USA) where these data was organised into three separate regions of interest (each on their own worksheet) to calculate the percentage lignin with the specific chemical shift values and placement shown in Table 3.8.

Table 3.8: Excel worksheet chemical shift signals

Worksheet title	Chemical shift range (ppm)	Intensity	Baseline
Total	0 – 250	Measured Data	Set as 0
GSlignin	120 – 165	Measured Data	Set as 0
Methoxy	54.5 – 58.5	Measured Data	Set as 0

Using the area under the NMR spectra enabled the calculation of bulk lignin present in the various samples. Having calculated the bulk lignin of various samples, the relative distribution of lignin within

droplets and solid particles was able to be quantified by analysing the separate fractions of 1) particle; 2) ethanol extracted fraction; 3) remaining solids post ethanol extraction. This enabled an experimental observation of process efficiency to be defined by creating a ratio based on the carbon chemical shifts for the different parts of lignin. This was conducted in MATLAB (MathWorks3, Massachusetts, USA) using the trapezium function having first generated an x/y plot including a baseline along y=0 as reference. The values of the area under the NMR spectrum against the baseline along y=0 are generated for the specific regions of interest from Table 3.8. Having generated values for each of the following Total, GSlignin, and Methoxy, using Equation 3.15 below a value of lignin percentage by carbon ratio can be generated. An example spectrum and subsequent breakdown prior to calculation is shown in Figure 3.7.

Equation 3.15: Equation used to calculate Total Percentage Lignin in Biomass using NMR and MATLAB method

$$Total\ \%\ lignin = \frac{GSlignin + Methoxy}{Total} \times 100$$

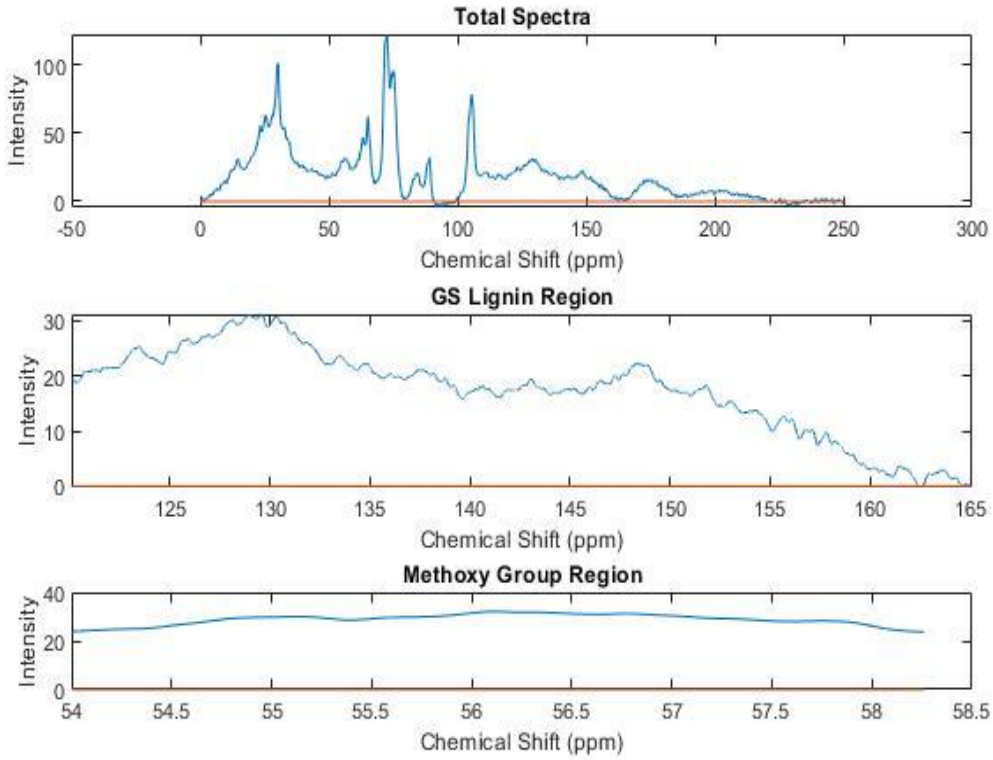


Figure 3.7: Example of the spectrum break down from MATLAB (3PHT BSG sample)

From the example spectra above, the total percentage lignin as calculated through carbon signals can be used to gain an insight estimate for the total lignin in the biomass. As this is a new method in terms of lignin quantification, it needs to be verified against the current standard method for lignin quantification which is the Acetyl Bromide Soluble Lignin Assay (shown in 3.4) and this comparison is highlighted in detail in Chapter 4.

3.7 Thermogravimetric analysis of lignin-rich feedstock

To calculate the total lignin content from a feedstock, a TGA profile was run before subsequent proximate analysis enabled the higher heating values and fixed carbon content to be determined. The conditions for this process were in an inert N_2 atmosphere. The different heating rate sections were: 5°C/min from 30–110°C where

the sample was held for 10min to calculate moisture content; a further ramp from 110–400°C at 5 °C/min; from 400–900°C the rate was 10°C/min where the sample was then held for 30min at 900°C; upon completion of the 30min, the atmosphere was switched to air and held for a further 15min to combust the sample for ash content quantification before being cooled. This method follows the ASTM D2015 standard test method with lignin chemical analysis following methods in accordance to ASTM D1103-80 and ASTM D1104-56 testing procedures (Demirbaş, 2001). This was conducted using a Simultaneous Thermal Analysis TGA/DSC 3+ (Mettler Toledo, Leicester, UK) using medium sized (70µl capacity) Alumina crucibles (part no. 00024123) which are capable of withstanding 2000°C. The lignin content of the feedstocks were calculated using Equation 3.16 through Equation 3.19 to calculate the higher heating value to reverse calculate the lignin content. The differences between Equation 3.17, Equation 3.18 and Equation 3.19 is based on the composition of the feedstock when considered a fuel, woody biomass or non-woody biomass. All of the equations have been used to calculate lignin but for the comparison with previous methods only the equation for non-woody biomass has been used since this is the one which most closely resembles the feedstocks used in this research.

Equation 3.16: Equation for calculating the higher heating value based on fixed carbon content used for all fuel samples (Demirbaş, 2001)

$$HHV = 0.196\ (FC) + 14.119$$

Equation 3.17: Equation for calculating the higher heating value based on lignin content for all fuel samples (Demirbaş, 2001)

$$\mathrm{HHV} = 0.0889(\mathrm{L}) + 16.8218$$

Equation 3.18: Equation for calculating the higher heating value based on lignin content for wood samples(Demirbaş, 2001)

$$\mathrm{HHV} = 0.0893(\mathrm{L}) + 16.9742$$

Equation 3.19: Equation for calculating the higher heating value based on lignin content for non-wood samples (Demirbaş, 2001)

$$HHV = 0.0877\ (L) + 16.4951$$

As another method which can be used for lignin quantification in biomass, this newly adopted TGA method needs further validation in comparison to the standardised ABSL method. This is covered in more detail in Chapter 4.

3.8 Method for Emulsion droplet analysis in W/O emulsions

Image analysis was used as a tool to quantify the differences between the water-in-oil emulsions produced using the particles produced using three passes on the microfluidizer followed by hydrothermal processing at 220°C for 120min in Chapter 6. The images were first sharpened and cleaned up using ImageJ using the standard functions with the further analysis for emulsion droplet size being conducted Campden BRI using the following procedure. Some assumptions were made in the analysis which are stated below in the method. The software used for this analysis was IDL (Harris Geospatial Solutions, Colorado, USA). Campden BRI wrote a specific coding program with the details of each stage of image editing prior to particles/droplet analysis outlined below.

1. The micrograph raw images exist as a Bitmap (BMP) RGB file with red, green, and blue channels with values from 0–255. It is a 24 bit colour image. All subsequent images are 8 bit images to retain full resolution during processing. Raw images are shown in Table 3.9 as "_raw".
2. These images need Thresholding whereby any values in greater than 100 (background) are set to 0 and anything else which is to be known as an object to 1. The dark objects (emulsion droplets or particles) are either very dark (<40 in all 3 channels) or the background is very light (>150 in all 3

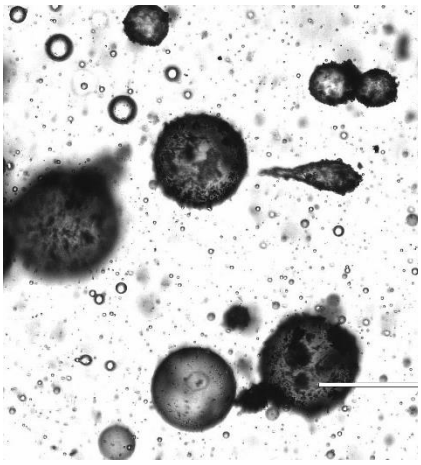
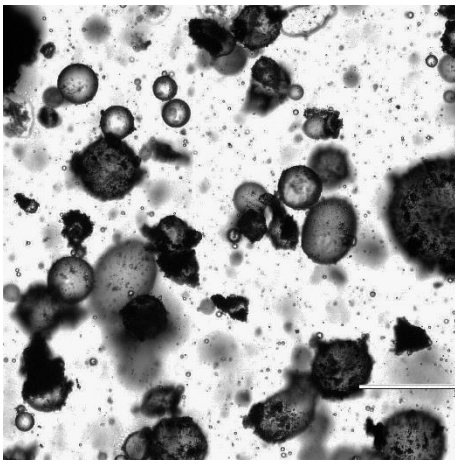
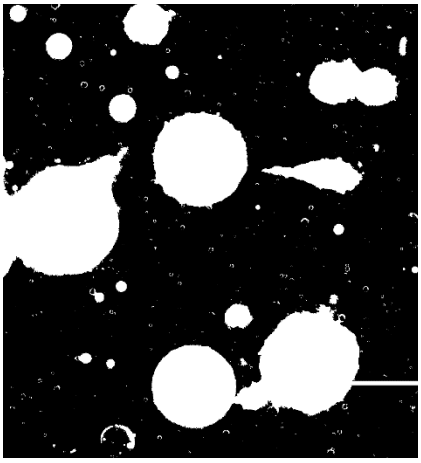
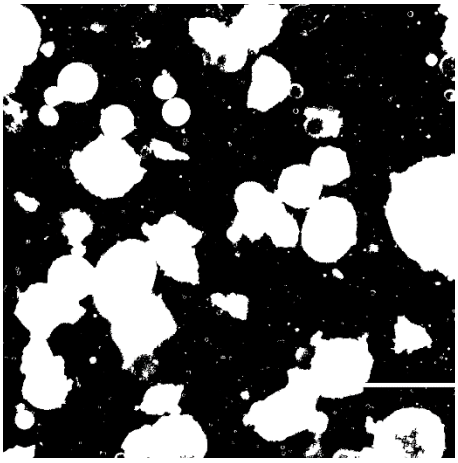
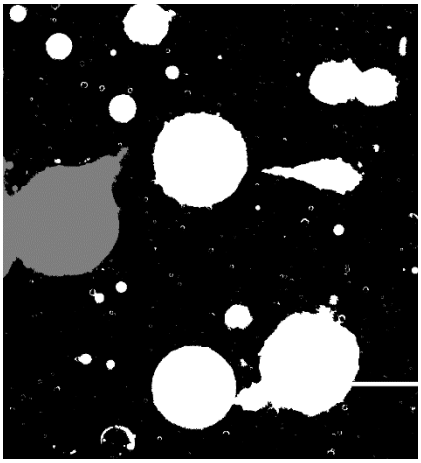
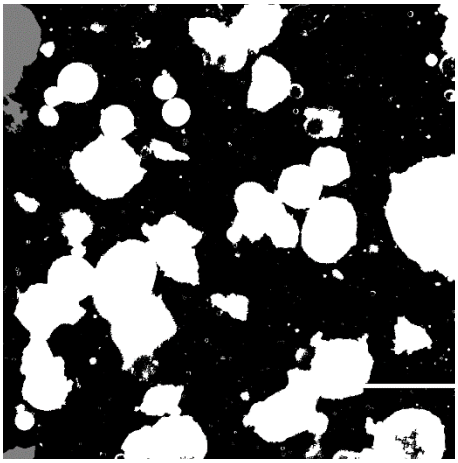
channels) and as such a threshold of 100 on the red channel was used. This is shown below as "_thres" (Table 3.9).

3. Holes in the new threshold image were subsequently filled to reduce the noise in the image by ensuring that the smallest areas where the pixel value was 0 with a surrounding pixel value of 1 are filled to also equal 1 (e.g. speckles within objects). This used a function confidential to Campden BRI.
4. Distinct objects (i.e. areas with pixel values 1 entirely surrounded by pixel value 0) are found and identified using blob analysis (this was another specifically written confidential function to Campden BRI).
5. If these objects are touching any edge of the image or are less than 10 pixels (approx. 2micron diameter), their pixel value is set to 0 and they are removed from the image as either noise (too small to be particles) or not fully captured in the image shown as "_thresnoedge" (Table 3.9). The program excludes any foreground regions that touch the edge of the image. Droplets touching the edge are shown in grey, non-edge-touching regions in white.
6. A new image is made as a Euclidean distance map of the cleaned binary image. In this image every pixel has a value equal to the Euclidean distance (the distance between two points) to the nearest background pixel in the image.

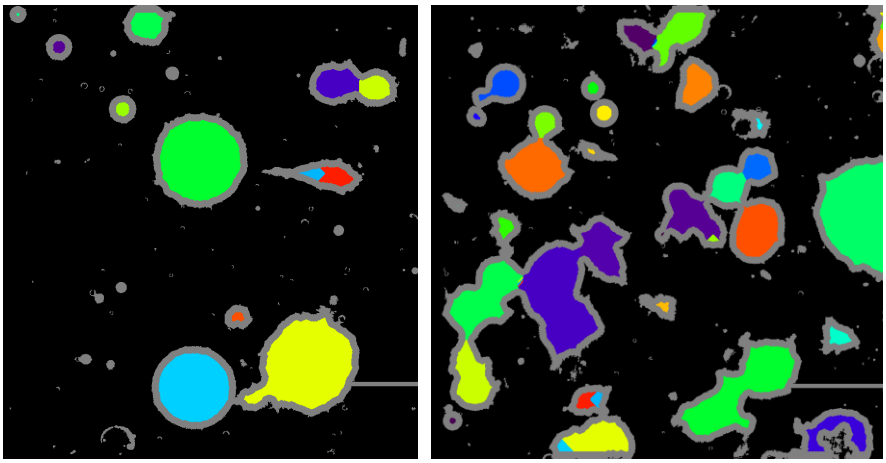
a. Two new images are created by eroding the Euclidean distance map. The candidate regions (white from the previous step) are shown in grey and are subsequently eroded to try to separate them by 15 pixels to find the centre of medium sized objects and 30 pixels to find the centre of large objects. Shown as "_largeseparated" (Table 3.9).
b. These values are fairly arbitrary, their main role being to effectively find and separate overlapping objects.

7. These eroded images are used to find and label large objects within the original image that may have been overlapped.
8. Any unlabelled objects in the original image are added back into the image and labelled themselves. These will generally be the smallest particles. Shown as "_separated" (Table 3.9). The (coloured) eroded regions have been dilated back to their original size and other regions that were lost at the eroding step have been added back, keeping them as separate regions, also coloured. Each of the differently coloured regions was then measured to provide the size distribution data.
9. All labelled objects are measured for area.
10. A circle equivalent length scale is assigned to each object using the concept of circle of equal projection area. This area is the equivalent area of a particle or structure of non-spherical origin (Sympatec, 2019). This approximates a diameter of the object, i.e. $D = 2\sqrt{A/\pi}$
11. A sphere equivalent volume is then calculated for each object as $V = \frac{4}{3}\pi\left(\frac{D}{2}\right)^3$
12. The volume fraction of each object is calculated as the ratio of that object volume to total object volume.
13. This is used to calculate X_{10}, X_{50}, and X_{90} values which are the 10^{th}, 50^{th}, and 90^{th}, percentile droplets. (i.e. the diameter of droplets where 10, 50, or 90% of the total droplet volume in the image is contained in particles of that diameter or less).

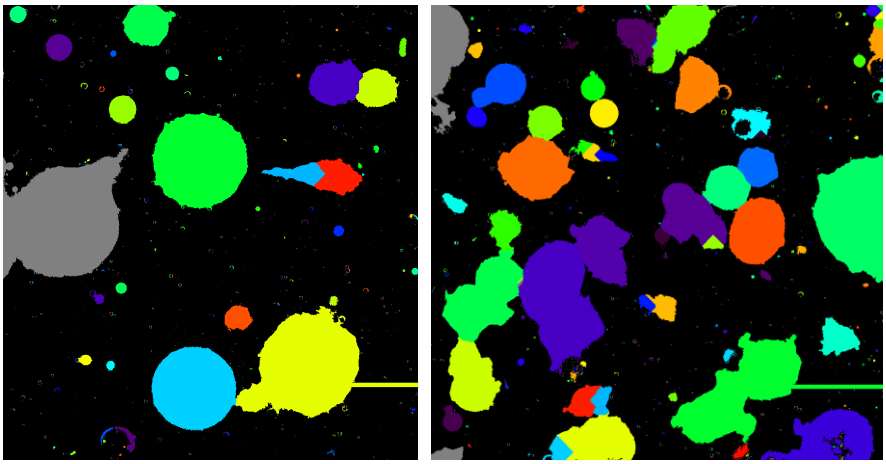
Table 3.9: Images showing the different stages associated with image analysis of emulsion droplets

Image type	70% Sunflower Oil	80% Sunflower Oil
_raw		
_thresh		
_threshnoedge		

_largesepa
rated



_separated



3.9 Production of hydrophobic particles without the use of temperature

3.9.1 Materials and Methods

3.9.1.1 Materials

Untreated BSG was used as sole feedstock in this experimental section and reverse osmosis (RO) water was used as the aqueous medium for the fluid process.

3.9.1.2 High pressure fluid process and separation

A 4 % concentration of milled untreated BSG particles was dispersed in water manually. The material was stirred as previously documented to avoid sedimentation during the first pass when filling the reservoir. A visual representation of how the microfluidizer works is shown in Figure 3.8. The material was then processed for a total

of 9 passes which was previously used as the "over processed" state looking at particle size reduction where the particle size D90 increased by nearly 50µm from the 3 pass samples to the 9 pass samples (result specifics shown in 6.3.1.1.1).

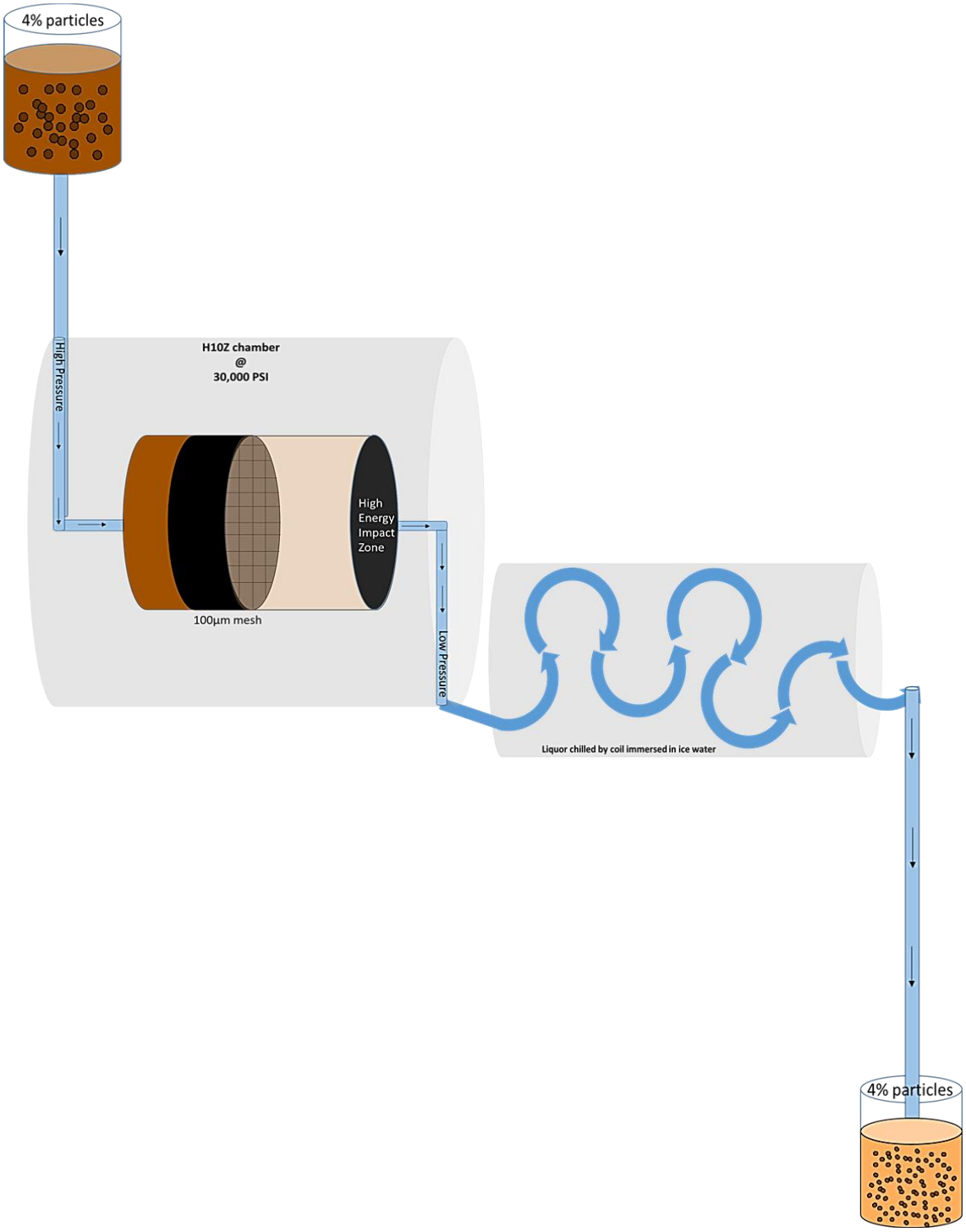


Figure 3.8: Process diagram of the mechanics of the microfluidizer when processing the particles in water mixture

After each full process in a batch format, the particles were centrifuged at 4000rpm for 3min as shown in Figure 3.9. This was conducted to separate the particles from the supernatant. The removed water was then replaced with fresh RO water before being processed for another subsequent time (Figure 3.10). As shown in Chapter 6, the liquid phase of the microfluidizer was shown to contain cellulosic material, amino acids and fat-soluble lipids. Therefore, this was removed to hypothetically maximise the change of getting lignin coverage on the particles without the need to use heat simply by removing aspects of the primary cell wall and polymer matrix. Coinciding with high levels of processing, the liquor was also removed to avoid progressive cellulose fibrillation with time and exposure to a high pressure homogenisation type process.

Results of this washing step showed that the introduction of the centrifugation step forms a soft pellet after 3min processing at 4000rpm. Calculations conducted on the batch upon separation showed that for 1000g of mixture at 4% concentration of UT BSG particles in water, the removed liquor accounted for 785.2g and the soft wet pellet accounted for 214.8g. Since the mixture contained 40g of BSG powder and 960ml water, if the liquor removed was assumed to only contain water then this was equal to removing 81.8% of the water in the initial mix. However, results in Chapter 6 show that this is not entirely the case and that some cellulosic material is also removed. This step was repeated after every batch process for the particles used to assess other functionality in 6.3.1.4.

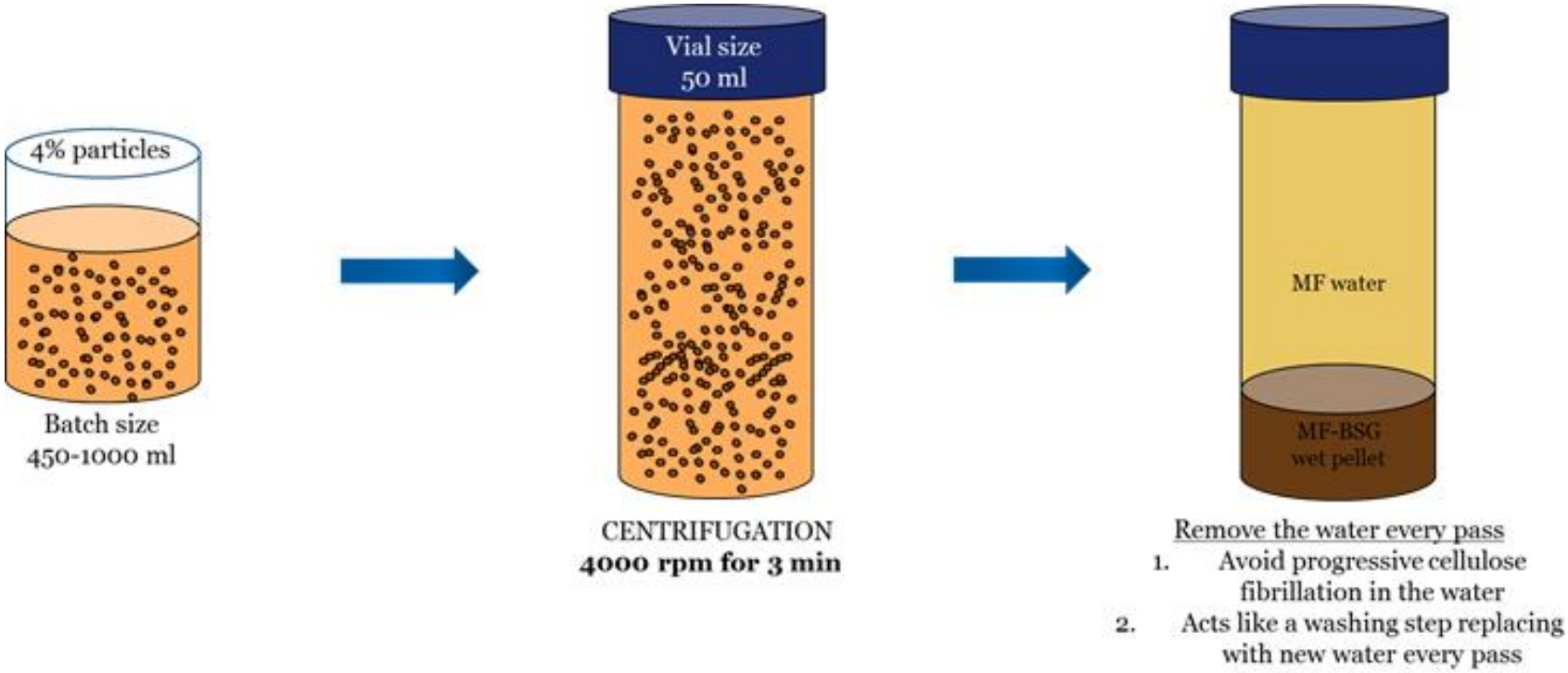


Figure 3.9: Visual representation of centrifugations and washing particles step

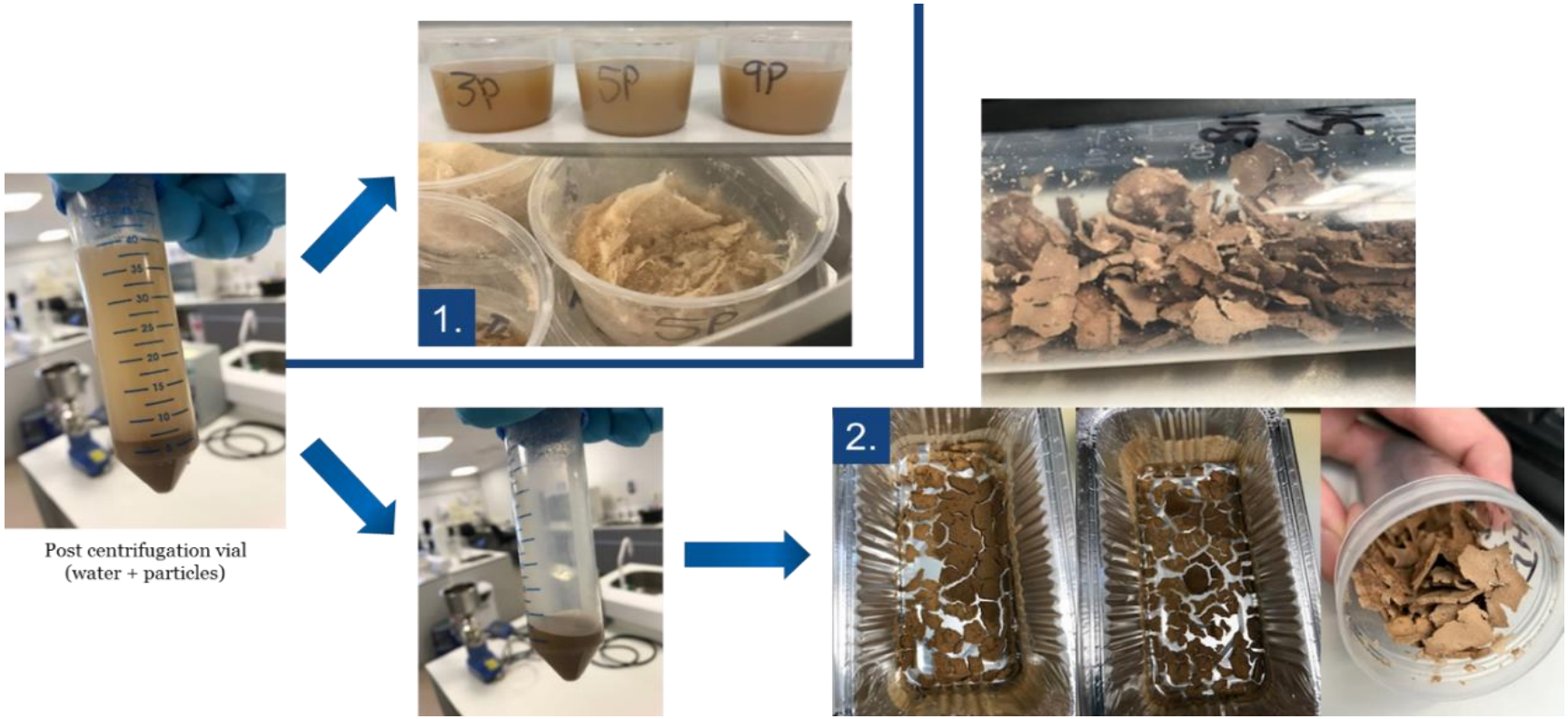


Figure 3.10: Results of successful centrifugation post 9 pass processing using high pressure

3.10 Production of lignin-emulsifier based cake

The cake recipe was taken from a Campden and Chorleywood Food Research Association publication, the emulsifier percentage used being 0.75% which is classified as the commercial optimum (Sahi and Alava, 2003). Baker's percentages as well as percentages in the recipe are shown below in Table 3.10.

This is calculated by taking $(100\% \times \frac{Weight\ of\ ingredient}{Weight\ of\ flour})$.

Table 3.10: Cake recipe used for all formulations

Ingredients	Bakers Percentage	Percentage (Recipe)	Weight (g)
Heat Treated Cake Flour	100	29.22	300.0
Caster Sugar	105	30.68	315.0
Vegetable Oil	15	4.38	45.0
Skimmed Milk Powder	8	2.34	24.0
Salt	2	0.58	6.0
Baking Powder	3.75	1.10	11.3
Water	68	19.87	204.0
Liquid Egg (Whole)	36	10.52	108.0
Dried Egg White	1.9	0.56	5.7
Emulsifier	2.55	0.75	7.7
Total			**1026.7**

The two different methods used for stabilising the emulsifier in cakes are as follows:

1. Mixing method using a Hobart mixer for direct suspension of the particles:
   - Sieve the dry ingredients
   - Whisk the liquid egg, 2min speed 2 in Hobart mixer (A120, Hobart Mfg.Co.Ltd, London, UK)
   - Add the dry ingredients and water, 1min speed 1 to incorporate the dry ingredients
   - Scrape down

- Mix 3min speed 3 to mix all ingredients and incorporate air
- Determine batter density
- Bake 230g in 7'' round cake tin at 185°C for 30min in a reel oven

2. Mixing method using a Silverson High Shear Overhead Mixer, pre-emulsify the particles
- Sieve the dry ingredients
- Pre-mix lignin based particles, water and oil with Silverson (L4M Series fitted with emulsor screen, Silverson, Chesham, UK) high shear mixer, 6000rpm 2min
- Whisk the liquid egg, 2min speed 2
- Add the dry ingredients and emulsion, 1min speed 1
- Scrape down
- Mix 3 min speed 3 to mix all ingredients and incorporate air
- Determine batter density
- Bake 230g in 7'' round cake tin at 185°C for 30min in a reel oven

Batter density is calculated using a 100ml container calibrated with water to represent 100g. The container is then filled with the batter and weighed with the specific gravity or batter density being determined as X/Y, where X is the weight of the batter in the container and Y is the weight of water which fits in the same space of container. This is important is because it determines the amount of air which is stabilised that in turn contributes to the viscosity of the batter. The higher the batter density the lower the amount of air stabilised in the matrix. Depending on the cake produced, the batter density is going to change. For example, a pound cake should have a batter density of around 0.8g/m^3 whereas a chocolate cake should have one around 0.9g/m^3 (Wing and Suas, 2009, BAKERpedia, 2019b).

Visually the cakes were observed for their crumb structure, any signs of tunnelling (large air pockets throughout the structure), uniformity and stability of air. This is covered briefly in Chapter 6 showing alternative functionality in another end product use instead of emulsions with the full details shown in Appendix A2.

4 The Quantification of lignin content: a comparison of analytical methods.

James Huscroft[1,2], Khalid Al-Mughairi[2], Robert Davis[3], Andrew Bosman[3], Bettina Wolf[1,a], Eleanor Binner[2], William MacNaughtan[1*]

[1]Division of Food, Nutrition and Dietetics, School of Biosciences, University of Nottingham, Loughborough, LE12 5RD, UK

[2]Faculty of Engineering, University of Nottingham, Nottingham, NG7 2QL, UK

[3]Campden BRI Limited, Chipping Campden, GL55 6LD, UK

[a]Present address: School of Chemical Engineering, University of Birmingham, Birmingham B15 2TT, UK

*Bill.MacNaugtan@nottingham.ac.uk

Abstract

For several years, lignin quantification has been notoriously difficult due to the number of different methods available. Each method delivers its own specific lignin extraction by extracting the parts of the plant cell wall which are susceptible to degradation and removal by the chosen solvent and quantifies exactly what is removed from the plant biomass. Since its development by Johnson *et al.* (1961), the 'Acetyl Bromide Soluble Lignin Assay' has been widely regarded as the standard method for lignin quantification since it was developed. Over the years, numerous additions and extra steps have been included to modify the assay to quantify exactly the component of the feedstock that is Acetyl Bromide soluble lignin. Here, this assay has been researched with regards to lignin monomeric fundamental composition, as well as its impact on 3 different lignin-rich feedstocks, each with differing monomeric composition. This assay was then compared to a newly developed solid state NMR method which is non-invasive and was used to determine lignin content from the ratio of carbons in the whole feedstock as well as a Thermogravimetric analysis (TGA) method. The Acetyl Bromide assay was found to be selective for coniferyl alcohol producing an overestimation (+20%) of the lignin content, whilst delivering an underestimation (-15%) of the lignin content based on the sinapyl alcohol content. The NMR method showed that the monomeric composition of a feedstock could be shown based on the carbon chemical shift of the individual alcohols when compared to the known lignin-rich feedstocks. The TGA method was found to be no use for quantifying lignin-rich feedstocks due the inaccurate ability to quantify total lignin in a feedstock by way of measuring fixed carbon content to calculate lignin.

4.1 Introduction

4.1.1 Lignin

As the second most abundant polymer in the natural world after cellulose; lignin, in its natural form; is a polymer formed of three different monolignols which are phenolic derivatives bonded together by radical coupling polymerisation reactions (Xu and Ferdosian, 2017). These three monolignols are derived from coumaryl alcohol (H), coniferyl alcohol (G) and sinapyl alcohol (S) and are mainly linked through alpha and beta ether linkages (Santos *et al.*, 2013, Haghdan *et al.*, 2016).

Depending on the extraction method, the lignin recovered will differ not only in composition but also the properties. For example, alkali lignin/kraft lignin is recovered from materials using NaOH, which breaks the polysaccharide associations. The Organosolv method involves heating the material in the presence of an aqueous organic solvent with an ethanol-water mixture producing a higher blend yield than that of the kraft procedure above (Singh and Dhepe, 2016). Another method which produces milled wood lignin involves extensive milling of wood in a ball mill to mechanically break down the linkages in the polymer (Xu and Ferdosian, 2017).

4.1.2 Methods used for lignin quantification

4.1.2.1 Principles of solid state NMR applied to plant cell walls

Over the last 25 years, ^{13}C solid state Nuclear Magnetic Resonance (NMR) as a method for the compositional analysis of plant cell walls has been widely used. Originally it was used to look specifically at plant materials found in the primary plant cell wall; predominantly for the identification of cellulose (Foster *et al.*, 1996). NMR has been used to identify the 2D and 3D structure of lignin within a feedstock and to analyse fractions produced by the progressive removal of the

organic components which make up the plant cell wall matrix. The chosen feedstock was primarily high pressure homogenised or hydrothermal processed Brewers' Spent Grain (BSG) with the fractions being cellulose, hemicellulose, lignin, pectin, lipids and proteins (Chapter 5 and Chapter 6). ^{13}C NMR spectra of these individual components, shows that based on their chemical shifts these can be distinguished in a complete spectrum (Manders, 1986, Gilardi *et al.*, 1995, Foster *et al.*, 1996, Kono *et al.*, 2002, Sanna *et al.*, 2011, Bernardinelli *et al.*, 2015). The primary focus of this work was detecting the presence, location and composition of the lignin i.e. the chemical composition of the monomers within the BSG lignin polymer. NMR determined lignin composition is based on the chemical shifts identified for the different lignin monomers namely H, G and S which have been characterised for hardwoods (Manders, 1986). Carbon atoms in the aromatic rings in these different phenyl alcohols were shown to have ppm values in the 120–165ppm region with the methoxy carbon having a value of 56ppm (Manders, 1986). Figure 4.1 and Table 4.1 show the structure of the different monomers and the chemical shifts of the different carbon atoms. A lignin extraction procedure has also been conducted followed by both solution state and solid state NMR experiments to quantify total lignin in Kenaf which is classified as a lignocellulosic biomass (Fu *et al.*, 2015). Other information can also be calculated from the NMR spectra. For example, the crystallinity of cellulose can be estimated from the chemical shift signals of the amorphous and crystalline signals present in the C4 region of 80–90ppm. The anomeric C1 carbon in cellulose, starch and pectin is approximately at 100ppm (Foster *et al.*, 1996, Gilardi *et al.*, 1995, Bernardinelli *et al.*, 2015). The carbonyl carbon in the lipid fraction of BSG, specifically oleic acid and palmitic acid as well as pectin correspond to approximately 180ppm (Gidley and Bociek, 1985, Gidley, 1992, Sanna *et al.*, 2011). The aromatic carbons of lignin are observed between 120 and

165ppm (Sanna *et al.*, 2011, Manders, 1986). The plant cell wall contains other polymers in addition to cellulose and lignin, the carbons of which can be found in the NMR spectrum since it is a bulk technique looking at the material in its entirety. Hemicellulose is found in the same region as cellulose i.e. between 56 and 110ppm. Pectin can be shown at different regions dependent on the degree of esterification (DE). Lower DE methoxy (-O-ME) pectin has a value of 54ppm whilst the higher DE methoxy pectin C6 chemical shift is found at ppm value of between 170–180 (assigned to 1,4-α-D-galacturonan with partial methyl esterification) where carbonyl ester groups in the lipid component of the material are also observed (Jarvis, 1984, Foster *et al.*, 1996, Sanna *et al.*, 2011).

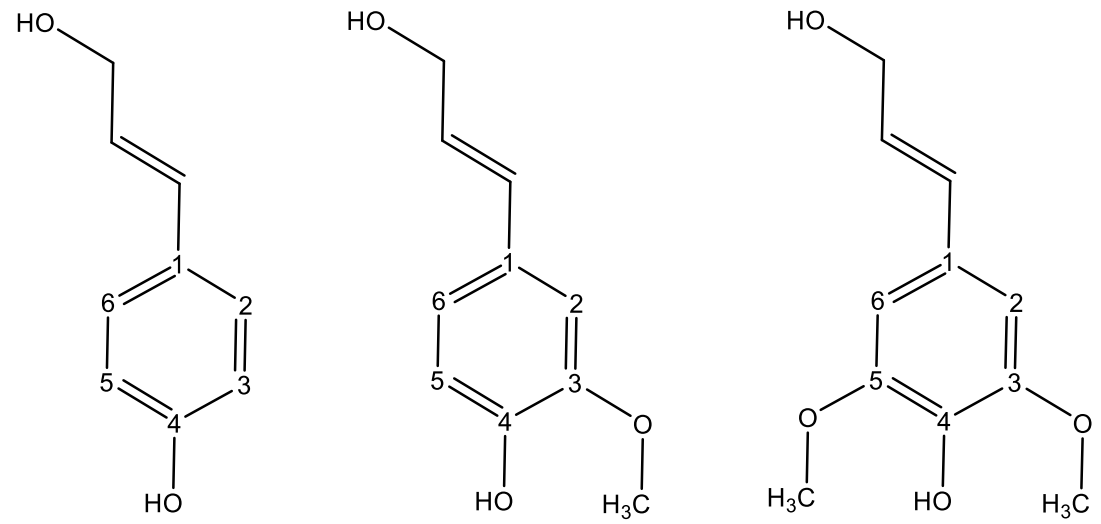


Figure 4.1: Numbering of carbon atoms in the aromatic ring for H, G and S lignin monomer alcohols (Manders, 1986)

*Table 4.1: Carbon atom chemical shift for lignin monomers shown in Figure 4.1 (Manders, 1986) (*o-alkylated being the inclusion of an O-CH3 group at both carbons)*

Carbon Atom on which Monomer	Associated chemical shift (ppm)
C-4 in H	160 – 162
C-3, C-4 in G	148
C-1 in G	134 – 136
C-1, C-4 in S	136
C-3, C-5 in S (o-alkylated)	153.5
C-3, C-4 in G	153.5 (upfield shoulder)
C-3, C-5 in S (non o-alkylated)	148

For the reasons outlined above, NMR was chosen as a technique suitable for chemical identification but deserves further consideration with regard to quantification. This could be used to identify the composition of the lignin at a monomeric level, to show whether lignin is present in untreated BSG and also whether it can be perceived that lignin has been relocated to the surface of the particulate emulsifier during the hydrothermal treatment by an increase in ethanol extractable yield (covered in more detail in 5.3.2.3). This should enable a detailed insight to be developed on what is present in the different constituents and where these are in relation to the different extracted fractions.

4.1.2.2 Acetyl Bromide Soluble Lignin (ABSL) chemical assay

The Acetyl Bromide wet chemistry assay has been used to quantify lignin in a variety of wood samples since it was created by Johnson *et al.* (1961). It is widely regarded as the benchmark method for lignin quantification. This assay involves the formation of Acetyl chemical derivatives to solubilise the lignin in the feedstock through the use of Acetyl Bromide and Acetic acid (Johnson *et al.*, 1961, Moreira-Vilar *et al.*, 2014). Other methods of lignin extraction can be used such as the Klason Lignin method, Dioxane Lignin, Organosolv lignin or the acid detergent lignin. These all produce different lignin derivatives based on the differences in the extraction

methods. These lignin samples can also be dissolved in different solvents. As an example, Organosolv lignin can be completely dissolved in dioxane and Brauns lignin in DMSO, ethanol or acetone. Acid lignin however cannot be solubilised in any solvents (Chen, 2014). The unmeasured residue of the digestion process (part of the assay) is often protein rich but may retain some lignin. This would not be measured as part of the assay. The amount of unmeasured lignin depends on the effectiveness of the digestion (Iiyama and Wallis, 1988). The modified Acetyl Bromide assay used by Iiyama and Wallis (1988) showed that the amount of lignin present in a number of wood samples was similar to the combined assays for Klason lignin and the acid soluble lignin, and so could be considered a measure of total lignin (Iiyama and Wallis, 1988).

Some cautionary information on the Acetyl Bromide assay has been published showing that a higher temperature of reaction will degrade other polysaccharides and so contribute to the soluble lignin fraction. The Acetyl Bromide reagent is also known to degrade xylans, specifically hemicellulose, which is a major component of plant cell walls (Hatfield *et al.*, 1999). If the degradation of xylans were to occur during the solubilisation of lignin, this would result in an overestimation of the total lignin concentration, as the same absorbance region of 280nm is used for the quantification of both. It was found that by lowering the temperature of the reaction from 70°C to 50°C and extending the time for the total reaction from 2 hours to 4 hours, then complete lignin solubilisation could occur with minimal degradation of xylans (Hatfield *et al.*, 1999). When comparing the Acetyl Bromide assay to other lignin methods, it was found that the ABSL assay gives relatively high numbers compared to other methods e.g. acidic detergent lignin, permanganate lignin or Klason lignin (Fukushima and Hatfield, 2004). Acid detergent lignin was found to give low values of lignin especially in grasses

whilst the Klason method appeared to overestimate the amount of lignin in legume based samples due to the presence of protein in the cell walls (Fukushima and Hatfield, 2004). A proposed reaction mechanism for lignin reacting with Acetyl Bromide was published by Hatfield and Fukushima (2005) and is shown in Figure 4.2A. Illustrated reaction mechanisms of lignin with Acetyl Bromide are shown in Figure 4.2B, Figure 4.3A and Figure 4.3B. The main mechanisms are o-acylation, bromine substitution and c-acylation (Lu and Ralph, 1996). Acylation is the process by which an Acetyl group replaces a hydrogen on a compound structure. Normally this occurs at an active hydrogen. Other mechanisms are o-alkylation which is the transfer of an alkyl group from one compound to another. Depending on the choice of solvents used as part of the Acetyl Bromide soluble lignin assay, the mechanisms previously stated will occur at different rates with the reactions being dependent on what is extracted based on solvent and processing conditions (Iiyama and Wallis, 1990, Lu and Ralph, 1996). It must also be noted that when calculating the lignin content, the feedstock itself will have an impact on the results. As a result, different extinction coefficients have been calculated dependent on the woody nature of the biomass to correct aspects of the calculated assay percentage. For example, Poplar as a wood species has an extinction coefficient of 18.21 whereas grasses have an extinction coefficient of 17.75 (Barnes and Anderson, 2017). Therefore, depending on the coefficient used in this assay, the percentage lignin will change from one feedstock to another.

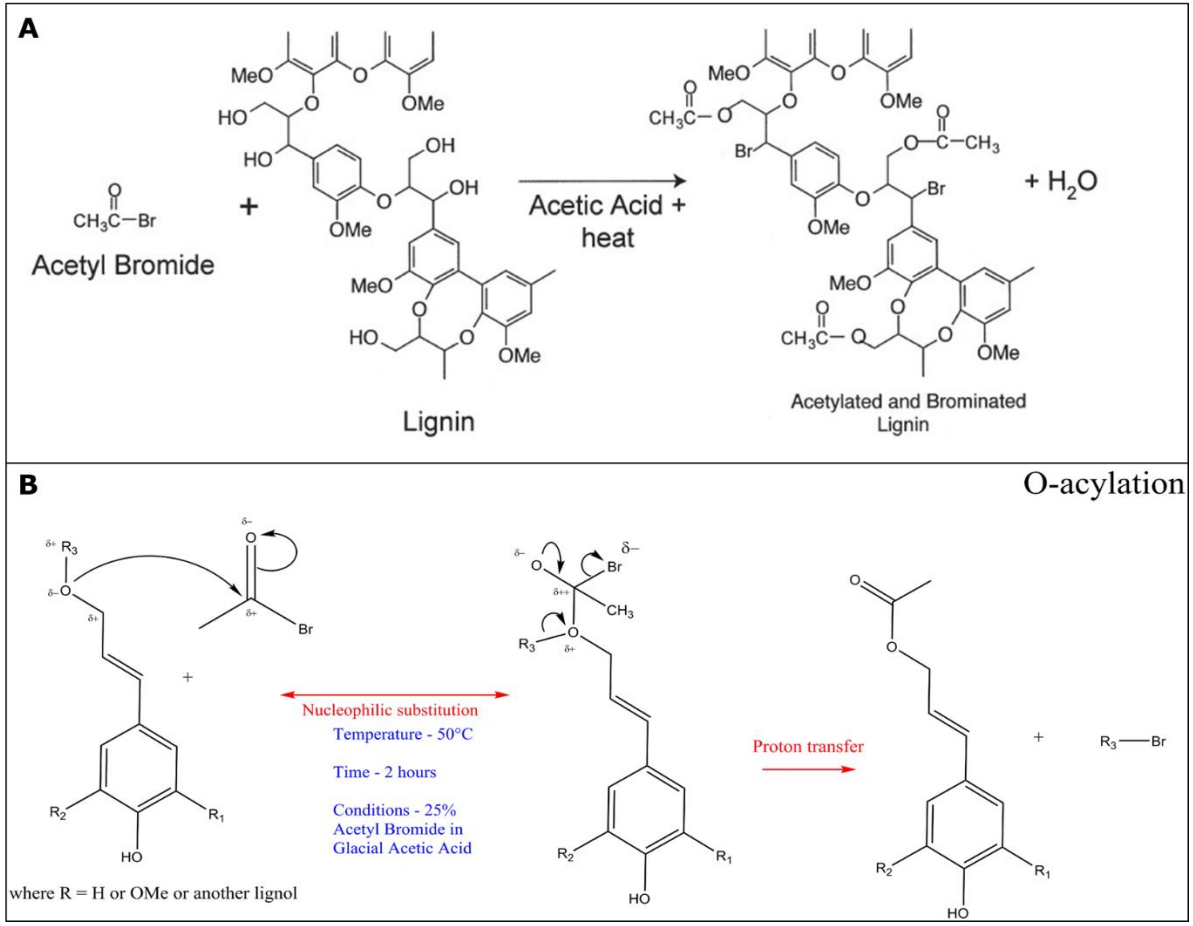


Figure 4.2: A) Proposed reaction mechanism of lignin reacting with Acetyl Bromide (Hatfield and Fukushima, 2005); B)one of three proposed reaction mechanics of Acetyl Bromide reacting with individual lignols or lignin produced on ChemDraw whilst referring to (Lu and Ralph, 1996)

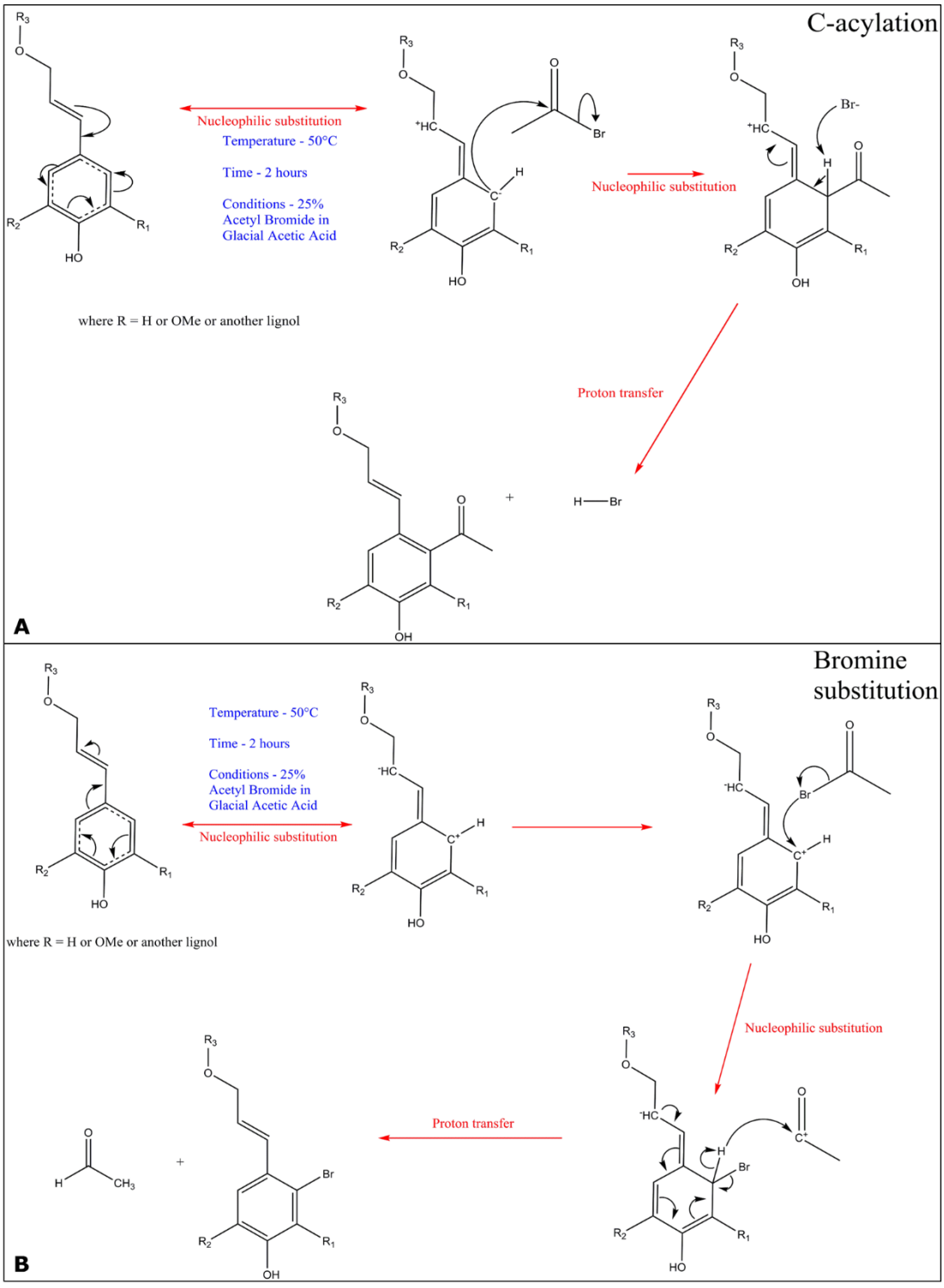


Figure 4.3: A) and B) the other two proposed reaction mechanics of Acetyl Bromide reacting with individual lignols or lignin produced on ChemDraw whilst referring to (Lu and Ralph, 1996)

4.1.2.3 Thermogravimetric analysis (TGA) for biomass lignin determination

TGA is normally used to quantify the temperature range where the thermal degradation of lignin takes place (Beall, 1968, Olatunji *et al.*, 2018). This temperature range has been found to begin at 100°C and continues up to 700°C (El Khaldi-Hansen *et al.*, 2016). The different degradation derivatives of lignin correspond to different regions on these curves; for example between temperatures of 230°C and 260°C the degradation of propanoid side chains and forms derivative compounds from the methyl and guaiacol constituents (El Khaldi-Hansen *et al.*, 2016).

TGA can be used to quantify the different components in the plant cell wall using a peak deconvolution method on the derivatives of the TGA curves. The areas under the differential weight loss peaks (derivatives) can be quantified and represent the degradation of lignin, cellulose and hemicellulose (Carrier *et al.*, 2011). The volatile components are usually characterised in an inert atmosphere (Nitrogen or Argon). The combustion processes are calculated using a reactive atmosphere such as oxygen or air (Demirbaş, 2001, Carrier *et al.*, 2011, Cotana *et al.*, 2014, Guo *et al.*, 2016). These deconvolution methods are used to look primarily at the degradation of components in lignocellulosic feedstocks and the range of temperatures which correspond to cellulose, hemicellulose and lignin (Guo *et al.*, 2016). The main degradative temperature regions observed in lignocellulosic compounds are 0–100°C; 100–200°C; 200–470°C; 470–650°C and 650–800/900°C (Ház *et al.*, 2013b). For combustion type reactions in the TGA, the heating rate is an important factor due to the kinetic nature of the reactions. The slower the heating rate, the more time available for the reaction to occur. A faster heating rate gives a greater temperature gradient and as such this gradient needs to be significant or the reaction must

have an increased time to generate the same combustion effects as a slower heating rate (Toloue Farrokh *et al.*, 2018). Differences in the composition of milled wood lignins of Chinese quince (stalks and fruits) have also been shown to have different temperatures for the maximum degradation rates (297°C and 281°C, respectively) with the fruit having a lower thermal stability than the stalk. This is likely to be due to the lignin content of the respective fractions (Yin *et al.*, 2017).

A highly significant linear correlation has been found between the lignin contents of biomass and the higher heating values (HHV) of the same biomass obtained using thermogravimetric analysis (Demirbaş, 2001). The resultant HHVs reported by Demirbaş for a given species are said to be specific for only the samples tested and cannot be correlated to the entire population of a given species (Demirbaş, 2001). The use of the HHVs calculated from lignocellulosic fuel samples has enabled the calculation of lignin content.

4.1.2.4 Pyrolysis Gas Chromatography/Mass Spectrometry for lignin quantification

Analytical pyrolysis involves the rapid pyrolysis of biomass and the measurement of the volatiles produced (Zhan *et al.*, 2017). The temperature dependence of lignin pyrolysis at 400°C, 500°C and 600°C showed that the relative abundances of pyrolysis compounds changed with pyrolysis temperature. An increase of phenols was observed with processing temperature. Polyaromatics also increased on going from 400°C to 500°C but decreased at 600°C. Catechols are not present at 400°C but are found at 500°C with no significant increase at 600°C (Zhan *et al.*, 2017). Pyrolysis Gas Chromatography/Mass Spectrometry (Py-GC/MS) shows that the generation of the lignin sub-units are a result of the cleavage of β-aryl ether bonds (Ház *et al.*, 2013a). Py-GC/MS is a tool which can

be used to measure not only the differences in total lignin percentages based on volatile release during pyrolysis, but also the different chemical components at a monomeric level and to observe compositional differences between different lignin sources, (van Erven *et al.*, 2017). In sapwood, heartwood and bark samples for example, the total lignin has been characterised using the generation of certain peaks from the lignin sub-units on the Py-GC/MS spectrum to calculate the H, G and S relative percentages for each feedstock (Lourenço *et al.*, 2014).

The four methods discussed have been used to quantify plant cell wall constituents; however, the success at quantifying lignin remains questionable. Since lignin is considered to be resistant to both chemical and biological degradation, Hatfield and Fukushima (2005) determined that for both invasive and non-invasive methods of lignin determination, there is no clear preferred method for the accurate measurement of lignin in a biomass (Hatfield and Fukushima, 2005).

Considering that there is no outright method for the best determination of lignin content in a given biomass, the three methods out of the four above which were selected were solid state NMR, Acetyl Bromide Soluble Lignin Assay and TGA. This was to enable a direct comparison with a standardised method (ABSL) to a newly adapted method of solid state NMR and an obscure TGA method for lignin quantification.

4.2 Materials and methods

4.2.1 Materials

Untreated Brewers' Spent Grain (UT BSG), Untreated Oat Husks and a hydrophobic BSG emulsifier (3PHT) were used as feedstocks to investigate the differences between the two methods. These samples and their descriptions are shown in Table 4.2.

Table 4.2: Sample names and descriptions for reference

Sample Name	Sample Description
UT BSG	Milled and dried BSG
UT Oat Husk	Milled and dried Oat Husk
3PHT BSG	BSG which has been high pressure homogenised and then hydrothermally treated post 3 passes through the Microfluidizer
L1	100% coniferyl alcohol
L2	75% coniferyl alcohol; 25% sinapyl alcohol
L3	50% coniferyl alcohol; 50% sinapyl alcohol
L4	25% coniferyl alcohol; 75% sinapyl alcohol
L5	100% sinapyl alcohol

The chemicals used for the Acetyl Bromide chemical assay are: Acetyl Bromide, glacial acetic acid, sodium hydroxide and hydroxylamine hydrochloride and dioxane. Low sulphonate content alkali lignin was used to generate the standard concentration of lignin calibration curve. This was then used as a reference and the absorbance used to calculate lignin percentage. All reagents were purchased from Sigma Aldrich.

4.2.1.1 Using lignin monomers as reference in the all analysis assays

To test the accuracy of the different assays outlined in 4.2.2 and 4.2.3, pure coniferyl alcohol (4-Hydroxy-3-methoxycinnamyl alcohol) and 85–90% pure sinapyl alcohol (4-Hydroxy-3,5-dimethoxycinnamyl alcohol) were purchased from Sigma Aldrich. Model lignin samples were created using different percentages of each alcohol as described below.

Using the monomers to represent lignin tested whether the assays preferentially detected one lignin monomer over another. The influence of the maturity of the biomass and plant cell wall on the concentrations of lignin monomers was also tested. During the four

stages of maturation, it has been shown that the G/S monomeric ratio changes as the amount of lignin decreases (Beaugrand *et al.*, 2004).

4.2.2 ^{13}C CPMAS solid state NMR

Samples chosen in 4.2.1 and 4.2.1.1 were analysed for composition. Differences in lignin percentages were characterised using NMR.

NMR was used to gain an insight into the composition of the BSG instead of conventional wet chemical methods. This was because NMR delivers quick analysis as a bulk measurement on solid samples whilst accounting for changes in mobility at a fundamental level without the need for wet chemical extractions for compositional quantification.

NMR spectra were obtained using solid state ^{13}C cross polarisation magic angle spinning (CPMAS). A ^{13}C CPMAS NMR spectrum of Adamantane was also recorded as an external standard with all subsequent chemical shifts (ppm) for the samples being referenced specifically to the up-field peak at 29.5ppm and operated under identical conditions.

^{13}C CPMAS NMR spectra were recorded on an NMR spectrometer (AVANCE III 600 MHz, Bruker UK Ltd, Coventry, UK) with a narrow bore magnet and a 4mm diameter triple resonance probe. The parameters and conditions used in CPMAS experiments were proton 90° pulse length 3μs, field strength of the proton and spin locking fields during the contact period 83 kHz. The samples were packed into 4mm outer diameter rotors and spun at 10 kHz or 12 kHz. The standard spinning speed was 10 kHz but occasionally a value of 12 kHz was used to ensure any spinning side bands would fall outside the lignin region of interest. For all CPMAS experiments, a contact time of 2ms was used. Recycle delay time was normally 2s, however,

a value of 5s was also used to check for relative changes in the intensity of lines across the spectra if relaxation between scans was incomplete.

Approximately 5k of data points were normally recorded and zero-filled to 16k. The experiments were apodized using an exponential window function with 50Hz line broadening. These data were Fourier-transformed and phased with zero and first order corrections. Baseline fitting routines were applied to all spectra using commercial software (MNOVA, Mestrelab Research S.L., Santiago de Compostela, Spain). Once the data was correctly phased and adjusted to a baseline, the spectra were analysed for the specific peaks and regions associated with the constituents of BSG based on published literature.

4.2.2.1 MATLAB calculation of Lignin percentage

Subject to the limitations and control experiments described and carried out earlier, bulk lignin percentage was calculated using the areas under different regions of the CPMAS spectrum. Having calculated the bulk lignin present in various samples, the relative distribution of lignin within droplets and solid particles was able to be quantified. This enabled an experimental observation of process efficiency to be defined by creating a ratio based on the carbon chemical shifts for the different parts of lignin (the methoxy group and also the aromatic regions in the different monomers). This was conducted in MATLAB (MathWorks, Natick, Massachusetts, USA) using the Trapezoidal numerical integration function having first generated an x/y plot of intensity against ppm shift values and including an appropriate baseline correction. The difficulties of baseline correction for some of the spectra are outlined in 4.3.2. Note: data must first be processed in MNOVA (Mestrelab Research S.L., Santiago de Compostela, Spain) and Microsoft Excel (Microsoft

Corporation, Washington, USA) prior to this analysis. Data processing is described in 3.6.

4.2.3 Acetyl Bromide Soluble Lignin (ABSL) Assay

This analysis was conducted by the Food Composition Section in the Chemistry Department at Campden BRI using an adapted method from a paper on extraction and isolation of lignin. The method, known as the Acetyl Bromide spectrophotometric method, is a standard method for the determination of lignin content (Fukushima and Hatfield, 2001). Biomass samples were heated at 50°C for 2 hours in a water bath in a solution of 25% Acetyl Bromide in glacial acetic acid inside Teflon capped boiling tubes. Lignin standards are prepared using 10mg of low sulphonate lignin which is dissolved in 5ml 80% aqueous dioxane and 0.5ml 25% Acetyl Bromide. They were then heated at 50°C for 30min. Calibration samples for analysis were made using the following components: Glacial acetic acid; 0.3M NaOH; 0.5M Hydroxylamine HCl as well as a known amount of sample taken from the supernatant. Standards and blanks were made by direct addition to the boiling tube. The tubes were homogenously mixed before the absorbance is measured at 280nm in a quartz cell.

Using lignin standards, a reference calibration curve is created based on the absorbance of the supernatant to UV light of wavelength 280nm. This reference curve is subsequently used for the analysis of all feedstocks and model compounds.

The absorbance of the feedstocks is then used to calculate the lignin percentage in the biomass. Equation 4.1 and Equation 4.2

are used to calculate the lignin content.

Equation 4.1: Calculating amount of lignin in mg/10ml for ABSL Assay

$$Amount\ of\ lignin\ \frac{mg}{10ml} = \frac{Absorbance\ of\ samples\ at\ 280nm}{value\ of\ calibration\ line\ gradient}$$

Equation 4.2: Calculating amount of lignin in g/100g for ABSL Assay

$$Lignin\frac{g}{100g} = \left(\frac{Amount\ in\frac{mg}{10ml}}{0.5}\right) \times \left(\frac{16}{Sample\ weight\ in\ mg}\right) \times 100$$

4.2.4 Thermogravimetric analysis for lignin percentage quantification

TGA was used as another quantification technique for the calculation of lignin and was conducted using a Simultaneous Thermal Analysis TGA/DSC 3+ (Mettler Toledo, Leicester, UK) using medium sized (70µl capacity) Alumina crucibles (part no. 00024123) which are capable of withstanding 2000°C.

The method used for this set of research has been described in 3.7 with full processing conditions outlined. This method follows the ASTM D2015 standard test method with lignin chemical analysis following methods in accordance to ASTM D1103-80 and ASTM D1104-56 testing procedures (Demirbaş, 2001). Further details of the method have been outlined previously in Section 3.7.

4.3 Results and Discussion

In this section, reasons for the differences between the Acetyl Bromide Soluble Lignin wet chemical assay and the newly developed ^{13}C solid state NMR method are addressed, as well as intrinsic properties of the methods themselves. The impact of lignin monomeric composition on the ABSL as well as the specific chemical shifts of the monomers on NMR quantification will be considered. Flaws in the methods are shown and investigated to develop a thorough understanding of how quantification can be reliably conducted using both methods.

4.3.1 Model lignin compounds characterised by two different analytical methods (Wet chemistry spectroscopy vs NMR spectroscopy)

During this research, p-coumaryl alcohol (H-lignin) was not investigated due its lack of abundance in nature. Gymnosperms or softwoods are predominantly G unit based with minimal H unit whereas hardwoods are primarily G and S units with trace amounts of H (Boerjan *et al.*, 2003).

For the first time, model lignin compounds have been used on the standardised Acetyl Bromide method and their impact on the results of the Acetyl Bromide assay with regards to quantification of percentage lignin reported. Previously, the Acetyl Bromide assay has been used to quantify lignin in many different feedstocks of both woody and non-woody origin. A standard lignin control of Sigma Lignin was run on the ABSL assay with the result of 98% ± 1% lignin as a calibration.

Figure 4.4 shows the recorded values of lignin percentage calculated as g/100g for each of the alcohol monomer mixtures in the Acetyl Bromide assay. If these alcohol monomers responded perfectly to the assay, then the expected result would be that each monomer would register a reading of 100g lignin/100g sample. As can be seen from Figure 4.4, this is not in fact the case and the response of each monomer to the ABSL assay differs depending on composition of G and S. Therefore, use of the Acetyl Bromide assay suggests that an overestimation of the total lignin content by up to 20% would occur if the feedstock were to be G-rich and an underestimation of the total lignin content by up to 15% would take place if it were S-rich. Examples of the G and S composition in nature are, softwood 90–95 G and 5–10 S; hardwood 50 G and 50 S; grasses 5 H, 75 G and 25 S (Azadi *et al.*, 2013). The total lignin percentages for soft are hard woods are 27–33% and 18–25% respectively (Azadi *et al.*, 2013).

Since the monomeric results on the ABSL assay are statistically different based on the composition of lignin at a monomeric level, the results of the quantified lignin percentages could also be different to the actual percentage. The results of the different monomeric compositions in Figure 4.5 imply that the differences in lignin composition will give different values of lignin percentage in biomass based on their intrinsic monomeric composition. Testing the hypothesis that the ABSL assay was selective for which lignin monolignol was primarily present in the feedstock showed that the assay would overestimate for coniferyl alcohol (G) and underestimate for sinapyl alcohol (S). The difference between 100% G and the 3 compositions 50/50 G/S; 25:75 G/S and 100% S has been shown to be significant at the $P<0.05$ level (de Groot, 1956) (see Figure 4.5). Based on these results, the differing monomeric composition in range of feedstocks implies that the measured lignin percentages could contain large errors.

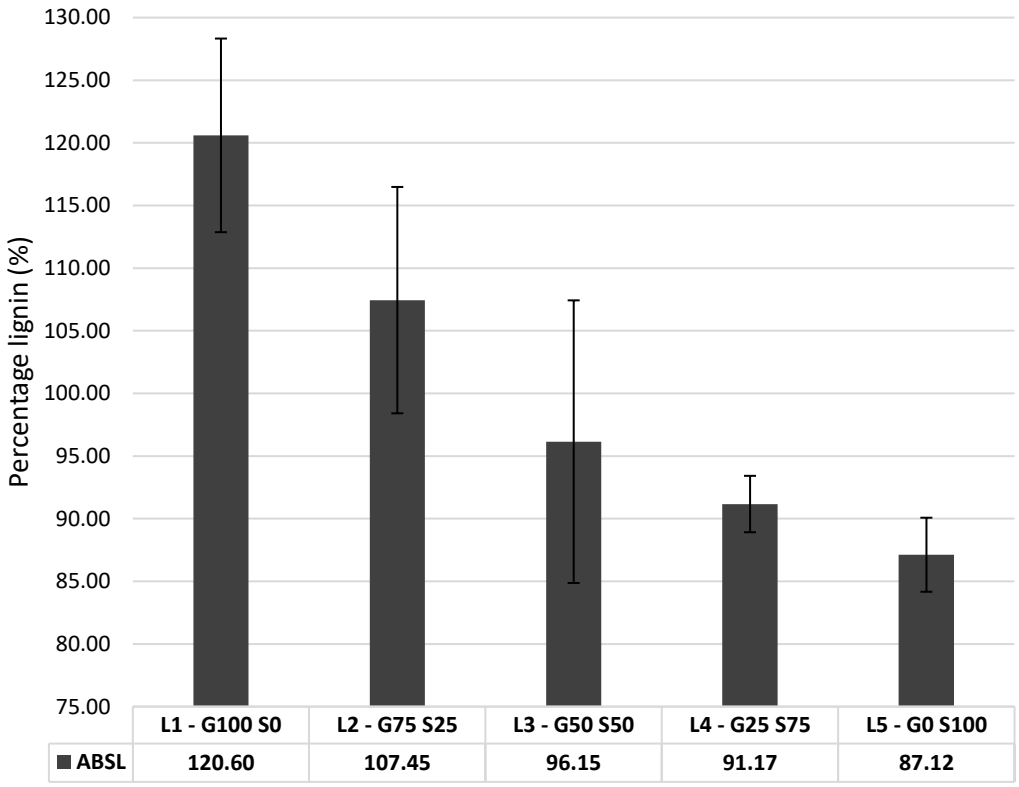


Figure 4.4: Results of ABSL when using mixtures of coniferyl alcohol and sinapyl alcohol mixtures to simulate lignin

Table 4.3: Statistical differences between samples characterised by ABSL when using mixtures of coniferyl alcohol and sinapyl alcohol mixtures to simulate lignin

Method	Tukey's multiple comparisons test	Adjusted P Value
ABSL	G100 vs. G75 S25	0.2747
ABSL	G100 vs. G50 S50	**0.0171**
ABSL	G100 vs. G25 S75	**0.0051**
ABSL	G100 vs. S100	**0.002**
ABSL	G75 S25 vs. G50 S50	0.4037
ABSL	G75 S25 vs. G25 S75	0.1329
ABSL	G75 S25 vs. S100	**0.0484**
ABSL	G50 S50 vs. G25 S75	0.9212
ABSL	G50 S50 vs. S100	0.6009
ABSL	G25 S75 vs. S100	0.9608

The difference between Sigma Lignin used as a standard, and the feedstocks was investigated. Sigma lignin is also the sample usually used as a reference in the assay. The UV light absorbance of the monomers at 280nm compared with Sigma Lignin is shown in Figure 4.5 provides further evidence that each monomer gives different results in the assay. The absorbance of Coniferyl alcohol is greater than that for Sigma Lignin whereas for Sinapyl alcohol it is less. It must also be noted that both Coniferyl alcohol and Sigma lignin have a linear relationship of concentration to absorbance whereas Sinapyl alcohol appears to have a low order polynomial relation. Therefore, the S monomer composition present in the feedstock will further impact on the linearity of lignin percentage as characterised by the Acetyl Bromide lignin assay. The results of this experiment show that based on the response to UV, the greater the amount of G monolignol present, the higher the overall lignin percentage calculated, similar to the results of the overestimation by 20% shown previously.

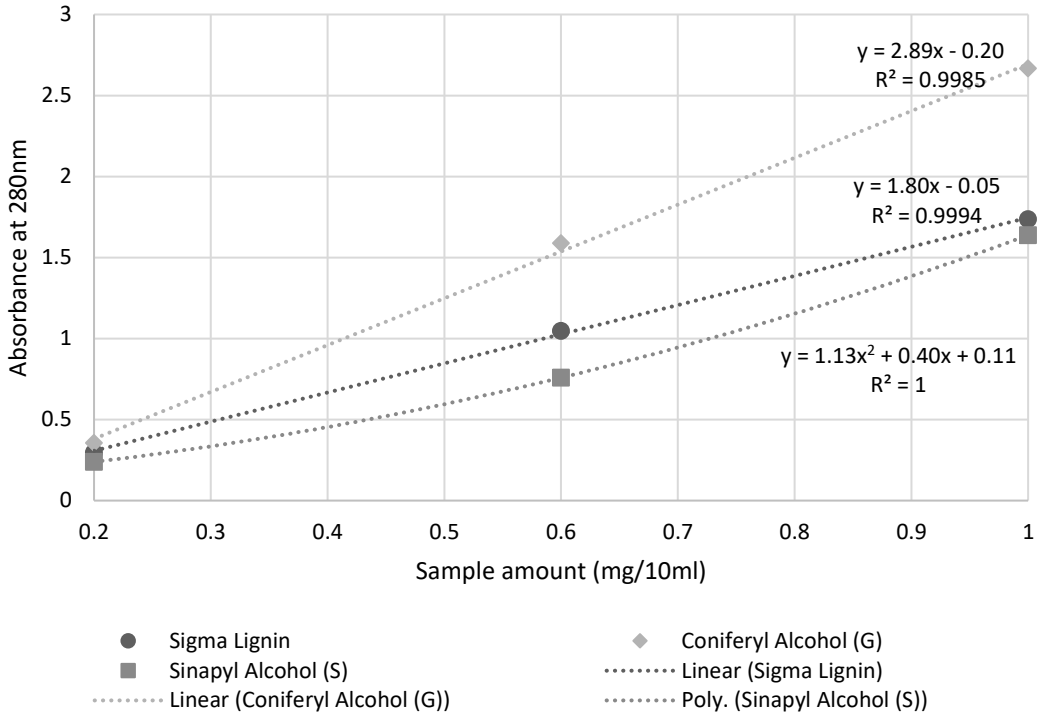


Figure 4.5 Absorbance of monomers at 280nm if treated as Sigma Lignin for standard reference

The results from using monomers to represent lignin have shown that they behave differently based on composition in the ABSL assay but also that there are different chemical shifts observed in the produced NMR spectra. As such, it must be noted that the translation of the work conducted on the monomers alone to represent lignin in the absence of other cell wall constituents may produce different results to when lignin (polymeric macromolecule) is present in a biomass that has not been processed.

In the NMR comparison using the monomers in place of lignin, the main difference from the ABSL method is that NMR records all solid carbon signals in the sample. Subject to the restrictions to be described, the NMR method will measure not only how much lignin is present but also the differences in the composition based on comparing the carbon ratio, if there are any other components to the feedstock. The region of interest (120–165ppm) contains both

the lignin carbons and the signals for the different monomers. The peaks observed are sharp which implies that the carbons present in the monomers all experience the same environment consistent with being in a crystalline form. The spectra of the pure monolignols, coniferyl alcohol and sinapyl alcohol are shown in Figure 4.6A. The main differences were that the peaks for coniferyl alcohol at approximately 148ppm were in the form of a triplet peak (one peak notable peak split into three) whereas the sinapyl alcohol displayed a singlet (peak (one peak notable only). The chemical shifts for the signals appear to be shifted by up to 5ppm when compared with the feedstocks (Figure 4.6B). A greater number of peaks are shown for coniferyl alcohol in the region of 120–165ppm compared to sinapyl alcohol. The presence of significant sidebands between 165 and 220ppm which are a close copy of the pattern between 95 and 160ppm can be seen. These are signals which must be included in the quantification of the percentage of lignin.

In contrast with this, the carbons in the feedstocks are disordered and as such experience multiple environments. This causes shifts and broadening in the peaks resulting in a broad spectrum whose maxima only loosely corresponds to the original peak positions in the monomers. However, the correlation between the peak positions of the monomers and the sigma lignin was closer than with the feedstocks Figure 4.6C. Of course, if samples are 100% G or S then the NMR method will give 100% unless there are contaminants in other regions of the spectrum. In this sense the NMR method does not distinguish between 100% G and S in the way that the wet chemistry method does. This lack of differentiating feature of the method when using known samples does not assist in true quantification. Nevertheless, when using the chemical shifts of the monomers to specifically highlight the regions where these monomers are represented on an NMR spectrum this in turn (in

samples such as Figure 4.6B-C) then a closer to realistic value of lignin percentage could be determined. Using the NMR method, true differentiation between samples could be conducted with regards to the different chemical shifts of the monomers. Using these specific differences between the monomers (assuming some kind of correction can be used due to the shift in peak values likely from chemical anisotropy), realistic G/S ratios could be determined for any biomass sample which contains lignin. This will need further testing to determine accuracy.

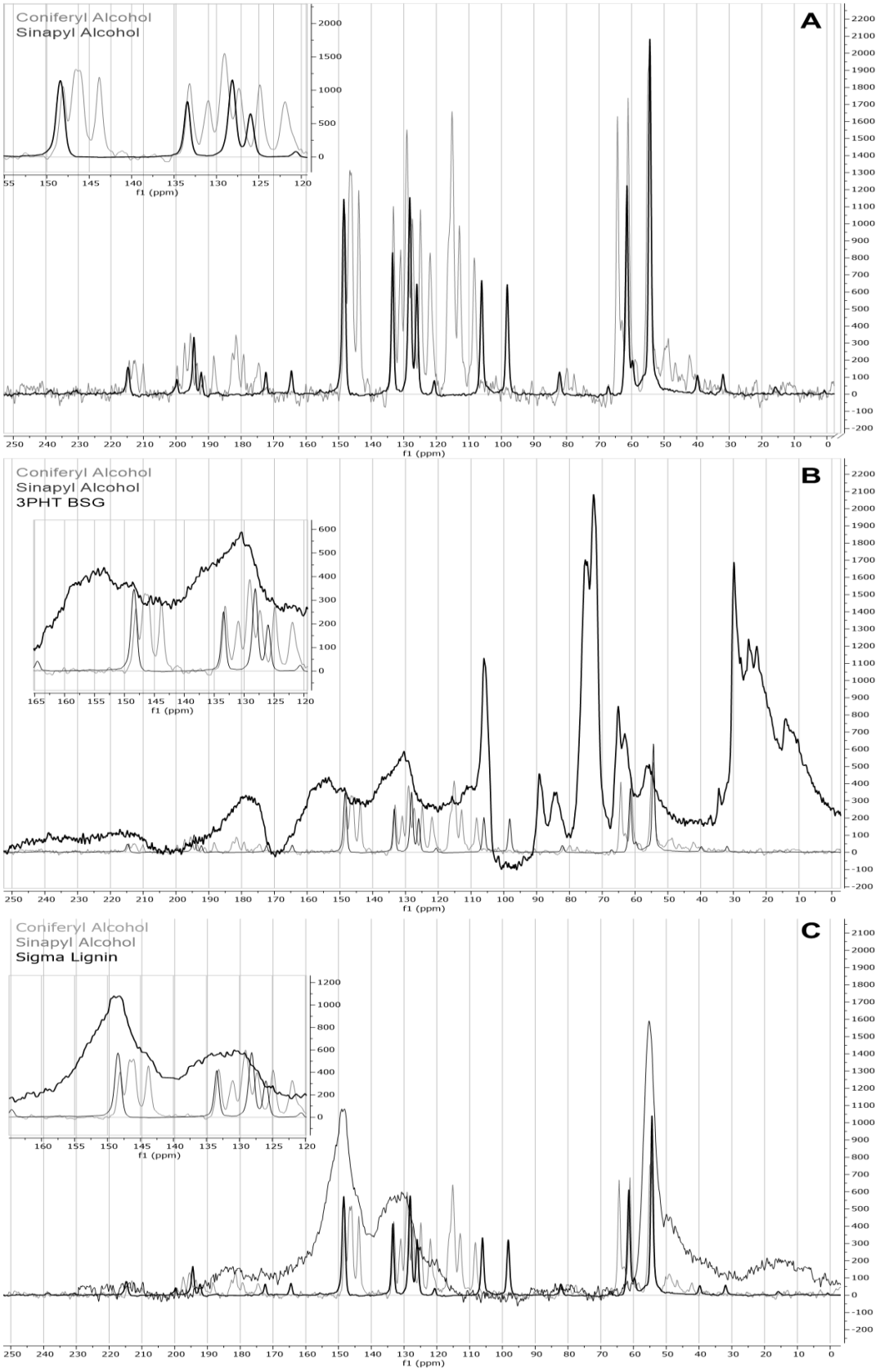


Figure 4.6: NMR spectra showing the peaks for coniferyl alcohol and sinapyl alcohol (A) & the same peaks showing the relation to a 3PHT BSG sample (B) & the same peaks showing the relation to a Sigma lignin sample (C) using the assignment regions in Table 4.1 for reference

The TGA method on the other hand as mentioned previously uses the calculated fixed carbon content to calculate the lignin percentage of the feedstock. Using what has been learned by running the monomers of coniferyl and sinapyl alcohol on the ABSL assay, three different ratios were selected to test on the TGA method. In the same principles as mentioned for all three methods, if the monomers behaved to represent lignin the results should show at 100% for all samples and different ratios. The NMR method is in principle the only method of the three where this is correct since carbon atoms are present in all constituents of the monomers. From Figure 4.7, the main notable result is that the TGA method does not give remotely accurate results close to the expected 100% lignin comparison. For the three samples L1, L3 and L5, the results show that the generated fixed carbon (as a result of removing all degradation matter and combusting the sample) does not give a representative value for the model samples with regards to how much lignin is present. The trend however for the TGA method follows a similar decrease in result to the ABSL method at considerably lower values. For example the L1 or 100% G samples records a higher value of lignin than L5 or the 100% S sample. Unless further testing is conducted to validate exactly what this method calculates then the recommendation would be to find an alternative. The TGA method is used as a comparative method again in 4.3.2 when actual biomass samples are used instead of model compounds.

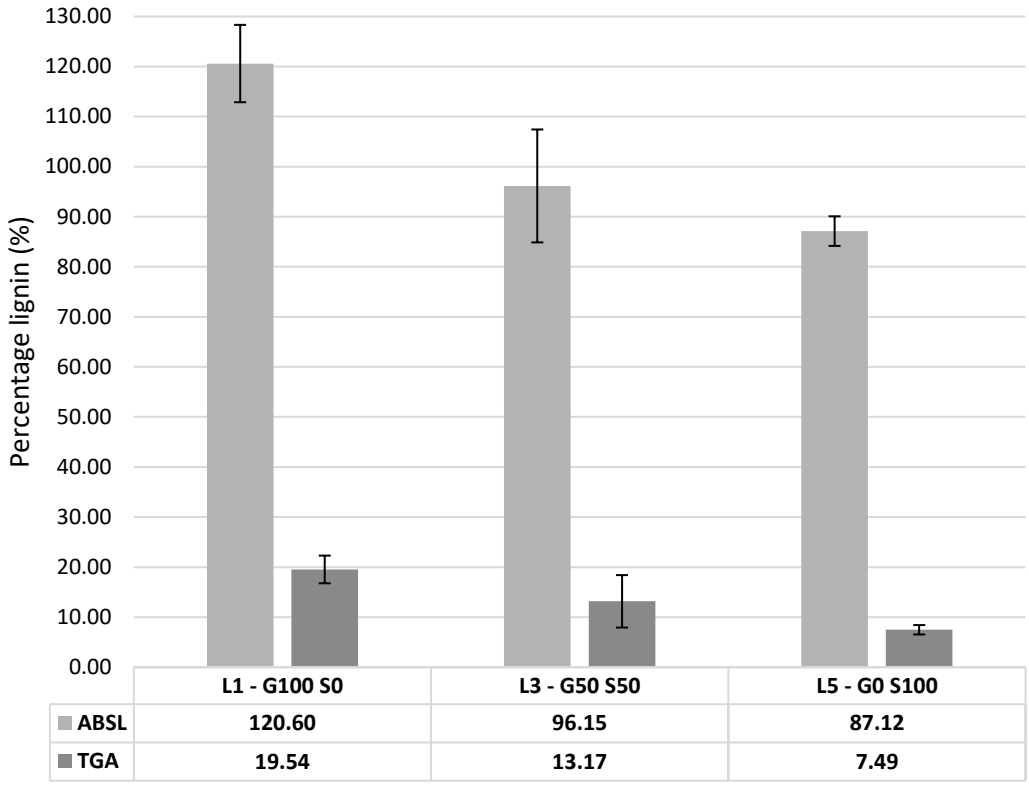


Figure 4.7: Results of TGA method compared to ABSL when using mixtures of coniferyl alcohol and sinapyl alcohol mixtures to simulate lignin

These results are on isolated fractions of lignin and do not take into consideration other factors present in a biomass. These include the covalent bonds linking lignin and hemicellulose as well as hydrogen bonding between cellulose and hemicellulose network of cellulose (Zhang *et al.*, 2011), plant cell wall composition and any additional processing steps which may remove aspects of the cell wall in the feedstock. As such, it is likely that these results for the individual monomeric alcohols could differ slightly to results of actual feedstocks.

4.3.2 Application of the three chosen methods for lignin quantification in three lignin-rich feedstocks

For feedstock quantification a separate calibration curve was created. The absorbance at different calibration points were used to generate a standard calibration line which is used to calculate the concentration of lignin in the biomass. The calibration curve resulted in a sample of 1mg/10ml lignin composition equating to an absorbance value of 2.14 at 280nm.

The different biomasses used were chosen because of their reported literature values for lignin percentage and composition (see Table 2.2, Table 2.3 and Figure 2.8 for more details). BSG contains between 12 and 28% lignin whereas oat husks contain 13.7% lignin (Welch *et al.*, 1983, Lynch *et al.*, 2016). The newly devised method of using NMR spectra to quantify how much lignin is present in the biomass requires initial processing of data. The reason for this is so all spectra have the same correction factors applied to them to minimise error. Triplicate runs were conducted on all biomass samples to estimate variation in the method using material from the same batch of experiments. The relative absorbance of the lignin in the material following the Acetyl Bromide assay were recorded and conducted in triplicate to gauge variation in sample as well as accuracy of the experimental procedure. Using the NMR method, UT BSG, UT Oat Husks and 3PHT BSG were found to contain 7.3% ± 0.4%, 9.5% ± 2.5% and 21.4% ± 0.9% lignin, respectively. This method produces a total percentage lignin based on the specific regions where lignin is visible on the NMR spectra and gives the lignin percentage as a ratio of total carbon in the biomass but does not include the amount of water (3%) or the non-carbon material present in the samples. The Acetyl Bromide assay for the same set of samples showed that UT BSG, UT Oat Husks and 3PHT BSG contains 9.0% ± 0.1%, 13.7% ± 0.2% and 13.9% ± 0.1% lignin,

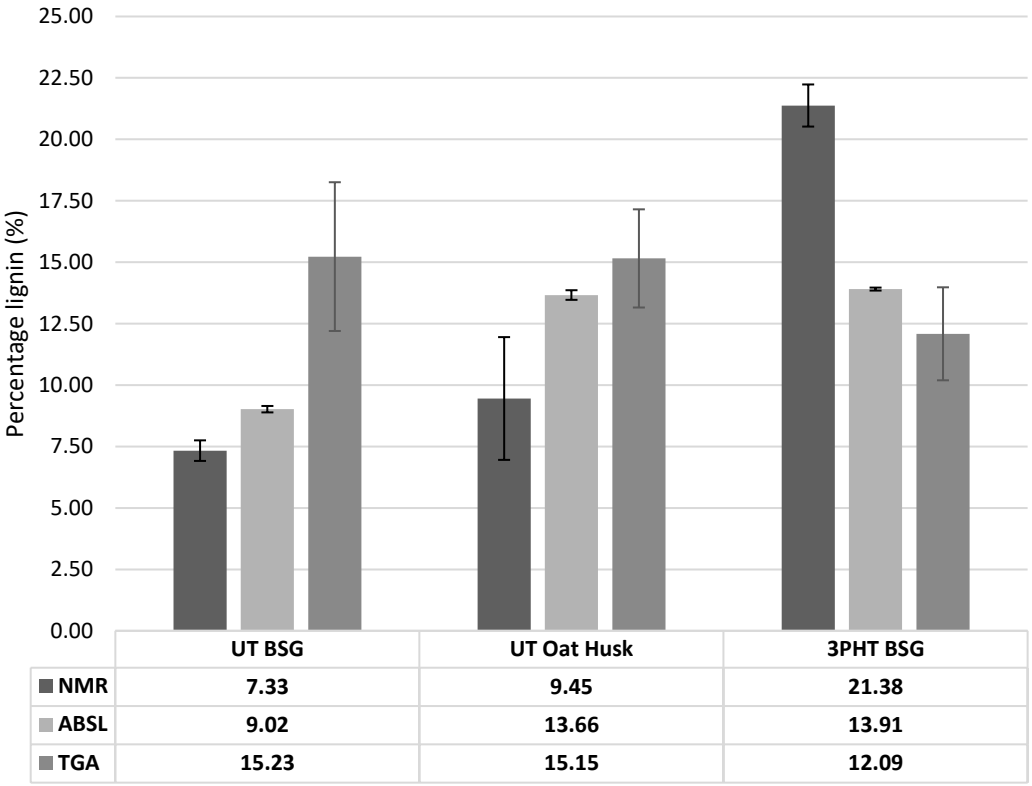
respectively. The differences in values in these three sets of experimental data, shown in Figure 4.8 and Table 4.4 could be for a number of reasons. A standardised one-way ANOVA with Tukey was used to look at the significance between the methods for each of the samples using GraphPad (GraphPad Software, San Diego, USA). The bulk comparison between the methods within the samples shown in Figure 4.8 has demonstrated that between the standardised Acetyl Bromide Soluble Lignin Assay and the newly devised NMR characterisation method, no significant difference is observed for using UT BSG. The TGA method when used on UT BSG shows significantly different results to both ABSL and NMR with a much large value of lignin detected (almost twice a large in both cases). Due to the nature of the TGA method, the lignin is calculated solely on the remaining mass after the process which is deemed to be the amount of fixed carbon.

For UT Oat Husk, different results appear in all three of the methods, but the NMR method delivers statistically different results to both TGA and ABSL (Figure 4.8). Finnish oat husks in literature contain 13.7% lignin (Welch *et al.*, 1983). This was taken as an estimate of the total percentage lignin which might be observed when using these different methods. Although this correlates closely to the ABSL quantified percentage, the difference between a Finnish oat variety and a native oat husk to the British Isles must be taken into consideration. As this was not tested the compositional difference cannot be accounted for but it is hypothesised that there will be some differences just as was shown for the UT BSG which from literature is 12-28% lignin where our batch was not as characterised by these methods (Lynch *et al.*, 2016).

3PHT BSG similarly to UT Oat Husk shows statistical differences between the NMR method and both TGA and ABSL as shown in Figure 4.8. This is likely to be due to the distortions in the spectrum caused

by the presence of mobile species (i.e. the droplets at the surface of the particle). The hypothesis that the droplets on the surface may be mobile is the because, although the lignin-based compound solidified into droplets upon cooling, when they are spun in the NMR the frequency of the spin might cause the sample to behave like a liquid. This has been observed in samples where moisture content is not controlled. An observation from the work presented in 4.3.1 was that the samples upon spinning occasionally changed state from a crystal-like powder at the start of the NMR experiment to a tar-like tacky liquid post experiment when the rotor was removed. Another limitation in the quantification method for lignin lies in the assignment of a reliable baseline. As can be seen in (spectrum Figure 4.9B) there appear to be "pedestals" beneath the peaks in the CPMAS spectra. The CPMAS method seeks to convert the very broad peaks observed in conventional NMR on solids, into sharp peaks with spectral detail. It does this by identifying the sources of broadening and addressing them by a series of manipulations such as spinning at the magic angle and the other methods already described, although this is dependent on the sample and the nature of the broadening. However, if there is a substantial liquid-like component in a sample (as there is in the sample which produced Figure 4.9B) then this will appear as a broad peak underneath the regions of the spectra having intense peaks. This was seen as noted in Figure 4.9B, but not in Figure 4.9A; the latter being a more solid sample. Moisture contents between samples A and B in Figure 4.9 were similar (<5%). As such, the NMR method has been shown to detect that when lignin is relocated to the surface of the particles (e.g. from UT BSG to 3PHT BSG) there is an increase in the amount of lignin present and the NMR method is a quantifiable technique where this can be measured and observed. From this technique as well the differences in the mobility of different lignin fractions can be observed as a result of the chemical shifts for the specific monomers. The references to the

solid sample are due to the droplets on the surface of the 3PHT BSG which are not present in UT BSG. A corrected baseline in the 3PHT BSG sample gave a lignin percentage of 12.17%, however, this baseline removed some of the data meaning this is not entirely accurate. Therefore, a correction factor may need to be included for samples which have slightly liquid components.



	UT BSG	UT Oat Husk	3PHT BSG
NMR	7.33	9.45	21.38
ABSL	9.02	13.66	13.91
TGA	15.23	15.15	12.09

Figure 4.8: Differences in lignin percentage between NMR, ABSL and TGA for three different feedstocks (UT BSG, UT Oat Husk and 3PHT BSG)

Table 4.4: Statistical differences between samples and methods shown in Figure 4.8

Sample	Tukey's multiple comparisons test	Adjusted P Value
UT BSG	NMR vs. ABSL	0.5108
UT BSG	NMR vs. TGA	**0.0037**
UT BSG	ABSL vs. TGA	**0.012**
UT Oat Husk	NMR vs. ABSL	**0.0709**
UT Oat Husk	NMR vs. TGA	**0.0216**
UT Oat Husk	ABSL vs. TGA	0.6112
3PHT BSG	NMR vs. ABSL	**0.0006**
3PHT BSG	NMR vs. TGA	**0.0002**
3PHT BSG	ABSL vs. TGA	0.2305

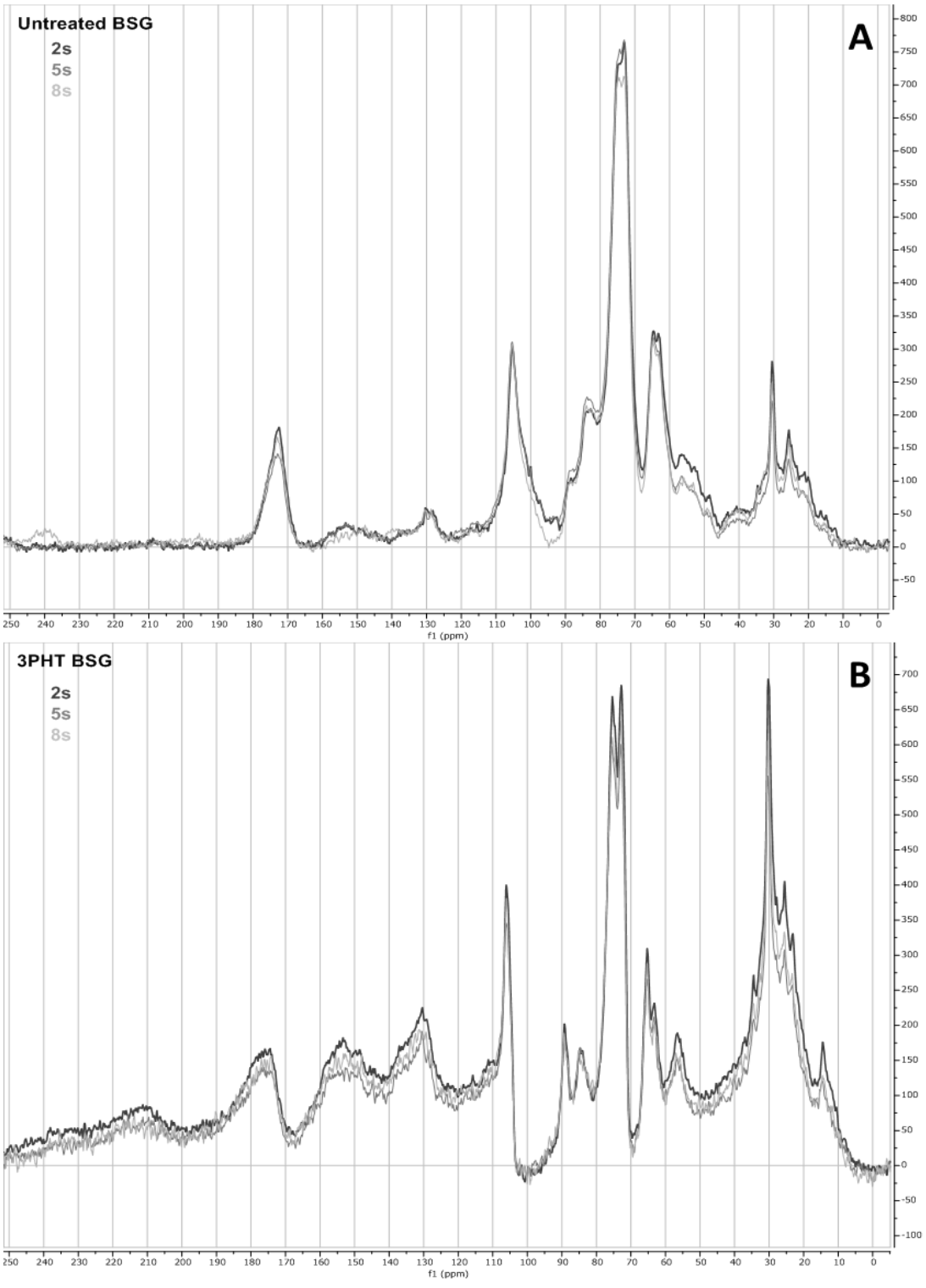


Figure 4.9: NMR spectra showing the comparison between the different recycle delay times for the same sample (A: UT BSG, B: 3PHT-BSG)

Due to the different industrial methods of lignin recovery outlined in 4.1.1, the quantified total lignin percentage will differ based on extraction method and whether it is still in its original form within a feedstock, or whether the feedstock has been processed in some way. Compared to other types of lignin extraction, the Acetyl Bromide assay gives a greater recovery of lignin as reported in the literature (Fukushima and Hatfield, 2004). The Acetyl Bromide assay is currently seen as the standard method for lignin quantification but it has been shown to deliver different results based on the reaction conditions used (Hatfield *et al.*, 1999). If during the preparation of samples during the Acetyl Bromide analysis, factors such as temperature, protein content and centrifugation conditions are overlooked then this will impact of the results of the measured lignin percentage (see Hatfield *et al.* (1999)).

There appear to be numerous drawbacks of using NMR as a method for lignin quantification. Multiple factors can impact on the generated spectra and affect the final quantified lignin percentage. Some of these are spin frequency, recycle delay (RD) times, contact time, moisture content and ionic content. If these are not controlled, then the results will differ not just between samples but also between replicates of the same sample. For example, if a sample was high in phospholipids then the relative carbon ratio observed would give an inaccurate measurement due to the abundance of phosphorous in the sample which would not be picked up by conventional ^{13}C solid state NMR. The dynamics of the cross polarisation magic angle spinning (CPMAS) experiments used in this work must be considered when using the spectra for quantification. When the sample is "spun" (pulses rotating the magnetisation), the nucleus of the atoms does not immediately return to its equilibrium position but in fact relaxes with regards to a specific time constant known as T_1. T_1 differs depending on many factors, specifically: temperature, environment

and whether or not a solvent is present or which solvent is present for example water content of the solid (in solution-state NMR) (Günther, 2013c). Pulse sequences such as the inverse recovery sequence can be used to measure this accurately. In order to truly quantify a measurement, the system must therefore be at equilibrium entirely. Once the system is at equilibrium and other issues accounted for, the measurement of areas under peaks will be quantitatively accurate. A method of assessing whether the system has returned to equilibrium involves making measurements with different recycle delay times which can be done using variable contact times. Relaxation delay (RD) is an important factor to consider since the differences in the relaxation times of hydrogen and carbon atoms differ, with hydrogen atoms returning to equilibrium much quicker than carbon atoms. This is because the RD times and the variation in the sample can have an impact on the individual groups which make up the overall material.

To look at this variation, experiments were conducted at different RD times, 2, 5 and 8 seconds. The corresponding results for both UT BSG and 3PHT BSG are shown in Table 4.5 and Figure 4.9 with the latter showing how the intensities of different regions either increase or decrease slightly based on RD time.

Based on the variation between the samples, specifically for 3PHT BSG, using the standard deviation generated above on the same batch of sample, the differences observed at the different RD times showed that there is no difference in the percentage of lignin calculated through NMR method for that particular sample at different RD times. Depending on the method used to calculate the area under the spectra, this can add error to the data. For example, if a Gaussian fitting of the peaks was used to best represent what is shown then this would change the shape and area of the curve. Due to the function used in MATLAB however, this should be averted

since it uses the Trapezoidal numerical integration function to create an approximation of the integral with the value on the Y-axis (Mathworks, 2005) and no parametric fit is used. Along with the usual limitations of the method, the molecular weight of the subunits (e.g. cellulose, hemicellulose, lignin, proteins, etc.) which are being measured need to be taken into consideration since the number of carbons being measured per subunit will give a different relative percentage if the molecular weight of the lignin is twice that of the cellulose. The spin frequency is another parameter that must be taken into consideration. The spinning sidebands which occur are as a result of the modulation of the signal recorded from the spinning rotor (BRUKER, 2003). These occur where the sample carbons show significant chemical shift anisotropy (for example carbonyls); spinning side bands will be observed at spacings of the spinning frequency, unless spinning frequencies are much higher than the spectral width of the anisotropy. As the anisotropy is field dependent, this is a much greater problem at high fields. At 600 MHz the maximum spinning frequency for a 4mm rotor is of the order of 15 kHz. This means that there is the possibility of a small but significant spinning side band contribution to the area under the peak for the lignin aromatic carbons from the central intense band of the spectrum and possibly from any carbonyl signal present. Once again, the simple experimental method to check this is to conduct experiments at different rotation frequencies (10 and 12 kHz) and determine whether the quantification method returns significantly different results.

This may have an impact for example if the large peak in the cellulose region when spun has side bands which fall in the lignin region (10 or 12 kHz) away from that peak then this could introduce error in the quantification. This should however be observed in the spectrum. The corresponding results for both UT BSG and 3PHT BSG

are shown in Table 4.5. The differences in percentages between the experiments are only marginal so therefore are shown to not directly affect the results with regards to quantification of lignin percentage by NMR.

Table 4.5: Percentage lignin calculated at different recycle delay (RD) time measurements and different spin frequencies

Parameter	UT BSG – total lignin (%)	HT BSG – total lignin (%)	3PHT BSG – total lignin (%)
RD 2s	7.33 ± 0.42	21.15	21.38 ± 0.86
RD 5s	8.07 ± 0.59	-	18.83 ± 1.43
RD 8s	6.74 ± 0.13	-	20.32 ± 2.80
10 kHz, 5s RD	8.34 ± 0.45	-	18.63 ± 1.43
12 kHz, 5s RD	8.13 ± 0.31	-	20.23 ± 0.44

* ”-“ no recorded data

4.4 Conclusions

The Acetyl Bromide Soluble Lignin assay was found to be selectively biased towards coniferyl alcohol (G-monomer) compared to sinapyl alcohol (S-monomer). It cannot effectively differentiate between samples which are compositionally different whilst also providing an accurate measurement for the amount of lignin present in the feedstock. The overestimation of quantified lignin percentage of up to 20% for a feedstock rich in coniferyl alcohol (G) or the underestimation up to 15% for a feedstock rich in sinapyl alcohol (S) shows that the inconsistency in measurement will greatly influence the measured figure. As such this must be taken into consideration and a correction factor introduced to obtain a more precise value. Unless another method to correctly calculate the G/S ratio of the monomers in the feedstock is employed alongside using ABSL, then the ABSL method will only be able to measure an estimate of lignin since no correction factor based on the actual composition can be effectively used.

The TGA method used in this research again did not accurately measure the total lignin present in the feedstock. Since it used the fixed carbon content alone to calculate the lignin percentage, this does not consider the degradation of lignin which occurs over an extended temperature range. Instead, this method uses the differences between two fixed points at the end of the process to determine how much lignin was present. A drawback of using the fixed carbon content solely is that other constituents of the plant cell wall (e.g. cellulose and hemicellulose) also contain carbon atoms and carbon-based structures which in turn will be measured. For characterising lignin, it is recommended that this method is not used and another TGA method potentially through peak deconvolution should be considered.

The NMR method out of the three selected in this research appears to give not only a quantifiable figure of total lignin percentage but also other information about the feedstock can be found. Although there have been some of the drawbacks highlighted (e.g. the impacts of recycled delay time) these have been found to not cause a large effect on the quantifiable percentage of lignin. As such, the newly developed NMR technique for quantifying lignin was found to deliver a quantifiable lignin content but could also be used to identify whether or not a feedstock is rich in coniferyl or sinapyl alcohol based on the chemical shift ppm values. Further investigative work should enable this method to be totally quantitative when a known amount of reference material is used to accurately measure the differences in signal intensities at known chemical shifts. This is turn could then potentially be used to characterise the G/S monomeric ratio in feedstocks enabling a much greater detailed understanding on composition.

There are questions which remain unanswered at present. For example, “what specifically is Acetyl Bromide soluble lignin?” and

"what is its composition?" and "which lignin fractions remain unquantified by ABSL?".

For the NMR method, future work will involve variable contact time experiments and the investigation of the dynamics of the CPMAS experiment to ensure that the behaviour of all components; lignin and other materials present in the feedstock is well defined in terms of all time constants. It would also be desirable to calibrate the system by adding a known reference such as Adamantane (regularly used in solid state NMR and used in all NMR experiments in this thesis as an external standard with all subsequent chemical shifts (ppm) for the samples being referenced specifically to the up-field peak at 29.5ppm) to the sample to enable a more robust quantification procedure for lignin.

Acknowledgments: This research was supported by the Engineering and Physical Sciences Research, University of Nottingham and Campden BRI. We would like to thank in the Division of Food Science, Steve Johnson, and Val Street for technical support and also Dr Clive Ford and Dr Charfedinne Ayed for assistance with the process of the chemical reactions. Professor Steven Walker of Campden BRI was a crucial partner in the commencement of this work.

Author contributions: J.H., K.A.M. and W.M., conceived and planned the experiments. J.H., K.A.M., R.D. and W.M. carried out the experiments and sample preparation. J.H. took the lead in writing the manuscript. All authors provided critical feedback and helped shape the research, analysis and writing of this manuscript.

All authors have approved and are accountable for the final version of the manuscript submitted.

Conflicts of interest: The authors declare no conflict of interest. The founding sponsors had no role in the design of the study; in the collection, analyses, or interpretation of data; in the writing of the manuscript; and in the decision to publish the results.

5 Hydrothermal processing as a route to yielding particulate emulsifiers from Brewers' Spent Grain as a lignin-rich by-product of the brewing industry

James Huscroft,[1,2] William MacNaughtan,[1] Graham Bown,[3] Joanne Gould,[1] Eleanor Binner,[2] Bettina Wolf[1,a*]

[1]Division of Food, Nutrition and Dietetics, School of Biosciences, University of Nottingham, Loughborough, LE12 5RD, UK

[2]Faculty of Engineering, University of Nottingham, Nottingham, NG7 2QL, UK

[3]Campden BRI Limited, Chipping Campden, GL55 6LD, UK

[a]Present address: School of Chemical Engineering, University of Birmingham, Birmingham B15 2TT, UK

[*]b.wolf@bham.ac.uk

Abstract

Particulate emulsifiers are a means of stabilising emulsions with long-term stability of the resultant process-induced droplet size distribution. Any emulsifier applied in foods is ideally clean-label and processing the emulsifier from a by-product of the same industry is a promising possibility. As such, hydrothermally processed ground coffee waste particles have previously been demonstrated to stabilise emulsions. Based on optical microscopy of the processed particles, this functionality was attributed to the relocation of the cell-wall component lignin to the surface of the particles during hydrothermal processing. Brewers' Spent Grain (BSG) was selected as another lignin-rich feedstock. The present study confirms these previous qualitative findings, supported by quantitative evidence. The thermal transition temperature of the BSG, determined via differential scanning calorimetry, was shown to aid in the relocation of lignin generating surface droplets imparted by hydrothermal processing. Increasing processing temperature further, and holding for longer, generated a greater number of surface droplets increasing the yield of the ethanol soluble extract. Utilising high resolution solid state NMR on the extract, the two phenylpropanoids guaiacyl (G) and syringyl (S) were identified. Following hydrothermal processing, their ratio shifted in favour of the more hydrophobic G as a result of physical extraction of S into the hydrothermal liquor resulting in particles being able to stabilise oil continuous emulsions, as opposed to aqueous continuous emulsions only prior to processing. It can be concluded that process induced functionalisation of lignin-rich particulate by-products presents a promising way of creating a range of particulate clean-label emulsifiers.

Keywords: lignin, hydrothermal processing, emulsifier, Pickering emulsions, Brewers' Spent Grain (BSG)

Highlights

- Brewers' Spent Grain particles as particulate emulsifiers
- Oil-continuous emulsions stabilised with hydrothermally processed particles.
- Processed particles feature surface-adhered lignin-rich droplets.
- Solid state NMR evidence for increased proportion of guaiacyl lignin.
- Hydrothermal process temperature linked to thermal transition of lignin.

5.1 Introduction

Lignin is an amorphous polymer found primarily in the secondary cell wall of vascular plants where it provides structural support and rigidity to the cell wall together with cellulose and hemicellulose (Rytioja *et al.*, 2014). It is the second most abundant natural polymer after cellulose (Thakur *et al.*, 2014). Lignin is composed of p-hydroxyphenyl (H), guaiacyl (G) and syringyl (S) units, which derive from the polymerisation of the three predominant monolignols p-coumaryl alcohol, coniferyl alcohol and sinapyl alcohol, see Figure 5.1 for their chemical structure, varying in ratio with plant species (Zhao and Dixon, 2011).

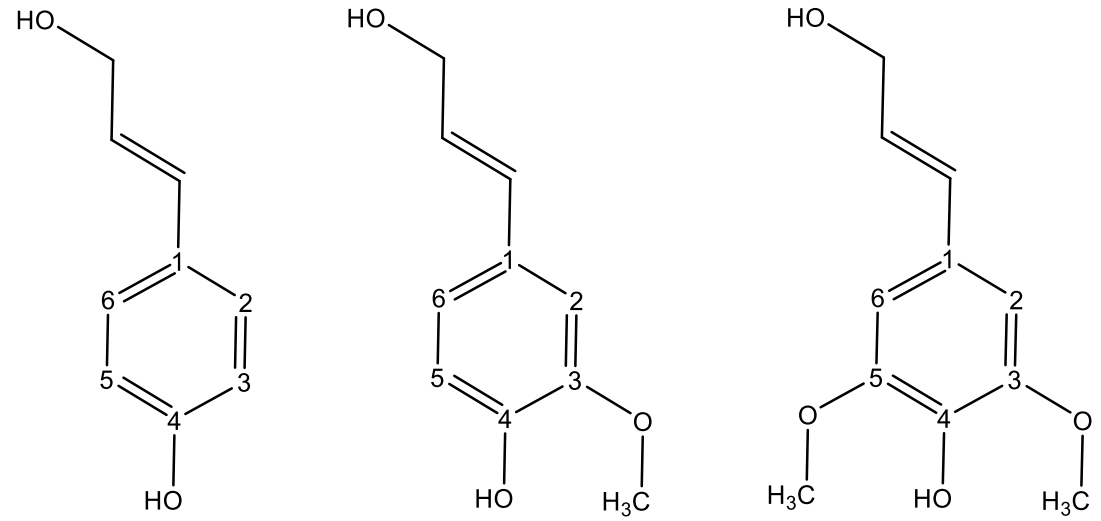


Figure 5.1: Chemical structure of the predominant precursor monolignols p-coumaryl alcohol, coniferyl alcohol and sinapyl alcohol incorporated into lignin in the form of p-hydroxyphenyl (H), guaiacyl (G), and syringyl (S) unit respectively.

The predominantly hydrophobic nature of lignin as a component of food (waste) particles has previously been linked to emulsion stabilisation (Gould *et al.*, 2016). Coffee waste and cocoa particles, recovered from consumer use or as by-product of chocolate manufacture, respectively, and milled, provided long-term stability of oil-in-water (O/W) emulsions through interfacial adsorption (Gould *et al.*, 2013, Gould *et al.*, 2016). The coffee particles were further exposed to hydrothermal treatment, following which these particles also stabilised water-in-oil (W/O) emulsions, although of limited stability as the particles migrated into the aqueous droplet phase over time (Gould *et al.*, 2016). While time of hydrothermal treatment was kept constant (1h), temperature was varied between 150–275°C following literature reports for the treatment temperatures of sugar cane bagasse to remove lignin. Hydrothermal processing is an established de-lignification pre-treatment strategy for plant biomass destined to enzymatic breakdown of the polysaccharide components to small sugars (Garrote *et al.*, 1999, Donohoe *et al.*, 2008, Boussarsar *et al.*, 2009, Ibbett *et al.*, 2011,

Ruiz *et al.*, 2013). Exposing aqueous dispersions of plant biomass to temperatures above the thermal transition temperature of lignin mobilises the lignin and it extrudes from the cell wall matrix towards the surface of the biomass. Once extruded to the surface, it coalesces in the form of surface-adhered droplets upon a reduction in temperature (Donohoe *et al.*, 2008), increasing the hydrophobicity of the particles thus enabling the stabilisation of oil phase continuous emulsions (Gould *et al.*, 2016). At the same time, aqueous soluble biomass is lost from the particle fraction into the hydrothermal treatment medium, increasing the hydrophobicity of the particles.

The performance of particulate emulsifiers is commonly characterised by the contact angle they assume at the oil/water interface (Binks *et al.*, 2010). The direct assessment of contact angles of irregularly shaped particles, such as the BSG particles selected for this study, is of no value. Instead, we have selected to apply high resolution ^{13}C solid state Nuclear Magnetic Resonance (NMR) spectroscopy to assess the composition of the particles to obtain compositional evidence for process-induced increased hydrophobicity. This technique has previously been used to characterise cellulose and pectin components in primary plant cell walls (Foster *et al.*, 1996) and also to analyse the lignin unit (H, G, S) composition of hardwoods (Manders, 1986, Fu *et al.*, 2015). The chemical shifts of constituents of lignocellulosic biomass, specifically cellulose, hemicellulose, lignin (H, G, S units), pectin, protein and lipids, have been widely published (Manders, 1986, Gilardi *et al.*, 1995, Foster *et al.*, 1996, Kono *et al.*, 2002, Sanna *et al.*, 2011, Bernardinelli *et al.*, 2015, Fu *et al.*, 2015).

BSG contains 12–28% lignin (Lynch *et al.*, 2016) and is an abundant by-product of beer production with 20 kg BSG being produced per 100l of beer (Mussatto *et al.*, 2006). In Europe, beer production is

over 52 million kl annually of which 4.3 million kl are produced in the UK (Kirin, 2017). In addition to lignin, BSG contains cellulose, hemicellulose, protein and lipids, in varying quantity depending on batch and origin (Lynch *et al.*, 2016). Other feedstocks could have equally been selected such as apple pomace, potato cuttings and coffee processing by-products, etc. The overall aim of this study was to validate hydrothermal processing as a process tool to functionalise lignin-rich particulate biomass as particulate emulsifiers, substantiated by compositional evidence.

5.2 Materials and methods

5.2.1 Materials

5.2.1.1 Brewers' Spent Grain

A single batch (120kg) of BSG from barley-based wort manufacture was collected from a local microbrewery (Nottingham, UK). It was dried overnight at 105°C using a dry heat oven (Compacta deck oven, Model CPMK4MDU438, Tom Chandley Ltd., Manchester, UK) until constant weight. The same dry heat oven was used throughout this study unless otherwise stated. The dried BSG was milled with a laboratory hammer mill (model 3100a, Perten Instruments, Hägersten, Sweden) fitted with a 0.8mm sieve and operated at 16,800rpm. Finally, the milled BSG was stored in hermetically sealed containers at a temperature of 12–18°C until further use. For the sake of simplicity, the dried and milled BSG is referred to as BSG in the following unless stated otherwise.

5.2.1.2 Other materials

Reverse osmosis water (resistivity of 14.2MΩ/cm^2 referred to as water throughout), to suspend the BSG, low sulphonate Kraft lignin (Sigma-Aldrich, Dorset, UK) as reference, referred to as SL hereafter for thermal property analysis, and ethanol (99.8% purity, Fisher Scientific, Loughborough, UK) to dissolve lignin and other ethanol

soluble components of the BSG. Sunflower oil purchased from a local supermarket served as oil phase for an emulsion assay to test the emulsifying ability of the processed BSG. A reference sample of Adamantane/ $C_{10}H_{16}$ (Sigma-Aldrich, Dorset, UK) was used for the Nuclear Magnetic Resonance (NMR) experiments. SL albeit water-soluble and therefore has been formed via a different extraction route to the extract was selected as a reference for both DSC and NMR as from literature a standardised lignin reference sample was not found.

5.2.2 Hydrothermal process and extraction methods processes

A hydrothermal process was applied to the BSG particles to relocate the internalised lignin to their external surface with the aim of creating a hydrophobic particulate emulsifier. A process set-up previously applied in-house to other lignin-rich feedstocks was employed (Ibbett *et al.*, 2011, Gould *et al.*, 2016) but with slight modification to the sample size and processing conditions. 4g of BSG was suspended through manual mixing in 40mL of water and sealed into stainless steel tubular reactors (length: 150mm tubing excluding end caps, 180mm including end caps and inner diameter: 22mm). Loaded reactors were heated in the aforementioned dry heat oven for 30, 60, 80 or 120min at temperatures between 140–220°C. The time window was chosen in line with previous works (Gould *et al.*, 2016) and the temperature range included 40°C either side of the transition temperature for the lignin component of the BSG, as reported in the results section. At the conclusion of the heating period, the reactors were removed from the oven and cooled for 15min under running cold water (5–10°C) before opening to recover the processed suspension. These particles were used to report the results in 5.3.2.1.

For the emulsions produced in 5.3.2.2, these particles were produced using a Monowave 300 Microwave Synthesis Reactor (Anton Paar, Graz, Austria). The Monowave was programmed to follow the same heating profile as was validated in thermal process trials in the oven using the steel tubular reactors (3.5.1 and 3.5.2).

The suspension was then filtered using a manually devised sieving system which had a pore size of 25μm. The solid residue was dried to constant weight in the oven for 3h at 105°C. Finally, the solids were stored in hermetically sealed containers at 12–18°C until assessment. The liquid filtrate was recovered for subsequent thermal property and chemical compositional analysis. It was frozen at -22°C and then transferred to a freeze drier (Lablyo FIT, FROZEN IN TIME Ltd, York, UK) fitted with a vacuum pump (RV3, Edwards, Burgess Hill, UK) and operating at -50°C and 2mbar pressure. Samples were left for at least 7 days after which they had reached constant weight. Finally, the freeze-dried BSG was stored in hermetically sealed containers at 12–18°C until assessment.

As a final set of samples for analysis, the droplets on the surface of the BSG particles that appeared as a result of the hydrothermal treatment were extracted with ethanol. Ethanol was selected as a good solvent for lignin (Sameni *et al.*, 2017) but it would also co-extract lipids and amino acids, expected to be present in BSG (Nozaki and Tanford, 1971, Holser, 2009, Sameni *et al.*, 2017). 4g of HT BSG particles (defined in Table 5.1) and 36g of ethanol were heated to 80°C under reflux for 1h. The suspension was then filtered under vacuum, utilising the same set up as described above. The ethanol was evaporated from the filtrate by leaving it in a fume cupboard for two days at 20°C. The retentate was dried overnight at 40°C in a convective fan oven (Sanyo Convection Oven MOV-112F,

Sanyo Electric Biomedical Company Ltd, Japan) to remove any residual ethanol.

A summary of the different samples prepared from the BSG is provided in Table 5.1.

Table 5.1: Samples prepared from BSG

Identifier and Sample Names	Description
UT BSG	Dried and milled BSG
HT BSG	UT BSG which has undergone different hydrothermal processing conditions
Extract	Ethanol extracted droplets from the HT BSG

5.2.3 Physicochemical Analysis Methods

5.2.3.1 Particle sizing

The particle size of UT BSG and HT BSG was analysed as the size of particulate emulsifiers is an important factor with regard to the size of emulsion droplets that can be stabilised (Weiss and Muschiolik, 2007). A low angle laser diffraction particle size analyser (LS 13320, Beckman-Coulter, High Wycombe, UK) fitted with an aqueous dispersion cell (Universal liquid module, LS13 320, Beckman Coulter, High Wycombe, UK) was used. The appropriate amount of particle suspension as indicted by the instrument's software was added, duplicate scattering patterns acquired, averaged and analysed by the software based on the Fraunhofer diffraction model. Replicate measurements were conducted, and the results are presented as averaged volume-based size distributions and the $x_{90,3}$. The $x_{90,3}$ was chosen as representative for the largest particle size. Due to the relevance of particle size in relation to emulsion dispersed phase droplet size, the X_{90}, was selected as the point of greatest interest. This is because if 90% of the particles were one order of magnitude less than the targeted maximum droplet size then the emulsion produced will likely have greater Pickering stability (Xiao *et al.*, 2016).

5.2.3.2 Scanning Electron Microscopy

The surface morphology of the BSG particles was visualised by acquiring micrographs on a scanning electron microscope (JSM 6060LV, JEOL, Tokyo, Japan). The particles were placed on SEM stubs with carbotape followed by drying under vacuum before being coated with gold sputtering (Leica SCD 0005, Leica Microsystems, Milton Keynes, UK) and transferred to the SEM stage for imaging.

5.2.3.3 Differential Scanning Calorimetry

The thermal properties of BSG particles were analysed with differential scanning calorimetry (DSC) to obtain transition temperatures primarily related to their lignin component. Approximately 10–20mg of a given sample were placed into a pre-weighed stainless steel pan, which was then sealed with an O–ring, weighed and introduced into the furnace of a DSC (DSC823^e, Mettler Toledo GmbH, Greifensee, Switzerland) equipped with a sample robot (TS0801R0, Mettler Toledo GmbH, Greifensee, Switzerland). The atmosphere in the furnace was maintained with an in-house designed nitrogen purge system and an external cooling unit (TC100, Peter Huber Kältemaschinenbau AG, Offenburg, Germany). An empty pan was used as reference. Three replicate samples were analysed while ramping temperature from 20–220°C at a rate of 5°C/min. Low sulphonate Kraft lignin was analysed as a lignin reference. Characteristic temperatures (onset and peak) of the thermograms were manually extracted.

5.2.3.4 Compositional analysis using ^{13}C Solid State Nuclear Magnetic Resonance

The ^{13}C NMR CPMAS method used was identical to that described earlier (Chapter 4) without the use of the lignin percentage quantification.

5.2.4 Particle functionality assay

Particle functionality, i.e., whether the particles were predominantly hydrophilic and would stabilise O/W emulsions, or whether they were predominantly hydrophobic, therefore stabilising W/O emulsions, was assessed by an emulsion assay following published protocol (Gould *et al.*, 2016). Assay sample size was 50g or 100g depending on the quantity of particles available from the hydrothermal process. 4g particles/100g emulsion were applied throughout as initial trials with UT BSG revealed that stable emulsions were formed. 24g or 48g of water was placed into a glass vial, 2g or 4g of particles layered on top followed by 24g or 48g of sunflower oil. Finally, the processing head of a higher shear overhead mixer (T25 Ultra-Turrax, IKA-Werke GmbH & Co. KG, Staufen, Germany) was lowered into the glass vial and the mixture processed for 1min at 24,000rpm then 1min at 16,000rpm.

Overall gravitational stability was observed visually through the development of phase boundary layers in the storage vials. Emulsion microstructure, and the microstructure of the BSG particles, was imaged with a digital inverted microscope (EVOS f1, Thermo Fisher Scientific, Loughborough, UK) in bright field and fluorescent mode. Glass slides were prepared for the O/W emulsions and the particles, whereas the W/O emulsions were imaged on PTFE slides to prevent coalescence of the hydrophilic droplets phase with the hydrophilic glass. No cover slip was used. Imaging in fluorescent mode with the microscope specific DAPI light cube (340–380nm) allowed identification of lignin as it autofluoresces when excited at 357nm (Vavrčík *et al.*, 2008).

5.3 Results and Discussion

5.3.1 Thermal properties and composition

The aim of this study was to prepare hydrophobic BSG particles through the relocation of lignin from the plant cell walls to the surface of the particles. This relocation can be affected by heat-induced mobilisation of the lignin in aqueous suspension. To establish the required minimum processing temperature, the thermal properties of UT BSG were characterised by DSC in comparison to the reference sample SL. The thermograms are reproduced in Figure 5.2 and the characteristic onset and peak temperature values around the lignin transition region, are reported in Table 5.2. The thermal transition of UT BSG is shifted to higher temperature due to the lignin being bonded to cellulose and hemicellulose within the cell wall matrix and when heated above this temperature the lignin undergoes a physical transitions induced by heat and becomes mobile such that it can start to migrate through the plant cell wall towards the surface of the particles (Donohoe *et al.*, 2008, Chen, 2014). From these data, the temperature range of 140–220°C was selected as hydrothermal processing conditions, corresponding to roughly ±40°C of the peak temperature. It must be noted that the transition temperatures characterised by DSC are in fact the mid-point. This was selected as it was the peak change in heat flow.

Table 5.2: Approximate Onset and Peak temperatures for different lignin samples characterised by DSC corresponding to the arrows in Figure 5.2

Sample	Onset Temperature (°C)	Peak Temperature (°C)
UT BSG	140	175
HT BSG – 200 °C 90 min	125	160
HT BSG Extract	100	135
SL	100	138

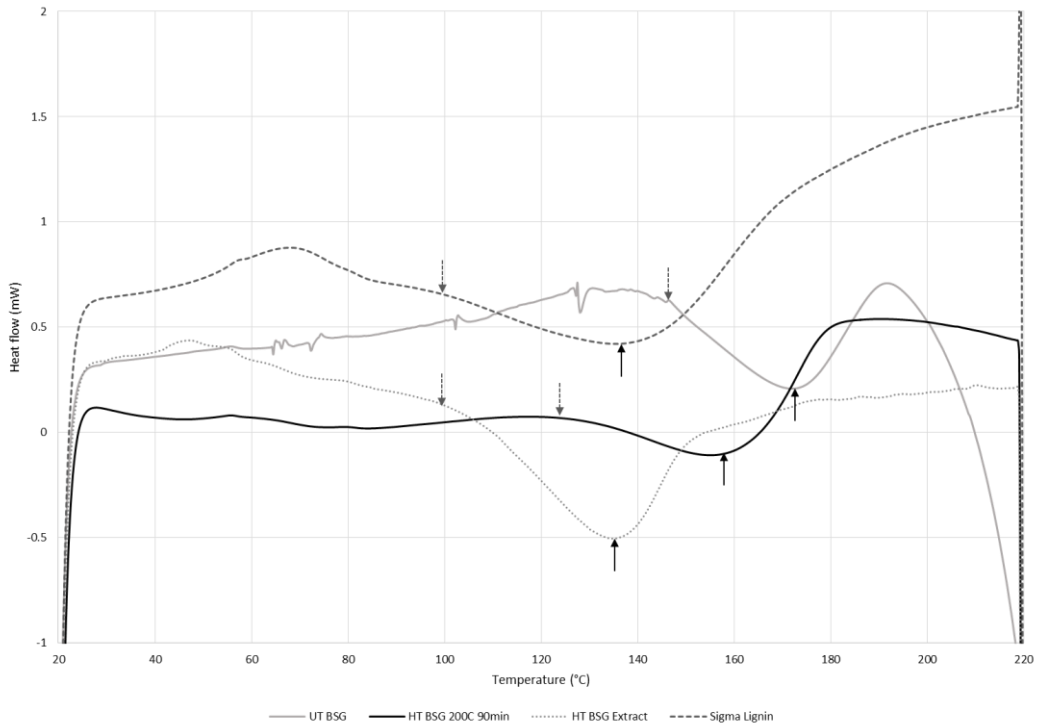


Figure 5.2: DSC thermogram of UT BSG (solid light grey), HT BSG 200°C for 90min (solid dark grey), HT BSG Extract (dashed light grey) and SL (dashed grey). Arrows: Solid black arrow is peak temperature and dotted grey arrow is onset temperature

The mechanism of how lignin changes state and migrates through the cell wall structure has been mentioned previously with Figure 2.12 showing what was proposed by Donohoe *et al.* (2008). Upon being heated above the transition temperature, following the collapse of cellulose microfibrils, lignin migrates through the cell wall structure and by thermal expansion goes from once internalised embedded in the cell wall to being relocated to the surface of the particle in the form of droplets. The diffusion of lignin through the particles appears to be a slow process with being not only caused by the temperature but also associated with time of the reaction (Figure

5.6 shows the formation of droplets relating to time and temperature). The NMR spectrum of the SL is shown in Figure 5.3A; the main identification being that it is comprised of G-lignin, based on the chemical shift of the carbon atoms, 148ppm is the primary peak associated with G-lignin as assigned from literature (Manders, 1986). This lignin standard is a lignosulphonate extract and can usually be dissolved in dilute alkali, water or salt solutions. The method of extraction has been shown to impact on the hydrophilicity and hydrophobicity of the lignin since Organosolv lignin is soluble in methanol, ethanol and DMSO, whereas alkali or lignosulphate lignin is soluble in dilute alkali or water. Soluble lignin has an amorphous structure (Chen, 2014). In comparison to UT BSG as determined by NMR shown in Figure 5.3B, SL differs since only lignin is present in its composition whereas, as expected, UT BSG was composed of cellulose, hemicellulose, pectin, lignin, lipids and proteins (Lynch *et al.*, 2016). SL, a water-soluble variant of lignin has a transition temperature of 138°C (Figure 5.2, Table 5.2). Since this lignin is water-soluble where the extract is not, this could mean that an entirely different fraction of lignin is present in the droplets.

Of the hydrothermally treated samples, the sample showed clearly recognisable lignin containing droplets on the surface (200°C, 90min), was selected for thermal and compositional analysis. The corresponding SEM images are presented below. The thermogram in Table 5.2 and the characteristic temperatures reported in Table 5.2 indicate that the thermal transition has shifted to lower temperature, even as low as the reference SL. The lowered transition temperature range supports the SEM evidence that the hydrothermal treatment liberated the lignin from the cell wall matrix. Some lignin is likely still present in the cell wall matrix, but this is yet to be confirmed.

The composition of the chosen hydrothermally treated sample in Figure 5.4A differs slightly to the UT BSG presented in Figure 5.3B.

Visually assessing the NMR spectra, lignin as a proportion of the material has increased whilst the cellulose region (60–110ppm) and some of the pectin and protein peaks associated with carbonyl groups at 180ppm has decreased. This is likely being removed, during the hydrothermal treatment, to the water fraction but further analysis is required to understand exactly to where this material has been relocated (see Figure 5.5). Another alternative that the findings are a result of cell wall degradation, β-elimination of pectin or even the early onset of hemicellulose pyrolysis around 220°C (Yang *et al.*, 2007).

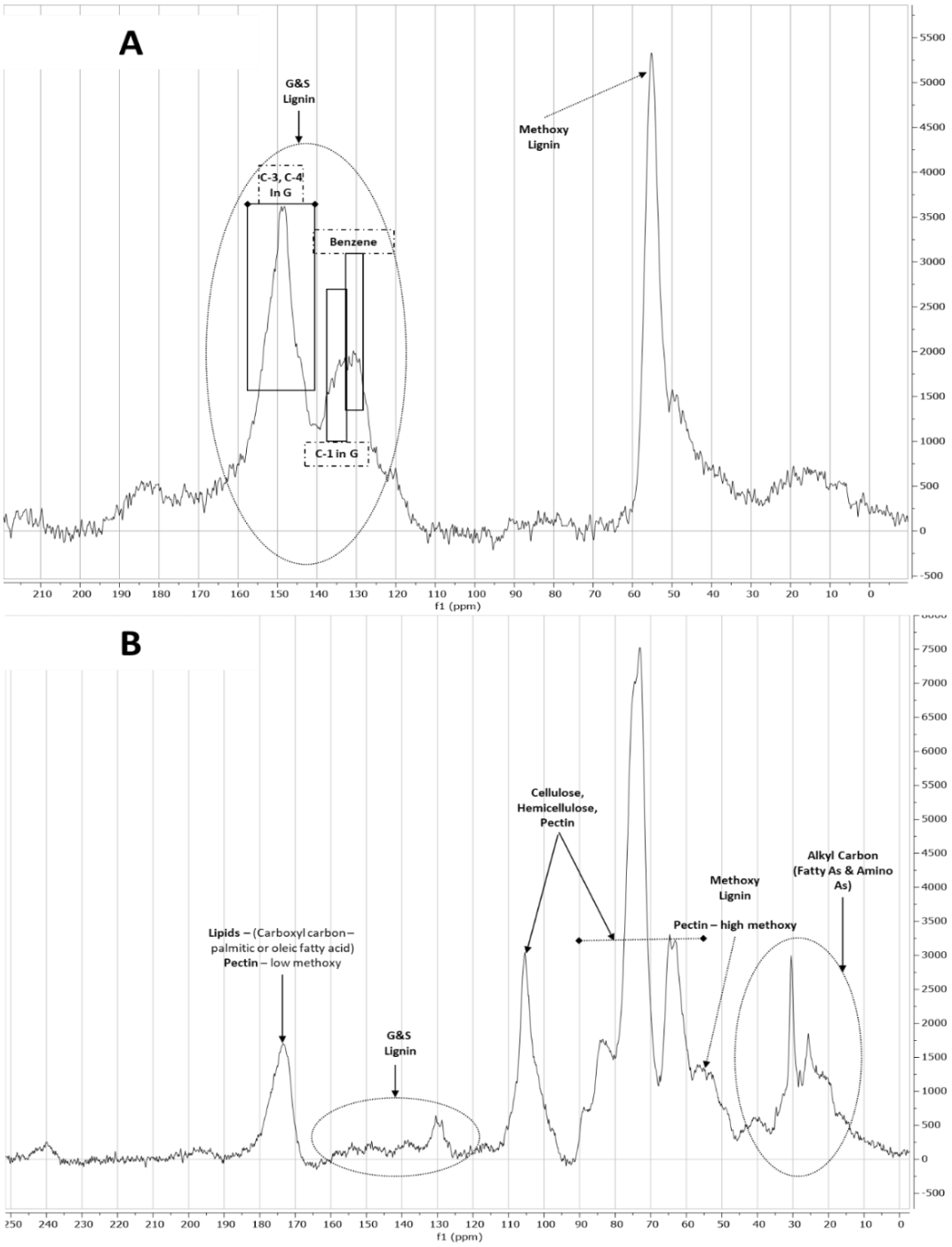


Figure 5.3: ^{13}C SS-NMR spectrum of A) Sigma Lignin (SL) and B) untreated and milled BSG (UT BSG)

The isolated droplets from the sample through ethanol extraction, termed extract, exhibit a different transition temperature to that when just relocated to the surface of the particles. As shown in Figure 5.4B, the composition of the extract at the surface of the particles contains lignin, lipids and protein. The transition temperature of the extract is 135°C (Table 5.2). It is hypothesised

that this fraction of lignin specifically might be a lower molecular weight fraction, which has been mobilised first. Figure 5.4B shows that the extract contains lipids, proteins and, most importantly, lignin. This confirms that the lignin in BSG is relocated to the surface as a direct consequence of the hydrothermal process. Since the droplets adhere to the surface of the particle and do not dissolve in water, they are in fact hydrophobic. The specific type of lignin stems from the monomer coniferyl alcohol, which corresponds to the monomeric component for G-lignin. Figure 5.4C shows the specific chemical shifts of the different carbon atoms around the benzene ring (Manders, 1986). In contrast to SL, the extract differs by being water insoluble, showing that the extract produced is more hydrophobic than the SL. The main peak occurs at 148ppm, which corresponds to carbons 3 and 4 on the benzene ring where at carbon 3, the carbon is o-alkylated by a methyl group as shown in Figure 5.1. The supernatant collected from the 200°C for 90min sample, was freeze dried and also characterised using NMR. Figure 5.5A shows that during the hydrothermal treatment certain components of the plant cell wall become water soluble, namely: fatty acids, amino acids, pectin, some cellulose and some lignin. Upon close inspection when focussing on the lignin region specifically (Figure 5.5B), the specific type of lignin stems from the monomer sinapyl alcohol, which corresponds to the monomeric component for S-lignin. Figure 5.5B shows the specific chemical shifts of the different carbon atoms around the benzene ring (Manders, 1986). Another observation from the NMR spectra shown in Figure 5.3B and Figure 5.4A is at the chemical shift between 80 and 90ppm. This specifically corresponds to the crystallinity index of cellulose using C4 as reference (Park *et al.*, 2009, Park *et al.*, 2010). As a result of hydrothermally processing BSG and converting the feedstock from UT BSG to HT BSG, it appears that the crystallinity of cellulose has increased whilst the amount of amorphous cellulose has decreased.

This is shown by changes in the heights of the peaks between 80 and 90ppm with the peak closest to 80ppm representing the amorphous nature of cellulose at C4 whilst the peak closest to 90ppm represents the crystalline nature of cellulose at C4 (Park *et al.*, 2009, Park *et al.*, 2010). Changes in the crystallinity of cellulose could be a consequence of the hydrothermal treatment whereby plant cell wall collapse occurs which enables to thermally transitioned lignin to migrate through the structure to the surface of the particles.

The separation of the different fractions into the droplets (ethanol soluble extract) and the water soluble fraction suggests that the separation of lignin from the plant cell wall could occur at different times and rates. Separation of the different monomers which make up lignin could be as a result of temperatures at which they undergo their physical transition and because of their different physical properties (e.g. hydrophobicity). From the online chemistry database, coniferyl alcohol (G-lignin) has a melting point of 74°C (NCBI, 2018a), whereas sinapyl alcohol (S-lignin) has a melting point of 61–65°C (NCBI, 2018c) and p-coumaryl alcohol (H-lignin) has a melting point of 213.5°C (NCBI, 2018b). Therefore, as a result of the differing number of methoxy groups between G and S (1 and 2, respectively) as well as the differences in melting point this suggests that both compounds will migrate and relocate at different temperatures. The removal of S-lignin from the plant cell wall to the hydrothermal water would suggest that as a result of the lower melting point temperature that this will migrate first and will ultimately be removed from the material which in turn will lower the molecular weight of the lignin and concentrating up the amount of G-lignin present in the plant cell wall. This in turn links with the result of the thermal transition temperature of the HT BSG extract being lower than the transition temperature of the lignin in UT BSG (135°C vs 175°C, respectively), suggesting that as a result of removing S-

lignin from the particles to the hydrothermal water and the extract no longer being bonded with other plant cell wall polysaccharides in the cell wall matrix the transition temperature decreases.

Combining inputs from the micrographs and NMR spectra, the relocation of G-lignin to the surface of the particles from the internal structure implies a change in the molecular weight of the overall lignin structure since at least one of the monomers is changing location, but this is yet to be confirmed. Following the ethanol extraction to remove the droplets and other ethanol soluble components from the particles, the transition temperature of the extract was found to be 135°C (Table 5.2).

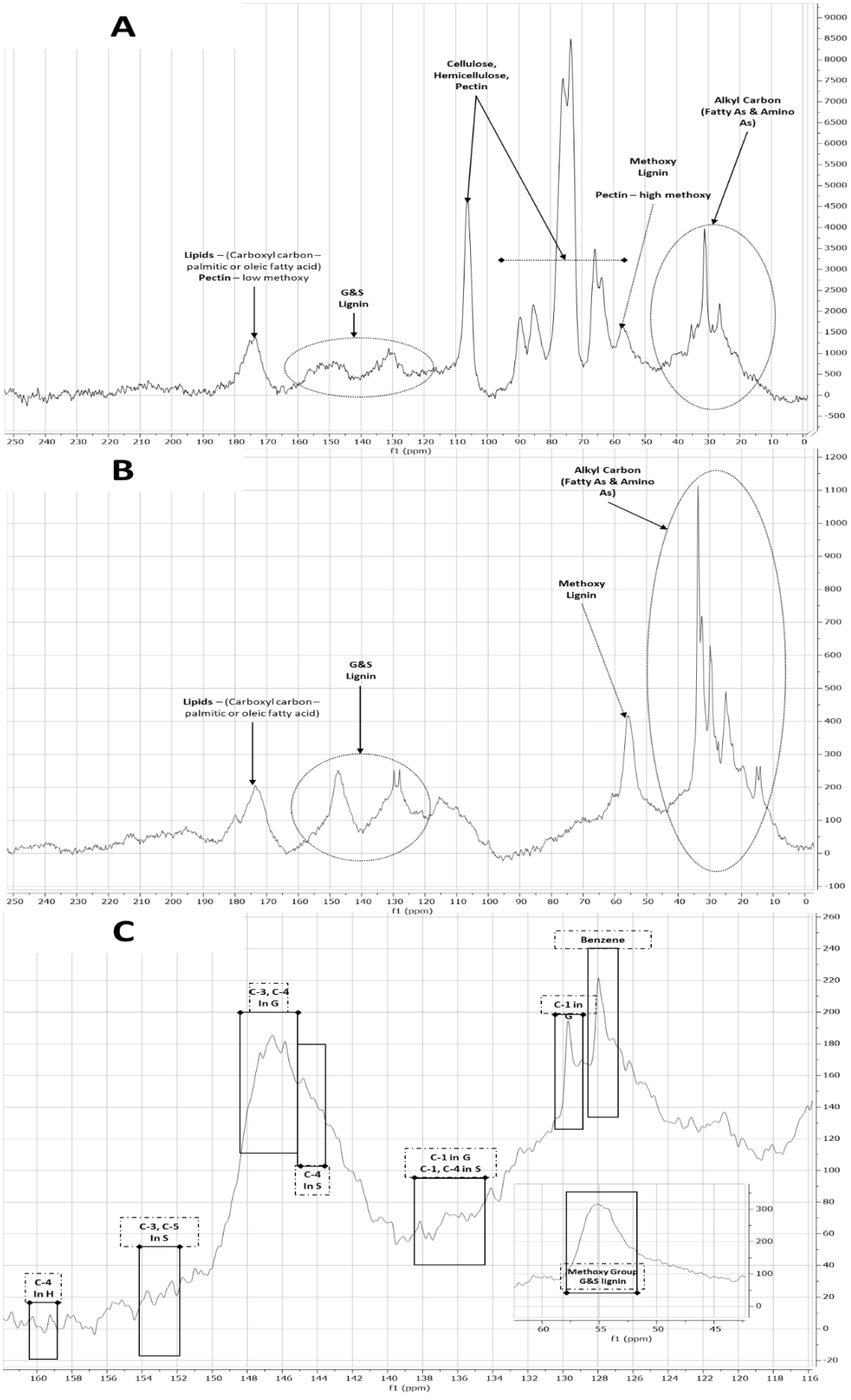


Figure 5.4: [13]C SS-NMR spectrum of: A) HT BSG – 200°C for 90min BSG; B) Extract from HT BSG; C) Extract from HT BSG (lignin region)

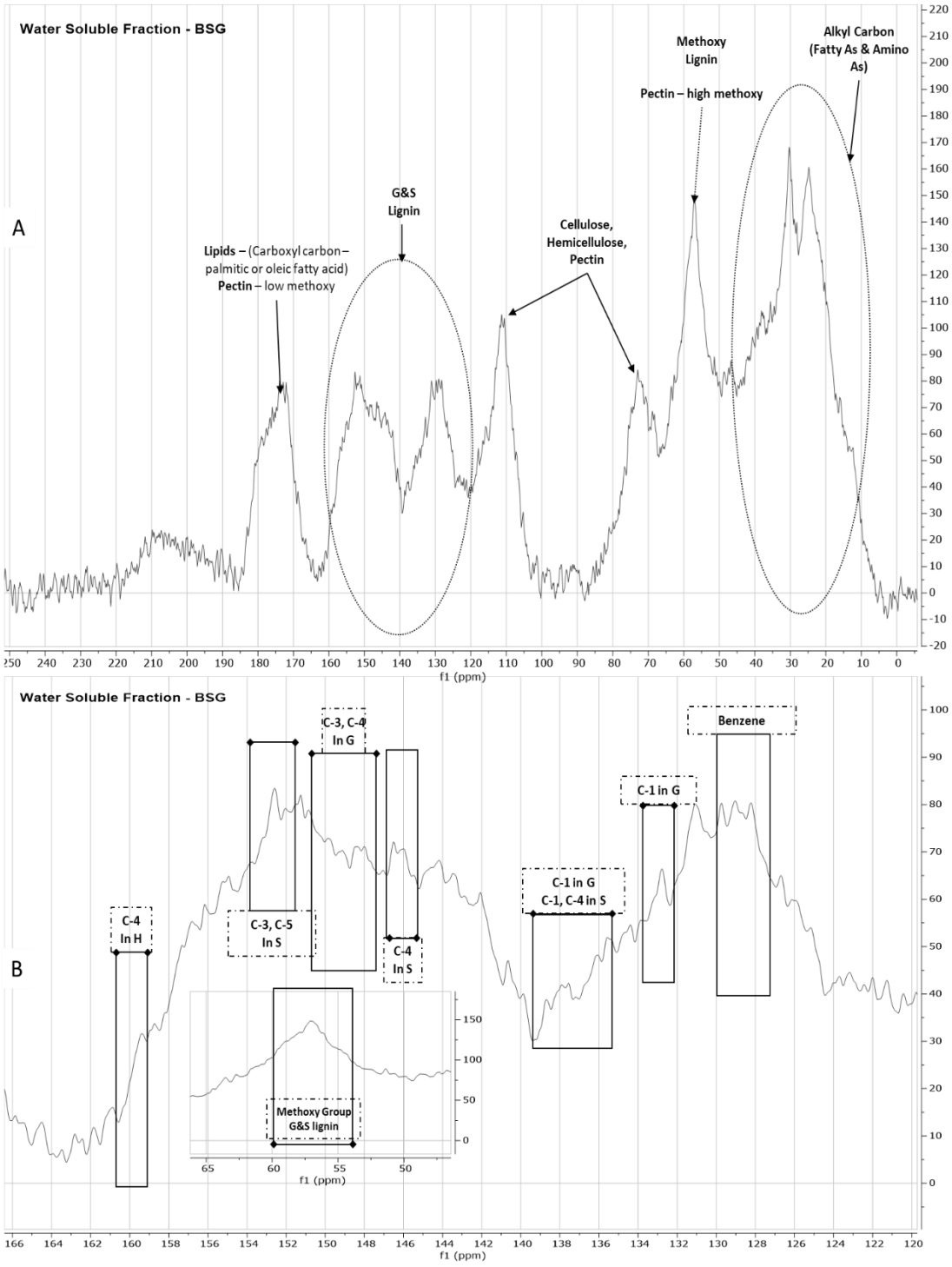


Figure 5.5: 13C SS-NMR spectrum of: A) HT BSG – 200°C for 90min hydrothermal water supernatant; B) HT BSG – 200°C for 90min hydrothermal water supernatant (lignin region)

When comparing the transition temperature of the untreated BSG to the micrographs of the hydrothermally treated samples in Figure 5.6, it is confirmed that that major transitions occur at or above the 180°C processing temperature. Below this temperature, no major

physical changes appear to occur however, above this temperature, time plays a role in the formation of the droplets and subsequently the changes in the material properties and physical characteristics. As such the droplets themselves as they were once embedded in the plant cell wall structure prior to being relocated and forming droplets now appear to become surface active and this is hypothesised to change the hydrophobicity of the particles.

Based on the composition of the untreated BSG due to the lack of droplets present at the surface of the particles, it is hypothesised that this will be a hydrophilic particle that will stabilise oil-in-water emulsions. The reason for this hypothesis is that lignin itself is a hydrophobic polymer and if a greater proportion of lignin is present at the surface (in this case as a result of relocated droplets) then the hydrophobicity of the surface itself might change. Although the particles are hypothesised to be interfacially surface active in their stability of o/w emulsions, another factor needs to be considered. This is that the particles are in fact just water absorbers. Since the UT BSG particles are in fact dried matter occurring from drying spent grain which has been removed after the mashing step in beer production, when the particles are added during emulsion preparation, they could in fact just be rehydrated and then stabilising the dispersed phase droplets. Additionally, as the particles are milled, the generation of regions of hydrophobic lignin could be the extra requirement which enables the stabilisation of oil dispersed phase droplets with the particles residing in the water.

In contrast, BSG that has been hydrothermally treated is hypothesised to be increasingly hydrophobic due to the mobilisation of lignin to the surface of the particles. Due to surface droplets, the particles are hypothesised to reside predominantly in the oil, but areas of the surface not coated in droplets could potentially be hydrophilic in property and as such enable the stabilisation of water

dispersed phase droplets. Therefore, certain samples, namely; 200°C for 90min; 200°C for 120min; 220°C for 120min are hypothesised to be the most hydrophobic due to the presence of now confirmed lignin-rich droplets and in turn are expected to stabilise water-in-oil emulsions.

It must be noted that when using the 4g sample of untreated BSG as the solids in the hydrothermal treatment, the total dried solids at the end of the process equates to 2.5g dried powder. Subsequent moisture content measurement found this dried powder to be <5% wet weight basis (wwb) as confirmed on the hydrothermally treated BSG sample processed at 220°C for 120min.

5.3.2 Surface morphology and emulsion functionality

5.3.2.1 Surface morphology and particle size

Numerous temperature and time combinations were trialled, but 6 specific crucial samples were selected for comparison.

In the SEM images presented in Figure 5.6, the surface morphology for various HT BSG particles can be observed. The chosen samples for comparison were UT BSG (a) and 5 HT BSG samples, namely, time and temperature conditions which were 140°C, 30min (b); 180°C, 120min (c); 200°C, 60min (d); 200°C, 90min (e); 220°C, 120min (f).

UT BSG was used as the basis for the observations for changes to the material through hydrothermal processing. UT BSG has a relatively smooth and flat surface with some sharp edges which were likely caused from the abrasive nature of the milling process. Processing at the onset transition temperature (140°C) for BSG lignin (sample b above) indicates that, minimal structural changes occur to the particle compared to UT BSG with the important observation being that no lignin droplets have been formed. There

has also been no change in the size of the particles as a result of the hydrothermal treatment with these data not shown.

At 180°C, or slightly above the characterised transition temperature, after 120min the surface changes to a smoother form causing an effect on the physicochemical properties of the material, however there are still no visible droplets. At 180°C, increasing the process time caused a larger the impact on the visible surface properties and structure of the material (further SEM micrographs shown in Appendix A1). Following the proposed mechanism of Donohoe *et al.* (2008), as 175°C was found to be the mid-point transition temperature for BSG lignin the changes to the surface appear to coincide with this temperature. This could be as a result of causing collapse to the cellulose microfibrils as well as changing the state of the lignin.

Increasing the heating temperature further to 200°C, 60min (d) processing time show similar visual degradation (melting of the surface) to the surface as for the sample of 180°C 120min (c), with no droplets still being present at the surface. However, the samples at 200°C for 90min (e) show visible droplets appearing on the surface of the material (Figure 5.6E). This was the first sample of all tested times and temperatures to show any visible droplets at the surface of the particles. Despite this work utilising a different lignin-rich by-product to that reported by Gould *et al.* (2016), the temperatures and the times to produce surface droplets are similar.

The most droplets and consequently the greatest surface coverage was produced at 220°C 120min (f). This therefore leads to the hypothesis that the process by which the droplets are produced is in fact kinetic, meaning that the production of droplets is actually a function of both time and temperature. The energy supplied in increasing the temperature of the processing medium eventually delivers enough energy to allow the change in state of the lignin

enabling movement. The heat also degrades parts of the cell wall, specifically hemicellulose (Fan *et al.*, 2016), and this is hypothesised to give the lignin channels in which to migrate through to the surface of the particle. Fan *et al.* (2016) also proposes the formation of another compound called "pseudo-lignin". Pseudo-lignin is considered to be a lignin-like product which is formed from the repolymerisation of polysaccharide degradation products. This can occur when processing under dilute acid conditions. Based on the changes to the ionisation constant of water, increasing temperature of water above 150°C, the number of H-bonds in water starts to decrease which ionises more H+ and OH- to the point that the concentration of both these ions is equivalent to that of a weak acid or weak base (Fan *et al.*, 2016). However, this research has shown that what is in fact extracted during the hydrothermal treatment (as a result of the ethanol extraction) is in fact lignin and not pseudo-lignin due to the lack of peaks present on the NMR spectrum shown in Figure 5.4B. This shows that under the conditions used in this research, pseudo-lignin is not produced. Process yields are discussed later in 5.3.2.3, but the increase in ethanol extracted material between the untreated sample and post hydrothermal process suggests that the increased liberation of plant cell wall constituents (namely lignin) is a direct consequence of the hydrothermal processing conditions used for BSG.

The size of these droplets differ slightly to those at 200°C 90min, which were between 2 and 10µm in diameter, since those produced at this higher temperature and longer processing time are <1 and up to 15µm in diameter and subsequently links with previous hypotheses that the emulsion droplets produced are to be limited by particle size meaning that the smaller particles act at the interface whereas the larger particles appear to act as a thickener and spacer to the droplets in the continuous phase. Another potential

explanation on how the larger particles behave in the emulsion system is a phenomenon called necking. Necking is defined as when one particle is shared between multiple dispersed phase emulsion droplets (Gould *et al.*, 2013). This occurs when a large concentration of particles is used in the preparation of the emulsion and as such the particle network not only stabilises the interface of the dispersed phase droplets, but the particles also act between droplets which in turn supresses the ability for the droplets to coalesce.

The lignin droplets appear in groups on the surface of the BSG particles. Previous work has shown that these groups of droplets appear on the surface of coffee particles and on corn stem rind in specific regions of the sample, which have physical structures such as pits, cell corners and delamination deposits, and this is still the case for BSG as an alternative lignin-rich feedstock (Donohoe *et al.*, 2008, Gould *et al.*, 2016).

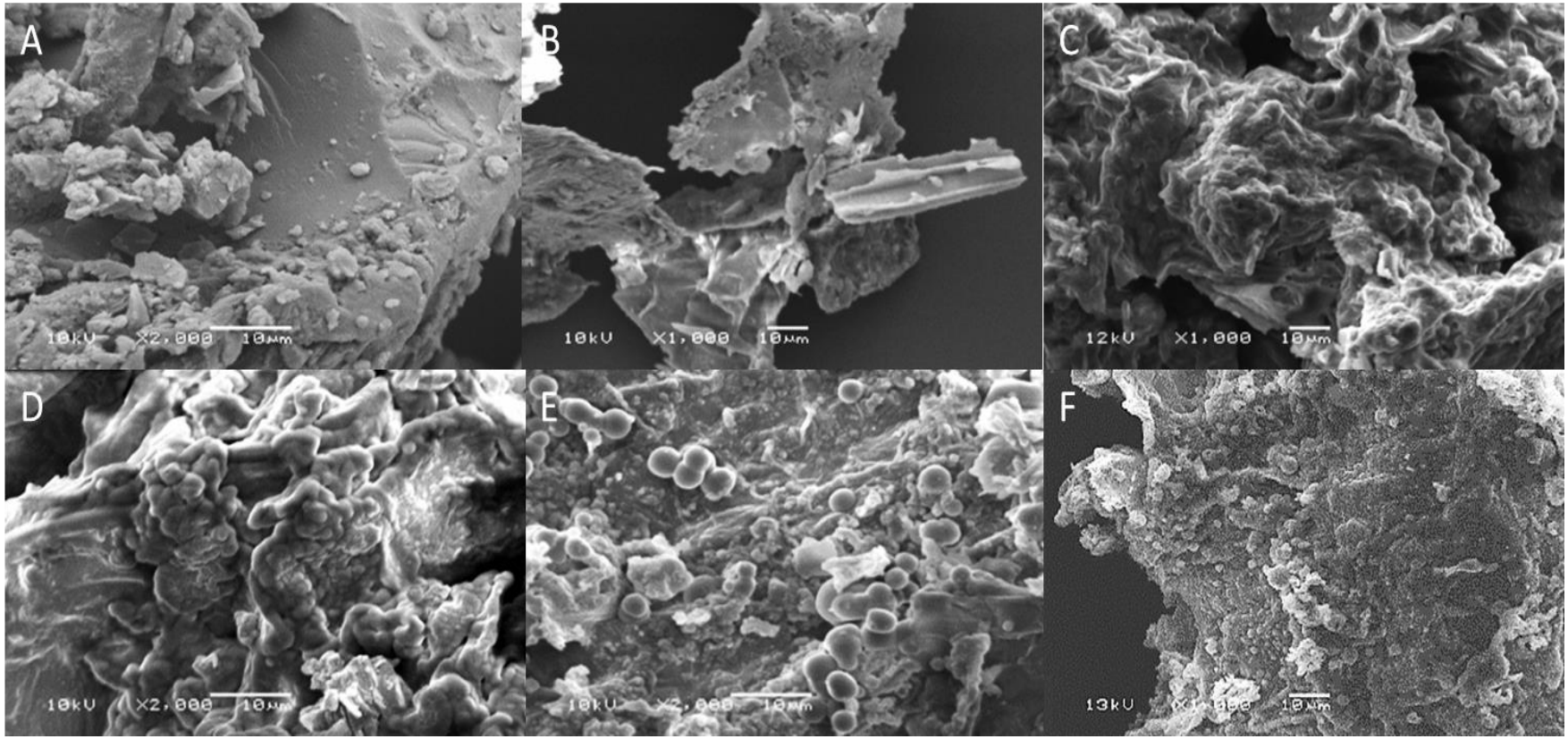


Figure 5.6: Scanning electron micrograph of selected BSG samples, specifically: A) UT BSG; B) 140°C 30min; C) 180°C 120min; D) 200°C 60min; E) 200°C 90min; F): 220°C 120min (scale bar = 10µm) note scale of image differs

5.3.2.1.1 Particle size

The milled BSG particles, prepared from dried BSG by hammer milling, varied in size, shape and roughness, outlined in 5.2.3.1 and show that the range in particle size reduction covers 2–400μm (Figure 5.7), as expected since the milling process produces irregular shapes due to abrasion and particle breakage, resulting in a large particle size distribution. To get a representative image of how the particle surface morphology appears, Figure 5.6 shows untreated milled BSG particles among a variety of different hydrothermally treated samples. The BSG particles are not smooth but in fact possess irregular edges. This dry hammer milling technique of particle size reduction produced a bimodal particle size distribution ranging from 2–400μm and $X_{90,3}$ being <234μm in diameter (Figure 5.7), due to the brittle nature of the dried material. This shows that the sample produced is not homogeneous and due to the large particle size distribution and therefore it is hypothesised that the size of the emulsion droplets is to be limited by this wide range of particle size due to the interfacial interaction and stabilisation by these particles. In comparison to the untreated sample, heating at 200°C 90min (the 1st sample showing visible droplets) the particle size, as a consequence of the hydrothermal process, is between 2 and 600μm, showing that during the hydrothermal treatment some aggregation occurs (Figure 5.6 and Figure 5.7). The pore size ranges (≤25μm) of the sieving technique also accounts for the loss of smaller particles in the particle size distribution data for the HT BSG sample. This is evident since the $X_{90,3}$ increases from 234μm to 373μm. It is hypothesised to be due to the adhesion of agglomerated lignin droplets on different particles during the cooling and drying of the particles. The droplets on the surface of the particle also affects the particle size, with the droplets being between 2 and 10μm in diameter.

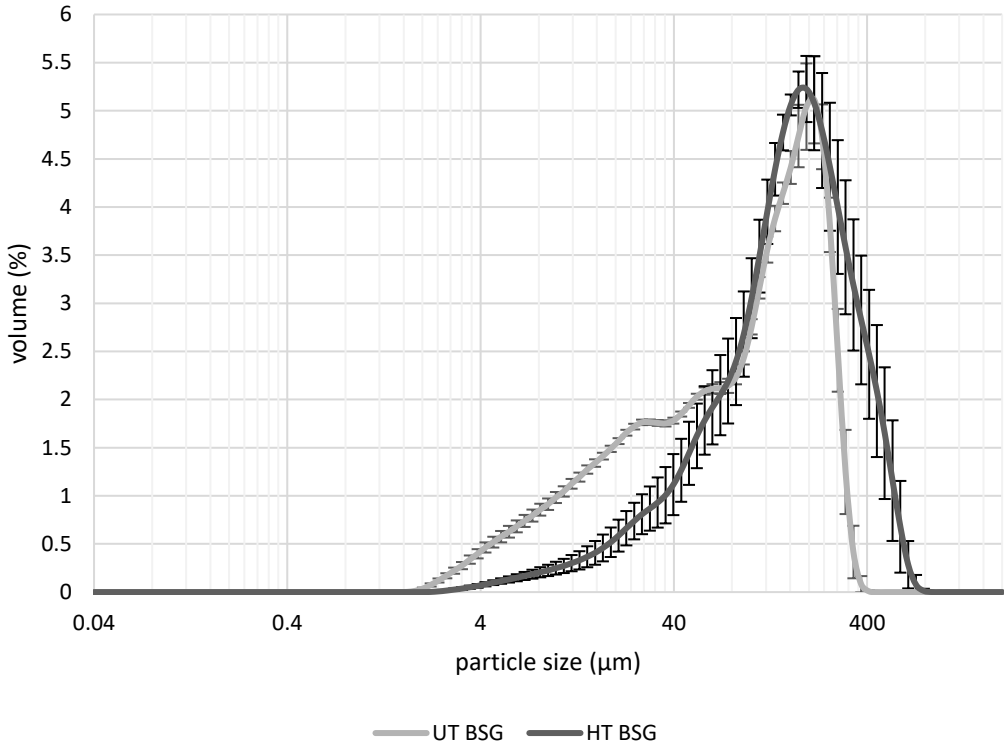


Figure 5.7: Particle size distribution of UT BSG re-suspended into water for analysis and dried HT BSG (200°C 90min) re-suspended into water for analysis (n=8, error bars represent ± 1 standard deviation).

5.3.2.2 Pickering Functionality

The emulsifying ability of the processed BSG samples was tested by processing emulsions with equal amounts of oil and water in the presence of 4% (w/w) of particles based on total emulsion, using the high shear overhead process outlined in section 5.2.4. The emulsions were assessed for phase continuity with a drop test, see also section 5.2.4. Stable emulsions were imaged utilising bright field or fluorescence microscopy to highlight the location of the lignin-based particles at the interface, exploiting the autofluorescence of lignin. To give some context to the results discussed below, if oil was stabilised in water using Tween 60 at 2% (w/w) the resulting droplets generated are around 10µm or if sodium caseinate was used at 0.02% a minimum droplet size of 30µm immediately after emulsification would be produced (Pichot *et al.*, 2010).

UT BSG stabilised O/W emulsions at a concentration of 4% (w/w) particles. As mentioned in 5.2.4, a stable emulsion is one that is stable against coalescence of the oil or water droplets and does not break over time of storage with the emulsion layer creaming or sedimenting to signify whether an O/W or a W/O emulsion was produced. Figure 5.8 indicates that the BSG particles are naturally hydrophilic in nature. Figure 5.9 shows the microstructure of a milled and untreated BSG Pickering particle stabilised O/W emulsion imaged at various days after production. Lignin autofluorescence in the particles themselves was used to show that these Pickering particles can stabilise the emulsion at the interface between the oil droplets and the water continuous phase. The oil droplets of the UT BSG stabilised emulsion on Day 0 appear to have a wide droplet size distribution ranging from ~10–200μm which has been characterised visually through the micrographs presented in Figure 5.9. This is caused by the wide particle size distribution of the particles produced during the milling pre-process and since no sieving process is employed, droplet size distribution is expected to be equally broad. The UT BSG O/W emulsion was stable at Day 7 (Figure 5.9) but the droplets had coalesced by Day 11 with visible phase separation and subsequent sedimentation of the particles residing in the water continuous phase.

To compare UT BSG to HT BSG (specifically 220°C 120min as this was where most droplets were observed), emulsions were prepared using identical methods and bulk ingredients with the only change being the particles used to stabilise the emulsion. The emulsions were tested immediately after production for type of emulsion produced (based on the sedimentation or creaming of the emulsion layer) and then imaged for comparison at a number of days postproduction (Day 1, Day 8 and Day 11) to look at emulsion droplet shelf stability. From both Figure 5.8 and Figure 5.9 the type of emulsion produced as well as the microstructure of the droplets is

visible. The hypothesis that the hydrothermal processing conditions affect the functional properties of the particles and through the creation of hydrophobic particles by the relocation of lignin to the surface appears to be the case here.

As shown previously in Figure 5.6, lignin droplets were produced starting at a temperature of 200°C 90min with most droplets observed at 220°C 120min. This shows that operating temperatures below the transition temperature of lignin specifically of BSG origin will not create hydrophobic particles and therefore means that regular thermal processing technologies currently in place within the wider food chain (e.g. retorts for canning) will not be suitable as options for scale-up. These W/O emulsions were also stable for than <1 week at room temperature showing visible separation from those that were stabilised by particles that had the most severe (220°C 120min) hydrothermal treatment.

When processing around the mid-point transition temperature (175°C), which for experimental purposes in the industrial deck oven was set at 180°C, the changes to the emulsions produced indicated that time and temperature play a crucial role in the formation of hydrophobic particles (Figure 5.6, Figure 5.8 and Figure 5.9). This signifies that hydrothermal processing impacting on particle hydrophobicity is influenced by the phase transition of the lignin in order to begin relocation to the surface of the particles (Gould *et al.*, 2016). This W/O emulsion (HT BSG 220°C 120min) was stable at day 7 however it appeared that this was more of a particle dispersion than an emulsion. Particles are shown to be stabilising at the interface between the water dispersed phase causing droplets and the oil continuous phase of the emulsion at Day 0 (Figure 5.9). Particle aggregation as a consequence of hydrothermal processing also affects the size of the droplets since the greater the particle size the smaller the surface area to volume ratio meaning that despite

smaller surface area these particles act more of a separator between water droplets and as a thickening agent in the continuous phase rather than stabilising the droplet interfaces similar to that of the UT BSG O/W stabilised emulsion in Figure 5.9.

For HT BSG processed at 200°C 90min, the particles produced stabilised W/O emulsions. It must be noted that the particles, which were considerably larger than the droplets also acted as a steric barrier between the water droplets which in turn prevents coalescence as well as being a thickener to the oil continuous phase or perhaps these particles are in fact "necking" which is the formation of a bridge between two dispersed phase droplets hindering the ability of them to coalesce.

The particles presented in Figure 5.6 would appear to have differing hydrophobicity by the number of surface droplets present. This suggests that processing at 220°C is more advantageous than processing at 200°C for the formation of increasingly hydrophobic particles as a result of more droplets and the greater emulsion stability observed in line with those previously reported. This is resultant of lignin relocation lignin to the surface of the particles which has been previously demonstrated to increase the hydrophobicity of the particles produced using a hydrothermal treatment (Gould *et al.*, 2016).

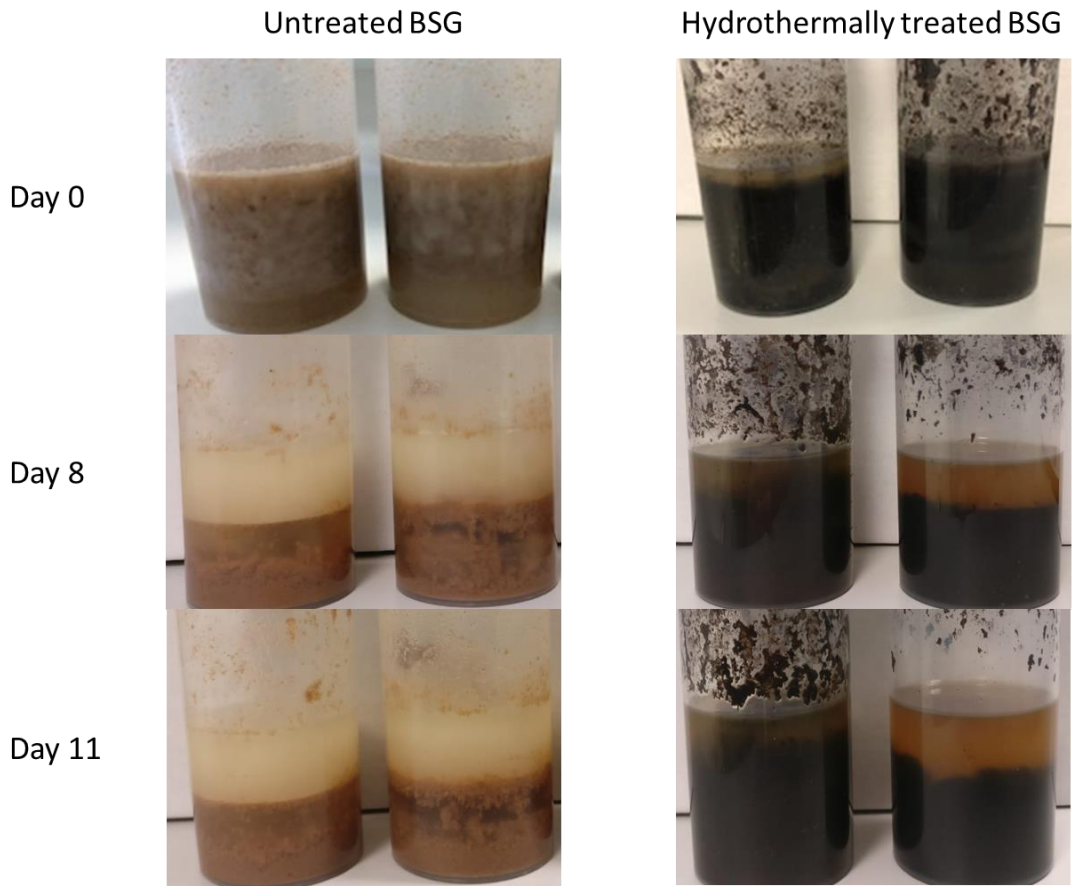


Figure 5.8: Images of emulsion vial for samples UT BSG and HT BSG 220°C 120min taken on Day 0, Day 8 and Day 11

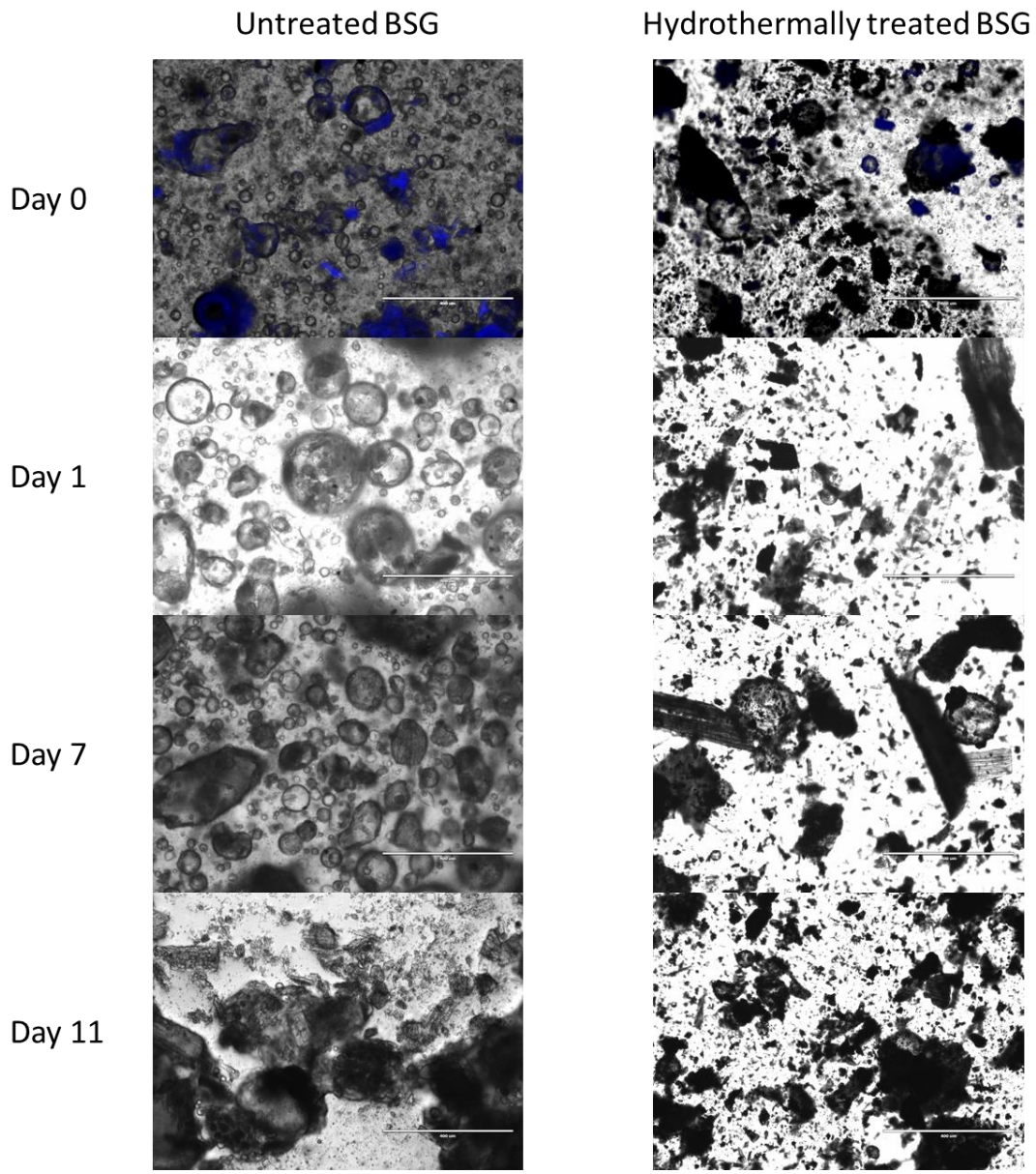


Figure 5.9: Emulsion micrographs for samples UT BSG and HT BSG 220°C 120min taken on Day 0, Day 1, Day 7 and Day 11 (scale bar = 400µm)

5.3.2.3 Process yields for BSG samples

Yields were calculated to understand the total production of relocated droplets at the surface of the particles relative to the UT BSG. The ethanol extraction was used to help isolate the surface droplets, or any material which is hydrophobic from the material since the nature of the extraction is that anything which is hydrophobic and soluble in ethanol should be extracted. Different

times for the ethanol extraction would be advantageous to be tested to find the point at which saturation of extracted material occurs, however, in this instance this was not conducted. The extracted components of UT BSG (which was used as a control for yield calculations) accounts for 10.42% ± 0.31% of the starting material, which shows that some ethanol soluble materials are extracted from the BSG without prior processing. Although this was not characterised on the NMR it is hypothesised that is will contain similar hydrophobic material to that which is present in the extract from HT BSG. Due to the composition of extract shown in Figure 5.4C, the aspects of the cell wall that are removed by ethanol are the lipids, proteins and maybe some lignin already present at the surface post milling, but this requires further analysis for confirmation. The main difference as a result of the hydrothermal process is that the amount of extract collected post treatment increases compared to UT BSG. This increase is hypothesised to be a result of lignin being relocated to the surface of the particle meaning it is no longer chemically bonded to the cellulose and hemicellulose in the cell wall matrix and thus making it more accessible and susceptible to the extraction process. Yields for the droplet residue were calculated as a percentage of the initial 4g UT BSG. HT BSG particles produced account for 62.4% ± 0.01% of the initial starting mass of UT BSG. This percentage factor was used to calculate the process yield for HT BSG. The average mass of the extract accounted for 21.58% ± 3.07% of the initial 4g UT BSG. This increase in the percentage extract is attributed to the relocation of lignin in the secondary cell wall to the surface of the particles. Therefore, this relocation enables a greater proportion of the overall material composition to be removed in the same ethanol extraction process.

5.4 Conclusions

To functionalise BSG into a hydrophobic particulate emulsifier, a hydrothermal treatment is required in order to change the physicochemical properties of the material. This treatment must be above the transition temperature of the lignin in the material in order to mobilise the internalised lignin to the surface of the particles. This occurs by causing cell wall collapse and lignin changing state such that it can migrate through the particles.

For BSG of 100% malted barley composition, the creation of hydrophobic lignin-rich droplets as confirmed through solid state NMR is as a direct consequence of the relocation of internalised lignin to the surface of the particles. Coalesced lignin droplets had a size range distribution on the surface of the particles between <1 and 15 microns in diameter depending on hydrothermal treatment.

Untreated BSG produced emulsions which are water-continuous with the particles adsorbed to the interface (shown by visible Pickering stabilisation in the emulsion micrographs) between the oil and water since the particles are predominantly hydrophilic by design. Using a hydrothermal process to functionalise BSG by relocating lignin in the form of droplets to the surface of the particles created hydrophobic particles that could stabilise oil-continuous emulsions with the particles adsorbed to the interface between the water and oil showing these particles are predominantly hydrophobic by design since they can stabilise W/O emulsions whilst preferentially residing in the oil. Although, these particles were shown to migrate to the water phase over time causing emulsion breakdown by phase separation. It is hypothesised that droplet size is particle size limited and since particle size increases as a result of the hydrothermal process due to aggregation, efforts must be taken to decrease particle size in order to become desirable for use in food applications.

Next steps – following the conclusions of this research, it is hypothesised that the inclusion of a high pressure homogenisation step (which transforms high pressure into shear forces) will aid in further particle size reduction assisting in stabilising smaller water droplets in W/O emulsions but also open up the structure making lignin more accessible during hydrothermal treatment. Further quantification of lignin content of the various BSG samples should be conducted.

Acknowledgments: This research was supported by the Engineering and Physical Sciences Research Council, University of Nottingham and Campden BRI. We would like to thank in the Division of Food Science, Steve Johnson and Val Street for technical support as well as the Nanoscale and Microscale Research Centre (nmRC) for providing access to instrumentation and Mrs Christine Grainger-Boultby for technical assistance. We would also like to thank Andrew Bosman, Richard Akkermans and Steven Walker of Campden BRI for being industrial partners in this research.

Author contributions: J.H., W.M., J.G., G.B., E.B and B.W. conceived and planned the experiments. J.H. and W.M. carried out the experiments and sample preparation. J.H. took the lead in writing the manuscript. All authors provided critical feedback and helped shape the research, analysis and writing of this manuscript. All authors have approved and are accountable for the final version of the manuscript submitted.

Conflicts of interest: The authors declare no conflict of interest. The founding sponsors had no role in the design of the study;

collection, analyses, or clarification of data; in the writing of the manuscript; and in the decision to publish the results.

6 Process design of an improved hydrophobic Pickering particle from Brewers' Spent Grain

James Huscroft,[1,2] William MacNaughtan,[1] Andrew Bosman,[3] Graham Bown,[3] Richard Akkermans,[3] Bettina Wolf,[1,a] Eleanor Binner[2*]

[1]Division of Food, Nutrition and Dietetics, School of Biosciences, University of Nottingham, Loughborough, LE12 5RD, UK

[2]Faculty of Engineering, University of Nottingham, Nottingham, NG7 2QL, UK

[3]Campden BRI Limited, Chipping Campden, GL55 6LD, UK

[a]Present address: School of Chemical Engineering, University of Birmingham, Birmingham B15 2TT, UK

*Eleanor.Binner@nottingham.ac.uk

Abstract

In Chemical Engineering, process design is a crucial aspect of a green unit operation specifically to transform one material into another. In the production of food, amending different parameters in the process can generate different products from the same starting material. Particulate emulsifiers are a method of stabilising emulsions for long periods of time. Previously, the use of ground coffee waste particles and BSG particles, transformed through hydrothermal processing, has been demonstrated to stabilise water-in-oil emulsions. However, emulsion droplet sizes were not in the order of magnitude ideal for food industry products. This was achieved through the relocation of hydrophobic lignin (cell wall component) to the surface of the particles. Implementing a high pressure homogenisation process prior to the hydrothermal process creates smaller particles than hydrothermal processing alone. The creation of smaller particles was confirmed by particle size analysis. Quantification of the liquid fraction from the high pressure homogenisation step showed that constituents of the primary cell wall (e.g. cellulose and hemicellulose) were removed during processing. For the hydrothermally treated samples, a greater surface coverage of lignin was confirmed by scanning electron microscopy and the droplets were found to have the same composition as that previously characterised by Nuclear Magnetic Resonance. Following hydrothermal processing, oil continuous emulsions could be stabilised, compared to water continuous emulsions only prior to processing. It can be concluded that additional process steps and amendments to process design induced improved functional lignin-rich particulate by-products for use as an emulsifier.

Keywords: lignin, Pickering emulsions, high pressure, non-chemical pre-treatment, hydrothermal processing, W/O emulsions, O/W emulsions

Highlights

- Lignin-rich hydrophobic particulate emulsifiers developed from Brewers' Spent Grain.
- High pressure homogenisation reduces particle size of particulate emulsifiers.
- Greater number of surface lignin droplets produced post hydrothermal treatment.
- Lignin droplets linked to severity of high pressure process conditions.

6.1 Introduction

Surfactants and amphiphilic biopolymers (mostly proteins) are commonly used to stabilise emulsion-based foods (Berton-Carabin and Schroën, 2015). However, these systems are thermodynamically unstable and tend to break down through aggregation and coalescence of the dispersed phase through time leading to phase separation which is the main requirement for using an emulsifier to avoid this and increase stability. Some changes in conditions can cause instability in emulsions, such as pH, temperature and salinity (Binks *et al.*, 2010, Dickinson, 2010, Murray *et al.*, 2011, Kalashnikova *et al.*, 2011, Pawar *et al.*, 2011, McClements, 2016a, Linke and Drusch, 2018). A growing concern amongst consumers is also that these emulsifiers may not be environmentally friendly and could cause adverse health effects. Pickering emulsions are stabilised by solid particles at the oil/water interface (Pickering, 1907). Unlike conventional emulsifiers, which can adsorb and desorb from the surface (this is an equilibrium effect), promoting emulsion droplet coalescence, Pickering Particles are considered to be irreversibly adsorbed, as the energy required for spontaneous desorption of the particles from the interface is extremely large compared with that of thermal energy (Gould *et al.*,

2016). Pickering emulsions therefore have the potential to create stable emulsions with prolonged shelf-life. They could also offer advantages such as fat reduction through the stabilisation of an encapsulated water phase in duplex (water-in-oil-in-water) emulsions (Gould *et al.*, 2016) or the encapsulation and sustained released of active ingredients (Linke and Drusch, 2018). For these reasons, the production of food-grade Pickering Particles has recently been the subject of significant research efforts (Berton-Carabin and Schroën, 2015, Xiao *et al.*, 2016, Ago *et al.*, 2016, Bai *et al.*, 2018, Calabrese *et al.*, 2018, Jiao *et al.*, 2018, Linke and Drusch, 2018, Lu *et al.*, 2018, Dammak *et al.*, 2019, Sanchez-Salvador *et al.*, 2019).

The focus of this paper is the production of Pickering Particles to stabilise water-in-oil (W/O) emulsions for application in foods such as margarines, low-fat spreads and confectionary fillings. The general requirements for solid particles to function as Pickering Particles are that (i) the particles should be partially wetted by both continuous and dispersed phase; (ii) they should preserve proper wettability to gain sufficient interfacial absorption efficiency, and (iii) particle size should be at least one order of magnitude smaller than the targeted emulsion droplet size (Xiao *et al.*, 2016). The wettability of the solid particles is the key property determining the formation and stabilisation of Pickering emulsions, and this can be semi-quantified by the contact angle θ, which is the angle formed at the three-phase boundary where solid particles, continuous and dispersed phase intersect. In the case of W/O emulsions, the particles must be preferentially wetted by the oil phase, but still capable of being wetted by the water phase (e.g. they are amphiphilic). Fat crystals are one option to stabilise W/O emulsions, with recognised applicability to foods such as edible spreads (Berton-Carabin and Schroën, 2015). However, due to their production

methods, thermally stable emulsifiers such as sodium stearoyl lactylate and high melting point phospholipids such as lecithin must be labelled as food additives and consumers therefore tend to not always accept these as clean label (Linke and Drusch, 2018). The addition of fat to food formulations is also counter-intuitive when fat reduction is a priority in the challenge to reduce non-communicable diseases such as diabetes in the obesity epidemic. The use of sustainable polysaccharide-based materials such as cellulose derivatives and starch-based materials is also common in the preparation of Pickering Particles. However, these materials are inherently hydrophilic, and require chemical modification in order to be able to stabilise W/O oil emulsions (e.g. stearolyated microcrystalline cellulose (microcrystalline cellulose modified with stearoyl chloride under heterogeneous conditions) (Pang *et al.*, 2018) and cellulose nanocrystals (Guo *et al.*, 2017)). Finally, the ability to stabilise W/O emulsions with hydrothermally modified lignin-rich particles has been demonstrated using ground coffee waste (Gould *et al.*, 2016) and Brewer's Spent Grains (BSG; Chapter 5). Lignin is a known emulsifier, with hydrophobic and hydrophilic regions. It is believed that the hydrophobicity of the coffee and BSG particles is increased during hydrothermal processing by relocating the hydrophobic lignin to the surface of the particles. The water-dispersed particles are heated in a sealed vessel in water at or above a lignin phase transition specific to that feedstock (Gould *et al.*, 2016); Chapter 5); above the phase transition the lignin becomes mobile, moving through the cell matrix. For BSG, the transition temperature has been characterised to be 175°C (Chapter 5). All transition temperatures characterised in this PhD are using the midpoint of the transition as the characterizable temperature for quantification. The hydrophobic lignin, in order to minimise contact with the hydrophilic solvent, forms droplets on the surface of the particles, which then solidify on cooling (Selig *et al.*, 2007), yielding

Pickering Particles that have been shown to stabilise W/O emulsions ((Gould *et al.*, 2016); Chapter 5). This approach has the advantage of using only food and drinks industry co-products and water, thereby producing clean-label potentially food-grade particles and at the same time valorising low value industrial feedstocks.

While ball milling followed by hydrothermal treatment of waste coffee grounds at 200°C for 1 hour was shown to increase hydrophobicity and yield particles that stabilised W/O emulsions, the droplet size was larger than would be applicable in food-based emulsions (butter having water droplets in final product ranging from 0.25 to 25μm (Juriaanse and Heertje, 1988)), ranging from 100μm to 300 μm, and the droplets were of irregular shape (Gould *et al.*, 2016). The authors attributed this to the interface being jammed with particles, resulting in prevention of further reduction in the interfacial area to a spherical droplet. This is known as arrested coalescence, and the authors surmised it may have been caused by the heterogeneous distribution of lignin droplets at the particle surface. In an attempt to understand how the processing conditions affected the hydrothermal functionalisation of lignin-rich biomass particles, Huscroft *et al.* (Chapter 5) hydrothermally treated hammer milled BSG at a range of temperatures below and above the lignin transition temperature (which was found to be 175°C for BSG lignin – quantified by the mid-point temperature), and also investigated the effect of heating time; the resulting hydrothermally treated particle sizes ranged from 2–600μm. The results indicated that the transition from hydrophilic to hydrophobic Pickering particles is a kinetic process, governed by both processing temperature and time. Emulsion tests indicated that all Pickering Particles produced below the phase transition temperature were hydrophilic. Although there was no visible formation of lignin droplets at 180°C, the maximum processing time (120 min) did yield hydrophobic Pickering particles

(as evidenced by the stabilisation of a W/O emulsion). Processing at 200°C for 90min or more yielded W/O emulsions which were stable for up to 7 days, which corresponded with the onset of <1–15μm lignin droplets at the particle surface (visible by Scanning Electron Microscopy). The presence of G lignin monomeric component, along with lipids, pectin, and fatty and amino acids at the particle surface were confirmed via Nuclear Magnetic Resonance. These results confirm the lignin transition temperature corresponds with the minimum processing temperature required and strengthens the hypothesis that hydrophobic lignin is predominantly responsible for the ability of these particles to stabilise W/O emulsions. However, referring to the requirement that the particles should be an order of magnitude smaller than the emulsion droplet size, and comparing the particle size (2–600μm) with the emulsion droplet size (e.g. 10–400μm for the 220°C treatment), particles above 10μm are unlikely to adsorb at the oil-water interface but would rather act as a thickener and spacer to the droplets in the continuous phase (Chapter 5). The phenomenon of necking is also considered which is where one particle bridges between two or more dispersed phase droplets which hinders coalescence. The key challenges to improve the performance of these hydrophobic Pickering Particles are therefore to address the problem of arrested coalescence caused by inhomogeneous surface activity across the particle surface and reduce the maximum particle size to avoid the presence of particles that do not adsorb at the oil/water interface.

There are a number of emerging techniques for the disruption of lignocellulosic biomasses that could potentially be applied for the production of clean-label products, including high pressure homogenisation (HPH), microwave treatment, ultrasound, electron beam irradiation and pulsed electric field (Turbak *et al.*, 1983, Herrick *et al.*, 1983, Hassan *et al.*, 2018). Of these, ultrasound

treatment and HPH also offer the benefit of particle size reduction below that achievable using standard milling techniques, which will be required to achieve emulsions that are suitable for food industry applications. In the production of Pickering Particles, HPH has been used to fibrillate cellulose into nanofibrils which can then be used to improve the strength of cellulose-based composite films (Lee *et al.*, 2009). Lignin-containing nanofibrils have been created from pulp fractions from the creation of Kraft wood. Post acid hydrolysis, HPH was utilised to generate different lignin containing cellulose samples which had become fibrillated post-processing (Wang *et al.*, 2012). HPH has also been used to create nanolignin particles of particle size <100 nm after 4 hours of mechanically-induced homogenisation. These particles were then used in nanolignin-polyvinyl alcohol (PVA) blends, which had an increased thermal stability compared with original lignin-PVA blends (Nair *et al.*, 2014). HPH was therefore selected as a promising method reduce the particle size and distributions, as well as improving Pickering particle production.

This paper reports efforts to improve the functionalisation of lignin-rich feedstocks for the production of hydrophobic Pickering particles through the addition of a HPH step prior to hydrothermal treatment. The specific objectives are to (a) reduce the particle size, ideally to below 10μm; (b) understand the surface activity that is imparted by lignin relocation, and (c) make the relocation of lignin as droplets homogenous across the particle surface. BSG was selected as the feedstock for continuity with previous work, and as a naturally fibre- and protein-rich (Lynch *et al.*, 2016) co-product of the food and beverage industry.

6.2 Materials and Methods

6.2.1 Materials

6.2.1.1 Brewers' Spent Grain

BSG from barley-based wort manufacture was sourced and prepared as reported previously (Chapter 5). Once dried, the BSG was then milled using a hammer mill (Perten Instruments Laboratory Hammer Mill 3100a, Perten Instruments, Hägersten, Sweden) fitted with 0.8mm sieve and operated at 16800rpm. The dried and milled BSG was stored in hermetically sealed containers at 12–18°C until use.

6.2.1.2 Other materials

Other materials utilised in this research included reverse osmosis water with a resistivity of 14.2MΩ/cm^2, referred to as water throughout, to suspend the BSG; low sulphonate kraft Lignin (termed Sigma Lignin, Sigma-Aldrich, Dorset, UK) used as reference for thermal property analysis and ethanol (Fisher Scientific, Loughborough, UK) to dissolve lignin and with it other ethanol soluble components of the BSG. Sunflower oil purchased from a local supermarket served as the oil phase to assay the emulsifying properties of the processed BSG, see 6.2.5. Further, Adamantane (Sigma-Aldrich, Dorset, UK), Coniferyl alcohol (G-lignin) and Sinapyl alcohol (S-lignin) (Sigma-Aldrich, Dorset, UK) were acquired as reference materials for the NMR analyses, see 6.2.4.1.

6.2.2 Processing

The processing of the untreated BSG particles consisted of high pressure homogenisation (HPH) followed by drying and subsequent hydrothermal treatment. The resulting solid and liquid phases were then separated for analysis. These unit operations are outlined in the remaining parts of this section. The various stages of production are shown in Figure 6.1 where different samples are produced. Table 6.1 shows the names and descriptions of the samples produced at the different stages of unit operations where xP refers to the number of

passes through the Microfluidizer (LM20, Microfluidics Corp., Massachusetts, USA) with x denoting a number; HT referring to whether the sample has had a hydrothermal treatment or not; FD refers to the freeze dried fraction for the respective sample and Extract meaning that it is the ethanol soluble fraction post extraction.

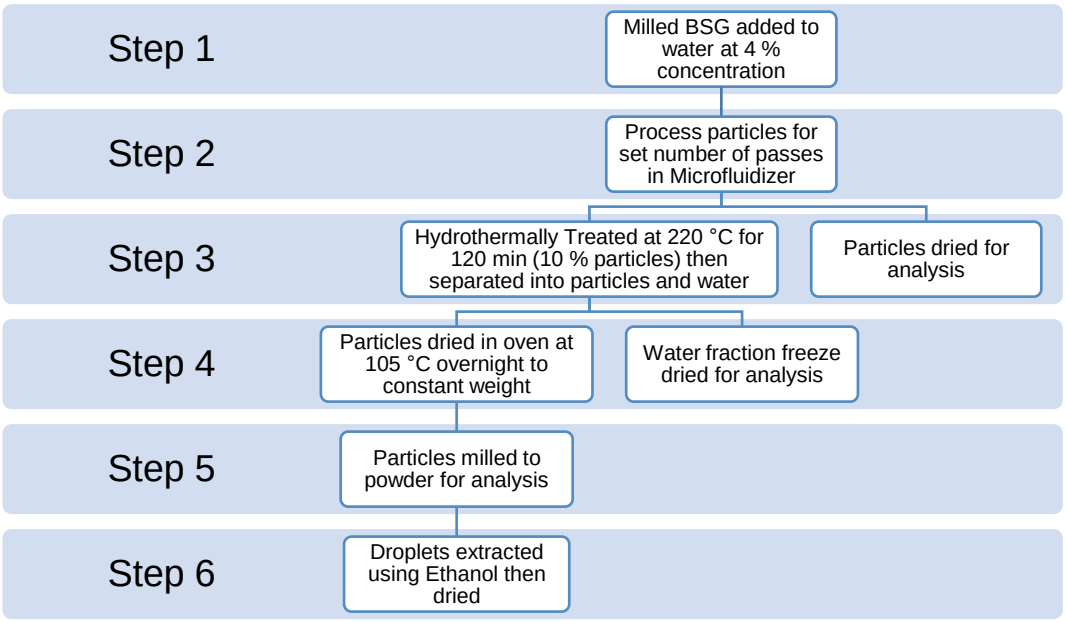


Figure 6.1: Process flow of unit operations to create Pickering Particles and characterised fractions

Table 6.1: Samples prepared from BSG

Identifier and Sample Names	Description
UT BSG	Dried and milled BSG
1P BSG	UT BSG which has undergone 1 pass at 2068 bar in the Microfluidizer
2P BSG	UT BSG which has undergone 2 passes at 2068 bar in the Microfluidizer
3P BSG	UT BSG which has undergone 3 passes at 2068 bar in the Microfluidizer
5P BSG	UT BSG which has undergone 5 passes at 2068 bar in the Microfluidizer
9P BSG	UT BSG which has undergone 9 passes at 2068 bar in the Microfluidizer
3P BSG SFD	UT BSG which has undergone 3 passes at 2068 bar in the Microfluidizer with water separated and freeze dried (SFD = supernatant freeze dried)
5P BSG SFD	UT BSG which has undergone 5 passes at 2068 bar in the Microfluidizer with water separated and freeze dried (SFD = supernatant freeze dried)
9P BSG SFD	UT BSG which has undergone 9 passes at 2068 bar in the Microfluidizer with water separated and freeze dried (SFD = supernatant freeze dried)
HT BSG	UT BSG which has undergone hydrothermal processing conditions of 220°C for 120min
3PHT BSG	UT BSG which has undergone 3 passes at 2068 bar in the Microfluidizer then hydrothermal processed at 220°C for 120min
5PHT BSG	UT BSG which has undergone 5 passes at 2068 bar in the Microfluidizer then hydrothermal processed at 220°C for 120min
9PHT BSG	UT BSG which has undergone 9 passes at 2068 bar in the Microfluidizer then hydrothermal processed at 220°C for 120min
HT BSG Extract	Ethanol extracted droplets from HT BSG
3PHT BSG Extract	Ethanol extracted droplets from 3PHT BSG
3PHT BSG Extract Solids	Remaining solids post Ethanol extraction of droplets from 3PHT BSG
HT BSG SFD	UT BSG which has undergone hydrothermal processing conditions of 220°C for 120min with water separated and supernatant freeze dried

6.2.2.1 High pressure homogenisation (Step 1 and 2)

Prior to addition of the water for use in the microfluidizer, the particles were milled according to the method described in 6.2.1.1 (this was Step 1 of the process chart in Figure 6.1).

100g of milled BSG was processed as a 4% w/w dispersion in water using a microfluidizer (LM20, Microfluidics Corp., Massachusetts, USA) operating at maximum pressure of 30,000 PSI (2068 bar). Hereafter the pressure used in the microfluidizer will be quoted in bar. The dispersion was well mixed to produce a homogenous sample prior to being processed. Samples were processed for a specific number of passes (1, 2, 3, 5 and 9). The processing range of passes was selected to assess changes to material properties at both minimal and extreme ends of processing to observe optimal particle size reduction. The coil in the machine was cooled under ice water to avoid any major temperature changes to the material other than that as a result of the exposure to high pressure. The dispersion (BSG particles is water) was processed as a batch operation.

6.2.2.2 Drying of high pressure liquor

The microfluidised BSG was oven-dried overnight to constant weight using a Model CPMK4MDU438, Compacta deck oven, Tom Chandley, Manchester, UK. This material (around 90g) was then milled using a benchtop Thermomix kitchen processor (Thermomix TM31, Vorwerk Elektrowerke, Wuppertal, Germany) operating at speed 8. The powder was then stored in hermetically sealed containers until use. Upon reflection, the drying step should be avoided in order to avoid the process of hornification occurring to the plant cell wall leading to irreversible collapse (Jayme, 1944, Laivins and Scallan, 1993, Stone and Scallan, 1965).

6.2.2.3 Hydrothermal processing and extraction procedures (Steps 3–6)

The dried post high pressure process BSG liquor was re-dispersed in water prior to being hydrothermally treated as previously reported (Ibbett *et al.*, 2011, Gould *et al.*, 2016) but with slight modification of sample size and processing conditions (5.2.2). Here, 30g of BSG was dispersed manually in 230mL of water and sealed into stainless steel tubular reactors, dimensions 850mm long and 22mm inner diameter (Tubing 316-T25M-S-2,0M-6ME and End Caps SS-1610-C, Swagelok, Warrington, UK). Loaded reactors were heated in a deck oven (Model CPMK4MDU438, Compacta deck oven, Tom Chandley, Manchester, UK) for 120min at processing temperature 220°C (Chapter 5). At the conclusion of the heating period, the reactors were removed from the oven and cooled overnight in a large reservoir of water. Alternatively particles were produced, shown in 6.3.3.2 using a Monowave 300 Microwave Synthesis Reactor (Anton Paar, Graz, Austria). The Monowave was programmed to follow the same heating profile as was validated in thermal process trials in the oven using the steel tubular reactors (3.5.1, 3.5.2 and 3.5.3).

The cooled suspension was then filtered under vacuum (Whatman Grade 1, Kent, UK) yielding separate solid and liquid fractions. The solids residue was subsequently dried for 3h at 105°C until constant weight. The so-obtained HT BSG was stored in hermetically sealed containers at ambient temperature (12–18°C) until assessment or the surface droplets were extracted using ethanol. The liquid fraction was frozen at -22°C before being freeze dried for subsequent analysis as previously reported (Chapter 5).

6.2.3 Physical material property analyses

6.2.3.1 Particle size measurement

The particle size of the BSG samples at various stages was measured to observe changes as a result of processing. This was conducted using a laser diffraction particle size analyser (LS 13320, Beckman-Coulter, High Wycombe, UK) utilising the Fraunhofer theory of the scattering of light by spherical particles in the instrument's software for data analysis measuring for particles above 0.8 μm. The attached dispersion cell filled with water was used to conduct the particle size analysis (Universal liquid module, LS13 320, Beckman Coulter, High Wycombe, UK) as previously outlined (Chapter 5). Pump speed used was 85% to avoid any sedimentation of the samples. Data is presented in volume based distributions. For comparison, the x_{90} was used to show the change in the particle size between the different numbers of passes. The x_{90} refers to the diameter of the particles where 90% of the total particles falls below this diameter threshold.

6.2.3.2 Microscopy

The particle microstructure, the surface morphology and the emulsion droplets were assessed using the same methods and techniques outlined previously (bright field microscopy and scanning electron microscopy in Chapter 5).

6.2.3.3 Thermal properties

The thermal properties of the different fractions of processed BSG were analysed to obtain phase transition temperatures primarily related to their lignin component. This method of differential scanning calorimetry (DSC) was the same as previously reported covering the range of the processing temperature for the hydrothermal process (Chapter 5).

6.2.4 Compositional analyses methods

6.2.4.1 ^{13}C solid state Nuclear Magnetic Resonance

NMR was used to gain an insight into the composition of the BSG. Following hydrothermal processing, NMR was also used to look for changes in composition due to the relocation of lignin to the surface of the particles. The different samples collected in section 6.2.2.3 were analysed for their composition. This enabled insight on where the different constituents identified for the untreated BSG were relocated during the hydrothermal process. The method was the same as used in the previous study (Chapter 4 and 5).

6.2.4.1.1 Lignin content and distribution of lignin within particles

Using the area under the NMR spectra which were produced in 6.2.4.1 enabled the calculation of bulk lignin present in the various samples (Chapter 4). Having calculated the bulk lignin of various samples, the relative distribution of lignin within droplets and solid particles was able to be quantified. This enabled an experimental observation of process efficiency to be defined by creating a ratio based on the carbon chemical shifts for the different parts of lignin. This was conducted in MATLAB (MathWorks, Natick, Massachusetts, USA) using the trapezium function having first generated an x/y plot including a baseline along y=0 as reference. Note: data must first be processed in MNOVA (Mestrelab Research S.L., Santiago de Compostela, Spain) and Microsoft Excel (Microsoft Corporation, Washington, USA) prior to this analysis (3.6.1).

6.2.5 Particle functionality assay

The ability of BSG particles to stabilise W/O or O/W emulsions was assessed using an emulsion assay involving different quantities of water and oil emulsion phases. This method has previously been shown to provide insight into particle classification based on the emulsion that was stabilised ((Gould *et al.*, 2016); Chapter 5). Stabilising O/W or W/O emulsions enabled a particulate emulsifier to

be classified as predominantly hydrophilic or hydrophobic ((Gould *et al.*, 2016); Chapter 5).

Particle functionality experiments (not shown) found that the number of particles required and still capable of stabilising an emulsion (hand shaken) for 3PHT particles was 2% w/w with those results used in this experimental section. To compare between HT W/O emulsions shown in Chapter 5 and 3PHT (the HPH particles with the smallest particle size and most surface droplets), 2% of milled particles w/w were used in a 50g emulsion using 50/50 water and oil concentrations. The particle concentration was halved as this was still capable of stabilising an emulsion. The methodology is the same as that mentioned in 3.1 with the addition of the particles to the perceived continuous phase (oil) prior to processing. The overhead high shear mixer (T10 Basic Ultra-Turrax, IKA England Ltd, Oxford, UK) instead of the Silverson L5M (previously in Chapter 5) was used due to sample size. The T10 Basic Ultra-Turrax was operated at 15000rpm for 30s following calculations of angular velocity and tangential velocity (3.1.1). The emulsion type was confirmed by observing gravitational stability through the development of phase boundary layers in the storage vials. The emulsions were also observed under a microscope to observe microstructure.

Subsequent work used the same 2% particle concentration w/w to assess the particle functionality at differing concentrations of oil and water from 10% oil – 90% oil at 10% increasing increments. The hypothesis being that there would be a point where along the range of O/W ratios, the particles would no longer stabilise weak O/W emulsions and a stable W/O emulsion would be formed. This inversion was hypothesised to be as a result of the concentration of oil being sufficient as to effectively act as a continuous phase in a W/O emulsion since the particles tend to preferentially reside in oil.

Particles which had not been through a hydrothermal treatment were also tested for their functionality with regards to emulsion stability. The 9P particles were used at an 8% concentration w/w to see whether they were capable of stabilising some form of particle stabilised emulsions. 8% w/w was chosen as from 3.1, this was the concentration where no free water was visible at the bottom of the vial for O/W emulsions. Since these particles were not subject to any hydrothermal treatment it was hypothesised that these would still be hydrophilic however the aggregation of the particles suggested this may not be the case (full methodology outlined in 3.9). Results for this are shown in 6.3.1.4.

6.2.6 Lignin-based Pickering emulsifiers used to replace conventional emulsifiers during cake baking

The methodology outlined in 3.10 was used to produce cakes where conventional emulsifiers were replaced with UT BSG and 3PHT BSG. Results are shown briefly in 6.3.4 with the full results summary shown in Appendix A2.

6.3 Results and Discussion

6.3.1 Effects of the Microfluidizer step on the BSG particles

6.3.1.1 Physical Characterisation

6.3.1.1.1 Particle Size

One objective of the high pressure homogenisation (HPH) step was to reduce the particle size, ideally to below 10µm. Figure 6.2A shows the mean particle size distribution of the untreated and HPH-treated particles. For clarity, 2P and 5P have been omitted from the figure. The data in Figure 6.2A shows that a single HPH pass reduced the particle size, but that the particle size distribution is still bimodal. Additional HPH passes (2P and 3P) reduce the particle size further, yielding a monomodal particle size distribution peaking at around 40 µm in both cases. Incremental HPH passes continued to yield monomodal distributions, but with an increasing peak particle size. Figure 6.2B shows x_{90} (the diameter of the particles where 90% of the total particles falls below this diameter threshold) for the non-HT samples. It shows a steady reduction in x_{90} from UT BSG to those of 1P to 2P to 3P with their x_{90} being 154µm ± 17µm; 107µm ± 0µm; 88µm ± 1µm and 80µm ± 4µm, respectively. After this point, the particles appear to aggregate, as their size increases the more they are processed. After 5P up to 9P, the particle size by x_{90} is 100µm ± 1µm and 127µm ± 3µm, respectively. It is hypothesised that since microfluidization is carried out in water, this aggregation effect could be caused by increasing hydrophobicity of the particles. However, this has not been tested as part of this research and is suggested as potential future work.

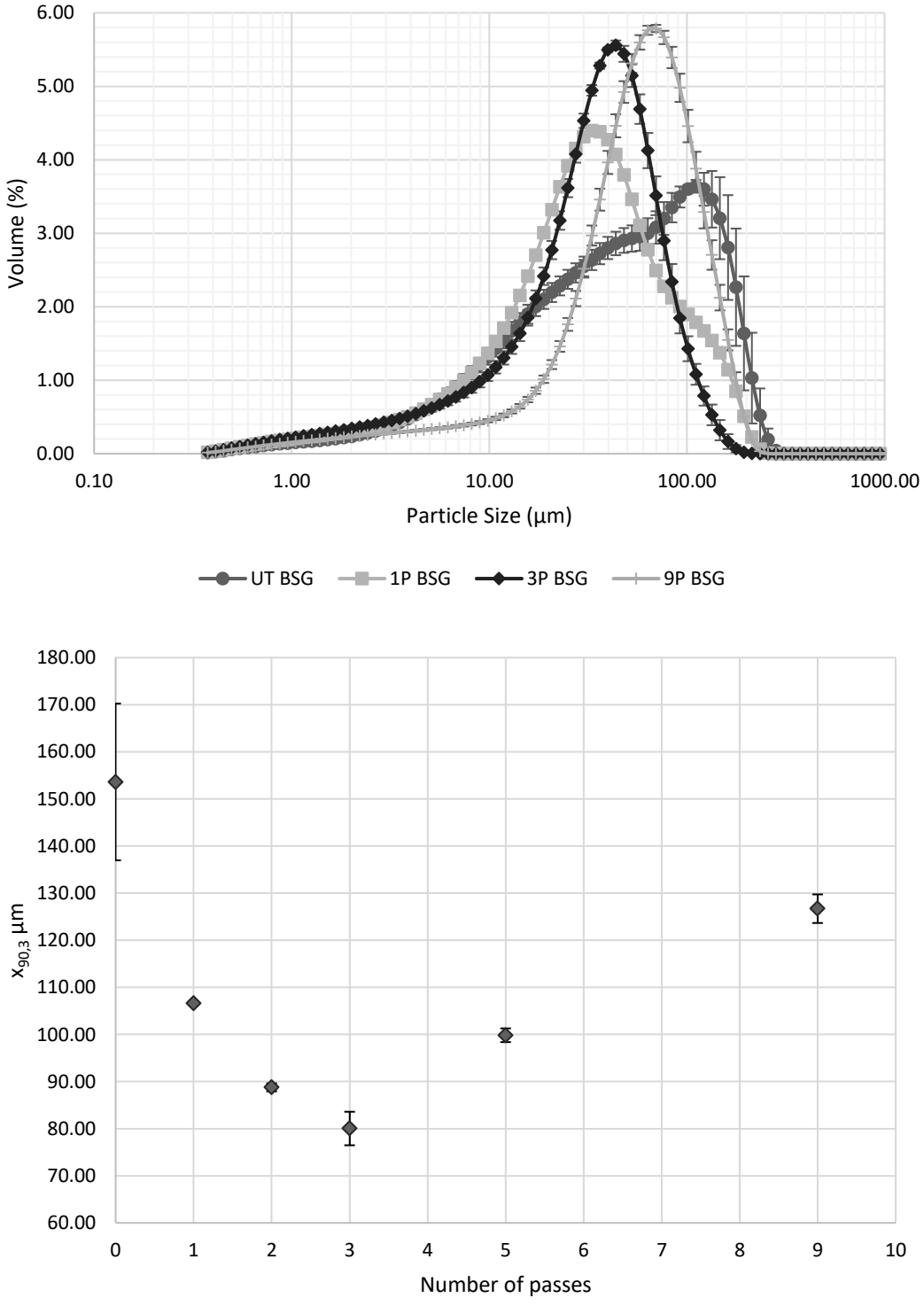


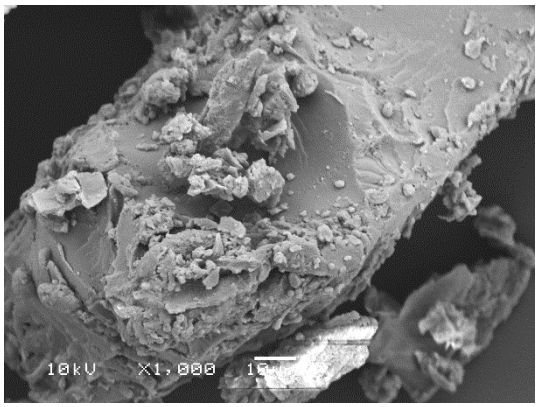
Figure 6.2: A) Mean particle size distribution of all Microfluidizer samples for analysis (n=3). The error bars show ± standard deviation; B) $x_{90,3}$ for the different particles produced using high pressure homogenisation (n = 3) measured using a Beckman-Coulter LS 13320

6.3.1.1.2 Surface morphology

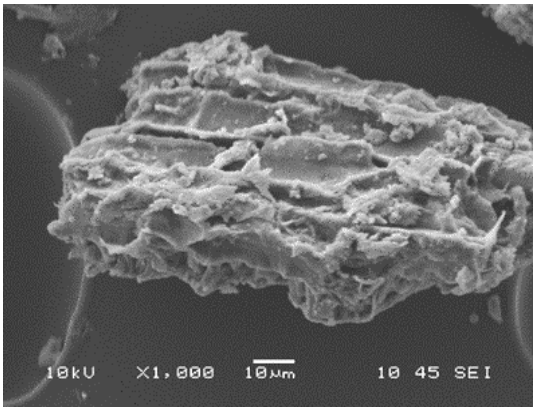
To address the objectives of understanding the surface activity of the functionalised particles, in particular how the HPH step may contribute to surface activity, SEM of the HPH-treated samples was carried out. Figure 6.3 shows SEM micrographs of the BSG before and after 1 – 9 passes at 2068 bar. The untreated and milled sample shows smooth surfaces interspersed with textured regions. Microfluidization creates high shear forces, and the changes in physical structure shown in Figure 6.3 (representative images of different passes), evidences these abrasive effects. The first three passes progressively show the development of crevices and valleys appearing on the smooth surfaces which is clear evidence for the removal of some material and that tissue rupture has been facilitated. Linking with the particle size data in Figure 6.2, the reduction in particle size up to three passes suggests that this could in fact be down to the removal of material layers in the particles.

If this was to be characterised at a molecular architecture level, it is hypothesised that some of the material which is removed would be that which is water soluble or in the case of cellulose that which is fibrillated (which might explain the visible change in viscosity of the batched liquor upon increased number of passes). If these materials were removed, then the hypothesis that the remaining material (e.g. that which is more intrinsically hydrophobic or possibly in this case lignin) is becoming greater in quantity and coverage at the particle surface and therefore making them more amenable to further (hydrothermal) processing. Changes to the chemical composition of the particles is covered in 6.3.1.2 where the removal of cellulosic material is discussed in more detail. Further HPH processing (5P and 9P) appears to completely remove the smooth surfaces, leaving only the textured regions, which appear less angular/more rounded than

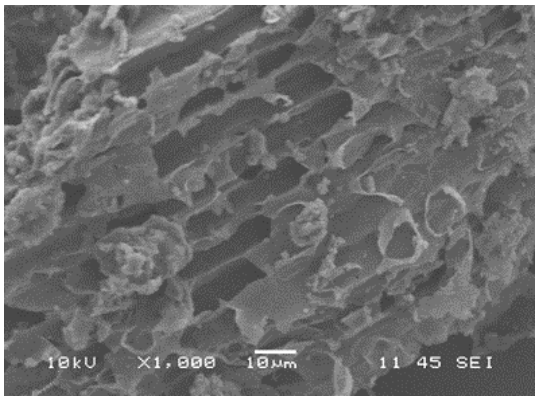
the textured regions of the untreated sample, possibly indicating a more homogeneous surface.



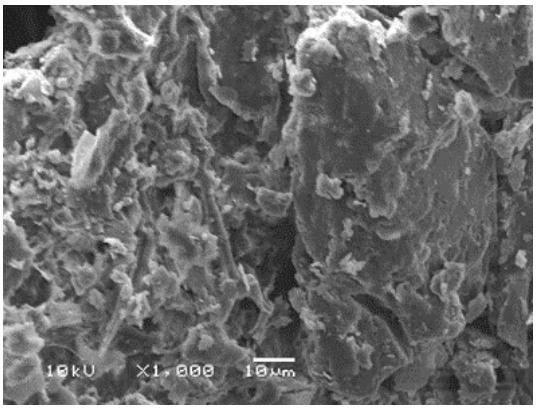
UT BSG



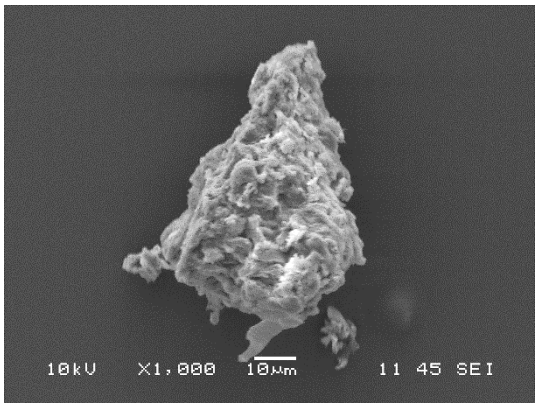
3P BSG



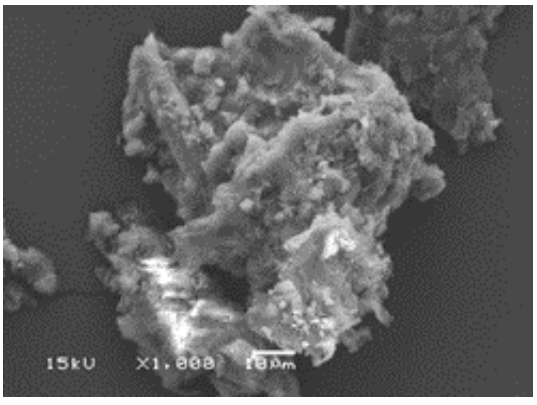
1P BSG



5P BSG



2P BSG



9P BSG

Figure 6.3: Changes to the material surface structure after being subject to 2068 bar using HPH, micrographs obtained using SEM (scale bar = 10µm)

6.3.1.2 Chemical characterisation

There was no detectable temperature increase after the high pressure homogenisation step, due to the material being cooled under ice. Without external cooling the temperature would have been expected to increase due to heat generation from the change in pressure as a result of the work input. In milk for example, with a starting temperature of 24°C, processing at 200MPa (29000 PSI/ 1999 bar), the temperature of the milk post high pressure homogenisation at the outlet valve was 60.3°C ± 1.0°C (Thiebaud *et al.*, 2003). External cooling was applied to the coil to mitigate the temperature increase as much as possible. The 4% w/w BSG suspension was also observed to change colour to a more homogeneous and lighter pale brown and showed an increase in viscosity. The viscosity was not measured but a visual change suggested a thickening of the mixture from pourable particles in water to a medium thickness gravy. These changes became more marked with increasing number of high pressure (HPH) passes. The colour change could be as a result of the generation of smaller particles due to light diffraction effects making the dispersion appear lighter. However, the increase in viscosity and change in colour, along with the fact that the suspension may have been subjected to elevated temperatures during the HPH process, indicate that some components may have been extracted from the particles into the water phase during processing. The evidence of the thickening of the suspension, the changes in colour and the changes to the particle structure shown in Figure 6.3 suggest that fibrillation of the liberated cellulose which is found in the water fraction has occurred (Agarwal *et al.*, 2018). Understanding any changes to the chemical composition of the particles prior to hydrothermal treatment will therefore help to understand the downstream functionalisation process. To do this, the composition of the supernatant (i.e. the

composition of the extracted compounds) was determined using NMR.

Upon separation of the particles and the supernatant fractions, the supernatant was freeze-dried to a sponge-like solid before being characterised by NMR. Figure 6.4 shows the spectrum of the freeze-dried supernatant after 3 passes. Similar results were obtained for the other samples (e.g. 5P and 9P). As can be observed, the main changes to the BSG upon being exposed to high pressure homogenisation is the removal of cellulose, pectin, a small amount of proteins/amino acids and lipids, as well as some lignin. These changes indicate the removal of components from all parts of the plant matrix, i.e. the middle lamella, primary and secondary cell wall and some intracellular components. However, the relatively small contribution of lignin to the composition of the supernatant (3.49% in 3P SFD; 6.80% in 5P SFD; 6.76% in 9P SFD based on carbon chemical shift ratios) and large contribution of cellulose and hemicellulose (74.93% in 3P SFD) shows that components of the secondary cell wall is more resilient to the abrasion caused by the high pressure produced shear forces, than the component of the primary cell wall; and therefore lignin is expected to be concentrated in the particles as a result of the HPH process. The lignin which is present in this phase is hypothesised to be fragments of lignin which have been cleaved during the high pressure homogenisation process. The preferential removal of the primary cell wall materials during HPH processing means that the lignin in the plant cell wall may become closer to the surface of the particles even before being subject to a hydrothermal treatment. This is hypothesised to occur as a result of a shaving type process occurring in the microfluidizer which removes the primary plant cell wall resulting in a smaller diffusion pathway for the lignin to migrate through during hydrothermal processing. This in turn could explain why in 6.3.1.4

9P BSG particles could stabilise limited shelf-life W/O emulsions. However, emulsion tests (results not shown) indicated that the material was still hydrophilic (for 3P BSG particles) despite this change in composition, and therefore hydrothermal processing is still required to functionalise the particles as hydrophobic Pickering Particles.

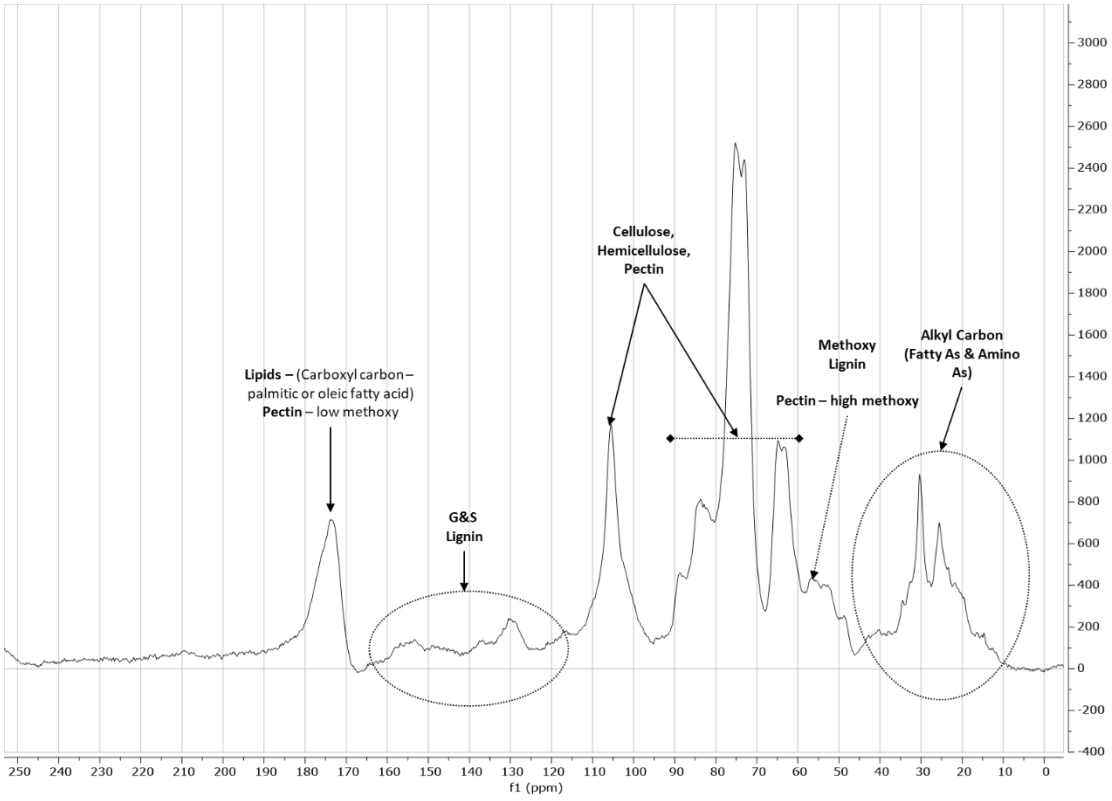


Figure 6.4: ^{13}C SS-NMR spectra of the 3P freeze-dried supernatant fraction of BSG post microfluidization

6.3.1.3 Thermal characterisation

In order to understand the impact the introduction of a high pressure homogenisation step may have on the hydrothermal processing conditions required to produce hydrophobic Pickering Particles; DSC was carried out to determine the lignin phase transition temperature. Previous work has shown that this phase transition temperature can be linked to the processing temperature required to effect the relocation of lignin to the surface of the particles (Chapter 5). Reference to the literature indicates that the inclusion of a high pressure physical pre-treatment step might lower the phase

transition temperature by removing some of the other cell wall components that are bonded to lignin (Chen, 2014). The mid-point phase transition temperature of BSG lignin is 175°C ± 4°C (Chapter 5). Figure 6.5 shows DSC thermograms for UT BSG and 1P – 9P BSG. All samples are within the range of 175°C ± 4°C, indicating that the HPH process does not affect the thermal properties of the lignin within the BSG. Therefore, the processing temperature required to hydrothermally activate BSG to become hydrophobic Pickering Particles is expected to remain the same regardless of the HPH pre-treatment step. However, the kinetics of the thermal process and lignin migration might change since the diffusion pathway lengths for lignin to migrate to the surface may be smaller as a result of the HPH homogenisation step.

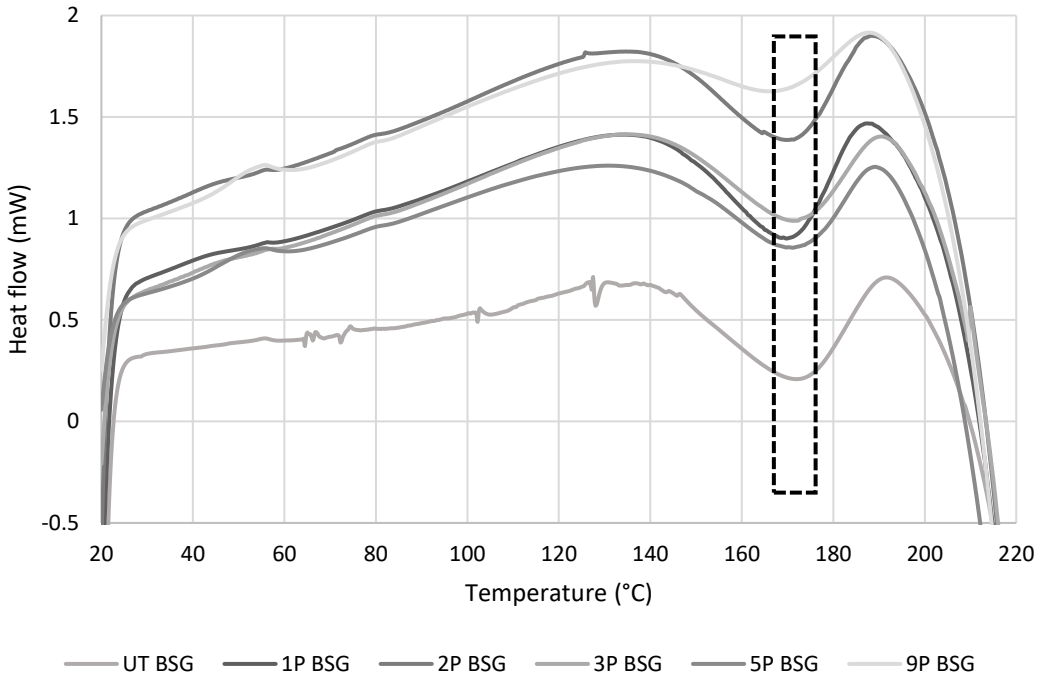


Figure 6.5: Multiple DSC thermogram showing all Microfluidizer BSG samples (phase transition temperature region for all samples shown in rectangle)

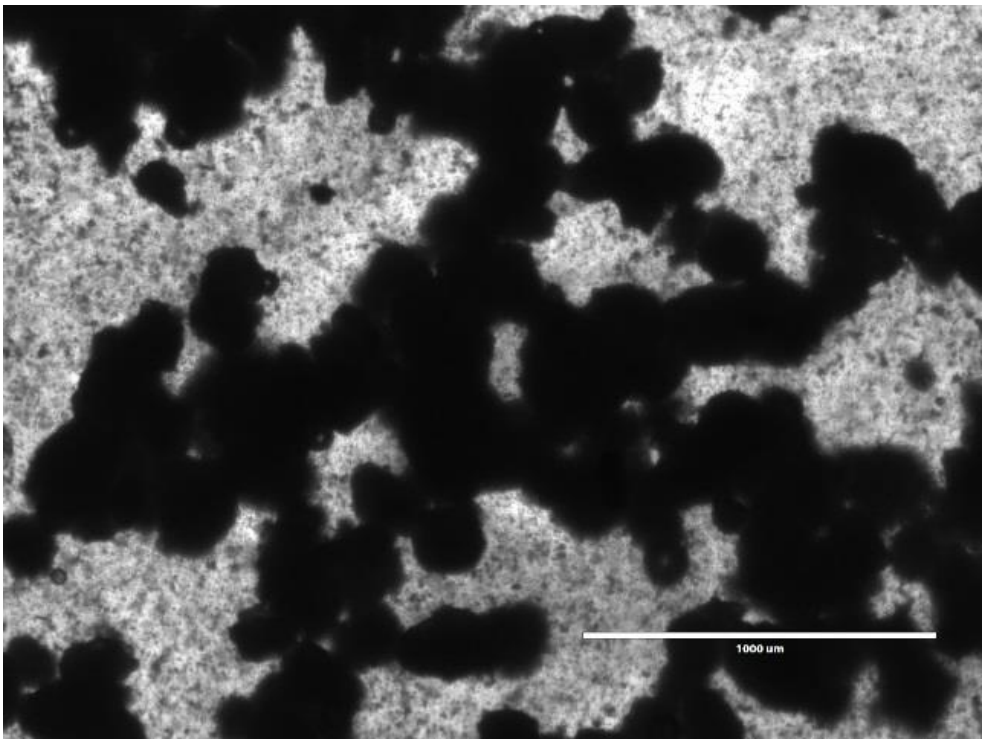
6.3.1.4 Effect of HPH processing for particle functionality

The use of the centrifugation step enabled the removal of the liquor which has previously been found to contain a majority of cellulose. This was removed in order to prevent the fibrillation of the cellulose

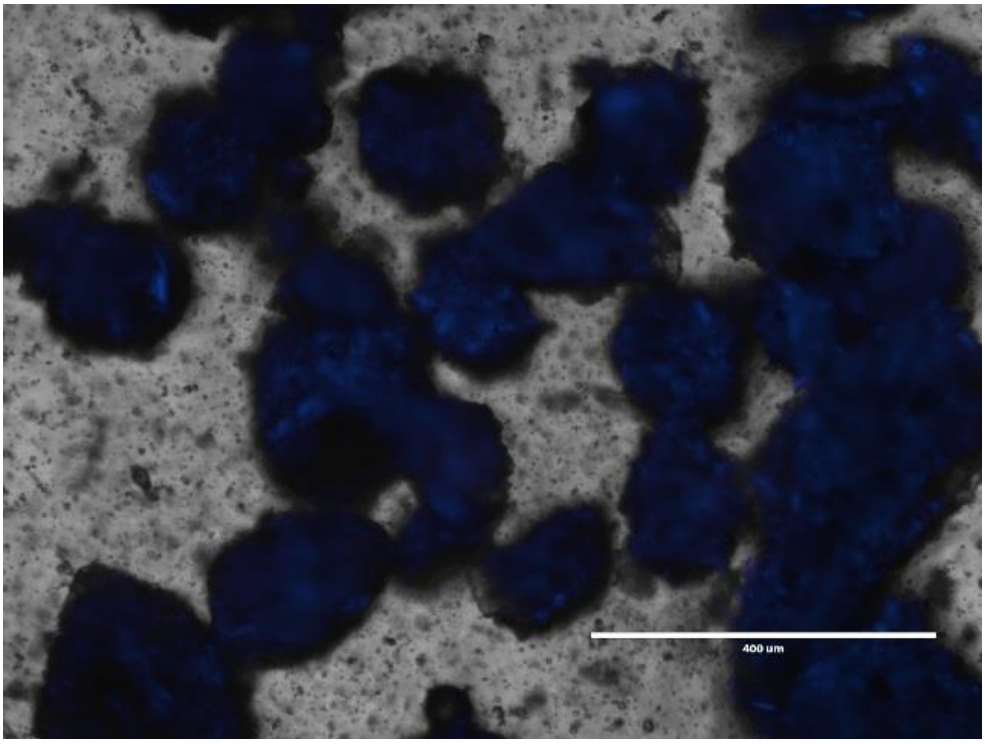
which would change the viscosity and properties of the mixture. This assessment was observed by eye during previous HPH processing experiments. The particles were washed in between each batch process but for assessment were dried prior to processing for storage. In hindsight, this drying step should have been avoided and another method of water removal should have been used. The reason for this is that during the HPH process, the cellulose in the cell wall begins to change structure and undergo fibrillation. This change in property to the cellulose also caused the pores between the cell wall to swell. Upon drying however, when water is evaporated from the plant cell wall (which is already swollen), the pores begin to shrink and eventually cause cell wall collapse which cannot be reversed as a result of drying and rewetting (Weatherwax, 1977, Luo and Zhu, 2011). This process is known as hornification (Jayme, 1944, Stone and Scallan, 1965, Laivins and Scallan, 1993).

The 9P particles in this instance were then used to test for their emulsion functionality despite the drying step. The hypothesis that these particles were to still be hydrophilic in property was tested however this was then disproved. At 8% particle concentration, the emulsion produced was a W/O emulsion. However, the stability of this emulsion is similar to that observed by hydrothermally treated (HT) BSG particles characterised in Chapter 5 and also HT spent coffee particles by Gould *et al.* (2016). If the W/O emulsion produced was in the ideal state, then the particles would permanently reside in the oil and stabilise the boundary interface between the water and the sunflower oil. This would occur due to parts of the particle being hydrophilic such that they can stabilise the W/O interface. Despite the emulsion produced being a W/O, this emulsion was stabilised with the particles residing predominantly in the water dispersed phase stabilising the interface from the inside-out rather than the preferential outside-in coating the interface. In some of the droplets,

the W/O emulsion showed that the particles which once were situated in the oil had migrated into the water phase over time. This was demonstrated in Figure 6.6 by the use of fluorescence microscopy whereby the particles can be seen fluorescing. The sizes of the droplets produced in the emulsion are shown to be huge (150+μm) and outside of the scope of food products.



A) 9P BSG W/O stabilised emulsion



B) 9P BSG W/O stabilised emulsion with fluorescence

Figure 6.6: Water-in-oil emulsion micrograph of 9P BSG particle stabilised emulsion. A) scale bar 1000μm; B) scale bar 400μm with fluorescence DAPI light cube (Excitation: 357/44, Emission: 447/60

6.3.1.5 Summary of HPH treatment

The addition of an HPH step to the particle functionalisation process results in particle size reduction and changes to the surface morphology of the particles. The best results in terms of particle size were achieved with 3 HPH passes, causing a reduction in x_{90} from 154µm ± 17µm for UT BSG to 80µm ± 4µm. This is still significantly larger than the target size of 10µm. The surface morphology after 3 passes appears more open than for UT BSG, potentially leaving the BSG more amenable to HPH processing. Further processing leads to particle agglomeration, which is undesirable, as a key objective is to minimise particle size. The HPH step as part of the particle size reduction is a physical process which transforms the surface morphology of the particles. Kinetically this occurs by the physical removal of primary cell wall cellulosic material from the within plant cell wall matrix. Specifically, cellulose and hemicellulose (including a small amount of lignin) as well as water soluble fatty acids and amino acids. The removal of this material is perceived to be from breaking down the structure of the plant cell wall when the high pressure in the system is transferred into high shear forces through the Z-chamber used. This indicates that the HPH pre-treatment may make the BSG more amenable to hydrophobic functionalisation. Since the removal of primary cell wall components has been demonstrated using NMR, a hypothesis that some of the internalised lignin has been moved closer to the surface (as a result of breaking down and removing cellulose and hemicellulose) can be suggested. This is supported by the evidence shown in 6.3.1.4 where 9P BSG particles were able to stabilise a W/O emulsion without the need for any hydrothermal processing. This observation implies that once internalised lignin has become available at the surface. Although the milling step prior to the HPH step will have a similar effect these produced O/W emulsions (as per Chapter 5), however, the addition of this HPH step when substantial pre-processing is conducted

appears to emancipate lignin enabling the particles to stabilise a W/O emulsion.

Conducting DSC on the materials showed that the use of a high pressure homogenisation pre-treatment step does not affect the thermal properties of the material, indicating that the processing temperature required to hydrothermally activate BSG to become hydrophobic Pickering particles to remains the same regardless of the HPH pre-treatment step and conditions applied. This was not the expected result due to the hypothesis that the HPH step might cleave some of the lignin causing it to fragment and in turn change the properties of the polymer such that the transition temperature might change.

6.3.2 Hydrothermal processing

6.3.2.1 Physical Characterisation

This section covers Step 3 onwards in Figure 6.1. Previously the time and temperature conditions were optimised to 220°C for 120min (Chapter 5), and these processing conditions were then used in this work minimise process variables. It must be noted that even though these conditions were changed, a result of the impact caused to the particle by the HPH process (e.g. facilitated tissue rupture) there could have been additional changes to the reaction kinetics meaning a lower time and temperature process could have been used. This however was not investigated in this work but is a recommendation for future works.

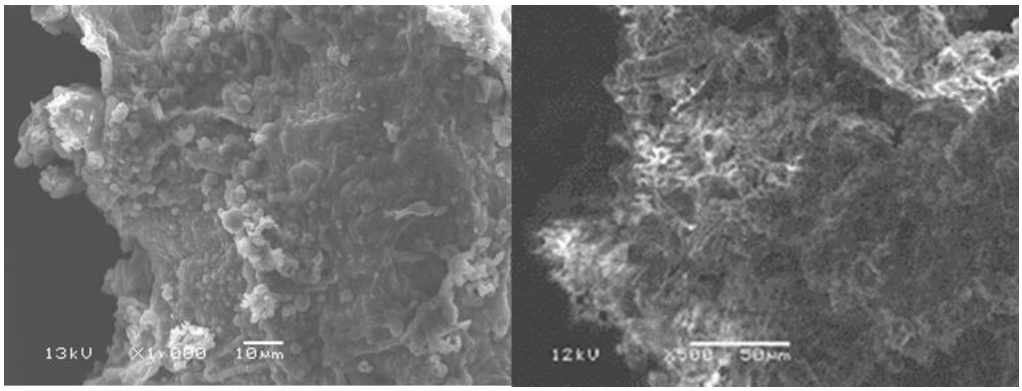
Figure 6.7 shows SEM images of the hydrothermally treated samples produced from BSG exposed to no HPH pre-treatment step (HT BSG), and 3, 5 and 9 HPH passes. There is a clear increase in the number and density of droplets on the surface of the 3PHT BSG compared with HT BSG. Including the HPH step results in a homogenous coverage of droplets throughout the sample on large

particles as well as the smaller particles, which is not observed on HT BSG nor in previous works (described in Chapter 5).

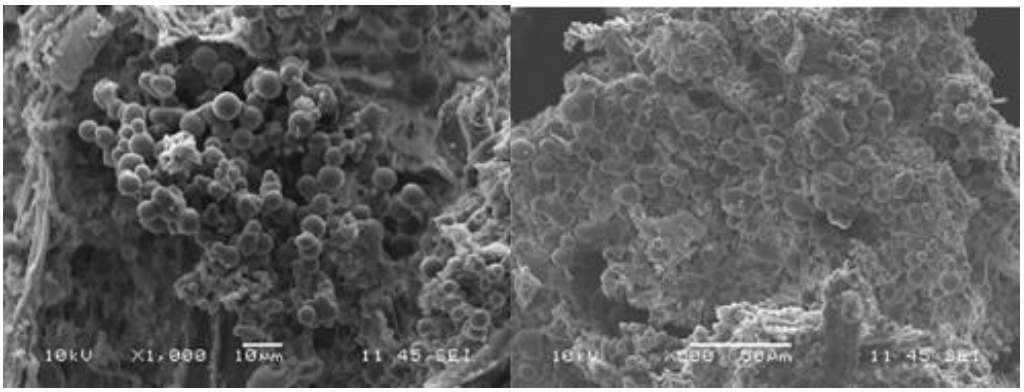
Differences between 3PHT BSG and samples that had been exposed to further HPH passes is less clear, but the lignin droplets do appear to have coalesced more after 5 and 9 passes than after only 3 passes. This suggests that a film of lignin might have been produced rather than droplets resulting in different surface characteristics. This corresponds with the SEM images of the HPH pre-treated particles (Figure 6.3), which showed homogenisation of the surface at 5+ passes resulting in the formation of a film comprised of coalesced lignin droplets following hydrothermal treatment.

Since the process of lignin relocation appears to be a kinetic process, the mobilised lignin or lignin components that will relocate to the surface first is likely to be that of lower phase transition temperature. Upon being heated at or above the transition temperature, lignin changes physical state from a glassy amorphous state in the cell wall to a flowable state whereby it can move and upon cell wall collapse (cellulose) it migrates through the cell wall and is relocated to the surface of the particles. The reason the process is hypothesised to be kinetic is because both time and temperature are crucial factors which impact on the generation of the droplets. As has been shown previously, processing temperature and length of total process changes the surface coverage on the particles. In this section, this is again is important from another angle. The removal of cell wall components assisted in the collapse of the cell wall prior to hydrothermal processing and in turn created smaller diffusion pathway lengths for the lignin to travel to reach the surface of the particle. This explains the formation of a greater number of droplets. The lignin was already closer to the surface or was in fact there initially ahead of hydrothermally treating the particles since the aim of this research was to produce improved lignin coated Pickering

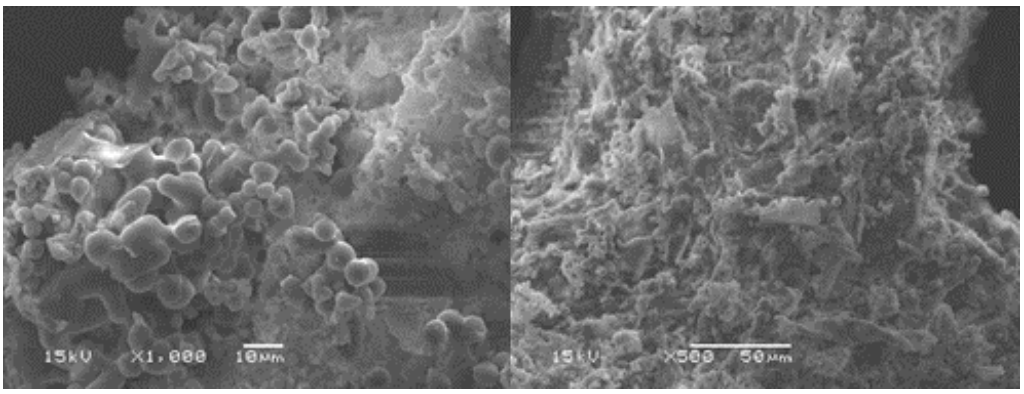
particles with the smallest particle size possible, the 3PHT BSG particles were chosen for characterisation since they had the smallest particle size initially and had the most visible surface droplets.



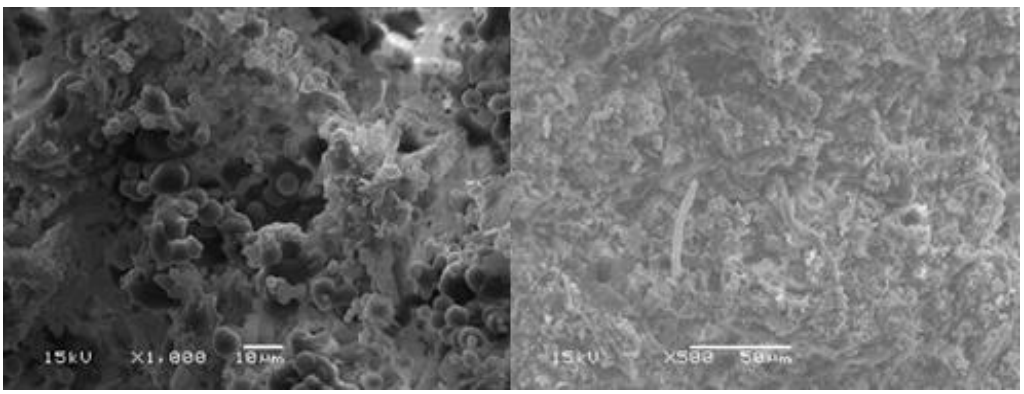
HT BSG (Chapter 5)



3PHT BSG



5PHT BSG



9PHT BSG

Figure 6.7: Surface morphology changes to the different BSG samples after pre-treatment and hydrothermal process observed with SEM (scale bar, Left = 10µm, Right = 50µm)

6.3.2.2 Chemical and thermal characterisation

The surface lignin droplets of the hydrothermally treated samples were isolated using the ethanol extraction to see whether HPH homogenisation affected the composition of the hydrophobic surface. Figure 6.8A shows the composition of the droplets determined by NMR for HT BSG Extract and 3PHT BSG Extract only, although the results were found to be similar for all extract samples. The extracts contain lipids, amino acids, pectin and lignin, and the addition of an HPH pre-treatment step was not found to affect this composition.

Figure 6.8B shows the lignin region (120–165ppm) in more detail. This was used as the basis of isolating which lignin fraction or combination was present in the droplets at the surface of the particles. Chemical shift values showed that the composition of the lignin was primarily coniferyl alcohol which is the alcohol monomer of G-lignin (Manders, 1986). Methoxy groups are present in both the G and S monomers of lignin as the signal at 54–56ppm shows, but due to the lack of specific peak for S in the region at 153.5ppm (C3, C5 of S), the methoxy group allocation is attributed to the group which is attached to C3 on coniferyl alcohol. It is hypothesised that coniferyl alcohol (G-monomer) is more hydrophobic than sinapyl alcohol (S-monomer) which is why it is found in the droplets and not removed into the water fraction of the hydrothermal process. Sinapyl alcohol (S-monomer) has been previously found in the hydrothermal water (Chapter 5). Pure samples of the different lignin monomers also have different melting points. From the online chemistry database, coniferyl alcohol (G-lignin) has a melting point of 74°C (NCBI, 2018a), whereas sinapyl alcohol (S-lignin) has a melting point of 61–65°C (NCBI, 2018c) and p-coumaryl alcohol (H-lignin) has a melting point of 213.5°C (NCBI, 2018b). Therefore, depending on the hydrothermal treatment, different components of the

internalised lignin will likely be liberated at different times and rates. The kinetics outlined previously would suggest that the hydrothermal processing temperature could break some of the bonds in lignin. S-lignin has the lowest melting temperature and is hypothesised to be liberated first and as it is also the most hydrophilic of the three monomers this could be a reason why S-lignin is not found in the droplets as it is in fact removed before the droplets are formed. Therefore, this could affect the number of droplets produced at the surface of the particles as well as their composition.

This is because of inductive and mesomeric resonance effects and the number of oxygen atoms present in the structure of the monomers. The greater the number of oxygens and subsequently methyl group ($O\text{-}CH_3$) attached, the greater the chance for the monomer to form hydrogen bonds with water when used as the processing solvent. The methyl group is more electron-donating than the oxygen by resonance due to the oxygen atom exerting an electron-withdrawing inductive effect. However, the lone pair of electrons on the oxygen in the hydroxyl group on carbon-1 exhibits the opposite effect to the oxygen atom attached to the methoxy group meaning that it becomes slightly electron donating (Soderberg, 2016). Therefore, the oxygen atom bonded to the methoxy group becomes slightly destabilised gaining a positive charge which can therefore bond with the OH^- when water dissociates upon heating in the high temperature water region (Fan *et al.*, 2016).

The differences in lignin percentage and transition temperature between HT BSG (non-HPH treated) and 3PHT BSG are shown in Table 6.2. For the solid particles (with droplets intact), HT BSG and 3PHT BSG appear to have similar lignin percentages as well as transition temperatures with HT BSG containing 21.15% lignin w/w with a transition temperature of 163°C and 3PHT BSG containing

21.38% lignin with a transition temperature of 158°C. However, there are noticeable differences when comparing the two particles at surface morphological level in Figure 6.7 which shows that the surfaces are vastly different in terms of their surface droplet coverage. The data in Table 6.2 also indicates that the percentage of lignin and the transition temperature (22.33% and 22.50%; 169°C and 170°C respectively for HT BSG and 3PHT BSG) of both sample extracts are close to those of the particles. It is hypothesised that the same fractions are being liberated from BSG forming droplets as this is likely the most stable form at lower entropy. In both cases however the surface droplet coverage has been greatly improved with the addition of the high pressure homogenisation step.

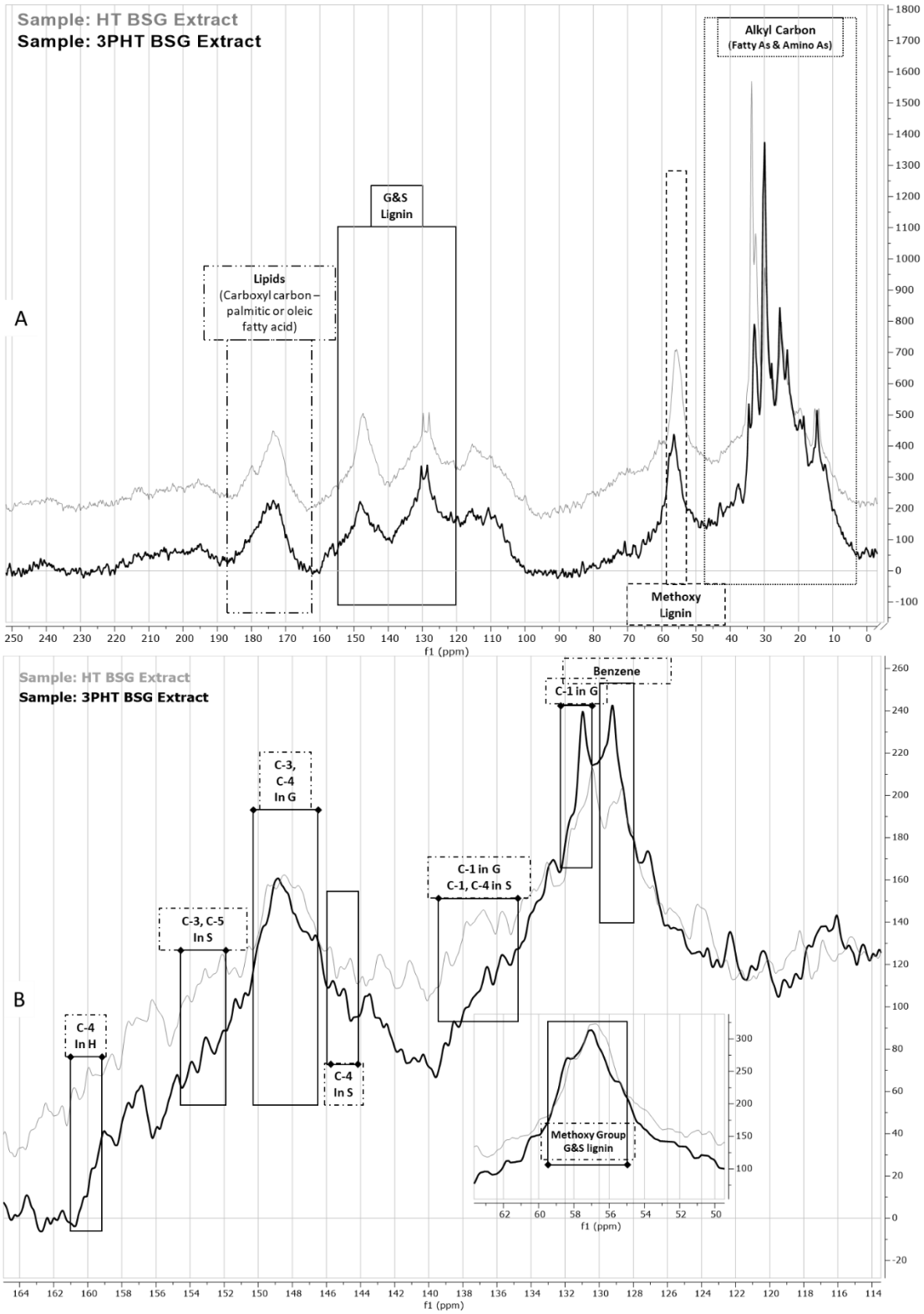


Figure 6.8: A) ^{13}C SS-NMR spectra for ethanol extracted surface droplets from HT BSG and 3PHT BSG; B) ^{13}C SS-NMR spectra for ethanol extracted surface droplets from HT BSG and 3PHT BSG (expanded lignin region)

Table 6.2: Total percentage lignin for different samples as calculated by areas under the specific lignin regions (chemical shifts) of the NMR spectra

Sample	Total lignin	Transition Temperature
UT BSG	7.33%	175°C
HT BSG	21.15%	163°C
HT BSG Extract	22.33%	169°C
3PHT BSG	21.38%	158°C
3PHT BSG Extract	22.50%	170°C

For 3PHT BSG, an extraction procedure was conducted to see where in the particle the lignin was present and to understand whether or not all of it has been mobilised to the surface. The extraction procedure isolated the droplets as an extract leaving behind a solid framework structure of the particle, from where the lignin has been relocated. Figure 6.9 shows the composition of the different constituents of the particle. From the NMR spectra, the framework solid structure of the particle can be seen to consist mainly of cellulose and hemicellulose with a small lignin signal still being present. The extract however is where the majority of the lignin can be found. This suggests that the majority of the lignin that was once in the secondary cell wall has been relocated to the surface of the particles. The mechanics of the ethanol extraction are such that any materials which are capable of being dissolved in ethanol will be extracted. This is not limited to just the surface of the particles and is in fact a total extraction procedure. As was shown in 5.3.2.3, for UT BSG around 10% of the mass is extracted by weight during the ethanol extraction however adding a hydrothermal process enabled greater recovery of ethanol extractable material that with no prior processing. As such this extra liberation of hydrophobic material is being attributed to the relocation of lignin to the surface of the particles following cell wall collapse during the hydrothermal process.

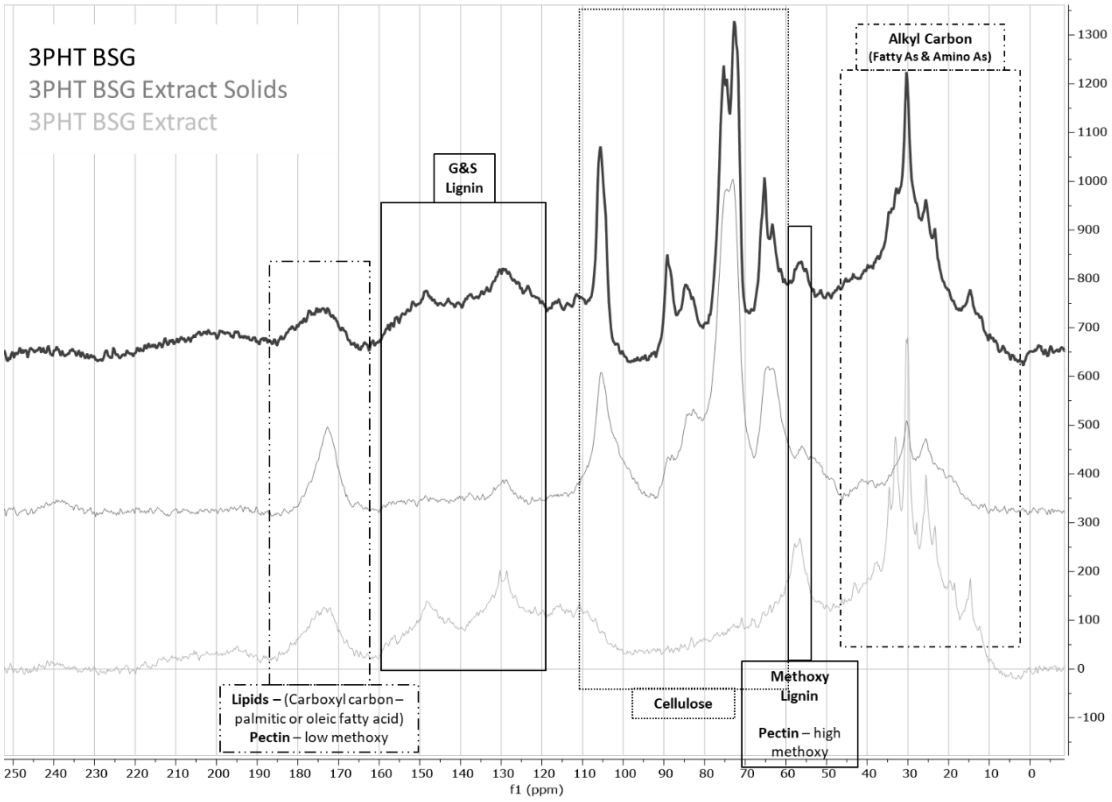


Figure 6.9: ^{13}C SS-NMR spectra for BSG particles which have had 3 passes at 2068 bar and subsequently hydrothermally processed

6.3.3 Particulate emulsifying capability

6.3.3.1 Preceding (HT BSG) vs current (3PHT) particle functionality

HT BSG particles were compared to the 3PHT BSG particles by preparing 50 g of 3PHT BSG emulsion at a 50/50 oil/water ratio and a concentration of 2% particles using the Ultra Turrax mixer. This was to assess whether the inclusion of the high pressure processing step before the hydrothermal treatment had improved particle performance and functionality for use as a particulate emulsifier capable of stabilising W/O emulsions. The differences between the emulsions (HT BSG and 3PHT BSG) are visible in Figure 6.10A and Figure 6.10B. For the HT BSG emulsion, the majority of the emulsion droplets coalesced on Day 1 showing instability as evidenced by lack

of visible individual water droplets. From initial observation, the particles themselves were stabilising the HT BSG emulsion whilst residing predominantly residing in the water dispersed phase (Figure 6.10A). The lignin droplets at the surface of the particles are proposed to stabilise an W/O emulsion. However, for the 3PHT BSG W/O emulsion imaged in Figure 6.10, distinct water dispersed phase droplets are visible. Irregular shaped water droplets became fewer in number with the 3PHT particles and this is attributed to the particles being adsorbed at the interface between the water and oil phases. The suggested increased hydrophobicity of the 3PHT BSG particles appears to halt complete coalescence of water droplets as a consequence of the interface being jammed with particles (Pawar *et al.*, 2011, Gould *et al.*, 2016). The emulsion produced by 3PHT BSG is highly viscous in consistency when compared to HT BSG, but this needs to be quantified in future works.

For the first time however, particles (3PHT) are visually stabilising the interface whilst residing predominantly in the oil continuous phase (even at a lower particle percentage) suggesting that the particles are more hydrophobic than the HT BSG ones produced previously. This is the first time in this system that W/O BSG emulsions were observed to be stabilised by hydrothermally treated particles, with particles jammed at the interface whilst residing predominantly in the oil.

Previous work by Gould *et al.* (2016) stated that an optimisation of the hydrothermal treatment may allow for a more homogenous deposition of particles and demonstrates control over surface chemistry/hydrophobicity and optimisation on the hydrothermal treatment of BSG (Gould *et al.*, 2016). This research has additionally shown that the inclusion of a high pressure homogenisation pre-treatment step can influence the surface coverage of droplets on BSG particles ((Gould *et al.*, 2016); Chapter 5). Subsequently these

particles have been demonstrated to be more hydrophobic than those previously created by their ability to stabilise of water droplet dispersed phase emulsions. The change in the hydrophobicity has been attributed to this increased ability to form particle stabilised emulsions however, particle size must also be considered. A greater proportion of the particle size distribution is in the smaller particle range with the X_{90} between UT BSG (153μm) and 3P BSG (80μm) being over 70μm different between the two. This suggest that particle size is another important factor in the stabilisation of Pickering emulsions. This further backs evidence by McClements (2016) which states that particle size is one factor which has to be considered in the stabilisation of emulsions (McClements, 2016a). This reduction in particles size means that a greater proportion of particles are in the magnitude capable of stabilising at the interface and where the "necking" phenomena of larger particles may be mitigated causing a more effecting Pickering stabilisation.

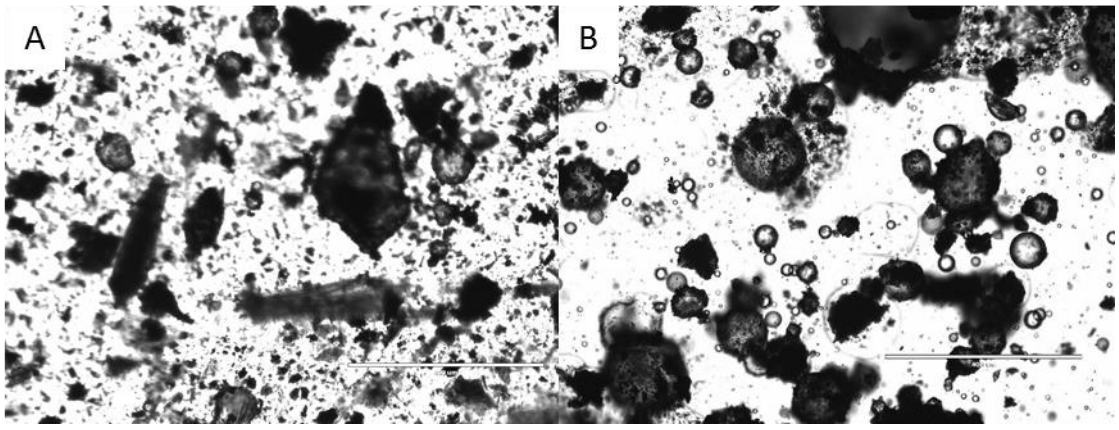


Figure 6.10: Micrographs of HT BSG at 4% particles (A) and 3PHT BSG at 2% particles (B) samples taken on Day 1 (scale bar = 400μm and particle being the dark/black parts of the micrographs)

6.3.3.2 Range of emulsifying capability for 3PHT BSG particles

Different percentages of oil and water were used to create a range of emulsions. This was in an attempt to understand the range of functional capability of the 3PHT BSG particles. A minimal particle concentration was used to show that 3PHT BSG particles could stabilise an emulsion at concentration 2% w/w. This method was used instead of contact angle between the particles adsorbed at the water dispersed phase droplet interface, which is the commonly utilised protocol to characterise the hydrophobicity of particles. This is because of the irregular shape of 3PHT BSG particles that would introduce error into the measurement. The measurement of contact angle shows whether particles are preferentially wetted by a hydrophilic or hydrophobic liquid phase (or polar/non-polar) and suggest which type of emulsion is likely to be stabilised. Therefore the emulsions produced using the protocol in section 6.2.5 were intended to give an understanding of the resulting O/W or W/O emulsifying capability of the processed BSG particles without the use of contact angle measurements, but by changing the concentration of the liquid phases.

Figure 6.11 shows the emulsions produced when imaged at Day 7 in the vials, to which the emulsions were transferred post-processing. The bright field micrographs were taken at Day 1. The vials show that the samples produced with ≤30% oil are in fact oil-in-water emulsions. These broke down immediately after processing by the visible phase separation of the oil and water. An important observation was that for the 40% samples, the emulsion produced was a very unstable O/W emulsion. For samples which contained 50% or more sunflower oil, W/O emulsions were produced when using 3PHT BSG as the particulate emulsifier at 2% concentration w/w. This shows that depending on the concentration of oil included, a water-in-oil emulsion can be produced using 2% 3PHT BSG

particles w/w shown by the gravitational separation of the emulsion layer being visible at the bottom of the vials in Figure 6.11. Micrographs showing the structure of the emulsions produced are shown in Figure 6.12 with these images taken on Day 1. Although the droplet sizes do not visually appear to change their size, the stability of the particles and where they are situated does. The particles in the 80% sample appear to suggest full jamming at the interface of the dispersed water droplets whereas in the 50% sample, droplets are still jammed at the interface, but the interface is not fully packed and is not homogenous. This is attributed to the greater proportion of water in the formulation resulting in a greater interfacial area of the water for a fixed quantity of particles. As such, the same number of particles based on the 2% w/w particle inclusion is attempting to stabilise 30% more water in the system.

With regards to the phase volume layers of the emulsion layers in all of the vials in Figure 6.11, for the W/O emulsions (50-90% oil), the 50% and 60% emulsions appear to take up half of the vial space whereas the 70-90% emulsions appear to take up about one third of the total phase volume. This is attributed to the concentration of the particles and the amount of water in the system although the results in Figure 6.12 and Table 6.3 show that the droplet sizes of the emulsions for all W/O emulsions appear to be in the same size distribution and order of magnitude regardless of composition. Since the number of particles stays the same and the amount of water dispersed phase gets smaller, the lack of change in the phase volume layer suggests that the concentration of the particles does in fact have an effect on the bulk phase volume. The representative 70%, 80% and 90% emulsion micrographs in Figure 6.12 show that there are minimal changes to droplet size despite the greater concentration of particles to dispersed water phase droplets.

The differences between the emulsions and their droplet sizes are visible in Figure 6.12, however, quantified differences between the samples is shown in Table 6.3. Here, the different droplet sizes based on the emulsions produced is shown. The differences in the variety of the droplet sizes across all ranges of X_{10}, X_{50} and X_{90} suggest that there is in fact no difference between the droplet sizes produced. The variation in droplet size implies that the particle size variation is still broad however, the clear Pickering stabilisation shown above 70% oil gives greater evidence that these particles are greatly improved to those previously generated in Chapter 5. The smaller particle size as well as the greatly increased surface coverage of droplets has assisted in effective Pickering stabilisation at the W/O interface however the broad particle size range is still an important factor affecting the size of the dispersed phase droplets. In order to effectively produce emulsions of greater long term stability, a narrower particle size variation must be generated which is ideally one order of magnitude smaller than the targeted droplet size.

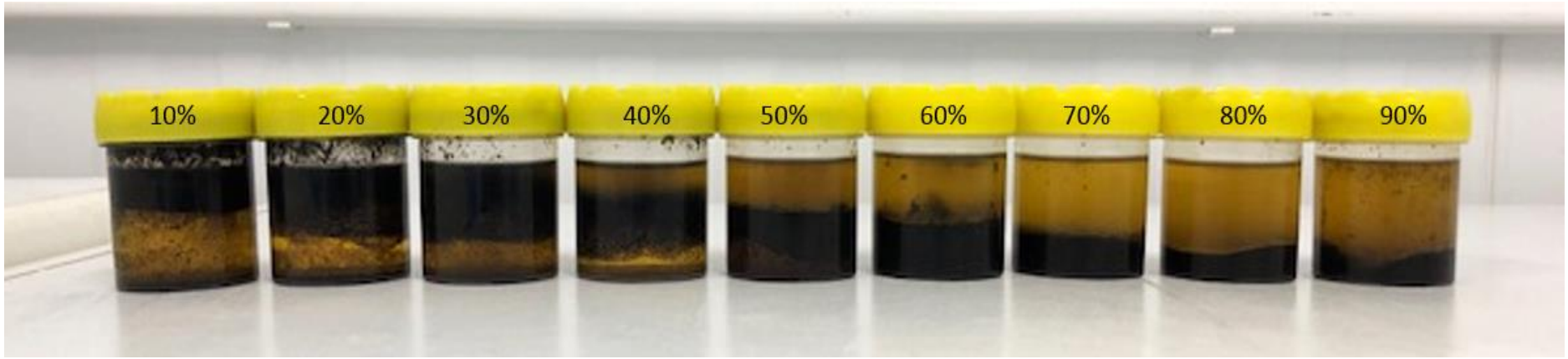
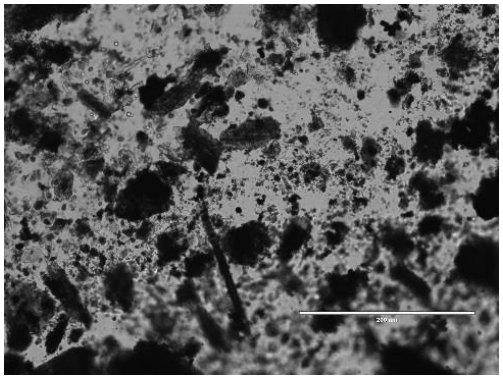
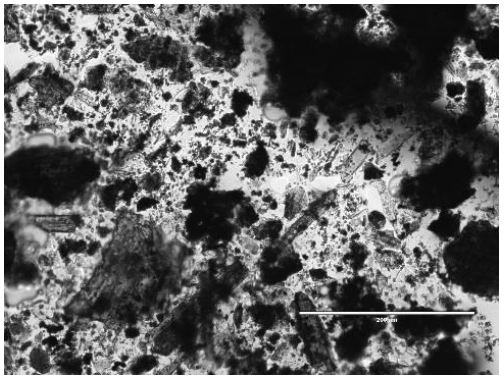


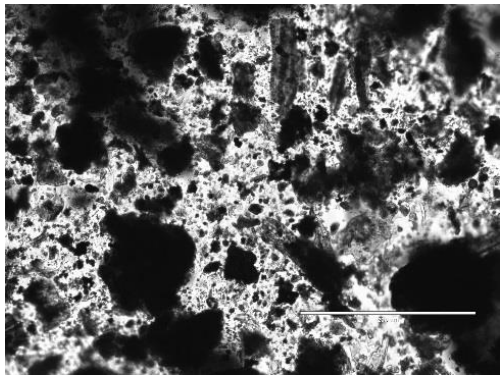
Figure 6.11: Vials containing emulsions at 2% particle concentration with different oil percentages.



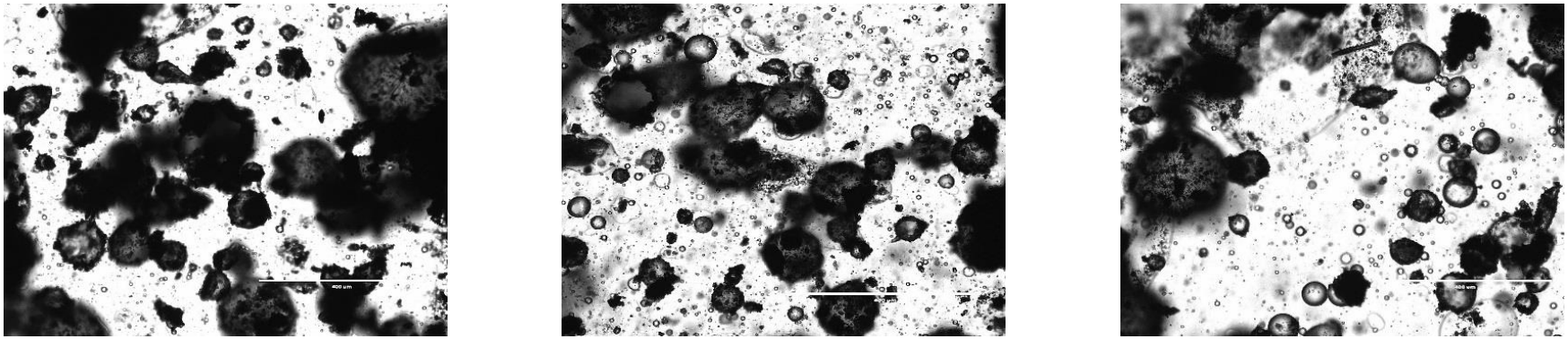
10%



20%



30%



40% **50%** **60%**

70% **80%** **90%**

Figure 6.12: Representative micrographs for all emulsions produced at different O/W concentrations. Percentage denoting the percentage oil in the system (scale bar = 400μm)

Table 6.3: Emulsion type and droplet size at X_{10}, X_{50} and X_{90} for the different emulsions produced with varying quantities of sunflower oil and water at 2% 3PHT BSG particles

Sample Name	Emulsion Formed	Average X_{10} (µm)	Average X_{50} (µm)	Average X_{90} (µm)
10 % SF Oil	O/W	27.68 ± 7.58	68.57 ± 21.58	105.92 ± 28.64
20 % SF Oil	O/W	31.69 ± 18.18	89.51 ± 59.29	119.39 ± 57.89
30 % SF Oil	O/W	39.34 ± 21.61	98.87 ± 51.28	121.33 ± 55.14
40 % SF Oil	BOTH	51.03 ± 29.54	121.77 ± 66.09	151.07 ± 59.17
50 % SF Oil	W/O	46.26 ± 14.17	121.60 ± 52.11	152.00 ± 47.16
60 % SF Oil	W/O	50.37 ± 20.09	126.32 ±61.02	148.36 ± 55.91
70 % SF Oil	W/O	59.52 ± 31.74	141.14 ± 69.57	167.55 ± 60.61
80 % SF Oil	W/O	63.97 ± 63.07	135.31 ± 67.13	168.40 ± 62.07
90 % SF Oil	W/O	55.32 ± 19.14	131.21 ± 55.52	158.24 ± 52.43

6.3.4 Additional particle functionality (cakes)

The difference between two emulsifiers was tested for use as an emulsifier in a foam-type product. Bread and cakes were initially selected as options to test the functionality. The BSG particles created could potentially be used to replace conventional emulsifiers in foam-type products. These could include, for breads: DATEM; SSL; GMS and Lecithins and for cakes: Polysorbate 60 and sorbitan monostearate. In breads, the emulsifiers named are used at up to 0.3%, 0.5%, 1%, and 0.5% respectively (Cauvain and Young, 2006). In cakes, the named emulsifiers are used at 0.46 % and 0.61 % of the total cake mix (FDA, 2018a, FDA, 2018b, BAKERpedia, 2019a). but due to the colour of the particles, cake was selected as this was perceived as the product where the particles may have the greatest potential use. Full differences in the particles (UT BSG and 3PHT BSG) and the conventional emulsifier is discussed in detail in Appendix A2.

A comparison of two cakes was selected for this section of the results, specifically the conventional emulsifier and 3PHT BSG. Figure 6.13 shows the structure of the cakes produced using the conventional emulsifier and the 3PHT BSG particles. The main

noticeable differences between the two are the crumb structures and the colour of the cake batters.

The conventional cake emulsifier produced a cake batter which is symbolic of most conventional cake batters (e.g. a Victoria sponge cake) whereas the 3PHT BSG particles when homogenised to form a W/O emulsion prior to being added to the other ingredients produced a batter which matched the colour of the emulsion produced in Chapters 5 and 6 for hydrothermally treated samples where droplets are produced.

The commercial emulsifier (Figure 6.13A) produced appeared to produce a much coarser structure for the crumb compared to a regular cake baking trial. This was hypothesised to be as a result of the emulsifier perhaps being old or out of date or that the concentration of the emulsifier was not great enough. The concentration of the emulsifier perhaps being too low could also be a reason why the batter density was almost equal to 0.9 which is at the higher end of acceptable for a conventional cake batter (full results in Appendix A2).

For the 3PHT BSG particles (Figure 6.13B), aside from the colour change other noticeable changes to the structure of the cake appeared. The underside of the cake even prior to cutting showed that holes had been produced in the crumb. Upon cutting, significant tunnel had appeared in the structure which despite not affecting the quality of the product is not a desirable visual for the consumer.

Although tunnelling is often linked to having a lower batter density and a finer crumb structure, some of the initial works shown in Appendix A2 showed that this cake had the highest density. As a result of this coarse crumb structure, it was hypothesised that the presence of particles in the crumb structure due to stabilising the emulsion may be puncturing some of the air pockets during baking

which in turn will generate tunnels due to the irregular shape of the particles.

Comparing the two cake structures, the addition of the particles has a clear changing behaviour to the structure of the batter as well as the end product of the cake. The particles act more like fibres than physical particles due to the puncturing effect of the particles to the batter and baked cake matrix. Research has shown that the addition of fibre to bread for example changes the structure of the crumb and the texture of the bread. The crumb gets coarser and the holes in the bread get larger often perceived to be due to the fibres puncturing the air pockets and bubbles within the gluten matrix when a dough is formed (Rosell and Santos, 2010, Sivam *et al.*, 2010). The same principle applies when making a batter for a cake. This puncturing effect increases bubble coalescence and also disproportionation (uptake of small bubbles by larger ones due to pressure differences) which can be shown upon baking by the large holes and tunnels appearing in the cake.



Figure 6.13: Produced cakes when using A) conventional cake emulsifier; B) 3PHT BSG particles pre emulsifier with water and oil before adding to a cake removing all conventional emulsifier from the batter

6.4 Conclusions

Processing BSG at 2068 bar under high pressure homogenisation conditions removes components of the feedstock that are routinely found in the primary cell wall namely: cellulose; hemicellulose; and pectin. However, this removal made no difference to the temperature required for BSG lignin to undergo a thermal transition. With regards to the aim of particle size reduction, the smallest particle produced was 3PHT BSG with the x_{90} being 80µm ± 4µm.

Using the HPH step to an "over processed" stage (9P) generated particles which aggregated during processing and also were able to stabilise W/O emulsions in similar Pickering stabilise to those which had no additional processing but were hydrothermally treated at 220°C for 120min.

Following hydrothermal treatment, the majority of once internalised lignin has been shown to be relocated to the surface of the particle. An important observation is that regardless of processing, and the inclusion of a HPH homogenisation step, the lignin droplet composition and bulk particle lignin percentage were comparable between HT BSG and 3PHT BSG.

At a 2% particle concentration, a W/O emulsion was produced at a maximum of 50% water. The droplet sizes were still larger than 100µm necessitating a requirement in future work to improve particle size reduction and lower the dispersed phase droplet size. For the first time, stabilised W/O emulsions with particles which reside predominantly in the oil continuous phase have been produced. This in turn confirmed that the inclusion of a high pressure homogenisation step prior to hydrothermal processing has indeed created a particulate emulsifier with increased water-in-oil emulsifying capability, than hydrothermal processing alone.

Additional works on particle functionality showed that the 3PHT BSG particles could replace a conventional cake emulsifier to stabilise a

cake batter. The 3PHT BSG cake differed to the conventional cake by being a darker colour but also had visible tunnelling effects in the baked cake which was attributed to the sharp irregular nature of the particles puncturing the bubble structure.

Future work following this research must aim to test these emulsions against shear stability; find a way of quantifying dispersed droplet size distributions through image analysis; and look for an alternative method of particle size reduction prior to hydrothermal processing or possibly a sieving step on dried particles before or after hydrothermal processing. If no further particle size reduction is possible then other products should be tested such as foams. With regards to the HPH homogenisation process, the drying step should be removed post processing to avoid plant cell wall hornification which could inadvertently increase the particle size and cause particle aggregation during drying.

Acknowledgments: This research was supported by the Engineering and Physical Sciences Research Council, University of Nottingham and Campden BRI. We would like to thank in the Division of Food Science, Steve Johnson and Val Street for technical support and the Nanoscale and Microscale Research Centre (nmRC) for providing access to instrumentation with Mrs Christine Grainger-Boultby providing technical assistance. We would also like to thank Steven Walker of Campden BRI for being industrial partner in this research.

Author contributions: J.H., W.M., G.B, R.A, E.B. and B.W. conceived and planned the experiments. J.H and W.M carried out all sample preparation and subsequent experiments. J.H. took the lead in writing the manuscript. All authors provided critical feedback and

helped shape the research at various stages, analysis and writing of this manuscript. All authors have approved and are accountable for the final version of the manuscript submitted.

Conflicts of Interest: The authors declare no conflict of interest. The founding sponsors had no role in the design of the study; in the collection, analyses, or interpretation of data; in the writing of the manuscript; and in the decision to publish the results.

7 Final conclusions and proposed next steps

The aims of this PhD were outlined in the motivation and objectives section at the beginning of this thesis. Namely:

1. The selection of an appropriate lignin rich feedstock for use in the experimental work.
2. To explore processing parameters and routes for Pickering particle generation; specifically, the time and temperature of the hydrothermal process necessary to form a hydrophobic Pickering emulsifier.
3. To explore whether an additional high pressure fluid process prior to hydrothermal processing generated particles of greater hydrophobicity than previously demonstrated and confirm whether this is linked to better emulsion stability with smaller particles and dispersed phase droplets.
4. To confirm whether these emulsions are usable in current food industry applications.
5. To quantify the lignin percentage in the particles using a newly developed method (Nuclear Magnetic Resonance) and compare this to the established wet chemical assay used widely in wood research, known as the Acetyl Bromide Soluble Lignin assay, as well as a known Thermogravimetric Analysis (TGA) method.

These objectives have largely been met, as shown in the results chapters 4, 5 and 6.

7.1 Final Conclusions

7.1.1 Feedstock selection

Following literature searches covering a wide array of lignin-rich materials, Brewers' Spent Grain (BSG) was selected as feedstock of choice. Since it is a highly abundant by-product of the brewing

supply chain as well as containing high levels of lignin, it was an appropriate feedstock for potential valorisation into new ingredients.

BSG from 100% malted barley was selected as BSG-based feedstock for this research and the ability of hydrothermal processing to generate a particulate emulsifier was investigated.

7.1.2 Time and Temperature parameters in hydrothermal processing

Untreated BSG had an onset thermal transition at 140°C with the peak in the transition occurring at 175°C. From DSC results it was difficult to determine the exact nature of this transition. It could have been an exothermic peak or a distorted glass transition. Upon hydrothermally treatment, the processing temperature must be above the peak transition temperature of lignin in BSG to mobilise the lignin to enable it to form droplets at the surface of the particles. The droplets at the surface of the particles have been confirmed to be lignin-rich specifically containing the monomeric fingerprint of coniferyl alcohol (G-monomer) based on the chemical shift pattern of the NMR spectrum. Sinapyl alcohol (S-monomer) was found in the aqueous phase which suggests that the lignin monomeric composition was depleted of S-lignin which created an environment rich in coniferyl alcohol. All of this was proved by the chemical shift signals of the various fractions by NMR. They were also found to have an onset thermal transition at 100°C with peak transition occurring at 135°C. These droplets were extracted from the HT BSG samples (heat treatment 200°C for 90min) and had a lower thermal transition temperature than the UT BSG with HT BSG extracted droplets having an onset thermal transition at 125°C with peak transition occurring at 160°C. From a literature review (using milled wood lignin from BSG as reference material and Table 2.3), coniferyl alcohol appears to be the main lignin monomer present in BSG at

more than twice the concentration to sinapyl alcohol (Rencoret *et al.*, 2015).

Of the processing conditions tested, the highest temperature and time conditions (220°C for 120min) generated the most droplets at the surface of the particles. (Scanning Electron Micrographs for all temperature treated samples are shown in Appendix A1). This suggest that increasing the temperature further may liberate more lignin droplets without the need for any additional processing or that for BSG which has no additional processing to milling that there may be a maximum amount of lignin-based material which can be extracted by hydrothermal processing alone.

7.1.3 High pressure processing technology applied for particle size reduction and emulsion droplet size reduction

The use of a microfluidizer (LM20) operating at 2068 bar prior to hydrothermally processing at 220°C for 120min resulted in a steady reduction in the particle size for UT BSG up to a maximum of 3 passes, generating a particle size with X_{90} of 80µm ± 4µm. An increase in processing to 5 or 9 passes generated particles with increased size probably as a consequence of particle agglomeration. Kinetically this occurs by the physical removal of primary cell wall cellulosic material from the within plant cell wall matrix. Specifically, cellulose and hemicellulose (including a small amount of lignin) as well as water soluble fatty acids and amino acids. The removal of this material is perceived to be from breaking down the structure of the plant cell wall when the high pressure in the system is transferred into high shear forces in the microfluidizer.

Including the high pressure homogenisation stage prior to hydrothermal treatment appears to have facilitated a more consistent release of lignin in BSG which was shown by the visible

generation of an increased number or even a full coverage by lignin-rich droplets at the surface of the particles. With regard to particle functionality, 2% 3PHT particles were capable of stabilising a W/O emulsion for sunflower oil and water ratios ranging from 50/50 to 90/10.

7.1.4 Relevant droplet size for food industry applications

Whether using just a hydrothermal treatment or including a microfluidization high pressure step beforehand, with BSG as the feedstock, dispersed phase emulsion droplets did not get into the desired order of magnitude for use in food industry emulsion applications. The target particle size was <10μm with ideal being 1–2μm in order to stabilise droplets <100μm but ideally in the range of 10–20μm.

However, if another step post hydrothermal treatment to separate particles in the desired order of magnitude was employed, then this size fraction of BSG particles could potentially be used in emulsion-based food products.

7.1.5 Lignin Percentage Quantification - Acetyl Bromide Soluble Lignin (ABSL) Assay, Thermogravimetric Analysis (TGA) and ^{13}C solid state Nuclear Magnetic Resonance (NMR)

To quantify lignin percentage in any biomass, the Acetyl Bromide soluble lignin (ABSL) chemical assay has traditionally been employed. Although many variants on this method have been used, such as the inclusion of additional steps, for instance introducing sodium hydroxide to precipitate out the protein in samples, a detailed study of the effects of feedstock composition on the Acetyl Bromide assay has not been carried out.

One of the chemical components of the ABSL assay, is Sodium Hydroxide (NaOH) which is used to precipitate the protein out of the sample to avoid being detected in the supernatant upon quantification. NaOH also can affect the plant cell wall of the biomass in other ways, for example it can aid in the delignification and dissolution of hemicellulosic polysaccharides albeit temperature dependent which in turn can add error to the quantified lignin percentage (Sun *et al.*, 1995). Additionally, NaOH has been shown to at relatively low percentage (2%) could effectively transform cellulose I into cellulose II whilst also removing hemicelluloses which again could add additional error to the quantification of lignin since the absorbance of hemicellulose is in the same range of UV light as lignin (Chen *et al.*, 2017).

To understand the fundamental processes underlying the Acetyl Bromide assay and how it behaves with feedstocks containing different lignin, monomeric alcohols (coniferyl alcohol and sinapyl alcohol) were substituted for lignin in varying ratios and studied under the same reaction conditions. The ABSL assay was compared to a newly developed quantitative NMR method and a Thermogravimetric analysis method which was tested using three different lignin-rich feedstocks. This study found that the Acetyl Bromide soluble lignin chemical assay differentially quantifies monomeric compositions depending on the chemical species present and as such cannot easily differentiate between the lignin in the feedstock and what its composition is. Samples which are over 75% coniferyl alcohol (G-monomer) are overestimated by as much as 20% on the total percentage lignin, whereas samples which are 75% sinapyl alcohol (S-monomer) are underestimated by up to 15%. With regards to feedstock variation this generates significant error when trying to characterise lignin. Since the assay quantifies lignin based on absorbance at 280nm, under the spectrophotometric conditions

used, coniferyl alcohol absorbs more UV at 280nm compared to the reference sample of Sigma Aldrich Low sulphonate content alkali lignin; whereas sinapyl alcohol absorbs less UV at 280nm compared to the reference sample of Sigma Aldrich Low sulphonate content alkali lignin, both of which will contribute to error in the assay. This could be a full explanation of why the ABSL assay estimates lignin contents differently for differing monomeric composition but could potentially be corrected by UV absorption coefficients. However this will need further testing as part of the future works.

For the TGA method when using monomers to represent lignin, this barely registered values for the percentage lignin since the method worked using the fixed carbon content to calculate lignin. As the sample make up was equivalent to 100% lignin this should have been shown by the method however for the varying percentage compositions the samples were calculated to be between 7.5% and 19.5% lignin. As such this method cannot accurately calculate lignin and therefore should not be used.

The main differing observations between the ABSL assay and the newly developed NMR method are that the ABSL quantifies a total lignin percentage that is entirely dependent on fundamental lignin monomeric composition whereas the NMR method can be used to quantify total lignin percentage independent of composition (based on some assumptions), as well as giving information on whether the feedstock is rich in either coniferyl alcohol or sinapyl alcohol based on the peaks and intensities of these peaks in the 120–165ppm region. The extra information characterised by NMR gives greater detail on the material composition than the ABSL assay and the TGA method in this instance. As such the NMR method with the addition of an extra quantification step proposed in future works should be used as a legitimate method for lignin quantification in biomass hereafter.

The percentage lignin requires further analysis to understand true limitations of NMR and this could be conducted by assessing the lignin percentage in a w/w experiment using a known amount of reference material which is also placed in the NMR rotor. Some of these suggestions were highlighted at the end of the conclusions and future work in 4.4. Upon using a reference sample of Adamantane in the rotor, a calculation of lignin percentage based on carbon chemical shift ratios can be characterised based on the relative intensities of the peaks. This will give a more accurate measurement of lignin in a feedstock with any correction factors being observed if coniferyl alcohol and sinapyl alcohol behave differently when they are spun.

7.2 Proposed next steps

Following on from the conclusions of this research, additional future research works are suggested in both immediate next steps and long-term objectives.

Some of the suggested future work has seen preliminary investigation and is reported in Appendices A2 to A5. These appendices and the relevance are highlighted in the following points:

1) Investigating how the Acetyl Bromide lignin assay behaves in relation to quantifying lignin in a feedstock. For the newly adopted NMR method further validation would involve using a reference material in the rotor to further calibrate the behaviour of the individual monomers. It is also essential to carry out some variable contact time experiments. This would identify whether or not there are different intensities of the NMR signal for both coniferyl alcohol and sinapyl alcohol similarly to the absorbance of UV in the ABSL assay. A number of different feedstocks with differing G/S monomeric ratios should be tested to further investigate the impacts of monomeric composition of the efficiency of lignin

quantification. Other methods of lignin quantification such as thermogravimetric analysis (TGA) using peak deconvolution and pyrolysis gas chromatography and mass spectrometry (Py-GC/MS) should be tested and quantified in relation to the NMR method to look for ways of using these methods synergistically.

2) With regard to the hydrothermal treatment, only BSG has been used a feedstock for generating particulate emulsifier. Due to the differences in composition in the lignin-rich by-products which are generated in the food and drink manufacturing supply chain, alternative hydrothermal processing conditions should be investigated (e.g. lower temperature and shorter time post HPH in the 3PHT BSG samples), as well as other feedstocks. This should identify whether there are any common themes between feedstocks and how they behave under hydrothermal conditions to generate hydrophobic particulate emulsifiers. With regard to the emulsions produced, the shear stability and rheological properties of these need to be investigated to understand the differences between not only the emulsifiers themselves from a functional perspective but also the stability of these emulsions. Aspects of this are already on-going as part of a patent application between the University of Nottingham and Campden BRI.
3) The droplet size of particle stabilised emulsions are notoriously difficult to quantify using laser light diffraction techniques. The particles which stabilise the interface contribute directly to the data alongside the dispersed phase emulsion droplets. Measuring the particle size distribution of the emulsifier separately could be carried out and this data could be subtracted from the droplet size distribution, either manually using micrographs or with some kind of image analysis

software. Additionally, oil continuous systems could be used to measure the water droplet sizes.

4) Since the particles produced are rather large for some current food industry emulsion applications, but are hydrophobic in nature, other possible products should be considered. Alternative products for stabilisation of the particles could be foams or chocolate.

This work has attempted to show that by using a hydrothermal treatment or adding a high pressure homogenisation process prior to hydrothermal treatment, a hydrophobic particulate emulsifier, which would reside predominantly in the oil phase of an emulsion can be created. Furthermore, there is potential for the development of a range of products from materials which are classified as lignin-rich supply chain by-products in the food and beverage industry.

References

AGARWAL, D., MACNAUGHTAN, W. & FOSTER, T. J. 2018. Interactions between microfibrillar cellulose and carboxymethyl cellulose in an aqueous suspension. *Carbohydrate Polymers,* 185**,** 112-119.

AGO, M., HUAN, S., BORGHEI, M., RAULA, J., KAUPPINEN, E. I. & ROJAS, O. J. 2016. High-Throughput Synthesis of Lignin Particles (approximately 30 nm to approximately 2 mum) via Aerosol Flow Reactor: Size Fractionation and Utilization in Pickering Emulsions. *ACS Applied Materials & Interfaces,* 8**,** 23302-10.

AL-JALALI, M. A. & MAHZIA, Y. M. 2014. Effect of electronegative elements on the NMR chemical shift in somesimple R-X organic compounds. *IOSR Journal of Applied Physics,* 6**,** 45-56.

ALBERSHEIM, P., DARVILL, A., ROBERTS, K., SEDEROFF, R. & STAEHELIN, A. 2011. Biochemistry of the Cell Wall Moleules. *In:* ALBERSHEIM, P. (ed.) *Plant Cell Walls: From Chemistry to Biology.* Abingdon, UK: Garland Science, Taylor & Francis Group, LLC.

ANDERSON, J. W. & BRIDGES, S. R. 1988. Dietary fiber content of selected foods. *The American Journal of Clinical Nutrition,* 47**,** 440-447.

AZADI, P., INDERWILDI, O. R., FARNOOD, R. & KING, D. A. 2013. Liquid fuels, hydrogen and chemicals from lignin: A critical review. *Renewable and Sustainable Energy Reviews,* 21**,** 506-523.

BAI, L., HUAN, S., XIANG, W. & ROJAS, O. J. 2018. Pickering emulsions by combining cellulose nanofibrils and nanocrystals: phase behavior and depletion stabilization. *Green Chemistry,* 20**,** 1571-1582.

BAKERPEDIA. 2019a. *Emulsifiers* [Online]. Portland, OR: Bakerpedia. Available: https://bakerpedia.com/ingredients/emulsifiers/ [Accessed 19 August 2019].

BAKERPEDIA. 2019b. *Specific Gravity* [Online]. bakerpedia.com. Available: https://bakerpedia.com/processes/specific-gravity-cakes/ [Accessed 11 July 2019].

BALLESTEROS, L. F., TEIXEIRA, J. A. & MUSSATTO, S. I. 2014. Chemical, Functional, and Structural Properties of Spent Coffee Grounds and Coffee Silverskin. *Food and Bioprocess Technology,* 7**,** 3493-3503.

BARNES, W. J. & ANDERSON, C. T. 2017. Acetyl Bromide Soluble Lignin (ABSL) Assay for Total Lignin Quantification from Plant Biomass. *Bio-protocol,* 7**,** e2149.

BARTOLOMÉ, B., SANTOS, M., JIMÉNEZ, J. J., DEL NOZAL, M. J. & GÓMEZ-CORDOVÉS, C. 2002. Pentoses and Hydroxycinnamic Acids in Brewer's Spent Grain. *Journal of Cereal Science,* 36**,** 51-58.

BEALL, F. C. 1968. Thermogravimetric analysis of wood lignin and hemicelluloses. *Wood Lignin and Hemicelluloses.* United States of America: US Department of Agriculture.

BEAUGRAND, J., CRONIER, D., THIEBEAU, P., SCHREIBER, L., DEBEIRE, P. & CHABBERT, B. 2004. Structure, Chemical Composition, and Xylanase Degrafation of External Layer isolated from Developing Wheat Grain. *Journal of Agricultural and Food Chemistry,* 52**,** 7108-7117.

BELKHEIRI, T., ANDERSSON, S.-I., MATTSSON, C., OLAUSSON, L., THELIANDER, H. & VAMLING, L. 2018. Hydrothermal liquefaction of kraft lignin in sub-critical water: the influence of the sodium and potassium fraction. *Biomass Conversion and Biorefinery,* 8**,** 585-595.

BENJAMIN, M., DOUGLASS, I. B., HANSEN, G. A., MAJOR, W. D., NAVARRE, A. J. & YERGER, H. J. 1969. A General Description of Commercial Wood Pulping and Bleaching Processes. *Journal of the Air Pollution Control Association,* 19**,** 155-161.

BERNARDINELLI, O. D., LIMA, M. A., REZENDE, C. A., POLIKARPOV, I. & DEAZEVEDO, E. R. 2015. Quantitative (13)C MultiCP solid-state NMR as a tool for evaluation of cellulose

crystallinity index measured directly inside sugarcane biomass. *Biotechnology Biofuels,* 8**,** 110.

BERTON-CARABIN, C. C. & SCHROËN, K. 2015. Pickering Emulsions for Food Applications: Background, Trends, and Challenges. *Annual Review of Food Science and Technology,* 6**,** 263-297.

BHATTACHARJEE, A., CHAKRABORTY, A. & MUKHOPADHYAY, G. 2018. DOUBLE EMULSIONS - A REVIEW WITH EMPHASIS ON UPDATED STABILITY ENHANCEMENT PERSPECTIVE. *World Journal of Pharmacy and Pharmaceutical Science,* 7**,** 475-493.

BINKS, B. P., FLETCHER, P. D., HOLT, B. L., BEAUSSOUBRE, P. & WONG, K. 2010. Phase inversion of particle-stabilised perfume oil-water emulsions: experiment and theory. *Physical Chemistry Chemical Physics,* 12**,** 11954-66.

BOERJAN, W., RALPH, J. & BAUCHER, M. 2003. Lignin biosynthesis. *Annual Review of Plant Biology,* 54**,** 519-46.

BOUSSARSAR, H., ROGE, B. & MATHLOUTHI, M. 2009. Optimization of sugarcane bagasse conversion by hydrothermal treatment for the recovery of xylose. *Bioresource Technology,* 100**,** 6537-42.

BRANDT, L. 1996. *Emulsifiers in Baked Goods* [Online]. Natural Products Insider. Available: https://www.naturalproductsinsider.com/archive/emulsifiers-baked-goods [Accessed 8 January 2019].

BRUKER. 2003. *AVANCE Beginners Guide - Chapter 5. The NMR Sample - 5.3 Sample Tube* [Online]. BRUKER Biospin. Available: http://triton.iqfr.csic.es/guide/man/beginners/chap5-3.htm [Accessed 12 December 2018].

BUDTOVA, T. & NAVARD, P. 2015. Cellulose in NaOH–water based solvents: a review. *Cellulose,* 23**,** 5-55.

BUFFLER, C. A. 1993. Dielectric Propeties of Foods and Microwave Materials. *In:* BUFFLER, C. A. (ed.) *Microwave Cooking and Processing: Engineering Fundamentals for the Food Scientist.* 1 ed. New York: Springer US.

BUNZEL, M., SEILER, A. & STEINHART, H. 2005. Characterization of Dietary Fiber Lignins from Fruits and Vegetables Using the DFRC Method. *Journal of Agricultural and Food Chemistry,* 53**,** 9553-9559.

BURROWS, D. 2015. *How coffee could 'give a lift' in another way* [Online]. Dartford: Recycling & Waste World. Available: http://www.recyclingwasteworld.co.uk/in-depth-article/spent-coffee-grounds/74144/ [Accessed 12 August 2019].

CALABRESE, V., COURTENAY, J. C., EDLER, K. J. & SCOTT, J. L. 2018. Pickering emulsions stabilized by naturally derived or biodegradable particles. *Current Opinion in Green and Sustainable Chemistry,* 12**,** 83-90.

CARRIER, M., LOPPINET-SERANI, A., DENUX, D., LASNIER, J.-M., HAM-PICHAVANT, F., CANSELL, F. & AYMONIER, C. 2011. Thermogravimetric analysis as a new method to determine the lignocellulosic composition of biomass. *Biomass and Bioenergy,* 35**,** 298-307.

CAUVAIN, S. P. & YOUNG, L. S. 2006. Ingredient qualities and quantities in the Chorleywood Bread Process. *In:* CAUVAIN, S. P. & YOUNG, L. S. (eds.) *The Chorleywood Bread Process.* 1st ed. Boca Raton, FL: Woodhead Publishing; CRC Press.

CEPI. 2019. *Types of Pulping Processes* [Online]. Brussels: Confederation of European Paper Industries. Available: http://www.cepi.org/node/22334 [Accessed 19th February 2019].

CHAWLA, S. P., KANATT, S. R. & SHARMA, A. K. 2015. Chitosan. *Polysaccharides.* Switzerland: Springer International Publishing.

CHEN, H. 2014. Chapter 2 - Chemical Composition and Structure of Natural Lignocellulose. *Biotechnology of Lignocellulose: Theory and Practice.* Beijing and Springer ScienceCBusiness Media Dordrecht: Chemical Industry Press.

CHEN, W.-H., PENG, J. & BI, X. T. 2015. A state-of-the-art review of biomass torrefaction, densification and applications. *Renewable and Sustainable Energy Reviews,* 44**,** 847-866.

CHEN, W. J., YANG, S., ZHANG, Y., WANG, Y. Y., YUAN, T. Q. & SUN, R. C. 2017. Effect of alkaline preswelling on the structure of lignins from Eucalyptus. *Scientific Reports,* 7**,** 45752.

CHEN, Y., SHARMA-SHIVAPPA, R. R., KESHWANI, D. R. & AND CHEN, C. 2007. "Potential of Agricultural Residues and Hay for Bioethanol Production. *Biological Systems Engineering: Papers and Publications,* Paper 79**,** 276-290.

CORONEL, P. M., SASTRY, S., JUN, S., SALENGKE, S. & JOSIP, S. 2009. Ohmic and Microwave Heating. *In:* SIMPSON, R. (ed.) *Engineering Aspects of Thermal Food Processing.* Florida: CRC Press.

COTANA, F., CAVALAGLIO, G., NICOLINI, A., GELOSIA, M., COCCIA, V., PETROZZI, A. & BRINCHI, L. 2014. Lignin as Co-product of Second Generation Bioethanol Production from Ligno-cellulosic Biomass. *Energy Procedia,* 45**,** 52-60.

CRAWSHAW, R. 2009. 16 - Food industry co-products as animal feeds. *In:* WALDRON, K. (ed.) *Handbook of Waste Management and Co-Product Recovery in Food Processing.* Woodhead Publishing.

CUISSINAT, C. & NAVARD, P. 2006. Swelling and Dissolution of Cellulose Part II: Free Floating Cotton and Wood Fibres in NaOH–Water–Additives Systems. *Macromolecular Symposia,* 244**,** 19-30.

DAMMAK, I., LOURENÇO, R. V. & SOBRAL, P. J. D. A. 2019. Active gelatin films incorporated with Pickering emulsions encapsulating hesperidin: Preparation and physicochemical characterization. *Journal of Food Engineering,* 240**,** 9-20.

DDBST GMBH. n.d. *Saturated Vapor Pressure - Calculation by Antoine Equation* [Online]. Dortmund: DDBST GmBH. Available: http://ddbonline.ddbst.com/AntoineCalculation/AntoineCalculationCGI.exe?component=Water [Accessed 26 September 2019].

DE GROOT, A. D. 1956. *The Meaning of "Significance" for Different Types of Research [Translated and Annotated by Eric–Jan Wagenmakers, Denny Borsboom, Josine Verhagen, Rogier Kievit, Marjan Bakker, Angelique Cramer, Dora Matzke, Don Mellenbergh, and Han L. J. van der Maas* [Online]. EJ. Wagenmakers. Available: https://www.ejwagenmakers.com/inpress/DeGroot1956_TA.pdf [Accessed].

DE OLIVEIRA, D. M., FINGER-TEIXEIRA, A., MOTA, T. R., SALVADOR, V. H., MOREIRA-VILAR, F. C., MOLINARI, H. B. C., MITCHELL, R. A. C., MARCHIOSI, R., FERRARESE-FILHO, O. & DOS SANTOS, W. D. 2015. Ferulic acid: a key component in grass lignocellulose recalcitrance to hydrolysis. *Plant Biotechnology,* 13**,** 1224-1232.

DEL RIO, J. C., LINO, A. G., COLODETTE, J. L., LIMA, C. F., GUTIERREZ, A., MARTINEZ, A. T., LU, F., RALPH, J. & RENCORET, J. 2015. Differences in the chemical structure of the lignins from sugarcane bagasse and straw. *Biomass and Bioenergy,* 81**,** 322-338.

DEL RIO, J. C., RENCORET, J., PRINSEN, P., MARTINEZ, A., T & RALPH, J. 2012. Structural Characterization of Wheat StrawLignin as Revealed by Analytical Pyrolysis, 2D-NMR, and Reductive Cleavage Methods. *Journal of Agricultural and Food Chemistry,* 60**,** 5922-5935.

DEMIRBAŞ, A. 2001. Relationships between lignin contents and heating values of biomass. *Energy Conversion and Management,* 42**,** 183-188.

DICKINSON, E. 2010. Food emulsions and foams: Stabilization by particles. *Current Opinion in Colloid & Interface Science,* 15**,** 40-49.

DICKINSON, E. 2019. Particle-based stabilization of water-in-water emulsions containing mixed biopolymers. *Trends in Food Science & Technology,* 83**,** 31-40.

DINAND, E., VIGNON, M., CHANZY, H. & HEUX, L. 2002. Mercerization of primary wall cellulose and its implication for the conversion of cellulose I→cellulose II. *Cellulose,* 9**,** 7-18.

DONOHOE, B. S., DECKER, S. R., TUCKER, M. P., HIMMEL, M. E. & VINZANT, T. B. 2008. Visualizing lignin coalescence and migration through maize cell walls following thermochemical pretreatment. *Biotechnology and Bioengineering,* 101**,** 913-25.

DUFFUS, L. J., NORTON, J. E., SMITH, P., NORTON, I. T. & SPYROPOULOS, F. 2016. A comparative study on the capacity of a range of food-grade particles to form stable O/W and W/O Pickering emulsions. *Journal of Colloid and Interface Science,* 473**,** 9-21.

EGGERS, J., LISTER, J. R. & STONE, H. A. 1999. *Coalescence of Liquid Drops* [Online]. Essen, Germany: Universit¨at Gesamthochschule Essen. Available: https://arxiv.org/pdf/physics/9903017.pdf [Accessed 23rd May 2019].

EL KHALDI-HANSEN, B., SCHULZE, M. & KAMM, B. 2016. Qualitative and Quantitative Analysis of Lignins from Different Sources and Isolation Methods for an Application as a Biobased Chemical Resource and Polymeric Material. *Analytical Techniques and Methods for Biomass.*

ENGINEERING TOOLBOX. 2004. *Water - Saturation Pressure* [Online]. Engineering Toolbox. Available: https://www.engineeringtoolbox.com/water-vapor-saturation-pressure-d_599.html [Accessed 21 November 2018].

EURLEX. 2011. *Commission Regulation (EU) No 1129/2011 of 11 November 2011 amending Annex II to Regulation (EC) No 1333/2008 of the European Parliament and of the Council by establishing a Union list of food additives Text with EEA relevance* [Online]. Brussels: European Commission (EUR-Lex). [Accessed 29 September 2019].

EVERS, T. & MILLAR, S. 2002. Cereal Grain Structure and Development: Some Implications for Quality. *Journal of Cereal Science,* 36**,** 261-284.

FAN, S., ZHANG, P., LI, F., JIN, S., WANG, S. & ZHOU, S. 2016. A Review of Lignocellulose Change During Hydrothermal Pretreatment for Bioenergy Production. *Current Organic Chemistry,* 20**,** 2799-2809.

FAO. 2002. *Chapter 2. Food security: concepts and measurement* [Online]. Food and Agriculture Organization of the United Nations. Available: http://www.fao.org/3/y4671e/y4671e06.htm [Accessed 20 August 2019].

FARUK, O. 2016. *Lignin in Polymer Composites,* Toronto, Elsevier.

FDA. 2018a. *PART 172 -- FOOD ADDITIVES PERMITTED FOR DIRECT ADDITION TO FOOD FOR HUMAN CONSUMPTION, Subpart I--Multipurpose Additives: Sec. 172.842 Sorbitan monostearate.* [Online]. Silver Springs, MD: US Food and Dug Administration. Available: https://www.accessdata.fda.gov/scripts/cdrh/cfdocs/cfcfr/CFRSearch.cfm?fr=172.842 [Accessed 19 August 2019].

FDA. 2018b. *PART 172 -- FOOD ADDITIVES PERMITTED FOR DIRECT ADDITION TO FOOD FOR HUMAN CONSUMPTION, Subpart I--Multipurpose Additives; Sec. 172.836 Polysorbate 60.* [Online]. Silver Spring, MD: US Food and Drug Administration. Available: https://www.accessdata.fda.gov/scripts/cdrh/cfdocs/cfcfr/CFRSearch.cfm?fr=172.836 [Accessed 19 August 2019].

FELIZARDO, M. P. & FREIRE, J. T. 2018. Characterization of barley grains in different levels of pearling process. *Journal of Food Engineering,* 232**,** 29-35.

FILLEY, T. R., CODY, G. D., GOODELL, B., JELLISON, J., NOSER, C. & OSTROFSKY, A. 2002. Lignin demethylation and polysaccharide decomposition in spruce sapwood degraded by brown rot fungi. *Organic Geochemistry,* 33**,** 111-124.

FLOWERS, P., THEOPOLD, K. & LANGLEY, R. 2018. *10.4: Phase Diagrams* [Online]. California: UC-Davis. Available:

https://chem.libretexts.org/Textbook_Maps/General_Chemistry/Book%3A_Chemistry_(OpenSTAX)/10%3A_Liquids_and_Solids/10.4%3A_Phase_Diagrams [Accessed 20 November 2018].

FOSTER, T. J., ABLETT, S., MCCANN, M. C. & GIDLEY, M. J. 1996. Mobility-Resolved 13C-NMR Spectroscopy of Primary Plant Cell Walls. *Biopolymers,* 39**,** 51-66.

FU, L., MCCALLUM, S. A., MIAO, J., HART, C., TUDRYN, G. J., ZHANG, F. & LINHARDT, R. J. 2015. Rapid and accurate determination of the lignin content of lignocellulosic biomass by solid-state NMR. *Fuel,* 141**,** 39-45.

FUKUSHIMA, R. S. & HATFIELD, R. D. 2001. Extraction and Isolation of Lignin for Utilization as a Standard to Determine Lignin Concentration Using the Acetyl Bromide Spectrophotometric Method. *Journal of Agricultural and Food Chemistry,* 49**,** 3133 - 3139.

FUKUSHIMA, R. S. & HATFIELD, R. D. 2004. Comparison of the acetyl bromide spectrophotometric method with other analytical lignin methods for determining lignin concentration in forage samples. *Journal of Agricultural and Food Chemistry,* 52**,** 3713-20.

GARROTE, G., CRUZ, J., DOMINGUEZ, H. & PARAJO, J. 2003. Valorisation of waste fractions from autohydrolysis of selected lignocellulosic materials. *Journal of Chemical Technology & Biotechnology,* 97**,** 392-398.

GARROTE, G., DOMINGUEZ, H. & PARAJO, J. C. 1999. Hydrothermal processing of lignocellulosic materials. *European Journal of Wood and Wood Products/Holz als Roh- und Werkstoff,* 57**,** 191-202.

GIDLEY, M. J. 1992. High-resolution solid-state NMR of food materials. *Trends in Food Science & Technology,* 3**,** 231-236.

GIDLEY, M. J. & BOCIEK, S. M. 1985. Molecular Organization in Starches: A 13C CP/MAS NMR Study. *J. Am. Chem. Soc.,* 107**,** 7040-7044.

GILARDI, G., ABIS, L. & CASS, A. E. G. 1995. Carbon-13 CP/MAS solid-state NMR and FT-IR spectroscopy of wood cell wall biodegradation. *Enzyme and Microbial Technology,* 17**,** 268-275.

GILL, P., MOGHADAM, T. T. & RANJBAR, B. 2010. Differential Scanning Calorimetry Techniques: Applications in Biology and Nanoscience. *Journal of Biomolecular Techniques,* 21**,** 167-193.

GOULD, J., GARCIA-GARCIA, G. & WOLF, B. 2016. Pickering Particles Prepared from Food Waste. *Materials,* 9.

GOULD, J., VIEIRA, J. & WOLF, B. 2013. Cocoa particles for food emulsion stabilisation. *Food & Function,* 4**,** 1369-75.

GRABBER, J. S. 2005. How do Lignin Composition, Structure and Cross-Linking Affect Degradability? A Review of Cell Wall Model Studies. *Crop Science,* 45**,** 820-831.

GÜNTHER, H. 2013a. Appendix 4 - Chemical Shifts and Substuent Effects S(delta) of 13C Resonances in Organic Compounds. *In:* GÜNTHER, H. (ed.) *NMR Spectroscopy: Basic Principles, Concepts and Applications in Chemistry.* 3rd ed. Weinheim, Germany: Wiley-VCH.

GÜNTHER, H. 2013b. Chapter 2 - The Physical Basis of the nuclear Magnetic Resonance Experiment. Part 1. *In:* GÜNTHER, H. (ed.) *NMR Spectroscopy: Basic Principles, Concepts, and Applications in Chemistry.* 3rd ed. Weinheim, Germany: Wiley-VCH.

GÜNTHER, H. 2013c. Chapter 8 - The Physical Basis of the Nuclear Magnetic Resonance Experiment. Part II: Pulse and Fourier-Transform NMR. *In:* GÜNTHER, H. (ed.) *NMR Spectroscopy: Basic Principles, Concepts, and Applications in Chemistry.* Third ed. Weinheim, Germany: Wiley-VCH Verlag GmbH & Co. KGaA.

GÜNTHER, H. 2013d. Chapter 14 - Nuclear Magnetic Resonance of Partially Oriented Molecules and Solid State NMR. *In:* GÜNTHER, H. (ed.) *NMR Spectrosopy: Basic*

Principles, Concepts and Applications in Chemistry. 3rd ed. Weinheim, Germany: Wiley-VCh.

GUO, F., WU, F., MU, Y., HU, Y., ZHAO, X., MENG, W., GIESY, J. P. & LIN, Y. 2016. Characterization of organic matter of plants from lakes by thermal analysis in a N2 atmosphere. *Scientific Reports,* 6**,** 22877.

GUO, J., DU, W., GAO, Y., CAO, Y. & YIN, Y. 2017. Cellulose nanocrystals as water-in-oil Pickering emulsifiers via intercalative modification. *Colloids and Surfaces A: Physicochemical and Engineering Aspects,* 529**,** 634-642.

GUPTA, A., ERAL, H. B., HATTON, T. A. & DOYLE, P. S. 2016. Nanoemulsions: formation, properties and applications. *Soft Matter,* 12**,** 2826-41.

GUTIÉRREZ-VALENZUELA, C. A., ESQUIVEL, R., GUERRERO-GERMÁN, P., ZAVALA-RIVERA, P., RODRÍGUEZ-FIGUEROA, J. C., GUZMÁN-Z, R. & LUCERO-ACUÑA, A. 2018. Evaluation of a combined emulsion process to encapsulate methylene blue into PLGA nanoparticles. *Royal Society of Chemistry Advances,* 8**,** 414-422.

GUTIERREZ, A., RODRIGUES, I., M & DEL RIO, J. C. 2006. Chemical Characterizaton of Lignin and Lipid Fractions in Industrial Hemp Bast Fibers Used for Manufacturing High-Quality Paper Pulps. *Journal of Agricultural and Food Chemistry,* 54**,** 2138-2144.

HA, M. A., VIETOR, R. J., JARDINE, G. D., APPERLEY, D. C. & JARVIS, M. C. 2005. Conformation and mobility of the arabinan and galactan side-chains of pectin. *Phytochemistry,* 66**,** 1817-24.

HAGHDAN, S., RENNECKAR, S. & SMITH, G. D. 2016. Chapter 1 - Sources of Lignin. *In:* FARUK, O. (ed.) *Lignin in Polymer Composites.* Vancouver: William Andrew.

HARHOLT, J., SUTTANGKAKUL, A. & VIBE SCHELLER, H. 2010. Biosynthesis of pectin. *Plant Physiology,* 153**,** 384-95.

HARTLEY, G. 2019. *What role does biomass have to play in our energy supply?* [Online]. Energy Saving Trust. Available: https://energysavingtrust.org.uk/blog/what-role-does-biomass-have-play-our-energy-supply [Accessed 22 January 2020].

HASSAN, S. S., WILLIAMS, G. A. & JAISWAL, A. K. 2018. Emerging technologies for the pretreatment of lignocellulosic biomass. *Bioresource Technology,* 262**,** 310-318.

HATFIELD, R. & FUKUSHIMA, R. S. 2005. Can Lignin Be Accurately Measured? *Crop Science,* 45.

HATFIELD, R. & VERMERRIS, W. 2001. Lignin Formation in Plants. The Dilemma of Linkage Specificity. *Plant Physiology,* 126**,** 1351 - 1357.

HATFIELD, R. D., GRABBER, J., RALPH, J. & BREI, K. 1999. Using the Acetyl Bromide Assay To Determine Lignin Concentrations in Herbaceous Plants: Some Cautionary Notes. *Journal of Agricultural and Food Chemistry,* 47**,** 628-632.

HAYHURST, A. N. 1997. Introduction to heat transfer. *In:* FRYER, P. J., PYLE, D. L. & RIELLY, C. D. (eds.) *Chemical Engineering for the Food Industry.* 1st ed. London: Blackie Academic and Professional.

HÁZ, A., JABLONSKÝ, M., ORSÁGOVÁ, A. & ŠURINA, I. 2013a. CHARACTERIZATION OF LIGNINS BY PY-GC/MS. *4nd International Conference Renewable Energy Sources 2013.* High Tatras, Slovak Republic.

HÁZ, A., JABLONSKÝ, M., ORSÁGOVÁ, A. & ŠURINA, I. 2013b. Determination of temperature regions in thermal degradation of lignin. *Renewable Energy Sources 2013.* High Tatras, Slovak Republic.

HE, Y., MOUTHIER, T. M., KABEL, M. A., DIJKSTRA, J., HENDRIKS, W. H., STRUIK, P. C. & CONE, J. W. 2018. Lignin composition is more important than content for maize stem cell wall degradation. *Journal of The Science of Food and Agriculture* 98**,** 384-390.

HERNANZ, D., NUNEZ, V., SANCHO, A. I., FAULDS, C. B., WILLIAMSON, G., BARTOLOME, B. & GOMEZ-CORDOVES, C. 2001. Hydroxycinnamic Acids and Ferulic Acid Dehydrodimers in Barley and Processed Barley. *Journal of Agricultural and Food Chemistry,* 49**,** 4884-4888.

HERRICK, F. W., CASEBIER, R. L., HAMILTON, J. K. & SANDBERG, K. R. Microfibrillated cellulose: morphology and accessibility. Applied Polymer Symposium., 1983. Journal of Applied Polymer Science., 797-813.

HOLSER, R. A. 2009. Temperature-dependent solubility of wax compounds in ethanol. *European Journal of Lipid Science and Technology,* 111**,** 1049-1052.

HOWARD, R. L., ABOTSI, E., JANSEN VAN RENSBURG, E. L. & HOWARD, S. 2003. Lignocellulose biotechnology: issues of bioconversion and enzyme production. *African Journal of Biotechnology,* 2**,** 602-619.

HU, C., ZHAO, Y., LI, K., ZHU, J. Y. & GLEISNER, R. 2015. Optimizing cellulose fibrillation for the production of cellulose nanofibrils by a disk grinder. *Holzforschung,* 69.

HUBBE, M. n.d. *Fibrillation* [Online]. North Carolina: North Carolina State University. Available: https://projects.ncsu.edu/project/hubbepaperchem/Defnitns/Fibrilzn.htm [Accessed 20 February 2019].

HYSLOP, G. 2019. *Kellogg's expands craft beer lineup made from cereal waste* [Online]. Bakery and Snacks Website. Available: https://www.bakeryandsnacks.com/Article/2019/06/18/Kellogg-s-expands-craft-beer-lineup-made-from-cereal-waste [Accessed 10 July 2019].

IBBETT, R., GADDIPATI, S., DAVIES, S., HILL, S. & TUCKER, G. 2011. The mechanisms of hydrothermal deconstruction of lignocellulose: new insights from thermal-analytical and complementary studies. *Bioresource Technology,* 102**,** 9272-8.

IIYAMA, K. & WALLIS, A. F. A. 1988. An improved acetyl bromide procedure for determining lignin in woods and wood pulps. *Wood Science and Technology,* 22**,** 271-280.

IIYAMA, K. & WALLIS, A. F. A. 1990. Dissolution of Wood with Acetyl Bromide Solutions-Reactions of Lignin Model Compounds. *Journal of Wood Chemistry and Technology,* 10.

JARVIS, M. C. 1984. Structure and properties of pectin gels in plant cell walls. *Plant, Cell and Environment,* 7**,** 153-164.

JAYME, G. 1944. Milkro-quellungsmessungen an Zellstoffenn. *Papier-Fabr/Wochbl Papierfabr,* 6**,** 187-94.

JENKINS, P. & SNOWDEN, M. 1996. Depletion flocculation in colloidal dispersions. *Advances in Colloid and Interface Science,* 68**,** 57-96.

JIAO, B., SHI, A., WANG, Q. & BINKS, B. P. 2018. High-Internal-Phase Pickering Emulsions Stabilized Solely by Peanut-Protein-Isolate Microgel Particles with Multiple Potential Applications. *Angewandte Chemie International Edition English,* 57**,** 9274-9278.

JOHNSON, D. B., MOORE, W. E. & ZANK, L. C. 1961. The spectrophotometric determination of lignin in small wood samples. *Tappi.,* 44**,** 793-8.

JOSHUA, H., SINEX, S. & JOHNSON, S. 2018. *11.5: Vapor Pressure* [Online]. California: UC-Davis. Available: https://chem.libretexts.org/Textbook_Maps/General_Chemistry/Map%3A_Chemistry_-_The_Central_Science_(Brown_et_al.)/11%3A_Liquids_and_Intermolecular_Forces/11.5%3A_Vapor_Pressure [Accessed 21 November 2018].

JUNG, H. & DEETZ, D. 1993. Cell wall lignification and degradation. *In:* JUNG, H., BUXTON, B., HATFIELD, R. D. & RALPH, J. (eds.) *Forage Cell Wall Structure and Digestibiliy.* Madison, WI: American Society of Agronomy.

JURIAANSE, A. C. & HEERTJE, I. 1988. Microstructure of Shortenings Margarine and Butter - A Review. *Food Microstructure,* 7**,** pp. 181-188.

KABALNOV, A. 1998. Thermodynamic and theoretical aspects of emulsions and their stability. *Current Opinion in Colloid & Interface Science,* 3**,** 270-275.

KALASHNIKOVA, I., BIZOT, H., CATHALA, B. & CAPRON, I. 2011. New Pickering emulsions stabilized by bacterial cellulose nanocrystals. *Langmuir,* 27**,** 7471-9.

KEELER, J. 2010a. Relaxation and the NOE. *In:* KEELER, J. (ed.) *Understanding NMR Spectroscopy.* 2nd ed. Chichester: John Wiley & Sons.

KEELER, J. 2010b. Setting the Scene. *In:* KEELER, J. (ed.) *Understanding NMR Spectroscopy.* 2nd ed. Chichester, UK: John Wiley & Sons, Ltd.

KIRIN. 2017. *Kirin Beer University Report Global Beer Production by Country in 2016* [Online]. Kirin Holdings Company Ltd. Available: https://www.kirinholdings.co.jp/english/news/2017/0810_01.html [Accessed 02 May 2018].

KONO, H., YUNOKI, S., SHIKANO, T., FUJIWARA, M., ERATE, T. & TAKAI, M. 2002. CP/MAS 13C NMR Study of Cellulose and Cellulose Derivatives. 1. Complete Assignment of the CP/MAS 13C NMR Spectrum of the Native Cellulose. *Journal of the American Chemical Society,* 124**,** 7506-7511.

KOSTAS, E. T., BENEROSO, D. & ROBINSON, J. P. 2017. The application of microwave heating in bioenergy: A review on the microwave pre-treatment and upgrading technologies for biomass. *Renewable and Sustainable Energy Reviews,* 77**,** 12-27.

KOZLIAK, E. I., KUBÁTOVÁ, A., ARTEMYEVA, A. A., NAGEL, E., ZHANG, C., RAJAPPAGOWDA, R. B. & SMIRNOVA, A. L. 2016. Thermal Liquefaction of Lignin to Aromatics: Efficiency, Selectivity, and Product Analysis. *ACS Sustainable Chemistry & Engineering,* 4**,** 5106-5122.

KU LEUVEN 2012. High pressure homogenisation. Leuven, Belgium: KU Leuven.

KUCHARSKA, K., RYBARCZYK, P., HOLOWACZ, I., LUKAJTIS, R., GLINKA, M. & KAMINSKI, M. 2018. Pretreatment of Lignocellulosic Materials as Substrates for Fermentation Processes. *Molecules,* 23.

KULKARNI, V. S. & SHAW, C. 2016. Chapter 7 - Preparation and Stability Testing. *Essential Chemistry for Formulators of Semisolid and Liquid Dosages.* Academic Press - Elsevier.

KURIAN, J. K., GARIEPY, Y., ORSAT, V. & VIJAYA RAGHAVAN, G. S. 2015. Comparison of steam-assisted versus microwave-assisted treatments for the fractionation of sweet sorghum bagasse. *Bioresources and Bioprocessing,* 2**,** 1-16.

LAIVINS, G. & SCALLAN, A. The mechanism of hornification of wood pulps. *In:* BAKER, C., ed. 10th fundamental research symposium, 1993 Oxford, UK. Pulp and Paper Fundamental Research Society, 1235-60.

LAM, S., VELIKOV, K. P. & VELEV, O. D. 2014. Pickering stabilization of foams and emulsions with particles of biological origin. *Current Opinion in Colloid & Interface Science,* 19**,** 490-500.

LEE, S.-Y., CHUN, S.-J., KANG, I.-A. & PARK, J.-Y. 2009. Preparation of cellulose nanofibrils by high-pressure homogenizer and cellulose-based composite films. *Journal of Industrial and Engineering Chemistry,* 15**,** 50-55.

LENIHAN, P., OROZCO, A., O'NEILL, E., AHMAD, M. N. M., ROONEY, D. W. & WALKER, G. M. 2010. Dilute acid hydrolysis of lignocellulosic biomass. *Chemical Engineering Journal,* 156**,** 395-403.

LESTER, E. 2018. Heating water and air in sealed container. *Swagelok Pressure Safety Course - Spreadsheet for Worse Case Scenario of sealed vessel rupture.* Nottingham: University of Nottingham.

LIBRA, J. A., RO, K. S., KAMMANN, C., FUNKE, A., BERGE, N. D., NEUBAUER, Y., TITIRICI, M.-M., FÜHNER, C., BENS, O., KERN, J. & EMMERICH, K.-H. 2011. Hydrothermal carbonization of biomass residuals: a comparative review of the chemistry, processes and applications of wet and dry pyrolysis. *Biofuels,* 2**,** 71-106.

LINKE, C. & DRUSCH, S. 2018. Pickering emulsions in foods - opportunities and limitations. *Critical Reviews in Food Science and Nutrition,* 58**,** 1971-1985.

LOURENÇO, A., NEIVA, D. M., GOMINHO, J., MARQUES, A. V. & PEREIRA, H. 2014. Characterization of lignin in heartwood, sapwood and bark from Tectona grandis using Py–GC–MS/FID. *Wood Science and Technology,* 49**,** 159-175.

LU, F. & RALPH, J. 1996. Reactions of Lignin Model ß-Aryl Ethers with Acetyl Bromide. *Holzforschung,* 50**,** 360-364.
LU, X., WANG, Y., LI, Y. & HUANG, Q. 2018. Assembly of Pickering emulsions using milled starch particles with different amylose/amylopectin ratios. *Food Hydrocolloids,* 84**,** 47-57.
LUKAS, K. & LEMAIRE, P. K. 2009. Differential scanning calorimetry: Fundamental overview. *Resonance,* 14**,** 807-817.
LUO, X. & ZHU, J. Y. 2011. Effects of drying-induced fiber hornification on enzymatic saccharification of lignocelluloses. *Enzyme and Microbial Technology,* 48**,** 92-9.
LUPOI, J. S., SINGH, S., PARTHASARATHI, R., SIMMONS, B. A. & HENRY, R. J. 2015. Recent innovations in analytical methods for the qualitative and quantitative assessment of lignin. *Renewable and Sustainable Energy Reviews,* 49**,** 871-906.
LYNCH, K. M., STEFFEN, E. J. & ARENDT, E. K. 2016. Brewers' spent grain: a review with an emphasis on food and health. *Journal of the Institute of Brewing,* 122**,** 553-568.
MAGNUSSON, E. & NILSSON, L. 2012. Emulsifying properties of egg yolk. *In:* SEGIL, W. (ed.) *Eggs: Nutrition, Consumption and Health.* Nova Science Publishers, Inc.
MANDERS, W. F. 1986. Solid-State 13C NMR Determination of the Syringyl/Guaiacyl Ratio in Hardwood. NBS Publication: U.S. DEPARTMENT OF COMMERCE, National Bureau of Standards, National Engineering Laboratory, Center for Fire Research, Gaithersburg, MD 20899.
MARTIN, C. J. & O'CONNER, D. A. 1977. An experimental test of Lindemann's melting law. *Journal of Physics C: Solid State Physics,* 10**,** 3521-3526.
MATHEW, S. & ABRAHAM, T. E. 2004. Ferulic acid: an antioxidant found naturally in plan cell walls and feruloyl esterases involved in its release and their applications. *Critical reviews in biotechnology,* 24**,** 59-83.
MATHWORKS. 2005. *MATLAB Function Reference - Trapz* [Online]. Available: http://matlab.izmiran.ru/help/techdoc/ref/trapz.html [Accessed].
MCCARDY, E. 1991. *The Nature of Lignin* [Online]. Alkaline Paper Advocate. Available: http://cool.conservation-us.org/byorg/abbey/ap/ap04/ap04-4/ap04-402.html [Accessed 12 June 2019].
MCCLEMENTS, D. J. 2016a. Emulsion Stability. *In:* MCCLEMENTS, D. (ed.) *Food Emulsions - Principles, Practices and Techniques.* 3rd ed. London: CRC Press.
MCCLEMENTS, D. J. 2016b. *Food Emulsions - Principles, Practices and Techniques,* Florida, USA, CRC Press.
MCCLEMENTS, D. J. & JAFARI, S. M. 2018. Improving emulsion formation, stability and performance using mixed emulsifiers: A review. *Advances in Colloid and Interface Science,* 251**,** 55-79.
MCGEE, H. 2004. Cold Egg Sauces: Mayonnaise. *In:* MCGEE, H. (ed.) *McGee on Food & Cooking.* London: Hodder and Stoughton.
MCKENDRY, P. 2002. Energy production from biomass (part 1): overview of biomass. *Bioresource Technology,* 83**,** 37-46.
MERCER, J. 1850. *Improvements in the preparation of cotton and others fabrics and other fibrous materials*. United Kingdom patent application British Patent 13,296.
METAXAS, A. C. & MEREDITH, R. J. 1988. Dielectric properties. *In:* METAXAS, A. C. & MEREDITH, R. J. (eds.) *Industrial Microwave Heating.* London: Peter Peregrinus.
MIEDES, E., VANHOLME, R., BOERJAN, W. & MOLINA, A. 2014. The role of the secondary cell wall in plant resistance to pathogens. *Front Plant Science,* 5**,** 358.
MISSOUM, K., BELGACEM, M. N. & BRAS, J. 2013. Nanofibrillated Cellulose Surface Modification: A Review. *Materials (Basel),* 6**,** 1745-1766.
MOHNEN, D. 2008. Pectin structure and biosynthesis. *Current Opinion in Plant Biology,* 11**,** 266-77.

MONDELĒZ INTERNATIONAL. 2018. *Mondelēz International Commits to Making All Packaging Recyclable by 2025* [Online]. Mondelēz International website: Mondelēz International. Available: https://ir.mondelezinternational.com/news-releases/news-release-details/mondelez-international-commits-making-all-packaging-recyclable [Accessed 10 July 2019].

MOREIRA-VILAR, F. C., SIQUEIRA-SOARES RDE, C., FINGER-TEIXEIRA, A., DE OLIVEIRA, D. M., FERRO, A. P., DA ROCHA, G. J., FERRARESE MDE, L., DOS SANTOS, W. D. & FERRARESE-FILHO, O. 2014. The acetyl bromide method is faster, simpler and presents best recovery of lignin in different herbaceous tissues than Klason and thioglycolic acid methods. *PLoS One,* 9**,** e110000.

MORRIS, G. A., FOSTER, T. J. & HARDING, S. E. 2000. The effect of the degree of esterification on the hydrodynamic properties of citrus pectin. *Food Hydrocolloids,* 14**,** 227–235.

MURPHY, L. R., MEEK, T. L., ALLRED, A. L. & ALLEN, L. C. 2000. Evaluation and Test of Pauling's Electronegativity Scale. *The Journal of Physical Chemistry A,* 104**,** 5867-5871.

MURRAY, B., DURGA, K., YUSOFF, A. & STOYANOV, S. 2011. Stabilization of foams and emulsions by mixtures of surface active food-grade particles and proteins. *Food Hydrocolloids,* 25**,** 627-638.

MUSSATTO, S. I., DRAGONE, G. & ROBERTO, I. C. 2006. Brewers' spent grain: generation, characteristics and potential applications. *Journal of Cereal Science,* 43**,** 1-14.

MUSSATTO, S. I., DRAGONE, G. & ROBERTO, I. C. 2007. Ferulic and p-coumaric acids extraction by alkaline hydrolysis of brewer's spent grain. *Industrial Crops and Products,* 25**,** 231-237.

NAIR, S. S., SHARMA, S., PU, Y., SUN, Q., PAN, S., ZHU, J. Y., DENG, Y. & RAGAUSKAS, A. J. 2014. High shear homogenization of lignin to nanolignin and thermal stability of nanolignin-polyvinyl alcohol blends. *Chemistry and Sustainability (ChemSusChem),* 7**,** 3513-20.

NATIONAL ACADEMIES OF SCIENCES, E., AND MEDICINE; . 2019. *Renewable Sources: Biomass* [Online]. Washington, DC: The National Academy of Sciences. Available: http://needtoknow.nas.edu/energy/energy-sources/renewable-sources/biomass/ [Accessed 22 July 2019].

NCBI. 2018a. *Coniferyl Alcohol* [Online]. National Center for Biotechnology Information. Available: https://pubchem.ncbi.nlm.nih.gov/compound/coniferyl_alcohol#section=Top [Accessed 27 April 2018].

NCBI. 2018b. *P-Coumaryl alcohol* [Online]. National Center for Biotechnology Information. Available: https://pubchem.ncbi.nlm.nih.gov/compound/p-Coumaryl_alcohol#section=Top [Accessed 27 April 2018].

NCBI. 2018c. *Sinapyl Alcohol* [Online]. National Center for Biotechnology Information. Available: https://pubchem.ncbi.nlm.nih.gov/compound/Sinapyl_alcohol#section=Top [Accessed 27 April 2018].

NOVAES, E., KIRST, M., CHIANG, V., WINTER-SEDEROFF, H. & SEDEROFF, R. 2010. Lignin and biomass: a negative correlation for wood formation and lignin content in trees. *Plant Physiology,* 154**,** 555-61.

NOZAKI, Y. & TANFORD, C. 1971. The Solubility of Amino Acids and Two Glycine Peptides in Aqueous Ethanol and Dioxane Solutions. *The Journal of Biological Chemistry,* 245**,** 2211-2217.

OLATUNJI, O. O., AKINLABI, S. A., MASHININI, M. P., FATOBA, S. O. & AJAYI, O. O. 2018. Thermo-gravimetric characterization of biomass properties: A review. *IOP Conference Series: Materials Science and Engineering,* 423.

OLKKU, J., SALMENKALLIO-MARTTILA, M., SWEINS, H. & HOME, S. 2005. Connection between structure and quality of barley husk. *Journal of the American Society of Brewing Chemists,* 63**,** 17-22.

OLSZEWSKI, M. P., ARAUZO, P. J., WĄDRZYK, M. & KRUSE, A. 2019. Py-GC-MS of hydrochars produced from brewer's spent grains. *Journal of Analytical and Applied Pyrolysis,* 140**,** 255-263.

PAAJANEN, A., CECCHERINI, S., MALONEY, T. & KETOJA, J. A. 2019. Chirality and bound water in the hierarchical cellulose structure. *Cellulose,* 26**,** 5877-5892.

PADALKAR, A. N., SHAHI, S. R. & THUBE, M. W. 2011. Micro particles: An approach for betterment of drug delivery system. *International Journal of Pharma. Research & Development,* 3**,** 99-115.

PANG, B., LIU, H., LIU, P., PENG, X. & ZHANG, K. 2018. Water-in-oil Pickering emulsions stabilized by stearoylated microcrystalline cellulose. *Journal of Colloid and Interface Science,* 513**,** 629-637.

PARK, S., BAKER, J. O., HIMMEL, M. E., PARILLA, P. A. & JOHNSON, D. K. 2010. Cellulose crystallinity index: measurement techniques and their impact on interpreting cellulase performance. *Biotechnology for Biofuels,* 3**,** 1-10.

PARK, S., JOHNSON, D. K., ISHIZAWA, C. I., PARILLA, P. A. & DAVIS, M. F. 2009. Measuring the crystallinity index of cellulose by solid state 13C nuclear magnetic resonance. *Cellulose,* 16**,** 641-647.

PATIL, R. A. 2012. *Cleavage of acetyl groups for acetic acid production in Kraft pulp mills.* Master of Science (MS) Open Access Thesis, Thesis - University of Maine.

PAULING, L. 1932. The Nature of the Chemical Bond. Iv. The Energy of Single Bonds and the Relative Electronegativity of Atoms. *Journal of the American Chemical Society,* 54**,** 3570-3582.

PAWAR, A. B., CAGGIONI, M., ERGUN, R., HARTEL, R. W. & SPICER, P. T. 2011. Arrested coalescence in Pickering emulsions. *Soft Matter,* 7**,** 7710.

PAWLIK, A., KURUKJI, D., NORTON, I. & SPYROPOULOS, F. 2016. Food-grade Pickering emulsions stabilised with solid lipid particles. *Food & Function,* 7**,** 2712-21.

PEPSICO. 2006. *Performance with Purpose: Strive to Achieve Zero Waste to Landfill* [Online]. PepsiCo. Available: https://www.pepsico.com/docs/album/esg-topics-policies/waste.pdf?sfvrsn=32345f87_4

https://www.environmentalleader.com/2018/07/pepsico-waste-diversion-packaging/ [Accessed 10 July 2019].

PERRY, R. H. 1997. *Perry's Chemical Engineers' Handbook*, McGraw-Hill.

PICHOT, R., SPYROPOULOS, F. & NORTON, I. T. 2010. O/W emulsions stabilised by both low molecular weight surfactants and colloidal particles: The effect of surfactant type and concentration. *Journal of Colloid and Interface Science,* 352**,** 128-35.

PICKERING, S. U. 1907. Pickering: Emulsions. *Journal of the Chemical Society, Transactions,* 91**,** 2001-2021

PRYNN, J. & SINMAZ, E. 2012. *Coffee shops just keep on buzzing* [Online]. London: Evening Standard. Available: https://www.standard.co.uk/news/coffee-shops-just-keep-on-buzzing-7303853.html [Accessed 2nd September 2019].

PUJOL, D., LIU, C., GOMINHO, J., OLIVELLA, M. A., FIOL, N., VILLAESCUSA, I. & PEREIRA, H. 2013. The chemical composition of exhausted coffee waste. *Industrial Crops and Products,* 50**,** 423-429.

RATKE, L. & VOORHEES, P. W. 2002. Coarsening - Basics and Growth Laws. *Growth and Coarsening: Ostwald Ripening in Material Processing.* Berlin: Springer Science & Business Media.

RAUDINO, A., SARPIETRO, M. G. & PANNUZZO, M. 2013. 4 - Differential scanning calorimetry (DSC): theoretical fundamentals. *In:* PIGNATELLO, R. (ed.) *Drug-Biomembrane Interaction Studies.* Catania: Woodhead.

RAYNER, M., MARKU, D., ERIKSSON, M., SJÖÖ, M., DEJMEK, P. & WAHLGREN, M. 2014. Biomass-based particles for the formulation of Pickering type emulsions in food and topical applications. *Colloids and Surfaces A: Physicochemical and Engineering Aspects,* 458**,** 48-62.

RAYNER, M., TIMGREN, A., SJOO, M. & DEJMEK, P. 2012. Quinoa starch granules: a candidate for stabilising food-grade Pickering emulsions. *Journal of the Science of Food and Agriculture,* 92**,** 1841-7.

REGRAINED. 2019. *What we do* [Online]. ReGrained Available: https://www.regrained.com/pages/what-we-do [Accessed 20 August 2019].

REINOLD, M. R. 1997. *Manual pra´tico de cervejaria,* Sao Paulo, Aden Editora e Comunicacoes Ltda.

RENCORET, J., PRINSEN, P., GUTIERREZ, A., MARTINEZ, A. T. & DEL RIO, J. C. 2015. Isolation and structural characterization of the milled wood lignin, dioxane lignin, and cellulolytic lignin preparations from brewer's spent grain. *Journal of Agricultural and Food Chemistry,* 63**,** 603-13.

RENCORET, J., RALPH, J., MARQUES, G. & DEL RIO, J. C. 2013. Structural Characterization of Lignin Isolated from Coconut (Cocus nucifera) Coir Fibers. *Journal of Agricultural and Food Chemistry,* 61**,** 2434-2445.

ROSELL, C. M. & SANTOS, E. 2010. Impact of fibers on physical characteristics of fresh and staled bake off bread. *Journal of Food Engineering,* 98**,** 273-281.

RUIZ, H. A., RODRIGUEZ-JASSO, R. M., FERNANDES, B. D., VICENTE, A., A & TEIXEIRA, J. A. 2013. Hydrothermal processing, as an alternative for upgrading agriculture residues and marine biomass according to the biorefinery concept: A review. *Renewable and Sustainable Energy Reviews,* 21**,** 35-51.

RYTIOJA, J., HILDEN, K., YUZON, J., HATAKKA, A., DE VRIES, R. P. & MAKELA, M. R. 2014. Plant-polysaccharide-degrading enzymes from Basidiomycetes. *Microbiology and molecular biology reviews,* 78**,** 614-49.

SAHI, S. S. & ALAVA, J. M. 2003. Functionality of emulsifiers in sponge cake production. *Journal of the Science of Food and Agriculture,* 83**,** 1419-1429.

SAMENI, J., KRIGSTIN, S. & SAIN, M. 2017. Solubility of Lignin and Acetylated Lignin in Organic Solvents. *Bioresources,* 12**,** 1548-1565.

SANCHEZ-SALVADOR, J. L., BALEA, A., MONTE, M. C., BLANCO, A. & NEGRO, C. 2019. Pickering Emulsions Containing Cellulose Microfibers Produced by Mechanical Treatments as Stabilizer in the Food Industry. *Applied Sciences,* 9**,** 1-15.

SANNA, A., LI, S., LINFORTH, R., SMART, K. A. & ANDRESEN, J. M. 2011. Bio-oil and bio-char from low temperature pyrolysis of spent grains using activated alumina. *Bioresource Technology,* 102**,** 10695-703.

SANTOS, R. B., CAPANEMA, E. A., BALAKSHIN, M. Y., CHANG, H.-M. & JAMEEL, H. 2012. Lignin Structural Variation in Hardwood Species. *Journal of Agricultural and Food Chemistry,* 60**,** 4923-4930.

SANTOS, R. B., HART, P. W. & JAMEEL, H., CHANG, HOU-MIN 2013. Wood Based Lignin Reactions Important to the Biorefinery and Pulp and Paper Industries. *BioResources,* 8**,** 1456-1477.

SAURA-CALIXTO, F., CANELLAS, J. & GARCIA-RASO, J. 1983. Determination of hemicellulose, cellulose and lignin contents of dietary fibre and crude fibre of severl seed hulls. Data comparison. *Zeitschrift für Lebensmittel-Untersuchung und -Forschung* 177**,** 200-202.

SCHAFER, J., WAGNER, S., TRIERWEILER, B. & BUNZEL, M. 2016. Characterization of Cell Wall Components and Their Modifications during Postharvest Storage of Asparagus

officinalis L.: Storage-Related Changes in Dietary Fiber Composition. *Journal of Agricultural and Food Chemistry,* 64**,** 478-86.

SCHULER, J., HORNUNG, U., KRUSE, A., DAHMEN, N. & SAUER, J. 2017. Hydrothermal Liquefaction of Lignin. *Journal of Biomaterials and Nanobiotechnology,* 08**,** 96-108.

SELIG, M. J., VIAMAJALA, S., DECKER, S. R., TUCKER, M. P., HIMMEL, M. E. & VINZANT, T. B. 2007. Deposition of lignin droplets produced during dilute acid pretreatment of maize stems retards enzymatic hydrolysis of cellulose. *Biotechnology Progress,* 23**,** 1333-1339.

SINGH, R. P. & HELDMAN, D. R. 2014. Heat Transfer in Food Processing. *In:* SINGH, R. P. & HELDMAN, D. R. (eds.) *Introduction to Food Engineering.* 5th ed. London: Academic Press, Elsevier.

SINGH, S. K. & DHEPE, P. L. 2016. Isolation of lignin by organosolv process from different varieties of rice husk: Understanding their physical and chemical properties. *Bioresource Technology,* 221**,** 310-317.

SIVAM, A. S., SUN-WATERHOUSE, D., QUEK, S. & PERERA, C. O. 2010. Properties of bread dough with added fiber polysaccharides and phenolic antioxidants: a review. *Journal of Food Science,* 75**,** R163-74.

SODERBERG, T. 2016. *7.4: Acid-base properties of phenols* [Online]. University of Minnesota: Chemistry LibreTexts. Available: https://chem.libretexts.org/Textbook_Maps/Organic_Chemistry_Textbook_Maps/Map%3A_Organic_Chemistry_with_a_Biological_Emphasis_(Soderberg)/Chapter_07%3A_Organic_compounds_as_acids_and_bases/7.4%3A_Acid-base_properties_of_phenols [Accessed 14.02 2018].

STATISTA. 2019a. *Distribution share of barley production worldwide in 2018/19, by country* [Online]. Hamburg: Statista. Available: https://www.statista.com/statistics/272760/barley-harvest-forecast/ [Accessed 12 August 2019].

STATISTA. 2019b. *World barley production 2008/2009 to 2015/2016 (in million metric tons)* [Online]. Hamburg: Statista. Available: https://www.statista.com/statistics/271973/world-barley-production-since-2008/ [Accessed 12 August 2019].

STELTE, W. 2013. Steam explosion for biomass pre-treatment. Denmark: Danish Technological Institute.

STONE, J. & SCALLAN, A. Influence of drying on the pore structures of the cell wall. *In:* BOLAM, F., ed. 3rd fundamental research symposium., 1965 Cambridge, UK. Pulp and Paper Fundamental Research Society, 145-174.

SUN, R., LAWTHER, J. M. & BANKS, W. B. 1995. Influence of alkaline pre-treatments on the cell wall components of wheat straw. *Industrial Crops and Products,* 4**,** 127-145.

SYMPATEC. 2019. *Particle Characterisation: Particle shape and shape descriptors* [Online]. Clausthal-Zellerfeld, Germany: Sympatec GmbH. Available: https://www.sympatec.com/en/particle-measurement/glossary/particle-shape/ [Accessed 12 April 2019].

TANG, J. 2005. Dielectric properties of foods. *In:* SCHUBERT, H. & REGIER, M. (eds.) *The microwave processing of foods.* Cambridge: Woodhead Publishing.

THAKUR, V. K., THAKUR, M. K., RAGHAVAN, P. & KESSLER, M. R. 2014. Progress in Green Polymer Composites from Lignin for Multifunctional Applications: A Review. *ACS Sustainable Chemistry & Engineering,* 2**,** 1072-1092.

THEANDER, O., AMAN, P., WESTERLUND, E., ANDERSSON, R. & PETTERSSON, D. 1995. Total Dietary Fiber Determined as Neutral Sugar Residues, Uronic Acid Residues, and Klason Lignin (The Uppsala Method): Collaborative Study. *Journal of AOAC International,* 78**,** 1030-1044.

THIEBAUD, M., DUMAY, E., PICART, L., GUIRAUD, J. P. & CHEFTEL, J. C. 2003. High-pressure homogenisation of raw bovine milk. Effects on fat globule size distribution and microbial inactivation. *International Dairy Journal,* 13**,** 427-439.

TOLBERT, A., AKINOSHO, H., KHUNSUPAT, R., NASKAR, A. K. & RAGAUSKAS, A. J. 2014. Characterization and analysis of the molecular weight of lignin for biorefining studies. *Biofuels, Bioproducts and Biorefining,* 8**,** 836-856.

TOLOUE FARROKH, N., SUOPAJÄRVIA, H., SULASALMIA, P. & FABRITIUSA, T. 2018. A thermogravimetric analysis of lignin char combustion. *10th International Conference on Applied Energy (ICAE2018),.* Hong Kong: Energy Procedia.

TURBAK, A. F., SNYDER, F. W. & SANDBERG, K. R. Microfibrilated cellulose, a new cellulose product: properties, uses, and commercial potential. Applied Polymer Symposium, 1983. Journal of Applied Polymer Science, 815-827.

UNITED NATIONS. 2015. *World population projected to reach 9.7 billion by 2050* [Online]. United Nations. Available: https://www.un.org/en/development/desa/news/population/2015-report.html [Accessed 08 July 2019].

US-EPA 1990. Chapter 10: Section 2 Wood Products Industry. September 1990 ed. United States: United States Enviromental Protection Agency.

VAN ERVEN, G., DE VISSER, R., MERKX, D. W. H., STROLENBERG, W., DE GIJSEL, P., GRUPPEN, H. & KABEL, M. A. 2017. Quantification of Lignin and Its Structural Features in Plant Biomass Using (13)C Lignin as Internal Standard for Pyrolysis-GC-SIM-MS. *Analytical Chemistry,* 89**,** 10907-10916.

VAVRČÍK, H., GRYC, V. & RYBNÍČEK, M. Fluorescence microscopy utilization for lignin detection in wooden cell walls in spruce. A technical note. TRACE - Tree Rings in Archaeology, Climatology and Ecology, 2008 May 3rd – 6th 2007, Riga, Latvia. GFZ Potsdam, p. 149 - 153.

VORAGEN, A. G. J., COENEN, G.-J., VERHOEF, R. P. & SCHOLS, H. A. 2009. Pectin, a versatile polysaccharide present in plant cell walls. *Structural Chemistry,* 20**,** 263-275.

WANG, X., CUI, X. & ZHANG, L. 2012. Preparation and Characterization of Lignin-containing Nanofibrillar Cellulose. *Procedia Environmental Sciences,* 16**,** 125-130.

WÄPPLING-RAAHOLT, B. & OHLSSON, T. 2005. Improving the heating uniformity in microwave processing. *In:* SCHUBERT, H. & REGIER, M. (eds.) *The microwave processing of foods.* Cambridge: Woodhead Publishing.

WEATHERWAX, R. C. 1977. Collapse of cell-wall pores during drying of cellulose. *Journal of Colloid and Interface Science,* 62**,** 432-446.

WEISS, J. & MUSCHIOLIK, G. 2007. Factors Affecting the Droplet Size of Water-in-Oil Emulsions (W/O) and the Oil Globule Size in Water-in-Oil-in-Water Emulsions (W/O/W). *Journal of Dispersion Science and Technology,* 28**,** 703-716.

WELCH, R. W., HAYWARD, M. V. & JONES, D. I. H. 1983. The Composition of Oat Husk and its Variation Due to Genetic and Other Factors. *Journal of the Science of Food and Agriculture,* 34**,** 417-426.

WING, F. & SUAS, M. 2009. *Advanced bread and pastry: a professional approach,* Detroit, Delmar Cengage Learning.

WOLF, F., KOEHLER, K. & SCHUCHMANN, H. P. 2013. Stabilization of Water Droplets in Oil with PGPR for Use in Oral and Dermal Applications. *Journal of Food Process Engineering,* 36**,** 276-283.

WRAP. 2018. *WRAP restates UK food waste figures to support united global action* [Online]. WRAP. Available: http://www.wrap.org.uk/content/wrap-restates-uk-food-waste-figures-support-united-global-action [Accessed 08 July 2019].

XIAO, J., LI, Y. & HUANG, Q. 2016. Recent advances on food-grade particles stabilized Pickering emulsions: Fabrication, characterization and research trends. *Trends in Food Science & Technology,* 55**,** 48-60.

XU, C. & FERDOSIAN, F. 2017. *Conversion of Lignin into Bio-Based Chemicals and Materials,* Germany, Springer.

YANG, H., YAN, R., CHEN, H., LEE, D. H. & ZHENG, C. 2007. Characteristics of hemicellulose, cellulose and lignin pyrolysis. *Fuel,* 86**,** 1781-1788.

YE, Y., FAN, J. & CHANG, J. 2012. Effect of reaction conditions on hydrothermal degradation of cornstalk lignin. *Journal of Analytical and Applied Pyrolysis,* 94**,** 190-195.

YIN, H. S., LIU, H. M. & LIU, Y. L. 2017. Structural Characterization of Lignin in Fruits and Stalks of Chinese Quince. *Molecules,* 22.

ZANDLEVEN, J., SORENSEN, S. O., HARHOLT, J., BELDMAN, G., SCHOLS, H. A., SCHELLER, H. V. & VORAGEN, A. J. 2007. Xylogalacturonan exists in cell walls from various tissues of Arabidopsis thaliana. *Phytochemistry,* 68**,** 1219-26.

ZHAN, S., CHENGUANG, W., KANG, B., XINGHUA, Z., CHILING, Y., RENJIE, D., LONGLONG, M. & CHANGLE, P. 2017. Py-GC/MS study of lignin pyrolysis and effect of catalysts on product distribution. *International Journal of Agricultural and Biological Engineering,* 10**,** 214-225.

ZHANG, X., YANG, W. & BLASIAK, W. 2011. Modeling Study of Woody Biomass: Interactions of Cellulose, Hemicellulose, and Lignin. *Energy & Fuels,* 25**,** 4786-4795.

ZHANG, Y., DIN, S., MIELENZ, J., CUI, J., ELANDER, R. & LASER, M. 2007. Fractionating recalcitrant lignocellulose at modest reaction conditions. *Biotechnology and Bioengineering,* 97**,** 214-233.

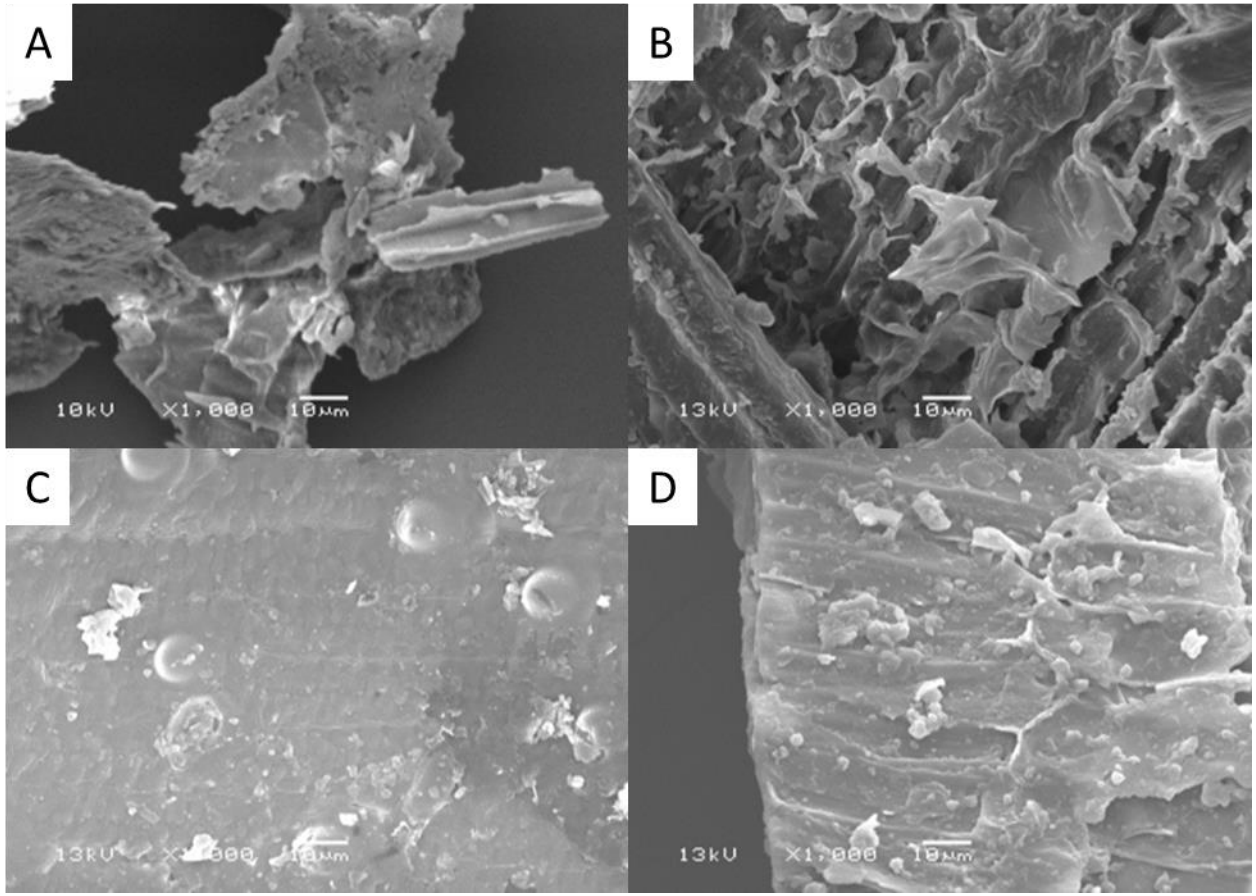
ZHAO, Q. & DIXON, R. A. 2011. Transcriptional networks for lignin biosynthesis: more complex than we thought? *Trends in Plant Science,* 16**,** 227-33.

ZHONG, R. & YE, Z. H. 2015. Secondary cell walls: biosynthesis, patterned deposition and transcriptional regulation. *Plant Cell Physiology,* 56**,** 195-214.

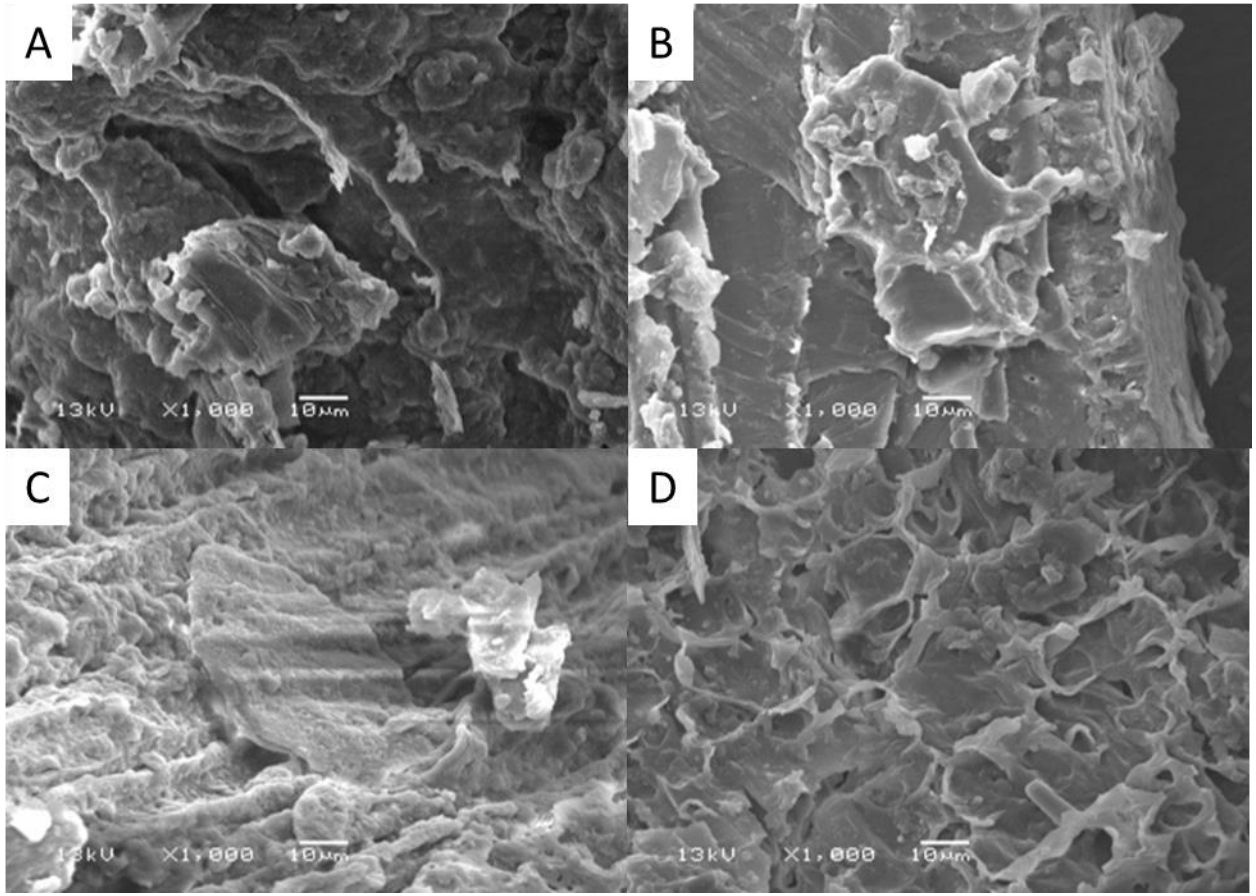
ZHOU, X., BROADBELT, L. J. & VINU, R. 2016. Mechanistic Understanding of Thermochemical Conversion of Polymers and Lignocellulosic Biomass. *Thermochemical Process Engineering.* Elsevier Inc.

Appendices

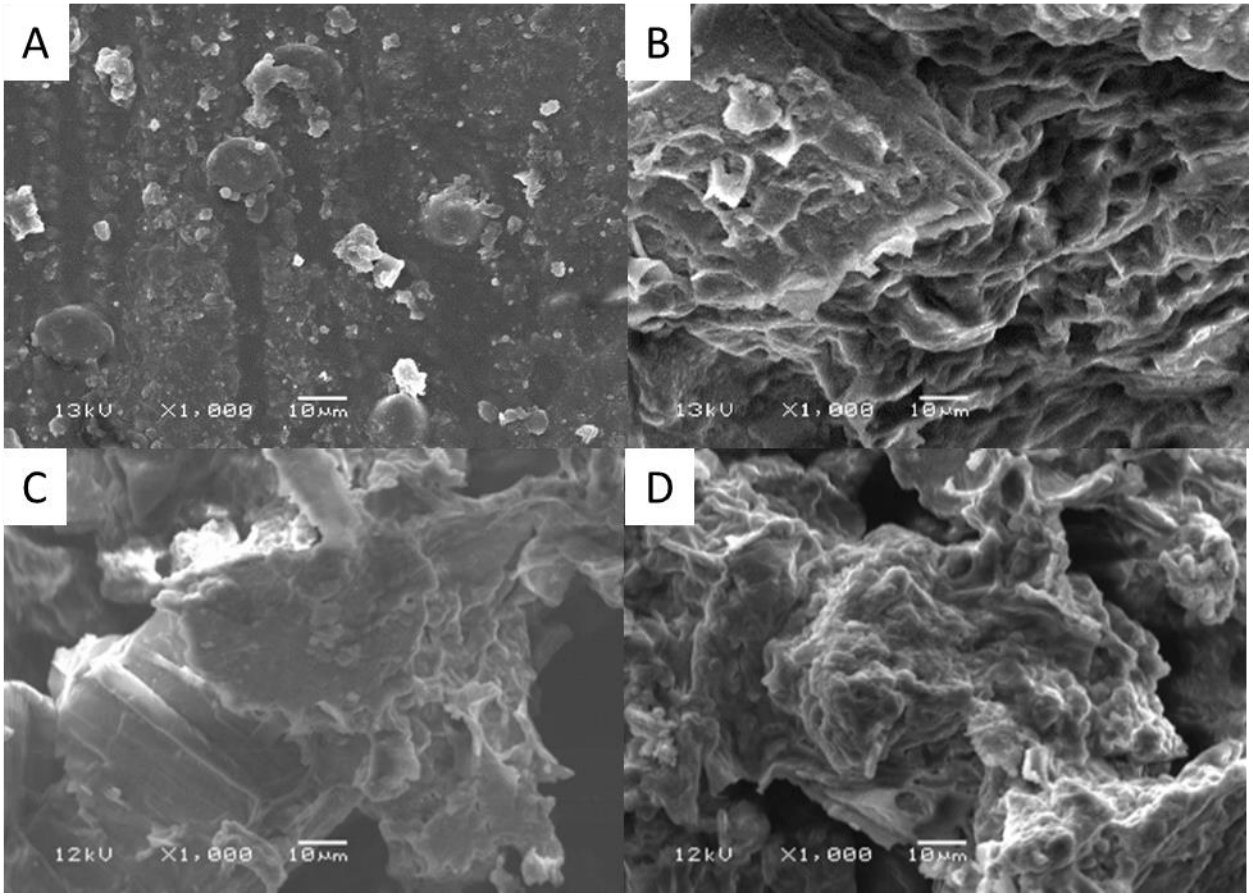
A1. Supplementary information for Paper 1 (Chapter 5) – All Scanning Electron Micrographs produced from different hydrothermal processing conditions



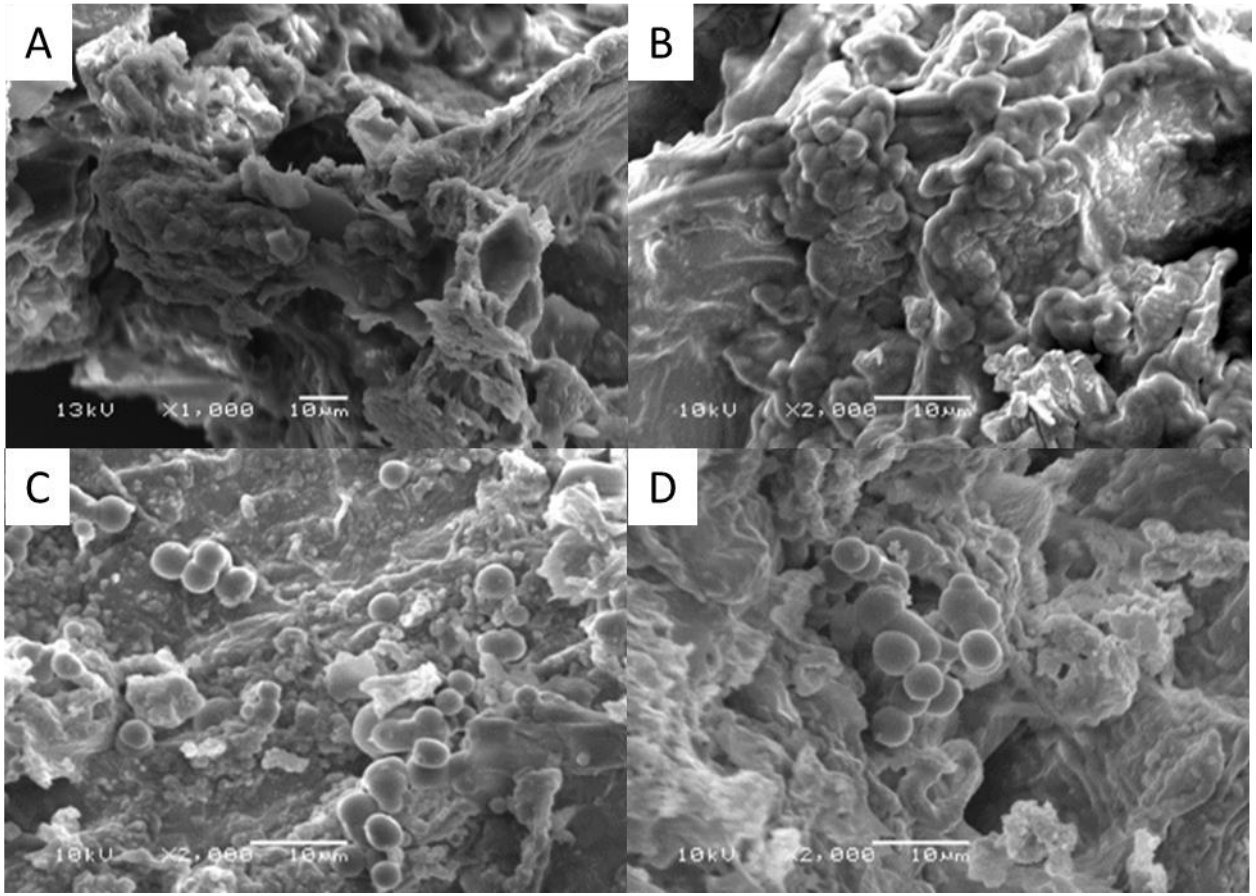
Appendix Figure 1: SEM Micrographs taken for hydrothermally treated BSG samples at 140°C for A) 30min; B) 60min; C) 90min; D) 120min



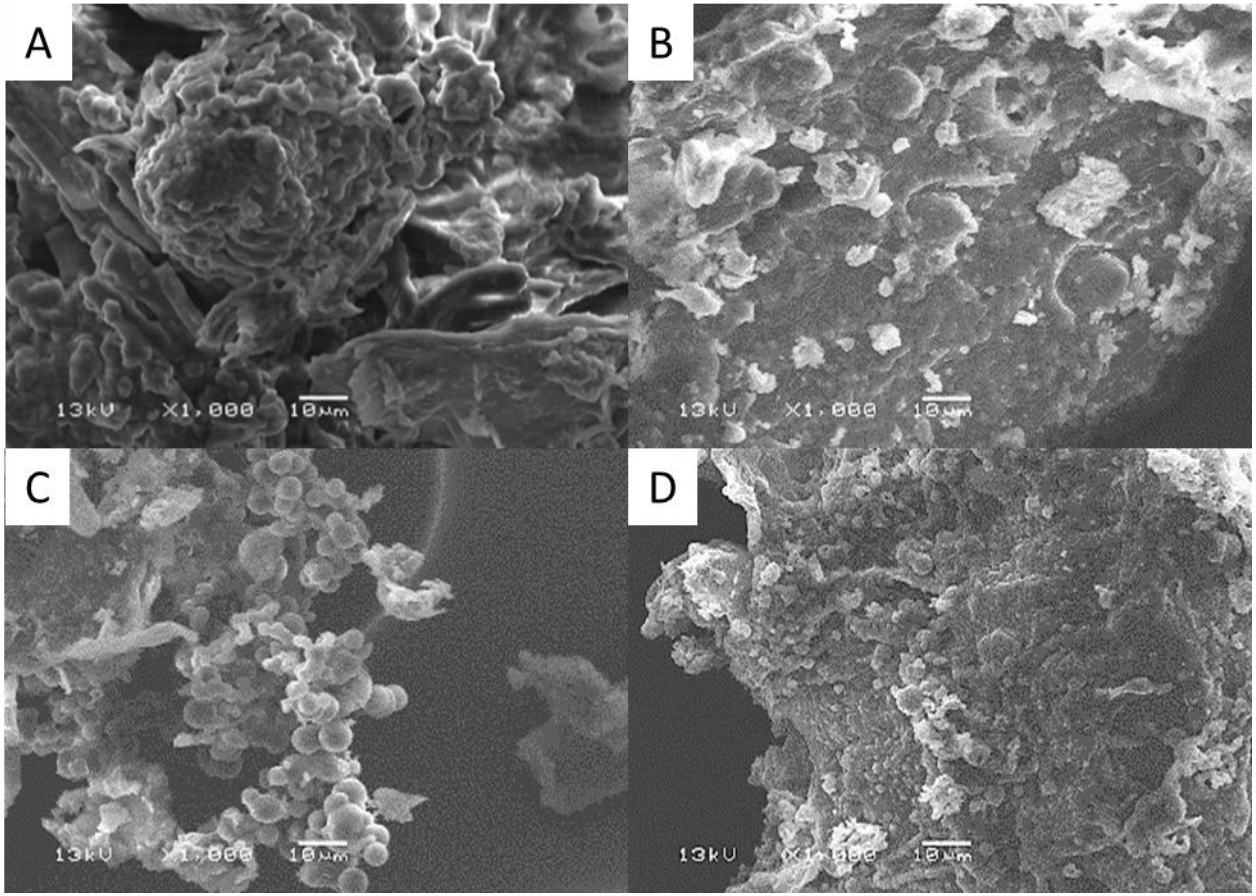
Appendix Figure 2: SEM Micrographs taken for hydrothermally treated BSG samples at 160°C for A) 30min; B) 60min; C) 90min; D) 120min



Appendix Figure 3: SEM Micrographs taken for hydrothermally treated BSG samples at 180°C for A) 30min; B) 60min; C) 90min; D) 120min



Appendix Figure 4: SEM Micrographs taken for hydrothermally treated BSG samples at 200°C for A) 30min; B) 60min; C) 90min; D) 120min



Appendix Figure 5: SEM Micrographs taken for hydrothermally treated BSG samples at 220°C for A) 30min; B) 60min; C) 90min; D) 120min

A2. Preliminary results for Lignin-based Pickering emulsifiers used to replace conventional emulsifiers during cake baking

Background and Objective

Emulsifiers are readily used in bakery and confectionary products within the food industry. They consist of a hydrophilic head and hydrophobic tail which during baking helps to stabilise the dough or batter whether the product is bread or a cake. The main function of emulsifiers in cakes is to aid in water binding which in turn will decrease the batter variability from batch to batch whilst improving air stability within the network. This in turn aids in creating a final texture of fine crumb structure whilst keeping the product saturated with moisture. Conventional emulsifiers used in baking are lecithins; sodium and calcium stearoyl lactylate; polysorbates; diacetyl tartaric acid esters of monoglycerides (DATEM) as well as mono and diglycerides. Out of all the emulsifiers stated, the cleanest label emulsifier is lecithin.

This study used hydrophilic and hydrophobic lignin-based particles, obtained from BSG to replace the conventional emulsifier used in cakes. The BSG particles have emulsifying properties in their natural form through Pickering stabilisation. With the addition of hydrothermal processing the functional properties have already been demonstrated to change from intrinsically hydrophilic to hydrophobic in nature.

A conventional sponge cake recipe was used for cake making, both the hydrophilic and hydrophobic particles were incorporated, using different ways of particle incorporation. The two methods of particle incorporation were direct addition to the batter mixture and pre-emulsified with the oil and water. Samples were compared to a

control using commercial cake emulsifiers. The different particles which are known from previous works to stabilise oil-in-water emulsions (UT BSG) and water-in-oil emulsions (3PHT BSG) were used compared to a conventional cake emulsifier to look specifically at changes to the bake crumb structure in the cake.

Results and Discussion

Before baking, the batter densities were measured for all cakes. The commercial emulsifier was used as reference not only in batter density but also for the visual representation and comparison of the cakes post-baking.

Batter densities were measured prior to baking with the results shown in Appendix Table 1. The lowest batter density was observed using the commercial emulsifier. The ideal batter density targeted in this research for cakes prior to baking was 0.8g/m^3 with all densities measured being higher than that. All cake batters using particulate emulsifiers were denser than the conventional emulsifier. The densest batter being the pre-emulsified hydrothermally treated particles. The differences in the batter densities across the different samples could give a clear indication of how the addition of the particles affects the final crumb structure. The reason being that the higher the batter density the less air has been incorporated during mixing generating a thinner viscosity. As a result of a higher batter density the cake will have a denser crumb structure. Tunnelling will usually appear when the batter density is too low as too much air has been incorporated into the batter during mixing which in turn creates a finer texture in the crumb.

Appendix Table 1: Batter Densities of all cakes baked

Sample	Treatment	Batter density (g/m^3)
1	Commercial emulsifier	0.895
2	Untreated particles (hydrophilic) suspended	1.07
3	Treated particles (hydrophobic) suspended	1.02
4	Untreated particles (hydrophilic) pre-emulsification	1.10
5	Treated particles (hydrophobic) pre-emulsification	1.28

Commercial emulsifier

Visually the cake produced using the conventional emulsifier had a uniform crumb structure which also appeared to be quite coarse. Not much visual tunnelling occurred showing that the emulsifier was able to stabilise the air bubbles successfully within the cake structure as visible in Appendix Figure 6. The structure of the cake in Appendix Figure 6 when compared regular cake baking trials appeared to be a lot coarser than expected. Possible explanations as to what may have caused this abnormality are that the emulsifier concentration was insufficient in percentage or that the emulsifier itself was out of date which were suggested by bakery scientists at Campden BRI.



Appendix Figure 6: Cake produced using conventional cake emulsifier

Untreated particles – suspended

The addition of the untreated BSG particles notably changed the colour of the cake batter to a darker hue however upon baking the colour difference appeared similar when compared to the control cake. The crumb structure of the cake shown in Appendix Figure 7 compared to Appendix Figure 6 was coarser. There were noticeable small holes and pockets visible throughout the cake. Small tunnels started to appear, and it is hypothesised that for all cakes with tunnelling, this was due to the rough nature of the particles puncturing the air pockets and generating the tunnels. As expected, the particles did not dissolve into the batter and the structure of the crumb indicates that the emulsifying properties of these particles are not comparable to the conventional emulsifier.



Appendix Figure 7: Cake produced using untreated BSG particles as direct replacement of the conventional emulsifier

Treated particles direct suspension.

Cake produced by hydrothermally treated particles added directly to and suspended in the batter mixer was noticeably darker than the conventional emulsifier, see Appendix Figure 8. This is because the particles themselves are intrinsically dark brown to black in nature. These particles are visible in the batter before baking. Pockets of particles are also visible in the cake noted by visible colour differences. This shows that using the particles as a direct addition to the cake replacing the conventional emulsifier is not a viable option similar to the cake using the untreated particles. Upon cutting the cake to observe the internal structure, holes and visible tunnels in greater quantity are produced with the structure being an increasingly course nature and less uniform across the entirety of the cake.



Appendix Figure 8: Cake produced using treated BSG particles as direct replacement of the conventional emulsifier

Untreated particles – pre-emulsification

To aid in the particle dispersion, particles were emulsified with the sunflower oil and water. These ingredients were ordinarily added to the cake batter as individual ingredients. Previously these particles have been shown to form stable oil-in-water emulsions.

Using Appendix Figure 6 as reference, Appendix Figure 9 shows a cake where the particles were pre-emulsified prior to addition to the cake batter. This produced similar structures to that observed previously in Appendix Figure 7 and Appendix Figure 8. No tunnels were observed at the bottom of the cake prior to cutting. However, upon cutting, considerable tunnels were observed suggesting that

the particles affect the air retention, whilst the crumb structure appeared to be finer but less homogeneous.



Appendix Figure 9: Cake produced using untreated BSG particles pre-emulsified as an O/W emulsion

Treated particles – pre-emulsification

The same principle of pre-emulsification was applied to the hydrothermally treated BSG particles (hydrophobic) before adding to the cake batter. Appendix Figure 10 shows the final cake produced. Holes in the cake have appeared at the bottom even prior to cutting. Upon cutting, significant tunnelling is present in the structure. These were in the greatest quantity of all cakes produced. The crumb structure is also coarser than the untreated particles and control reference using the conventional emulsifier. Although tunnelling is often linked to having a lower batter density and a finer crumb structure. The initial works showed that this cake batter had the highest density. Despite this observation, it is hypothesised that the presence of particles in the crumb structure due to stabilising the emulsion may be puncturing some of the air pockets during baking which in turn will generate tunnels.



Appendix Figure 10: Cake produced using treated BSG particles pre-emulsified as a W/O emulsion

When comparing the cakes, it appears that the particles have a distinct behaviour in the cake structural matrix as well as impact on the colour. The particles themselves seem to act like fibres in the matrix rather than conventional emulsifiers. Research has shown that the addition of fibre to bread for example changes the structure of the crumb and the texture of the bread. The crumb gets coarser and the holes in the bread get larger often perceived to be due to the fibres puncturing the air pockets and bubbles within the gluten matrix when a dough is formed (Rosell and Santos, 2010, Sivam *et al.*, 2010). The same principle applies when making a batter for a cake. This puncturing effect increases bubble coalescence and also

disproportionation (uptake of small bubbles by larger ones due to pressure differences) which can be shown upon baking by the large holes and tunnels appearing in the cake. Upon treating the particles to render them increasingly hydrophobic, they generate a greater number of holes and tunnels in the crumb which suggests that the particles are sharper through processing despite the presence of the lignin droplets. Directly applying the particles of any kind into the batter formed fewer holes and tunnels than pre-emulsifying them with the oil and water in the recipe. It is hypothesised that this pre-emulsification step stabilised the water as a dispersed phase in the emulsion but upon mixing with the other ingredients in the Hobart mixer, this emulsion is broken down creating the pockets of inhomogeneity shown above in Appendix Figure 9 and Appendix Figure 10. For the differences in colour between the cakes, the noticeable changes are as a result of the colour of the particles. The use of pre-emulsification of the hydrophobic 3PHT particles generated a darker cake crumb than any other produced cake. This is because the particles themselves are dark in hue and that the pre-emulsified mixture is a greater proportion of the overall mixture of ingredients than if they were added individually.

Conclusions and Recommendations

This set of preliminary test baking has shown that it is possible to replace a conventional emulsifier used in cake baking with particulate emulsifiers created from BSG whether of untreated (hydrophilic) origin or hydrothermally treated (hydrophobic) origin. Further work is required to fully understand the behaviour of the particles in a cake-like structure as well as looking at different concentrations of the ingredient in the batter.

Since the hydrothermally treated particles have a dark brown hue, the type of cakes in which this could be used without causing a physical colour change is also required to be tested with chocolate sponge or coffee sponge type cakes being the likely option for most effective colour masking. Also since the particles are dark brown, the nutritional value of them must also be considered since they are both high in protein and fibre, but further testing will be required on acrylamide to ensure that the addition of the emulsifier is still within the limits allowed in a product.

Alternative products of potential use are biscuits or chocolate where the fat phase volume is greater than that in cakes. Breads are also another option however it is hypothesised that similar tunnelling and puncturing of the bubble structure may appear due to the fibrous nature of the particles.

Acknowledgements: We would like to thank specific staff members at Campden BRI who conducted the work specifically Anne Vissers as well as Sarab Sahi and Dr Gary Tucker for input in idea generation.

A3. MATLAB code for calculating lignin percentage from NMR data

Specific code for use in MATLAB – example based on file name "3PHT BSG.xlsx".

```
dataset = xlsread('3PHT BSG.xlsx','Total');

x = dataset(:,1);
y = dataset(:,2);
y2 = dataset(:,3);

Total = trapz(x,y) - trapz(x,y2);

datasetL = xlsread('3PHT BSG.xlsx','GSlignin');

xL = datasetL(:,1);
yL = datasetL(:,2);
y2L = datasetL(:,3);

GSlignin = trapz(xL,yL) - trapz(xL,y2L);

datasetM = xlsread('3PHT BSG.xlsx','Methoxy');

xM = datasetM(:,1);
yM = datasetM(:,2);
y2M = datasetM(:,3);

Methoxy = trapz(xM,yM) - trapz(xM,y2M);

figure;
subplot(3,1,1);
plot(x,y,x,y2);
title('Total spectra range');

subplot(3,1,2);
plot(xL,yL,xL,y2L);
title('G & S Lignin range');

subplot(3,1,3);
plot(xM,yM,xM,y2M);
title('Methoxy range');
```